

UNIVERSITY OF NOTTINGHAM

School of Chemical, Environmental and Mining Engineering



**THE CHARACTERISATION AND COMBUSTION
OF SOUTH AMERICAN COALS**

By

**Richelieu Barranco Melendez
BEng**

**Thesis submitted to the University of Nottingham
for the degree of Doctor of Philosophy**

September 2001

ACKNOWLEDGEMENTS

I would like to express my sincere gratitude to the following people and institutions, for the assistance and help I have been given during the project:

Dr Mike Cloke, my supervisor, for his constructive guidance, financial help, encouragement and advice throughout the duration of the research.

Staff at Powergen UK plc, Ratcliffe-on-soar, Nottingham, for their invaluable provision of the combustion rigs and related facilities, for their assistance in the running of the rigs and the supply of coal samples.

Dr Edward Lester, for his help in all aspect of the experimental work and his assistance in the running of the DTF rig; Dr Andrew Gilfillan and Dr Alan Thompson, for the proof reading of this thesis and useful suggestions; and Dave Clift, for the photographic work and petrographic-related matters.

The Colombian Institute of Science, COLCIENCIAS, and Universidad del Atlantico-Colombia, for providing the funding for this project; and to Carbones del Caribe-Colombia, Inspectorate de Colombia, SGS-Colombia, and Carbones del Guasare-Venezuela for supplying some of the coal samples.

The Chemical Engineering Laboratory Staff, in particular, Marion, Mick, Fred and Phil for their help and support during my experimental work.

Tom Gilbertson for his friendship and his hospitality during my stay in the UK.

My parents, Oswaldo and Ana, my brothers, Oswaldo and Holman, and my sister, Bertha, for their patience and continuous encouragement.

Finally to all those who directly or indirectly participated of my effort to carry out this research, especially, my colleagues and friends, Ricardo, Juan, Astrid, Marley, Tomasa, Aaron, Jesus, Manuel, Heriberto, Rosalba, Uraporn, Karuna, Mathew, Zelia, Laura, Miguel, Janos, Patricia, Fabio, Andrew, Eduardo, David, Svenja, Shola, Karen and Doug for their friendship and their encouragement.

TABLE OF CONTENTS

| | |
|-------------------------|-----|
| ACKNOWLEDGEMENTS | i |
| LIST OF FIGURES | vii |
| LIST OF TABLES | xii |
| ABSTRACT | xv |

CHAPTER 1 INTRODUCTION

| | |
|---|---|
| 1.1 The Origins of Coal | 1 |
| 1.2 Coal Combustion | 3 |
| 1.3 Char Formation and Characterisation | 4 |
| 1.4 Aims of the Project | 6 |

CHAPTER 2 LITERATURE REVIEW

| | |
|------------------------------------|----|
| 2.1 Coal Origins and Formation | 8 |
| 2.2 Coal Classification | 9 |
| 2.3 Coal Petrography | 10 |
| 2.3.1 Coal Macerals | 12 |
| 2.3.1.1 Vitrinite Group | 12 |
| 2.3.1.2 Liptinite Group | 14 |
| 2.3.1.3 Inertinite Group | 15 |
| 2.3.2 Coal Lithotypes | 16 |
| 2.3.3 Coal Microlithotypes | 17 |
| 2.4 South American Coals | 19 |
| 2.4.1 Coal Occurrences and Geology | 19 |
| 2.4.2 Colombian Coals | 20 |
| 2.4.3 Venezuelan Coals | 23 |
| 2.5 Coal Combustion | 26 |

| | | |
|-----------------------------------|---------------------------------------|----|
| 2.5.1 | Coal Pyrolysis and Devolatilisation | 27 |
| 2.5.1.1 | The Effect of Experimental Conditions | 27 |
| 2.5.1.2 | The Effect of Coal Properties | 28 |
| 2.5.2 | Char Formation and Morphology | 29 |
| 2.5.3 | Char Burnout and Reactivity | 30 |
| 2.5.4 | Rank Effects | 33 |
| 2.5.5 | Macerals Effects | 35 |
| 2.5.5.1 | Vitrinite | 36 |
| 2.5.5.2 | Liptinite | 37 |
| 2.5.5.3 | Inertinite | 38 |
| 2.5.6 | Particle Size Effects | 40 |
| 2.5.7 | Mineral Effects | 41 |
| CHAPTER 3 EXPERIMENTAL | | |
| 3.1 | Coal Sample Preparation | 42 |
| 3.1.1 | Origin of Samples | 42 |
| 3.1.2 | Screening | 42 |
| 3.1.2.1 | Wet Sieving | 42 |
| 3.1.2.2 | Alpine Jet Sieve | 44 |
| 3.2 | Coal Sample Characterisation | 44 |
| 3.2.1 | Proximate Analysis | 44 |
| 3.2.2 | Elemental Analysis | 46 |
| 3.2.3 | Petrographic Characterisation | 48 |
| 3.2.3.1 | Sample Preparation | 48 |
| 3.2.3.2 | Polishing Procedure | 48 |
| 3.2.3.3 | The Microscope | 48 |
| 3.2.3.4 | Maceral Analysis | 50 |
| 3.2.3.5 | Vitrinite Reflectance Measurements | 51 |
| 3.2.4 | Image Analysis | 51 |
| 3.2.4.1 | The Image Analyser | 51 |
| 3.2.4.2 | The Reactivity Assessment Program | 52 |

| | |
|---|----|
| 3.3 The Drop Tube Furnace | 54 |
| 3.3.1 Description of Rig | 54 |
| 3.3.1.1 Gas Supply | 54 |
| 3.3.1.2 Feeder System | 57 |
| 3.3.1.3 Heating System and Controls | 58 |
| 3.3.1.4 Reaction Tube and Probes | 58 |
| 3.3.1.5 Filter System | 58 |
| 3.3.2 Drop Tube Furnace Experiments | 59 |
| 3.3.3 DTF Re-firing Experiments | 59 |
| 3.4 The 1 MW Combustion Test Facility | 60 |
| 3.4.1 Description of Rig | 60 |
| 3.4.2 Combustion Experiments | 61 |
| 3.5 Char Characterisation | 61 |
| 3.5.1 Loss-on-Ignition Test | 63 |
| 3.5.2 Microscopic Analysis | 63 |
| 3.5.2.1 Char Block Preparation | 63 |
| 3.5.2.2 Morphological Characterisation | 64 |
| 3.5.3 Image Analysis | 64 |
| 3.5.4 Intrinsic Reactivity Analysis | 65 |
| 3.5.5 Scanning Electron Microscopy Analysis | 66 |

CHAPTER 4 DROP TUBE FURNACE EXPERIMENTS

| | |
|---|----|
| 4.1 Initial Drop Tube Furnace Experiments | 67 |
| 4.1.1 Coal Characterisation | 68 |
| 4.1.2 Drop Tube Furnace Conditions | 70 |
| 4.1.3 Char Collection Efficiency | 71 |
| 4.1.4 DTF Volatiles and R Factor | 74 |
| 4.1.5 Char Intrinsic Reactivity | 77 |
| 4.1.6 Optical and Automatic Image Analyses of Chars | 79 |
| 4.2 Further Drop Tube Furnace Experiments | 83 |
| 4.2.1 Proximate and Ultimate Analysis of Coals | 83 |

| | | |
|---------|--|-----|
| 4.2.2 | Petrographic Characterisation of Coals | 85 |
| 4.2.3 | Image Analysis of Coals | 88 |
| 4.2.4 | Drop Tube Furnace Conditions | 89 |
| 4.2.5 | Char Collection Efficiency | 89 |
| 4.2.6 | DTF Volatiles and R Factor | 92 |
| 4.2.7 | Char Intrinsic Reactivity | 92 |
| 4.2.7.1 | Peak Temperature | 92 |
| 4.2.7.2 | Burnout Temperature | 98 |
| 4.2.8 | Optical Morphology and Automatic Analysis of Chars | 99 |
| 4.2.9 | Correlation of Char Properties and DTF Volatiles with Coal Characteristics | 107 |
| 4.2.9.1 | Automatic Char Analysis | 108 |
| 4.2.9.2 | DTF Volatiles and Char Intrinsic Reactivity | 112 |

CHAPTER 5 DTF CHAR RE-FIRING EXPERIMENTS

| | | |
|-------|--|-----|
| 5.1 | Coal Selection and Properties | 115 |
| 5.1.1 | Proximate and Ultimate Analysis | 115 |
| 5.1.2 | Petrographic Characterisation | 118 |
| 5.1.3 | Image Analysis | 118 |
| 5.2 | Drop Tube Furnace Conditions | 120 |
| 5.3 | Char Collection Efficiency | 121 |
| 5.4 | DTF Volatiles and R Factor | 123 |
| 5.5 | Properties of the Pyrolysed Char | 126 |
| 5.5.1 | Char Intrinsic Reactivity | 126 |
| 5.5.2 | Optical Morphology and Automatic Analysis | 130 |
| 5.5.3 | Correlation of DTF Volatiles and Char Properties with Coal Characteristics | 132 |
| 5.6 | Properties of the Re-Fired Chars | 135 |
| 5.6.1 | Char Reactivity and Burnout | 135 |
| 5.6.2 | Char Intrinsic Reactivity | 142 |
| 5.6.3 | Scanning Electron Microscope Examination | 144 |
| 5.6.4 | Correlation of Re-fired Char Properties with Coal Characteristics | 153 |

CHAPTER 6 EXPERIMENTS IN THE 1MW RIG

| | |
|---|-----|
| 6.1 Introduction | 155 |
| 6.2 Sample Preparation | 156 |
| 6.3 Coal Properties | 159 |
| 6.4 Test Programme | 162 |
| 6.5 Properties of the Chars from the Near-Burner Region | 167 |
| 6.5.1 Intrinsic Reactivity | 167 |
| 6.5.2 Automatic Char Analysis | 168 |
| 6.6 Properties of the Chars from the Convective section | 173 |
| 6.6.1 Loss-on-Ignition and Unburnt Combustible | 173 |
| 6.6.2 Intrinsic Reactivity | 178 |
| 6.7 Summary | 185 |

CHAPTER 7 CONCLUSIONS AND FURTHER WORK

| | |
|---|-----|
| 7.1 Drop Tube Furnace Experiments | 186 |
| 7.2 Experiments in the 1MW Combustion Rig | 188 |
| 7.3 Recommendations for Further Work | 189 |

| | |
|-------------------|-----|
| REFERENCES | 190 |
|-------------------|-----|

| | |
|---------------------|-----|
| PUBLICATIONS | 202 |
|---------------------|-----|

| | |
|-------------------|-----|
| APPENDICES | 203 |
|-------------------|-----|

| | |
|--|-----|
| APPENDIX A. Vitrinite Reflectance Histograms of the Coal Fractions | 204 |
|--|-----|

| | |
|---|-----|
| APPENDIX B. Grey Scale Histograms of the Coal Fractions | 210 |
|---|-----|

| | |
|--|-----|
| APPENDIX C. DTA Profiles of the Chars as a Function of DTF Temp. | 216 |
|--|-----|

| | |
|---|-----|
| APPENDIX D. F-Distribution, F-values [Confidence level 95%: $\alpha = 0.05$] | 226 |
|---|-----|

| | |
|---|-----|
| APPENDIX E. DTA Profiles of the Pyrolysed Chars | 227 |
|---|-----|

| | |
|--|-----|
| APPENDIX F. DTA Profiles of the Re-fired Chars | 230 |
|--|-----|

LIST OF FIGURES

CHAPTER 2

| | | |
|------------|--------------------------|----|
| Figure 2.1 | The three maceral groups | 13 |
| Figure 2.2 | Tenuispheres | 31 |
| Figure 2.3 | Crassispheres | 31 |
| Figure 2.4 | Tenuinetworks | 32 |
| Figure 2.5 | Crassinetworks | 32 |
| Figure 2.6 | Inertoids | 32 |
| Figure 2.7 | Fusinoids/Solids | 32 |

CHAPTER 3

| | | |
|-------------|---|----|
| Figure 3.1 | Location of the South American coal samples used in this study | 43 |
| Figure 3.2 | The Alpine Air Jet Sieve | 45 |
| Figure 3.3 | The Stanton Redcroft STA 1000 thermo-gravimetric analyser | 45 |
| Figure 3.4 | TGA curve showing proximate analysis of coal | 47 |
| Figure 3.5 | The Leco 600 CHNS analyser | 47 |
| Figure 3.6 | The Pressi Mecapress C and Struers Prontopress-2 mounting presses | 49 |
| Figure 3.7 | The Struers Pedemat Rotapol polisher | 49 |
| Figure 3.8 | The Leitz Ortholux II POL-BK microscope | 50 |
| Figure 3.9 | The IBAS 2000 Image Analyser | 52 |
| Figure 3.10 | A typical reflectance histogram of coal | 53 |
| Figure 3.11 | Schematic of the Drop Tube Furnace | 55 |
| Figure 3.12 | The main working are of the Drop Tube Furnace | 56 |
| Figure 3.13 | The screw feeder system of the Drop Tube Furnace | 57 |
| Figure 3.14 | Schematic of the 1 MW Combustion Test Facility | 62 |
| Figure 3.15 | The distance transform mapping process | 65 |
| Figure 3.16 | A typical burning profile from the intrinsic reactivity analysis | 66 |

CHAPTER 4

| | | |
|-------------|---|-----|
| Figure 4.1 | Temperature profiles along the reaction zone in the DTF | 71 |
| Figure 4.2 | A plot of R Factor as a function of operating temperature and particle size for the three coals | 76 |
| Figure 4.3 | Peak temperature as a function of coal particle size and DTF operating temperature | 78 |
| Figure 4.4 | Burnout temperature as a function of coal particle size and DTF operating temperature | 78 |
| Figure 4.5 | Scanning Electron Micrograph showing typical network structure of Bijao chars | 81 |
| Figure 4.6 | Scanning Electron Micrograph showing cenospheres from Caypa chars. | 81 |
| Figure 4.7 | Scanning Electron Micrograph showing cenospheres and fusinoid chars in La Jagua. | 82 |
| Figure 4.8 | Changes in ACA5 as a function of temperature and particle size | 82 |
| Figure 4.9 | A plot of ACA5 against % unreactives | 83 |
| Figure 4.10 | A plot of R Factor as a function of operating temperature for the 53-75 μm char fractions | 95 |
| Figure 4.11 | A plot of R Factor as a function of operating temperature for the 106-125 μm char fractions | 95 |
| Figure 4.12 | A Plot of peak temperature as a function of the DTF operating temperature for the 53-75 μm char fractions | 96 |
| Figure 4.13 | A Plot of peak temperature as a function of the DTF operating temperature for the 106-125 μm char fractions | 96 |
| Figure 4.14 | A Plot of burnout temperature as a function of the DTF operating temperature for the 53-75 μm char fractions | 97 |
| Figure 4.15 | A Plot of burnout temperature as a function of the DTF operating temperature for the 106-125 μm char fractions | 97 |
| Figure 4.16 | A Plot of ACA5 against DTF temperature for the 53-75 μm char fractions | 106 |

| | | |
|-------------|--|-----|
| Figure 4.17 | A Plot of ACA5 against DTF temperature for the 106-125 μm char fractions | 106 |
| Figure 4.18 | Actual values of ACA5 against predicted values following linear regression with maceral content - DTF temp.: 1300°C | 109 |
| Figure 4.19 | Actual values of ACA5 against predicted values following linear regression with maceral content and rank - DTF temp.: 1300°C | 109 |
| Figure 4.20 | A Plot of ACA5 against % unreactive as a function of DTF temperature | 110 |
| Figure 4.21 | Actual values of ACA5 against predicted values following linear regression with image analysis, grey scale histograms- DTF temp.: 1300°C | 111 |

CHAPTER 5

| | | |
|-------------|---|-----|
| Figure 5.1 | Temperature profiles as a function of residence time along the reaction zone in the DTF | 121 |
| Figure 5.2 | A plot of DTF volatiles as a function of particle size for each coal | 125 |
| Figure 5.3 | A plot of R Factor versus particle size for each coal | 125 |
| Figure 5.4 | DTA burning profiles for the 53-75 μm fraction pyrolysed chars | 128 |
| Figure 5.5 | A plot of peak temperature as a function of mean particle size for the pyrolysed chars | 129 |
| Figure 5.6 | A plot of burnout temperature as a function of mean particle size for the pyrolysed chars | 129 |
| Figure 5.7 | Grey scale histograms for the 106-125 μm coal fractions showing the different grey scale bands | 134 |
| Figure 5.8 | Unburnt combustible against % unreactives for the 200 ms re-fired chars | 139 |
| Figure 5.9 | Unburnt combustible against % unreactives for the 400 ms re-fired chars | 139 |
| Figure 5.10 | Unburnt combustible against % unreactives for the 600 ms re-fired chars | 140 |

| | | |
|-------------|--|-----|
| Figure 5.11 | Relation between unburnt combustible of the 400 ms re-fired chars and the automatic char analysis of the pyrolysed chars | 141 |
| Figure 5.12 | Relation between unburnt combustible of the 400 ms re-fired chars and the peak temperature of the pyrolysed chars | 142 |
| Figure 5.13 | DTA burning profiles for the 400 ms re-fired chars (Fraction II) | 145 |
| Figure 5.14 | SEM photomicrograph of Bijao coal/chars, fraction II | 147 |
| Figure 5.15 | SEM photomicrograph of La Loma coal/chars, fraction II | 148 |
| Figure 5.16 | SEM photomicrograph of La Jagua coal/chars, fraction II | 149 |
| Figure 5.17 | SEM photomicrograph of El Cerrejon coal/chars, fraction II | 150 |
| Figure 5.18 | SEM photomicrograph of Caypa coal/chars, fraction II | 151 |
| Figure 5.19 | SEM photomicrograph of Guasare coal/chars, fraction II | 152 |

CHAPTER 6

| | | |
|-------------|---|-----|
| Figure 6.1 | Vitrinite reflectance histograms of Thoresby coal grinds | 163 |
| Figure 6.2 | Vitrinite reflectance histograms of Carbocol coal grinds | 164 |
| Figure 6.3 | Grey scale histograms of Thoresby coal grinds | 165 |
| Figure 6.4 | Grey scale histograms of Carbocol coal grinds | 166 |
| Figure 6.5 | DTA burning profiles for Thoresby chars from Port 1 | 169 |
| Figure 6.6 | DTA burning profiles for Carbocol chars from Port 1 | 170 |
| Figure 6.7 | A plot of BT as a function of percentage of particles above 150 μ m for chars from Port 1 | 171 |
| Figure 6.8 | A plot of BT against % unreactives for chars from Port 1 | 171 |
| Figure 6.9 | A plot of ACA5 against % unreactives for chars from Port 1 | 172 |
| Figure 6.10 | A plot of ACA5 against percentage of particles above 150 μ m for chars from Port 1 | 173 |
| Figure 6.11 | A plot of unburnt combustible against percentage of particles above 150 μ m for Thoresby chars from Ports 2 and 3 | 175 |
| Figure 6.12 | A plot of unburnt combustible against % unreactives for Thoresby chars from Ports 2 and 3 | 175 |
| Figure 6.13 | Comparison of Malvern size parameter for Thoresby chars from Port 2 | 177 |
| Figure 6.14 | DTA burning profiles for Thoresby chars from Port 2 | 180 |
| Figure 6.15 | DTA burning profiles for Thoresby chars from Port 3 | 181 |

| | | |
|-------------|--|-----|
| Figure 6.16 | DTA burning profiles for Carbocol chars from Port 2 | 182 |
| Figure 6.17 | DTA burning profiles for Carbocol chars from Port 3 | 183 |
| Figure 6.18 | PT and BT data as a function of the percentage of particles above 150 μ m for Thoresby chars from Ports 2 and 3 | 184 |
| Figure 6.19 | PT and BT data as a function of the percentage of particles above 150 μ m for Carbocol chars from Ports 2 and 3 | 184 |

LIST OF TABLES

CHAPTER 2

| | | |
|-----------|---|----|
| Table 2.1 | The ASTM coal classification system | 11 |
| Table 2.2 | Microlithotypes and inorganic associations of coal | 18 |
| Table 2.3 | Colombia coal reserves | 21 |
| Table 2.4 | Quality of Colombian coals from La Guajira and Cesar counties | 23 |
| Table 2.5 | Venezuela coal reserves | 24 |
| Table 2.6 | Quality of coal from Paso Diablo – Guasare basin | 25 |
| Table 2.7 | Char morphology classification | 31 |

CHAPTER 4

| | | |
|------------|---|----|
| Table 4.1 | Proximate and elemental analyses for the three coals | 69 |
| Table 4.2 | Petrographic and image analyses for the six coal fractions | 69 |
| Table 4.3 | Ash content of coals and chars | 72 |
| Table 4.4 | Char yield and collection efficiency data for the three coals | 72 |
| Table 4.5 | Proximate and DTF volatiles and R Factor data for the three coals and chars | 75 |
| Table 4.6 | Intrinsic reactivity data of chars as a function of temperature and particle size | 77 |
| Table 4.7 | Manual char analysis for the samples at 1000°C | 80 |
| Table 4.8 | Manual char analysis for the samples at 1150°C | 80 |
| Table 4.9 | Manual char analysis for the samples at 1300°C | 80 |
| Table 4.10 | Proximate analysis data for the coal fractions | 84 |
| Table 4.11 | Ultimate analysis data for the coal fractions | 86 |
| Table 4.12 | Petrographic Analysis of the coal fractions | 87 |
| Table 4.13 | Ash content of coal and chars | 90 |
| Table 4.14 | Char yield and collection efficiency results | 91 |

| | | |
|------------|--|-----|
| Table 4.15 | Proximate and DTF volatiles and R factor data for the ten coals and chars | 93 |
| Table 4.16 | Char intrinsic reactivity data as a function of temperature and particle size | 94 |
| Table 4.17 | Manual char analysis results for the samples at 1000°C | 100 |
| Table 4.18 | Manual char analysis results for the samples at 1150°C | 101 |
| Table 4.19 | Manual char analysis results for the samples at 1300°C | 102 |
| Table 4.20 | Summary of manual char analysis at the three DTF temperatures | 103 |
| Table 4.21 | Automatic char analysis data as a function of DTF temperature | 104 |
| Table 4.22 | Percentage of material at different grey scale bands on grey scale histograms of the coals | 113 |
| Table 4.23 | Coefficients of determination and F values results from the regressions of char properties and DTF volatiles with coal characteristics | 114 |

CHAPTER 5

| | | |
|-----------|---|-----|
| Table 5.1 | Proximate analysis data for the coal fractions | 116 |
| Table 5.2 | Ultimate analysis data for the coal fractions | 117 |
| Table 5.3 | Petrographic Analysis of the coal fractions | 119 |
| Table 5.4 | Ash content of coal fractions and pyrolysed and re-fired chars | 122 |
| Table 5.5 | Char yield and collection efficiency for the pyrolysed and re-fired chars | 123 |
| Table 5.6 | Proximate and DTF volatiles and R factor data for the coals and the pyrolysed chars | 124 |
| Table 5.7 | Intrinsic reactivity data for the pyrolysed chars as a function of particle size | 127 |
| Table 5.8 | Manual and automatic char analysis results | 131 |
| Table 5.9 | Summary of the manual char analysis results | 132 |

| | | |
|------------|---|-----|
| Table 5.10 | Percentage of coal material at different grey scale bands | 133 |
| Table 5.11 | Correlation coefficients and F values results from the regressions of the pyrolysed char properties with coal characteristics | 135 |
| Table 5.12 | Unburnt combustible and burnout results for the re-fired chars | 138 |
| Table 5.13 | Char intrinsic reactivity data as a function of temperature and particle size | 143 |
| Table 5.14 | External appearance of pyrolysed and re-fired chars, fraction II | 146 |
| Table 5.15 | Correlation coefficients and F Values results from the regressions of char properties with coal characteristics | 154 |

CHAPTER 6

| | | |
|-----------|--|-----|
| Table 6.1 | Size distribution specifications for combustion tests | 157 |
| Table 6.2 | Summary of results of the grinding and blending | 158 |
| Table 6.3 | Proximate analysis data for the coal grinds | 160 |
| Table 6.4 | Ultimate analysis data for the coal grinds | 160 |
| Table 6.5 | Petrographic Analysis of the coal grinds | 161 |
| Table 6.6 | Intrinsic reactivity data for the chars obtained at Port 1 | 167 |
| Table 6.7 | Automatic char analysis data for the char from Port 1 | 172 |
| Table 6.8 | Loss-on-ignition and unburnt combustible data for chars from Ports 2 and 3 | 174 |
| Table 6.9 | Intrinsic reactivity data for the chars from Ports 2 and 3 | 179 |

ABSTRACT

On an international basis, coal is used extensively for power generation and this is likely to remain the case well into this century. Although many standard tests are currently used to assess and select coals for combustion purposes, these have proven to be unable to predict coal burnout behaviour. For a power station based on coal combustion, a clear knowledge and understanding of the coals offered in the market is essential to achieve optimum conversions and to meet environmental constraints. There is, therefore, a need to develop suitable and efficient methods and techniques to characterise coals so that the combustion plant performance can be predicted more effectively.

In the present work, a series of experiments were conducted to characterise chars obtained from a Drop Tube Furnace (DTF) and a 1 MW combustion rig from which the effect of particle size distribution on coal reactions during devolatilisation and combustion of pulverised coal have been studied. The effect of temperature on coal pyrolysis in the DTF was also assessed. The coals used in this study were mainly from South America whose coals are widely traded internationally, and were characterised by standard tests and a novel automated image analysis technique called the Reactivity Assessment Program (RAP). The morphology of the chars were examined manually and using an automated image analysis technique and thermogravimetric analysis.

The aim of this study was to provide a better understanding of the RAP and the automatic image analysis of chars, particularly related to South American coals. The results indicated that temperature significantly influences the coal behaviour during devolatilisation, and hence, the reactivity and morphology of the char generated. The structure and morphology of the char were found to play a significant role in burnout of the residual char, with a significant effect of coal type and particle size.

Multiple linear regressions of char properties, such as intrinsic reactivity,

morphology, and burnout, against particle size and maceral content of the feed coal were performed. The results showed that there was only a good correlation of high temperature volatiles with macerals. Subsequently when rank was included in the regressions, the correlation remarkably improved in all cases. However, when a novel approach which involved the correlations of char properties with bands of the grey scale histogram (RAP profile) of the coals was performed, much better correlations were achieved. The initial improvement is related, evidently, to the inclusion of the variation of vitrinite structure with rank. The grey scale histogram of coal takes this stage further by including the variation in reflectance for all the macerals. Therefore, the results indicate that the RAP analysis provides a simple and objective technique to predict the combustion behaviour of coals.

CHAPTER 1 INTRODUCTION

1.1 The Origins of Coal

Coal is the altered remains of prehistoric vegetation that originally accumulated as plant material in swamps or river deltas. With burial, caused by movements of the earth's crust, the plant material underwent physical and chemical changes and was further transformed into coal. Since coal-forming plant growth has occurred throughout the last 400 million years, a wide variety of coal types exist corresponding to various stages of coalification. Initially, the peat, the precursor of coal, was converted into *lignite* or *brown coal* (coals with low organic maturity). Over many more millions of years, additional changes in the lignite progressively increased its maturity and transformed it into the range known as *sub-bituminous* coals. As this process continued, these coals became harder and more mature, at which point they are classified as *bituminous* or *hard coals*. Under the right conditions, the progressive increase in the organic maturity continued ultimately to form *anthracite* (World Coal Institute, 2000).

The degree of coalification undergone by a coal, as it matures from peat to anthracite, has a remarkable effect on its physical and chemical properties, and is referred to as the *rank* of the coal. Low rank coals, such as lignite and sub-bituminous coals, are typically softer, friable materials with a dull, earthy appearance and are characterised by high moisture levels and a low carbon content, and hence a low energy content. Higher rank coals are typically harder and stronger and often have a black vitreous lustre. Increasing rank is accompanied by an increase in the carbon and energy contents and a decrease in the inherent moisture content (Smoot, 1993).

Coal is not a homogenous substance but contains various discrete entities named *macerals* (Stopes, 1935). Macerals are analogous to the minerals of inorganic rocks and are divided into three main groups known as *vitrinite*, *inertinite* and *liptinite*. Each group exhibits its own physical and chemical properties and they vary with increasing rank. There is general agreement about the origin and evolution of the different maceral groups and also about the variations in their chemical composition brought about by their distinct genesis. Despite the clear differences among these microscopic components, the behaviour of each maceral during any of the coal conversion processes is still a matter of discussion. The maceral composition of a coal can be estimated by performing a microscopic identification and this is known as *petrographic analysis*. This analysis is often carried out in order to distinguish different coals.

Efforts have been made to classify the vast number of coals into broad classification systems, and to relate similarities among other coals to their potential behaviour in coal conversion processes. The most common of these is the ASTM (American Society of Testing Materials) Classification, which is based upon fixed carbon and heating value of the coals. This is discussed in more detail in the following chapter, section 2.2.

Coal is the most abundant, safe and secure fossil fuel worldwide. It has been estimated that, in 1996, there were around one thousand billion tonnes of total coal reserves economically accessible (BP Amoco plc, 2000). These reserves are geographically spread over all continents and are currently mined in more than 50 countries. In particular, the largest reserves occur in North America, Eastern Europe and Asia. At current levels of production, coal reserves are forecast to last for over 200 years (Smoot, 1993). Some coal reserves which are not economically recoverable under present conditions may become accessible as further improvements are made in mining technology. On an international basis, coal is used for combustion for electric power generation and this is likely to remain the case well into the century.

1.2 Coal Combustion

Coal has been used as an energy source for hundreds of years. It not only made possible the changes of the industrial revolution but also promoted the electric era in the last century. Globally, coal is a competitive fuel for the generation of electricity and is at present the major energy source for power generation. Current estimates show that around 37% of global electricity is generated from coal (World Coal Institute, 2000). Additionally, significant developments continue to be made in improving utilisation efficiencies so that the energy generated per unit mass of coal may be increased. Apart from this, coal is of paramount importance in the iron and steel industry and is directly or indirectly essential for many aspects of everyday life.

Many standard tests are currently used by power stations to assess and select coal. Certain characteristics such as rank, fuel ratio, particle size, maceral content, and ash yield have been found to influence the burnout performance of coal. There has been, however, with the increasing trade of thermal coal, a growing concern that most of these properties are unable to successfully predict coal combustion behaviour. The international coal market has provided utility operators with a wider selection of coals of varying geological origins. This has led to operational problems, particularly in power stations that are accustomed to handle only local coals. In some cases, in order to assess the suitability of a coal, expensive full-scale tests are required. There is, therefore, a need to develop internationally acceptable methods for assessing coal characteristics so that the combustion plant performance can be predicted more effectively.

The maceral composition of coals, along with rank, is one of the characteristics that account for the wide range of variability in the physicochemical properties of coals. An understanding of the maceral composition of coals would therefore seem to be a useful prerequisite before utilisation of coals in the combustion process. However, there is no clear understanding about the transformation undergone by the different macerals when subjected to the conditions typical of pulverised fuel (pf) combustion. In general, liptinite and vitrinite are more

reactive and therefore burn more effectively than inertinite (Nandi et al., 1977; Smith et al., 1993). Nevertheless, this is not always the case, and although it is useful to obtain the maceral composition of a coal, there are other aspects affecting the reactivity of maceral groups such as origin and rank. As a result, maceral content may not successfully predict combustion behaviour.

The main drawback in the use of petrographic analysis in predicting combustion performance is that reactivity of the macerals can vary depending on the rank of the original coal. An image analysis technique which takes this problem into consideration has been developed at Nottingham (Cloke et al., 1997b). This analysis, known as the Reactivity Assessment Program (RAP), accounts for both maceral type and reflectance (expressed on a grey level scale) of the whole coal, and assumes that macerals with the same reflectance have the same reactivity. Because the effects of rank of all the macerals is taken into account it should be possible to assign a grey level threshold and divide the macerals into reactive and unreactive fractions. This technique has been proven to successfully predict the burnout potential of coals from different origins (Cloke et al., 1997a & b). The RAP technique has been used in this project to assess the behaviour of some South American coals during pyrolysis and burnout.

1.3 Char Formation and Characterisation

Char formation and burnout are typically studied at a laboratory scale to address a wide variety of combustion concerns ranging from char reactivity and morphology to environmental aspects such as pollution control and ash deposition. Drop Tube Furnace (DTF) and other small-scale furnace systems are widely used for this purpose. These systems are capable of reproducing high heating rates, high reaction temperatures, and atmospheres similar to those found during combustion in full-scale boilers. Among the different methods of burning coal in power station boilers, only pulverised fuel combustion is considered in this research. A DTF and a 1MW Combustion Test Facility were the main combustion apparatus used in this work to produce partially combusted chars.

The structure and reactivity of the resultant char are largely consequences of the pyrolysis behaviour of the parent coal. It is generally agreed that intrinsic char reactivity decreases with increasing coal rank, particle size, density of the char, and content of 'unreactive' maceral forms in the char (Carpenter & Skorupska, 1993). The nature and structure of the char formed vary with coal rank and type, particle size, and operating conditions, such as final temperature, heating rate and residence time. Similarly, the plastic properties of the different coal macerals and their degree of association will determine the morphology of chars, i.e., increased diameter due to swelling, sphericity, and thickness of walls (Alvarez et al., 1998). These properties could have a major influence on the efficiency with which a char will be combusted. The reactivity of the char is an important consideration in relation to aspects such as incomplete combustion leading to carbon in fly ash. The extent to which loss of this unburnt coal can be minimised will significantly affect the economy of the coal combustion process.

It has been proposed that the morphological characteristics of intermediate chars which remain after pyrolysis have a greater effect on burnout characteristics in comparison with the intrinsic reactivity (Cloke et al., 1997b). The morphological features of these chars can, in turn, be related to the properties of the coal and particularly to its maceral composition. Generally speaking liptinite, and vitrinite produce porous cenospheric thin-walled chars (Skorupska et al., 1987; Bend et al., 1992). Chars generated from the pyrolysis of inertinite range from porous thick-walled chars to fused solids, depending on their reflectance, although some inertinites have been found to produce reactive chars (Vleeskens & Nandi, 1986). A maceral is deemed to be reactive if it exhibits thermoplasticity during pyrolysis and char formation, and the type of char generated has thin walls, is fused and highly porous.

Classification methods to describe the morphological features of char produced after partial combustion of coal have been developed (Jones et al., 1985; Tsai & Scaroni, 1987; Lightman & Street, 1968; Bailey et al., 1990). Study of the char types from a wide variety of coals revealed complex char structures that cannot easily be accommodated within these classification systems. The microscopic

examination involved in this analysis has proven to be highly subjective and open to large degrees of error. Once again, Lester et al. (1996a) developed an automatic technique using image analysis which allows the relative thickness of char to be measured and thus provides an indication of combustion reactivity (see chapter 3, section 3.5.3). This image analysis technique is rapid and far more objective compared with manual assessments, and, therefore, has been used to assess the majority of chars generated throughout this project.

1.4 Aims of the Project

Fundamental understanding of the effect of operating conditions and coal properties on the coal reaction behaviour is essential for the development of advanced clean coal technologies. In the present work, a series of experiments were conducted to characterise chars obtained from a DTF from which the effect of temperature and particle size on coal reactions during devolatilisation and combustion have been studied. The coals selected for these experiments are mostly from South America, mainly from Colombia and Venezuela, and were chosen owing to their availability, their reasonable combustion potential, and their actual or future potential marketing as thermal coals. The coals were characterised by using standard methods, petrographic analysis, and, more importantly, the Reactivity Assessment Program. The morphological nature and the intrinsic reactivity of the remaining chars were investigated by means of image analysis and thermo-gravimetric analysis respectively.

Coal combustion is hardly ever completed in practical pf combustion systems and a small proportion of the fuel is emitted from the boiler as partially burnt char. The economy of the combustion process depends heavily on the extent to which this loss of unburnt coal can be minimised. Another study was undertaken in the DTF to investigate coal properties which have an impact on burnout, and whether they are relevant in predicting coal combustion behaviour. For this purpose, various coals from South America were re-fired in the DTF over a range of residence times in order to provide a relative comparison of the combustion rates of each coal. Three size fractions for each coal were used in order to evaluate the

effect of particle size in the re-firing process. Correlations are drawn between predicted and actual burnout characteristics with maceral composition, rank and reflectance (grey level) of the macerals as determined from the RAP.

The required performance of pulverised fuel milling plants has been largely based on the best practically attainable fineness from conventional equipment. This does not necessarily produce the optimal particle size distribution for a particular coal. By taking into consideration the potential improvements in mill product quality available through new classification technologies, a recent study in a 1MW Combustion Test Facility (CTF) was carried out by Powergen, in collaboration with Nottingham University. The primary aim of the combustion tests undertaken on the CTF was to quantify the effect of particle size distribution on combustion performance. More specifically, it was intended that the tests should assess the improvement in combustion performance that could be achieved by retrofitting commercially available “high performance” static or dynamic classifiers to existing plant. A coarse size distribution was also tested to assess the impact of poor mill maintenance. These tests were compared with baseline results from the coals ground to a specification representative of the currently accepted standard for pf fineness ($> 70\%$ by mass $< 75 \mu\text{m}$, $< 1\%$ by mass $> 300 \mu\text{m}$). A Colombian and a British coal were used and were selected to be representative of extremes in fuel characteristics experienced by coal importing utilities in Europe.

CHAPTER 2 LITERATURE REVIEW

The following review firstly surveys the origins and formation of coal and provides information regarding its petrographic composition and classification. Secondly, a brief summary of the geology and occurrences of South American coals is presented with particular emphasis on Colombian and Venezuelan coals. Thirdly, it considers the coal combustion process including its different stages of pyrolysis and devolatilisation, and char formation and burnout. Finally, the influence of coal properties and experimental conditions on this process is also addressed. It is anticipated that this review will form a comprehensive background for the following chapters.

2.1 Coal Origins and Formation

Coal, one of the most important sources of energy, has been defined from different points of view. It is deemed as a physically heterogeneous fossil fuel and chemically complex solid (Tsai, 1982; Grainger and Gibson, 1981; Osborne, 1988). It is, geologically, conceived as a rock, a sediment, a conglomerate composed primarily of fossilised plant remains named *macerals* and of inorganic crystalline minerals (Davidson, 1980; Van-Krevelen, 1993; Matthias, 1992). It is also defined as a complex colloidal system, an enigma in solid-state physics and as an intriguing object for chemical and physical analysis (Van-Krevelen, 1993). Coal is not another kind of carbon. It mainly consists of organic material containing carbon, hydrogen and oxygen, together with smaller amount of nitrogen, sulphur and some trace elements.

Many theories have been suggested in order to elucidate or explain the formation of a coal deposit. However, it is generally agreed that the organic coal material was formed from partially decomposed and subsequently metamorphosed plant debris which, under the influence of pressure and temperature, caused by

overlying sediments, movements of the earth crust and forces of erosion, underwent coalification over a period of up to several hundred million years.

During the coalification process or maturity of the coal there is a gradual increase in carbon content of fossil organic material in the plant debris as it becomes transformed from peat to lignite and then through the higher ranks of coal to anthracite. The degree of coalification is expressed as the rank of the coal. Similarly, the kind and condition of decaying vegetation; the depth; the average temperature; the degree of acidity; and the natural movement of the earths crust are determining factors of the nature, the quality and the relative position of the coal seams, and hence of the type of coal that will finally be formed.

In general terms, the plant debris consisted of trees, ferns, rushes, lycopods, and several thousand plant species that have been identified in coal beds. Similar types of plant remains may be found in all types (ranks) of coal but, of course, the relative amounts vary considerably. On this basis, it is not surprising that coal differs markedly in composition from one location to another. Indeed, pronounced differences in coals from one particular seam are not uncommon, due not only to the wide variety of plant debris that could have formed the precursor but also to the many different chemical reactions that can occur during the maturation process. These differences, which could occur at all stages, created the dissimilarities in the characteristics of the various coals.

2.2 Coal Classification

Owing to the worldwide occurrence of coal, its great diversity, and different potential applications, a great deal of effort has gone over the years into the development of systems of classification. The purpose of any of these classification systems is to group similar features together and to distinguish those that are not. Some workers (Van-Krevelen, 1993; Carpenter, 1988) have identified two kinds of classification of coals which serve different purposes: “scientific” and “commercial”. Scientific systems deal with origin, constitution and basic or fundamental properties. Commercial systems are concerned with

aspects such as market value, utilisation, technological properties and suitability for particular end uses. The majority of the classification systems of coal comprise both scientific and commercial features but either of them may be used for classification of any world coal.

Coal classification systems are based on two main chemical analyses, ultimate and proximate, which provide the percentage of the main chemical elements present in coal (carbon, hydrogen, nitrogen, oxygen, total sulphur and chlorine) and the relative amounts of moisture, volatile matter, ash and fixed carbon respectively. A number of technological properties of coal such as the calorific value, fusibility of coal ash, free swelling index and plasticity of coal, among others, have also been introduced as second classification parameters to characterise coal in different fields of utilisation.

From the different classification systems proposed so far, the ASTM (American Society for Testing of Materials) is the most commonly used. This system, as many others, is hierarchical and is based upon proximate analysis, calorific value and agglomerating tendency. Coals that exhibit a fixed carbon content greater than 69% are classified by their volatile matter and fixed carbon values. Lower rank coals are differentiated according to their calorific value. The agglomerating characteristics are used to differentiate coals of similar rank. Table 2.1 shows this classification system (ASTM D388, 1991).

Nowadays, the ECE (Economic Commission for Europe) Coal Committee is working (in close co-operation with the ICCP, the International Committee for Coal Petrology) on an international classification of coals which will cover the geological aspect of coal resources, coal mining and industrial uses.

2.3 Coal Petrography

The systematic study of coal as an organic sedimentary rock in terms of discrete microscopic constituents is the scientific discipline known as *coal petrography*. Its main goal is to look backward and attempt to understand fully how coal was

formed. Petrography is of great importance as it is known that the different petrographic constituents of coal may behave differently under various processing conditions.

Table 2.1 The ASTM Coal Classification System

| Class/Group | Fixed Carbon Limits | Volatile Matter Limits | Gross Calorific Value ^b | Agglomerating Character |
|---------------------------------|------------------------|------------------------|------------------------------------|-------------------------|
| | (% dmmf ^a) | (% dmmf) | (BTU/Lb) | |
| <i>I. Anthracitic</i> | | | | |
| 1. Meta-anthracite | >98 | <2 | ... | Non-agglomerating |
| 2. Anthracite | 92-98 | 2-8 | ... | |
| 3. Semianthracite | 86-92 | 8-14 | ... | |
| <i>I. Bituminous</i> | | | | |
| 1. Low Volatile | 78-80 | 14-22 | ... | Commonly agglomerating |
| 2. Medium Volatile | 69-78 | 22-32 | ... | |
| 3. High Volatile A | <69 | >31 | >14000 | |
| 4. High Volatile B | ... | ... | 1300-14000 | |
| 5. High Volatile C | ... | ... | 11500-15000 | |
| | | | 10500-11500 | Agglomerating |
| <i>I. Sub-bituminous</i> | | | | |
| 1. Sub-bituminous A | ... | ... | 10500-11500 | Non-agglomerating |
| 2. Sub-bituminous B | ... | ... | 9500-10500 | |
| 3. Sub-bituminous C | ... | ... | 8300-9500 | |
| <i>I. Lignitic</i> | | | | |
| 1. Lignite A | ... | ... | 6300-8300 | Non-agglomerating |
| 2. Lignite B | ... | ... | <6300 | |

^a dmmf= Dry, Mineral Matter-Free Basis; ^b Moist, Mineral Matter-Free Basis. Moist refers to coal containing its natural moisture but not including visible water on the surface of the coal.

2.3.1 Coal Macerals

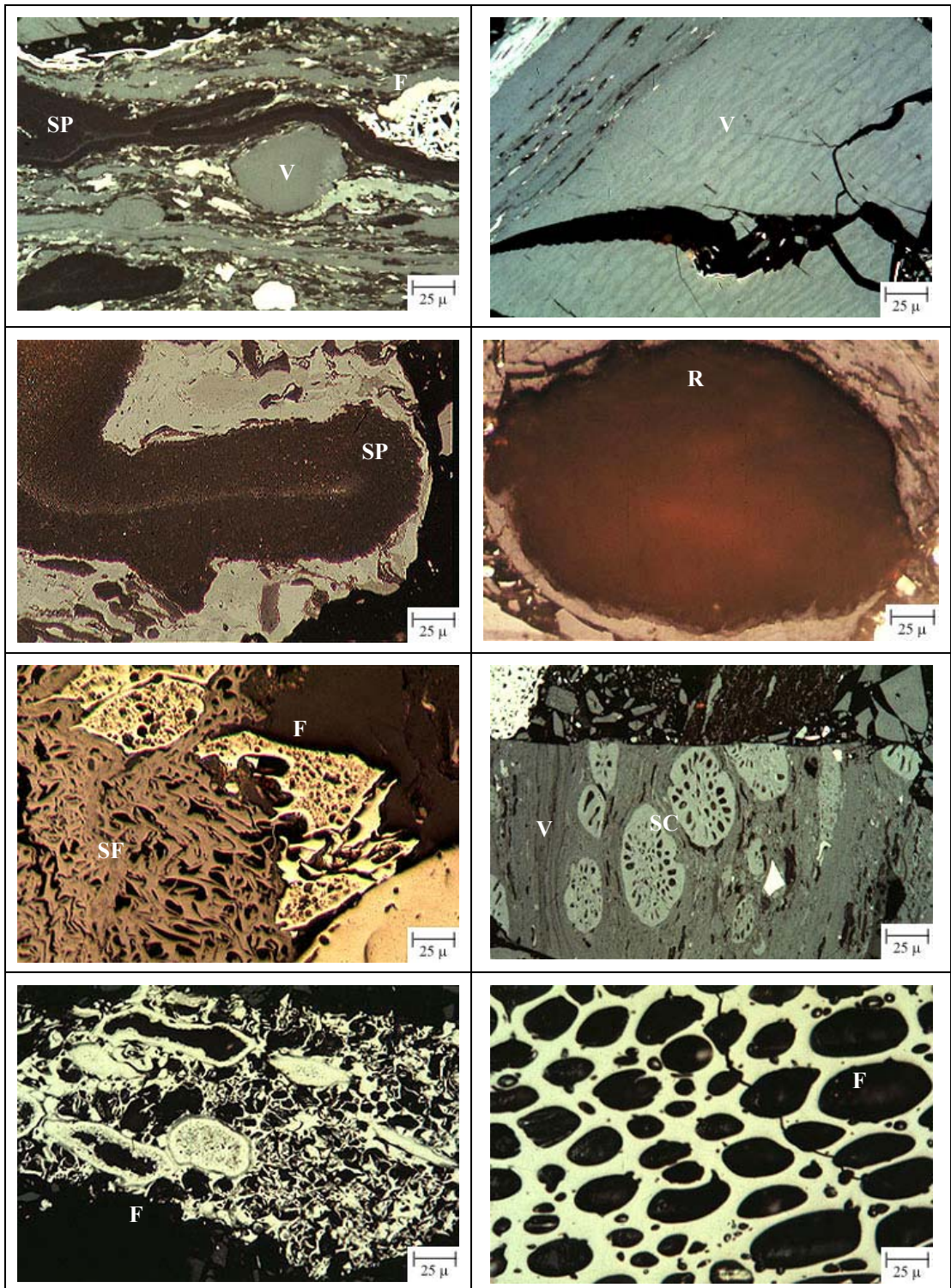
Coal is not a homogenous substance, but contains various discrete organic constituents, named *macerals* by Stopes (1935) to correspond to the minerals of inorganic rocks. The term maceral comes from Latin and means *to soften* or *weaken*, with or without heat, or to wear away. This analogy among macerals is not a strict one; maceral groups are not crystalline. They were derived from the structure of different plant materials and in different environments during the coalification process and they were also altered to various extents by geochemical forces after burial. Consequently, each maceral has specific physical and chemical properties and they vary in composition, morphology, structure and reflectance. Nevertheless, as metamorphosis progresses, the apparent differences between the maceral groups become less evident.

Coal macerals may be divided broadly into three main maceral groups or principal petrographic components: Vitrinite (huminite in low rank coals and lignites), liptinite and inertinite. These macerals can be identified by microscopy and concentrates can be prepared. Their properties are found to be different, although the apparent differences become less evident as rank increases (Grainger and Gibson, 1981; Bustin et al., 1983). Each maceral group includes a series of sub-macerals which can be regarded as belonging together due to similar optical and chemical properties. Figure 2.1 shows some photographs in which the differing reflectances and the various structures of the three maceral groups can be observed (Crelling, 1998).

2.3.1.1 Vitrinite Group

Vitrinite is commonly the most predominant petrographic constituent of coals and the most consistent in its properties. In most coals the vitrinite content is greater than both liptinite and inertinite. Many scientific investigations of coal have, therefore, concentrated mainly on the vitrinite component, which can often be prepared in reasonable purity from large lumps of coal. (Grainger and Gibson, 1981)

Figure 2.1 The three maceral groups



V=Vitrinite, Liptinite (SP=Sporinite, R=Resinite), Inertinite (F=Fusinite, SF=Semifusinite, SC=Sclerotinite)

The vitrinite group is deemed to be derived from the cell wall material (woody tissue) of plants, which are chemically composed of polymers, cellulose and lignin. It mainly originated from trunks, branches, stems, leaves and roots. When a polished coal sample presents a quite clear picture of the structure of the woody tissue of a vitrinite particle, the maceral is called *telinite* (tela = tissue). When structureless, it is named *collinite* (derived from greek: kolla = glue). Collinite was formed when cell walls were thickened with gelatinous humus and hence it is responsible for the colloidal medium which dominates in all bright coal. The vitrinite telinite is relatively rare but the structureless vitrinitic groundmass, called *telocollinite*, is common. If broken gelified grains are mixed together or with other constituents of the vitrinite group, the maceral is called *vitrodetrinite*. Generally, identification of vitrinite macerals is difficult and confusion is possible, particularly when continuous transitions occur between vitrinite and inertinite. For practical purposes, the undifferentiated vitrinite content of a coal is usually sufficient.

Vitrinite is typically shiny and glass-like in appearance. Observed in transmitted light it is translucent and of a light or dark orange colour, whereas under reflected light it is grey to yellowish white, depending on the coal rank. In bituminous coals, the vitrinitic macerals show fissures and appear medium grey in reflected light under oil immersion under the microscope. The reflectance of vitrinite is intermediate compared with the other maceral groups and provides an excellent indication of the coal rank since it increases as coalification advances. Accordingly, the measurement of the vitrinite reflectance on a polished coal surface has been selected as the parameter to determine the rank of a coal.

2.3.1.2 Liptinite Group

The liptinite group is usually a minor component of coal. The former term *exinite* was originally used to describe the chemical-resistant exines of spores in coal. Subsequently, the designation of liptinite was incorporated in order to cover all the chemically distinct plant material other than woody tissues such as spores, cuticles, suberine, resins, waxes, fats and oil of vegetable origin. This group

formerly comprised the macerals sporinite, cutinite, resinite, alginite, suberinite and liptodetrinite which are characterised by low reflectance and by green-yellow to brown-red fluorescence. Further to this, when a coal sample is viewed under blue light, four other macerals may be identified; *fluorinite*, *bituminite*, *exsudatinite* and *chlorophyllinite*.

The outstanding petrographic feature of the liptinite group is that they all have a reflectance that is lower than the vitrinite macerals in the same coal. This group of macerals is very sensitive to advanced coalification and so they begin to disappear in coal of medium volatile rank and are absent in coals of low-volatile rank (Crelling, 1987). Liptinites are the most volatile and lightest, with a specific gravity range from 1.18 to 1.28 for bituminous coals. This maceral group also has the highest hydrogen content and contains more aliphatic groups if compared with vitrinite and inertinite of coals of the same rank (Chen and Bodily; 1985; Taulbee et al., 1989; Dyrkacz et al., 1984; Dormans et al., 1957). As far as porosity is concerned, liptinites are deemed to be the least porous, appearing as a featureless material with irregular and tubular macropores (Harris and Yust, 1976).

2.3.1.3 Inertinite Group

Inertinite comprises a group of macerals derived from plant remains similar to vitrinite. However, oxygen has usually played a stronger role during the first stage of deposition and has been incorporated into the macerals. Depending upon the extent of the oxidation process, part of the cell structure of the woody material may appear to be preserved retaining the original well-defined plant tissue structures whilst in others they are not clearly perceived. Accordingly, transitions between inertinite and vitrinite are to be expected. The most abundant inertinite macerals are *fusinite* and *semifusinite*. Fusinite usually shows well-conserved and easily recognised cellular structures. Semifusinite, on the other hand, is intermediate between fusinite and vitrinite showing tissue structures that are not always easy to recognise and its reflectance is lower than that of fusinite.

Compared with the other macerals in coal, inertinite has the highest carbon and oxygen content, is the densest, and is the least volatile with lowest H/C ratio (Stach et al., 1982). Generally, Inertinites have a higher reflectance than that of vitrinites, although the differences become less evidence with increasing rank. Fusinite is always the highest reflecting inertinite maceral and is distinguished by cell-texture. It is normally broken into small shards and fragments. Semifusinite has the largest range of reflectance among the coal macerals going from the upper end of the vitrinite range to fusinite. Semifusinite is normally the most abundant of the inertinite submacerals.

2.3.2 Coal Lithotypes

An important contribution that can be made by petrographic analysis is to add to the understanding of the effect that the maceral composition has on the behaviour of coal in most of the technological processes of utilisation. The way in which macerals are distributed and associated with each other is also significant in determining the behaviour of coal during utilisation. These associations of macerals, at the macroscopic level, lead to the formation of particular layers named *lithotypes*.

Coal lithotypes represent the macrostructure of coal and are, in fact, descriptive of the coal. A piece of coal usually shows a distinctive banded appearance that may not only be due to the deposition of different organic substances, but also to the accumulation of debris of diverse plants and their different parts during the formation of the organic sediment. Two distinct bands can be conveniently recognised by their general appearance as bright or dull. The bright bands are deemed to result from the main structural portions of plants: wood or cortex, whereas, the dull bands are considered to originate from a variety of plant debris such as cellular tissue, leaves, spores, pollen grains, cuticle, and other amorphous materials.

The complexity of coal maceral associations observed in further macroscopic examinations of coal lead workers to classify them in terms of four

macroscopically different bands. Thus, bright coal has been further subdivided into *vitrain* and *clarain* whilst the dull coals are subdivided into *fusain* and *durain*. Each of these lithotypes has definite individual features which are summarised below (Kural, 1994; Van-Krevelen, 1993).

Vitrain. Occurs as precise narrow bands usually not greater than 0.5 inches thick. It appears as uniform and vitreous bright layers showing orthogonal cracks which easily produce angular grains.

Clarain. Occurs in bands that are horizontal to the bedding plane and of variable thickness. It appears less vitreous and less bright than vitrain bands.

Durain. Appears as bands of variable thickness which may be parallel to the bedding plane and which may have bands of clarain intercalated between its own bands. Durain shows dull and hard layers with a close and firm texture.

Fusain. This lithotype occurs primarily as patches that are parallel to the bedding plane. It consists of fibrous and soft layers which can be easily fractured and separated from a coal lump.

2.3.3 Coal Microlithotypes

At the microscopic level, the associations of coal macerals are named *microlithotypes*. They have been classified into three main groups: *monomaceral*, *bimaceral* and *trimaceral* according to whether a microlithotype contains one, two or three maceral groups. The monomaceral microlithotypes “*vitrite*”, “*liptite*” or “*fusite*” must contain not less than 95% vitrinite, liptinite or inertinite and not more than 5% other maceral groups, respectively. The bimaceral and trimaceral microlithotypes are subdivided into three categories according to the maceral composition as shown in Table 2.2 (Kural, 1994; Stach et al., 1982).

The composition of the coal microlithotypes seems to be limited by the types of organic matter present in the original coal precursor. In the case that a

considerable amount of mineral matter is present in the microlithotype to be identified, the material is referred to as “*carbominerite*”. The types of carbominerites usually recognised and the composition of mineral species present are also shown in Table 2.2.

Table 2.2 Microlithotypes and inorganic associations of coal

| Group | Name | Composition |
|----------------------|----------------------------------|----------------------------------|
| | | (vol%) |
| <i>Monomaceral</i> | Vitrite | Vitrinite (V) > 95 |
| | Liptite | Liptinite (L) > 95 |
| | Inertite | Inertinite (I) > 95 |
| <i>Bimaceral</i> | Clarite | V + L > 95 (each > 5%) |
| | Vitrinertite | V + I > 95 (each > 5%) |
| | Durite | I + L > 95 % (each > 5%) |
| <i>Trimaceral</i> | Duroclarite | V > I, L (each > 5%) |
| | Trimacerite Vitrinertoliptite | L > I, V (each > 5%) |
| | Clarodurite | I > V, L (each > 5%) |
| <i>Carbominerite</i> | Carbargilite | Coal + 20-60% clay minerals |
| | Carbopyrite | Coal + 5-20% sulphide minerals |
| | Carbankerite | Coal + 20-60% carbonate minerals |
| | Carbosilicite | Coal + 20-60% quartz |
| | Carbopolyminerite | Coal + 20-60% various minerals |

The chemical properties of microlithotypes are very similar to those of macerals of which they primarily consist. Their physical properties are not only related to those of the macerals but also to the combined effect of their associations.

2.4 South American Coals

2.4.1 Coal Occurrences and Geology

The South American continent has abundant energy resource potential. Coal and peat deposits have been found in all countries although available estimates of the amount of coal and peat present have been based on inadequate and, sometimes, unreliable information. The range of physical and chemical characteristics of coal and peat is undefined in most reported resource areas. However, the resource potential for the use of coal and peat as energy sources is large. A better understanding of the quality and quantity of these resources is required for planning and efficient utilisation in an environmentally acceptable manner.

The age of South American coal deposits ranges from Late Mississippian (Lower Carboniferous) to Quaternary, although the deposits are mainly of the Tertiary and Cretaceous periods (Weaver and Wood, 1994). Some of the age determinations of these coals have been based on investigations of the fossil flora in the coal beds or in immediately adjacent strata and of the fossil fauna in adjacent terrestrial and marine rocks. Most of South America's coal-bearing rocks are concealed from view by thick jungle and associated soils; younger volcanic rocks; non-coal-bearing Tertiary and Quaternary valley fill adjacent to mountain ranges and complex structural features within barely accessible high mountain ranges. These factors have made it extremely difficult for geologists and explorers, who have mostly worked without the aid of adequate maps, to find and evaluate the coal potential of South America.

The oldest known coal beds, from the Late Mississippian period, are located in Brazil and Peru. They are reportedly thin and none have ever been mined. Coal beds of Pennsylvanian and Permian age are known in Brazil, Argentina and Peru, and they are of particular economic value to Brazil. Coal beds of Triassic age are rare in South America, and they are only in north-western Argentina and northern Chile. Jurassic coal deposits are generally of small lateral extent and are found only in Argentina and Peru. In these two countries and in Colombia, coal beds of

Cretaceous age have been identified. They are concentrated in the intermontane valleys of the Andes. Tertiary coal fields and occurrences comprise approximately one-half of all coal deposits of all ages in South America. The extent of Tertiary coal deposits is several times greater than the extent of all other deposits of other ages. More than 55 percent of these coal fields and occurrences are in Venezuela. Most of the estimated tonnage of Tertiary coal underlies the Amazon River drainage basin in Brazil, Peru and Colombia. The remainder of the Tertiary coal appears to be evenly distributed throughout the coal-bearing nations of the continent. Tertiary coal is not found in Paraguay and Uruguay (Weaver and Wood, 1994).

South America was part of Gondwanaland until Cretaceous times, when continental fragmentation occurred. In mid-Cretaceous times Africa and South America drifted apart and by the late Cretaceous age, the South Atlantic Ocean had formed. In late Cretaceous to Tertiary times, conditions within many intermontane basins of the evolving cordillera of northern South America were suitable for the development of coal-forming deposits (Walker, 1993). The El Cerrejon, La Jagua, and La Loma coal fields of the eastern Cordillera de Colombia and the coal fields of the neighbouring Zulia region of Venezuela are the most significant of these deposits. The geological history of Colombia and northern Venezuela is fairly complex as a result of the interactive effects of the differential movements of a number of adjacent crustal plates.

Since the significant coal deposits of South America occur in northern Colombia and Venezuela, coals from only these two countries were discussed in this study. These coals are widely traded internationally.

2.4.2 Colombian Coals

There are 36 identified coal basins in Colombia grouped into seven main coal regions (Jamieson 1985; Gomez, 1995). The export mines are located in the counties of La Guajira and Cesar, 120-350 km from Atlantic ports (Coalportal, 2000a). The coal samples examined in this work were all from these counties and

from Cordoba. In these coal zones the seams are generally thicker and less disturbed than those in the inland coal fields of Cundinamarca, Boyaca, Santander, Antioquia, and Cauca that are geared towards domestic markets for coking and thermal coal (see Table 2.3)

Colombia has proven coal reserves of 6,648 Mt, with another 2,596 Mt estimated, these being the highest figures in Latin America. This is high-grade, low-pollutant coal which is much sought after in international markets. Colombia exports 85% of total production making it one of the largest exporters in the world. Coal ranks third in the list of exports (8%) after coffee and oil (Coinvertir, 2000). The largest proportion of resources lies in the La Guajira and Cesar counties, which reflect the greater export potential of these coal fields rather than the actual distribution of coal. Thermal coals account for approximately 90% of Colombia's measured coal resources, with measured reserves of coking coal in the counties of Cundinamarca and Boyaca amounting to only 670 Mt. Measured resources of anthracite are only 18 Mt and are confined to the county of Santander.

Table 2.3 Colombia coal reserves

| County | Measured Reserves | Indicated Reserves | Coal Type |
|----------------------------------|-------------------|--------------------|----------------|
| | (Mt) | (Mt) | |
| <i>Guajira</i> | 3,670 | - | Thermal |
| <i>Cesar</i> | 1,933 | 589 | Thermal |
| <i>Cundinamarca and Boyaca</i> | 412 | 1,221 | Thermal/Coking |
| <i>Cordoba</i> | 381 | 257 | Thermal |
| <i>Antioquia</i> | 90 | 225 | Thermal |
| <i>North Santander</i> | 68 | 101 | Thermal/Coking |
| <i>Santander</i> | 57 | 114 | Thermal/Coking |
| <i>Valle del Cauca and Cauca</i> | 37 | 89 | Thermal |
| Total | 6,648 | 2,596 | Thermal/Coking |

The Cesar coal zone has four important coal fields: Boquerón, El Descanso, La Jagua and La Loma (Gomez, 1995). La Loma and La Jagua deposits are near the towns of the same name. In the Cordoba county the Alto San Jorge-San Pedro is the main coal basin and consists of two major fields: Alto San Jorge, in the west, and San Pedro, in the east. The coal sample Bijao, which was used in this study, came from the San Pedro coal field.

The El Cerrejon deposit, located in La Guajira county, north-eastern Colombia, extends for some 50 km from north to south and is up to 5 km wide. Substantial resources of coal occur close to surface (Walker, 1993). Development of Colombian coal for export has centred on the El Cerrejon deposits from which the first shipments of 1Mt were made in 1984. Colombia had entered the international coal export market and by 1987 shipments had grown to about 9.6 Mt. A completely new infrastructure was required for the project, including transport and port facilities, which were installed with the aim of being able to handle increasing tonnages of export coal. El Cerrejon is now claimed to be the largest export mine in the world with 1998 sales of 18.7 Mt (Ecocarbon, 1998). The main market for this coal has been Germany, Holland, Denmark, North America and the United Kingdom.

The Cerrejon deposit is divided into three blocks, North, Central and South. The North block covers an area of 380 km² with about 55 seams and contains high-volatile B bituminous rank coal according to the ASTM coal classification system. The Central block extends over 100 km² with 38 seams. This block also contains high-volatile B bituminous rank coal at surface mineable depth. The South block covers an area of 200 km² with at least 15 seams. It is the least explored of the three blocks (Walker, 1993). The coal sample Carbocol comes from the North block, Prodeco and Caypa comes from the Central Block and Oreganal from the South Block.

As coal from El Cerrejon, coals from Cordoba and Cesar are of bituminous rank, ranging from bituminous A through C. These coals generally have low ash and

sulphur contents and have been found to exhibit no coking properties (Gomez, 1995). A summary of the properties of the coals from La Guajira and Cesar region is presented in Table 2.4 (Walker, 1993, International Coal Report, 1991, Gomez, 1995).

The two mines in Colombia that currently have access to modern transportation systems and ports have a major cost advantage over all other mines. Output from these mines is expected to double within the next 10 years, growing from 35.7 Mt in 2000 to 70.5 Mt in 2010 (Fossil Energy International, 2001)

Table 2.4 Quality of Colombian coals from La Guajira and Cesar counties

| Coal Property | La Guajira –El Cerrejon | | | Cesar | |
|------------------------------|-------------------------|-----------|-------|-----------|-----------|
| | North | Central | South | La Jagua | La Loma |
| <i>Heating Value</i> (MJ/Kg) | 26.9-28.5 | 27.4-28.4 | 28.2 | 23.1-31.2 | 32.1-32.2 |
| <i>Moisture</i> (wt%) | 8.3-10.3 | 10.0-12.0 | 11.0 | 11.8 | 10.3-14.3 |
| <i>Volatiles</i> (wt%) | 31.5-36.5 | 35.0-37.0 | 36.6 | 33.6-40.0 | 41.8-43.5 |
| <i>Ash</i> (wt%) | 5.5-11.5 | 5.0-7.0 | 4.5 | 0.6-5.1 | 1.4-6.2 |
| <i>Sulphur</i> (wt%) | 0.4-0.8 | 0.6-0.8 | 0.5 | 0.4-0.8 | 0.3-0.8 |

2.4.3 Venezuelan Coals

Venezuelan coal resources were discovered in the early 19th century, but it was not until 1988 that the coal industry began to play a role in international markets (Vasquez, 1991). Venezuela possesses the second largest inventory of coal in South America after Colombia. Total resources are estimated at 8,283 Mt, of which 6,643 occur in the Guasare Basin, in Zulia county, on the far western border of Venezuela, adjoining the Colombian Cerrejon coalfield. The Guasare coalfield is in the best position to increase Venezuela's coal exports with the Paso Diablo-Socuy Complex likely to remain the nation's largest (Coalportal, 2000b).

The major coal producing regions in the country are Zulia, Tachira and Anzoategui (see Table 2.5). Total reserves in Tachira amount to 1,541 Mt, the majority of which is best suited for coking. Production is centred near the town of Lobatera, some 12 km north of San Cristobal. However, the largest reserves are located around Santo Domingo. Anzoategui is Venezuela's third major coal region, with total reserves estimated at 133 Mt. Production is centred around two mining areas; Fila Maestra and Naricual. The Maturin coal sample also comes from this region. Coal production in Anzoategui totalled 272 Mt in 1992, most of which was exported to Europe (Corporate Information, 2001).

Table 2.5 Venezuela coal reserves

| Coalfield/County | Reserves (Mt) | | Possible Resources | Total Resources |
|---------------------------------|---------------|--------------|--------------------|-----------------|
| | Measured | Indicated | (Mt) | (Mt) |
| <i>Guasare Basin</i> | 983 | 2,060 | 3,600 | 6,643 |
| <i>Others</i> | 34 | 62 | 64 | 160 |
| <i>Zulia county</i> | 1,017 | 2,122 | 3,664 | 6,803 |
| <i>Santo Domingo</i> | 135 | 145 | 22 | 302 |
| <i>Lobatera</i> | 9 | 7 | 9 | 25 |
| <i>Las Adjuntas</i> | 30 | 61 | 184 | 275 |
| <i>Other</i> | 4 | 40 | 425 | 469 |
| <i>Tachira county</i> | 178 | 253 | 640 | 1,071 |
| <i>Naricual</i> | 117 | 23 | 19 | 159 |
| <i>Fila Maestra</i> | | 2 | 5 | 7 |
| <i>Anzoategui county</i> | 117 | 25 | 24 | 166 |
| <i>Falcon county</i> | 16 | 27 | 111 | 154 |
| <i>Others</i> | | | 89 | 89 |
| Total | 1,328 | 2,427 | 4,528 | 8,283 |

Zulia state is the most important coal-producing region in Venezuela in which the Guasare coal basin is located. Guasare has proven reserves of 353 Mt and total reserves estimated at 8,489 Mt. This coal is of bituminous rank and is an excellent quantity steam coal for electrical power generation (high heat value, low sulfur and ash). In late 1987, the first coal was produced from Paso Diablo and exported to Italy and France. Paso Diablo is Venezuela's largest coal mine. Production at Paso Diablo totalled 4 Mt in 1994, 15 percent more than in 1993. Approximately 75 percent of Guasare coal exports went to western Europe. Paso Diablo is estimated to have economically recoverable reserves of some 200 Mt. Maximum yearly production at the mine is likely to reach a level of 10 Mt in the near future. Table 2.6 shows quality information for Guasare basin coal obtained from the Paso Diablo mine (Walker, 1993).

Table 2.6 Quality of coal from Paso Diablo – Guasare basin

| Coal Property | Guasare Basin-Zulia |
|------------------------------|---------------------|
| | Paso Diablo Mine |
| <i>Heating Value</i> (MJ/Kg) | 29.4 |
| <i>Moisture</i> (wt%) | 7.0 |
| <i>Volatiles</i> (wt%) | 34.5 |
| <i>Ash</i> (wt%) | 7.5 |
| <i>Sulphur</i> (wt%) | 0.6 |

Venezuela has increased coal production by 8% between 1998 and 1999 to about 7.4 Mt per annum. Without opening new mines during 2000, the industry predicts a 20% increase in production to reach 9.0 Mt this year. The majority of coal produced is exported because there is little domestic demand for coal. The power sector has large reserves of oil, gas and hydroelectric power and consequently has no plans at this stage to invest in coal-fired power generation. Venezuelan production had lagged in previous years as a result of delays in developing export infrastructure (Coalportal, 2000b).

Venezuela's coal exports in 1999 totalled 6.9 Mt, a 16.9% increase over 1998 when exports totalled 5.9 Mt. During 2000 Paso Diablo produced about 6.5 Mt, a 23% increase on 1999 exports, which totalled 5.3 Mt. The principal coal export markets are in Europe (40%), i.e. the Netherlands, France, Germany, and Italy, where Venezuela favourably competes with American higher sulphur content coal. About 30% of the market is in the USA, and 30% in Central and South America (Coalportal, 2000b).

2.5 Coal Combustion

The combustion processes in industrial combustors occur in complex turbulent gas and solid phase flame reactors. Among the different methods of burning coal in power station boilers, only pulverised fuel combustion is considered in this research. During this process, a mixture of air and finely ground coal is introduced into the utility boiler in which most of the particles (>70%) are typically below 75 μm (Essenhigh, 1981; Carpenter and Skorupska, 1993), although, the actual particle size distribution is generally dependent on the rank of the coal (Clarke, 1988). The coal particles are subjected to temperatures between 1300 and 1700°C and rapid heating rates around 10^4 - 10^6 °C/s (Skorupska and Marsh, 1989), depending on the size of the particles.

During combustion, coal not only produces a large quantity of gaseous products of changing composition, but also a residual solid ('char') whose chemical and physical structure undergoes changes during burnout. Moreover, a large quantity of heat energy is released, transferred, and emitted from the distinctive reaction region containing hot gases, fine particles, and products of the reaction. For maximum efficiency, all the carbonaceous material of the residual char should be consumed by the oxidising atmosphere within the operational time of approximately one second (Skorupska and Marsh, 1989).

Laboratory experiments were designed to simulate the coal combustion process as closely as possible. However, since this process is extremely complex it is conveniently divided into two separate stages: rapid pyrolysis and devolatilisation

of the coal producing a solid char, followed by the relatively slow process of char combustion. These two processes, which are partly overlapping, may be the rate-determining step and may be related to both reaction conditions and properties of the coal (Laurendeau, 1978; Essenhigh, 1981; Morrison, 1986). Therefore, the performance of a particular coal in the boiler will be governed by its behaviour in each of the stages of pyrolysis and char combustion.

2.5.1 Coal Pyrolysis and Devolatilisation

Rapid heating rates have a substantial effect on the coal particles during pyrolysis, initially inducing thermal decomposition of the carbonaceous material, accompanied in many cases by swelling and followed by release of volatiles. The overall yield of substances from coal on heating includes volatile gas release (e.g. CO, CO₂, H₂, HCN and light hydrocarbons), and, at higher temperatures, heavier, high molecular weight compounds (e.g. tars, bitumens). Volatiles released during devolatilisation can account for up to 50% of the heating value of the coal (Sarofim and Beér, 1979). The rate of volatile release is important in determining the ignition characteristics of a coal flame which affects the efficiency of pollutant formation (Carpenter and Skorupska, 1993).

The extent of devolatilisation during pf combustion has a significant effect on the characteristics of the residual char. For instance, a higher volatile yield produces smaller quantities of chars with lower densities, higher porosities and significantly different pore structure (Jamaluddin, 1992). Both the volatile yield and composition during pyrolysis can be affected by the operating conditions of the process as well as the properties of the coal. These two topics are discussed below.

2.5.1.1 The Effect of Experimental Conditions

The rate and final temperature of heating during pyrolysis have been found to influence the quantity of volatiles evolved and the composition of the residual char (Solomon et al., 1986). Nevertheless, investigations have shown that it is the final

temperature which mainly determines the total yield of volatiles (Jamaluddin, 1992; Lester et al., 1994). Furthermore, the gaseous environment in which the pyrolysis takes place has also been identified as an important factor affecting devolatilisation. For example, by increasing the heating rate, McCown et al (1982) found that there was an increase in volatile yields under nitrogen atmosphere, whereas a decrease was noted when using hydrogen.

On the other hand, work on the effect of pressure revealed that an increase in pressure decreases the rate of volatiles release, reduces tar yield, and affects the quantity and type of volatile species (Lee et al., 1991). The type of product released during devolatilisation and pyrolysis from a single coal is also influenced by the geometric configuration of the experimental equipment utilised (Skorupska, 1987).

2.5.1.2 The Effect of Coal Properties

The ultimate yield of volatile matter and composition is not only affected by the experimental conditions during pyrolysis but also by coal properties such as particle size, coal rank, maceral composition and mineral matter content.

Studies involving the pyrolysis of concentrated coal macerals and coals of diverse petrographic composition indicate that the total yield of volatiles decreases in the order liptinite > vitrinite > inertinite (Howard, 1981, Stach et al., 1982). The volatiles evolved from vitrinitic coal particles generally contain a higher proportion of phenolic and aromatic compounds whereas liptinites usually yield volatiles with a higher proportion of hydrocarbons (Howard, 1981; Stach et al., 1982; Nip et al., 1987).

Volatile yield and composition also vary as a function of rank. Ultimate yields have been shown to be very similar at about 50 wt% for coals through the high-volatile bituminous rank, then decrease in higher ranked coals (Skorupska, 1987). Nevertheless, the proportion of gases and tars differ extensively with gases

governing the yields of low-ranked coals whereas tars dominate the yields of bituminous and coals of higher rank (Solomon, 1986, Smoot, 1993).

Coals of medium rank exhibit thermoplastic behaviour, and plasticise when heated. This thermoplasticity normally occurs in coals with 81-92% C, although it depends on oxygen and hydrogen content, and heating rate (Smoot, 1993). The fluid behaviour of coals becomes more apparent at high heating rates. However, cross-linking reaction temperatures can be rapidly reached, as the heating rate becomes excessively high, and hence, the thermoplastic behaviour of coals is impeded. As coal pores melt and fuse, the subsequent formation of light gas and tar vapour-filled bubbles results in swelling. Volatiles are transported via bubble formation. By contrast, high rank coals normally exhibit little fluidity and plasticity, and preserve their pore structure during devolatilisation. In this case, volatiles are transported by diffusion via pore structures (Smoot, 1993).

2.5.2 Char Formation and Morphology

Following the process of coal devolatilisation and the combustion of volatiles, the slower process (> 1 s) of char combustion occurs. The overall reaction scheme involving this process includes the diffusion of mass (reactants and products species) and heat across the char particle boundary layer (gas/solid interface), accompanied by the diffusion of mass and heat through the char particle structure and a heterogeneous gas/solid reaction (Laurendeau, 1978; Skorupska, 1987).

The rate of oxidation is deemed to be controlled by chemical kinetics, mass transport processes, or a combination of the two, depending upon the temperature under which the reactions take place, the size and the porosity of the particle undergoing oxidation (Essenhigh, 1981; Morrison, 1986; Laurendeau, 1978; Young and Smith, 1987). For instance, at low temperature ($< 1000^{\circ}\text{C}$), where the reactivity of the char is low, the rate of combustion will be controlled by chemical kinetics, reactivity of the carbon, hydrogen and other heteroatoms such as nitrogen and sulphur. As the temperature increases, the chemical reactivity

increases and oxygen pore diffusion and bulk diffusion become more important in determining the overall rate of char combustion (Bailey et al., 1990).

Experiments have shown that combustion of char is the rate-determining step in the overall combustion of pulverised fuel. While devolatilisation takes place in less than 50 ms, char combustion may take several seconds (Bailey et al., 1990). It is therefore important to consider how original coal structure, and volatile yield and composition during rapid pyrolysis have an effect on the physical and chemical structure of the char, as these properties control the overall reactivity of the char combustion reactions (Carpenter and Skorupska, 1993; Skorupska, 1987).

Classification systems for chars have been presented by various authors (Lightman and Street, 1968; Jones et al., 1985a; Young et al., 1986; Tsai and Scaroni; 1987). Studies of chars produced from a wide variety of coal ranks have revealed some complex char structures that cannot be easily accommodated within these classification systems. In 1990, Bailey et al. (1990) developed a new classification system which is based on the physical properties that determine char reactivity. The most important parameters considered in the determination of the different char types were wall thickness, porosity and basic char structure. A modified set of Bailey's char classification system was used in this work to classify the different chars obtained after pyrolysis (Table 2.7). Photographs of these char types are provided in Figures 2.2 to 2.7 (Alvarez and Lester, 2001).

2.5.3 Char Burnout and Reactivity

The structure and reactivity of the resultant char are largely consequences of the pyrolysis behaviour of the parent coal. Basically, the characteristics of the char that influence the progress of burnout are the external dimension of the particles; the volume; size and distribution of pores within the particles; the total internal surface area of the char available for reaction and the intrinsic reactivity (Bailey et al., 1990). The intrinsic reactivity of char can be defined as the rate of reaction between the oxidising gas and the internal surface, in the absence of any mass transfer or pore diffusion limitation, i.e. the rate of the chemical reaction alone (Harris and Smith, 1991). For the purpose of this work, the parameters of peak temperature (PT) and burnout temperature (BT) are used to represent intrinsic reactivity as defined by Unsworth et al. (1991). This provides a comparative

measure between different char samples. The intrinsic reactivity analysis procedure is presented in the following chapter, section 3.5.4.

Table 2.7 Char morphology classification

| Char Type | Description |
|-----------------------|--|
| <i>Tenuisphere</i> | Spherical to angular, porosity >80%, >50% of wall area <3 μ m. |
| <i>Crassisphere</i> | Spherical to angular, porosity >60%, >50% of wall area >3 μ m. |
| <i>Tenuinetwork</i> | Internal network structure, porosity >70%, >50% of wall area <3 μ m. |
| <i>Crassinetwork</i> | Char with internal network structure, porosity >40%, >50% of wall area >3 μ m or char with a fused and unfused part, porosity 40-60%. More than 25% but less than 75% unfused. |
| <i>Inertoid</i> | Dense char, porosity 5–40%, can be either fused or unfused. |
| <i>Fusinoid/Solid</i> | Inherited cellular fusinite structure or solid particle with <5% porosity. |

Figure 2.2 Tenuispheres

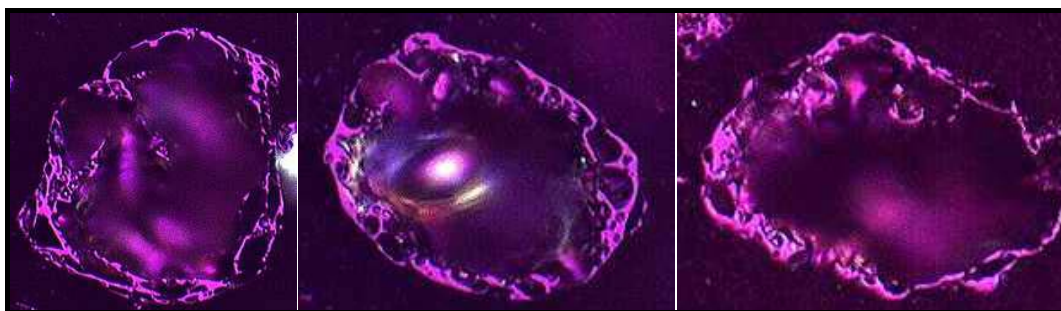


Figure 2.3 Crassispheres

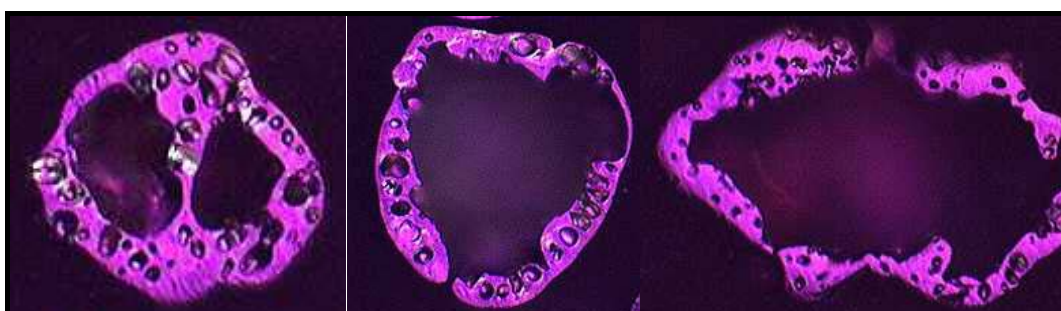


Figure 2.4 Tenuinetworks

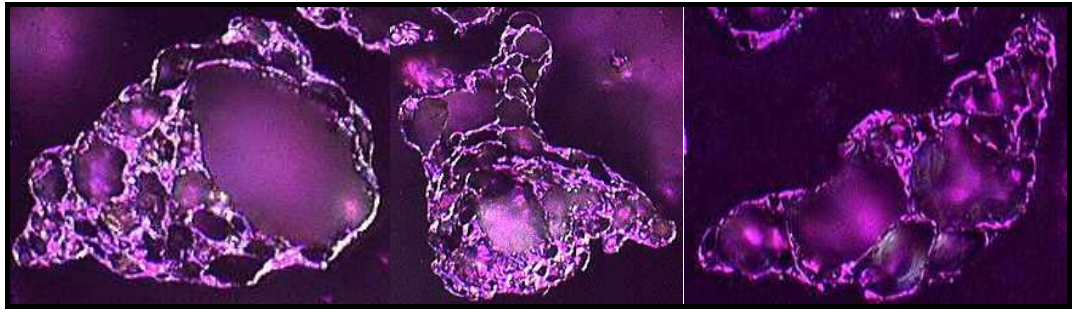


Figure 2.5 Crassinetworks

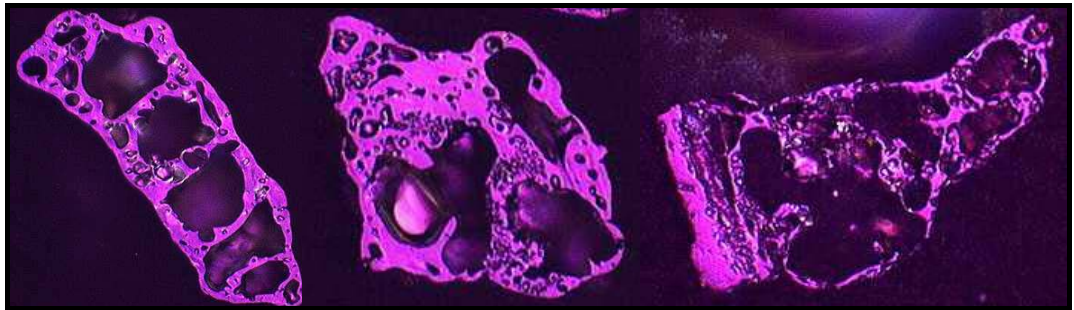


Figure 2.6 Inertoids

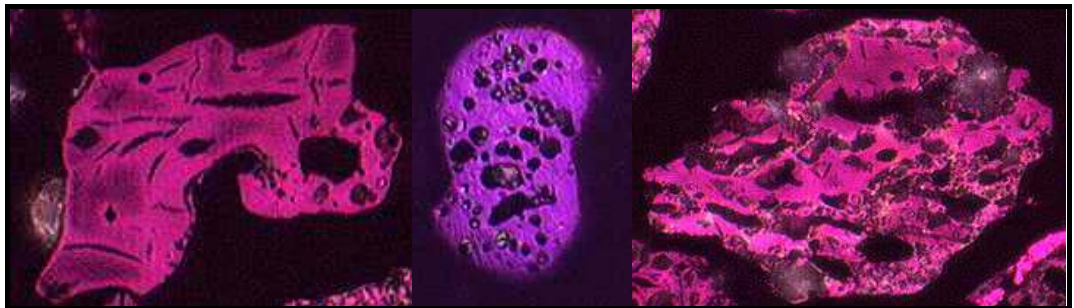
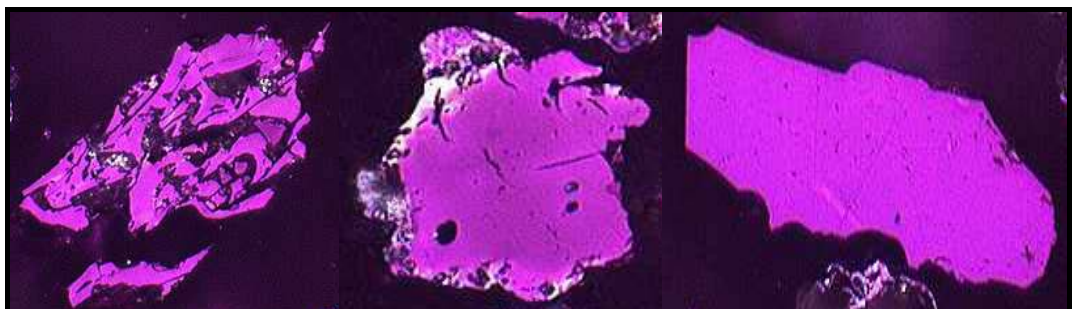


Figure 2.7 Fusinoids/Solids



It is generally agreed that intrinsic char reactivity decreases with increasing rank of the coal, anisotropy of the char material, particle size, density of the char, and content of 'unreactive' inertinite forms in the char (Carpenter and Skorupska, 1993). The nature and structure of the char vary with coal rank and type, particle size as well as operating conditions, such as final temperature, heating rate and residence time (Lester, 1994 a & b; Cloke and Lester, 1994). Similarly, the plastic properties of the different coal macerals and their degree of association will determine the morphology of chars, i.e., increased diameter due to swelling, sphericity, and thickness of walls. These properties could have a major influence on the efficiency with which a char will be combusted (Alvarez et al., 1998).

The extent of the overall coal burnout is influenced by the amount of char formed on pyrolysis and by how fast the char burns out. Burnout is dependent on the size and morphology of the chars, which determine the rate of mass transfer to and within particles, and on the chemical reactivity of chars, which determine the rate of surface reactions (Unsworth, 1991). The reactivity of the char is an important consideration in relation to aspects such as incomplete combustion leading to excessive carbon in fly ash. The extent to which loss of this unburnt coal can be minimised will significantly affect the economy of the coal combustion process.

2.5.4 Rank Effects

There is general agreement concerning the influence that rank or vitrinite reflectance has on the performance of coal in combustion (Carpenter, 1988; Essenhigh, 1981; Kopp and Harris, 1984; Steller et al., 1991; Bailey et al., 1990). Vitrinite reflectance, for instance, is found to be a good parameter to differentiate burnout performance of coal with significant differences in rank (Bailey et al., 1990). Similarly, coal rank has shown to be a major factor governing combustibility and reactivity in pulverised coal combustion (Steller et al., 1991; IEA Coal Industry Advisory Board, 1985; Milligan et al., 1997). However, other technological properties of coal, such as petrographic composition, mineral matter, and caking capacity also play a part. Correspondingly, particle size, as well as combustion conditions have a relative effect on combustion rates, so that

any attempts made to establish empirical correlations between parameters of combustion behaviour and rank, are generally valid only for coals with similar particle size at specific operating conditions (Carpenter, 1988).

Efficiency of combustion can also be related to rank. For example, work carried out by Vleeskens and Nandi (Vleeskens, 1983; Nandi et al., 1977), showed that combustion efficiency, measured as the amount of combustible material remaining, decreased with increasing rank. Nevertheless, the level of unburnt fuel is expected to vary with different experimental conditions, e.g. maximum gas temperature and oxygen concentration (Shibaoka et al., 1985). On the other hand, the reactivity of coals of similar rank have been shown to be related to differences in ash and inertinite contents (Steller et al., 1991). In some studies, these inert constituents were found to be more significant than rank in predicting coal combustion efficiency (Vleeskens and Nandi, 1986).

Experiments have shown that variations in the rank in combination with the maceral composition have an effect on the specific physical and chemical properties of chars (Crelling et al., 1988; Skorupska et al., 1989). From experiments based upon nine vitrinite-rich coals of increasing rank in an entrained flow reactor, Bend et al. (1992) found that char characteristics such as optical texture, the degree of vesiculation, porosity, surface area, and thermoplasticity are related to the molecular structure of the original vitrinite and vary as a function of rank.

It is generally agreed that char reactivity in pf combustion increases with decrease in rank (Bend et al., 1992; Morgan and Roberts, 1987; Haley et al., 1991). Accordingly, it might be expected that the lower rank fuels would be the preferred feedstock of a power station. However, these coals have lower calorific values and are less efficient as an energy source than bituminous coals. Hence, for many reasons, in order to evaluate coals for combustion, it is essential to investigate the separate effects of a classification parameter but its interpretation should be referred to the other technological properties.

2.5.5 Macerals Effects

Maceral composition has an important influence on the combustion of pulverised coal. Differences in their chemical and physical properties as well as their response to process conditions are reflected in their combustion behaviour producing differences in char yield and char morphology, i.e. different particle densities and porosity and varying chemical structure. Several studies (Lightman et al., 1968; Jones et al., 1985b; Milligan et al., 1997) have demonstrated how different macerals behave under simulated pf combustion conditions and have shown the diverse morphologies of the partially reacted char particles (Street et al., 1969; Hamilton, 1981).

Generally speaking, vitrinite and liptinite are chemically reactive during pyrolysis (Nandi et al., 1977; Milligan et al., 1997). In the case of inertinite, however, there are some points of controversy. Several workers have considered this maceral group as inert during combustion and this behaviour has been attributed to being primarily due to its aromatic nature (Milligan et al., 1997).

Part of the inertinite group, mainly low reflectance semifusinite, may also be deemed as reactive (Vleeskens and Nandi, 1986). Workers in South Africa and Australia, for instance, have emphasised the fact that, although southern hemisphere coals are highly rich in macerals of the inertinite group, the properties of this group can range from being almost inert to showing a reactivity close to that of vitrinite (Phong-Anant, 1991, Thomas et al., 1989a). This debate has led researchers to define a coal maceral in terms of its reactivity. Thus, a maceral is deemed to be reactive if it exhibits thermoplasticity during pyrolysis and char formation, and the type of char generated is referred to as fused char by several workers (Thomas et al., 1989b). Further to this, the proportion of the reactive fraction of a coal has usually been determined by combining the liptinite and vitrinite percentages with the fusible inertinite fraction of the inertinite (Thomas et al., 1989b).

The relationship between char type and petrographic composition is not a simple one (Thomas et al., 1991), and the effect of macerals on combustion reactivity is unpredictable (Milligan et al., 1997). There is also evidence to suggest that interaction between macerals may occur which affects the coal combustion process (Milligan et al., 1997; Crelling et al., 1992). The type of maceral interaction depends on rank. Therefore, in order to predict the reactivity of a coal it is necessary to have an understanding of maceral composition. The effect of individual macerals on coal pyrolysis and combustion is further examined in the following sections with particular emphasis on the inertinite group.

2.5.5.1 Vitrinite

Of the three maceral groups vitrinites exhibit greater thermal alteration and their behaviour during combustion is best understood (Shibaoka et al., 1985). The degree of oxidation or pyrolysis of a coal is related to the rank of the vitrinite content (Carpenter, 1988). Vitrinites have been found to combust at slightly higher temperatures than the other macerals, although they burn considerably faster and more intensely (Crelling et al., 1992). Although vitrinite is generally deemed to be reactive, Bengtsson (1987a) noted that pseudovitrinite behaved as relatively unreactive since a considerable amount of unburnt material in the fly ash was observed. Some workers have also identified some inertinite to be more reactive than some vitrinites (Thomas et al., 1989b; Suarez et al., 1991; Phong-Anant et al., 1989; Cai et al., 1997).

Pyrolysis of high vitrinite coals may produce vesiculated and swollen chars depending on the fluidity development and rate of volatile release. Pure vitrinite chars are mainly highly vesiculated and porous cenospheric (hollow, single chambered, thin-walled or tenui- spherical particles) (Skorupska et al., 1987; Bend et al., 1992, Thomas et al., 1989a; Lightman and Street, 1968). However, the extent of porosity development in the char is found to be highly rank dependent (Bend et al., 1992, Bailey et al., 1991; Hamilton, 1981). With decreasing rank vitrinite-rich coals generate chars that are of increasing structural complexity (Hamilton, 1981). Tenuispheres with high porosity as well as

networks have been regarded as the major chars produced from vitrinite coals of lower rank (Lightman and Street, 1968, Bailey et al., 1990), whilst higher ranked coals may give crassinetworks and crassispheres (Oka et al., 1987). Thin-walled or tenui-networks or porous mixed chars have also been produced from vitrinite-rich particles but their formation has been attributed to association of different macerals with vitrinite (Bend et al., 1989).

2.5.5.2 Liptinite

The liptinite group of macerals, which has the highest hydrogen content, volatile yield, and heating value, is regarded as the most reactive maceral group in coals of the same rank. Because of the aliphatic nature of the organic matter of the liptinite macerals, they usually decompose as volatile matter leaving a small amount of combustible remaining (Skorupska et al., 1989). Thus, liptinite promotes good ignition and burnout and, in some cases, when the coal is liptinite-rich, a low ignition temperature is expected (Tsai and Scaroni, 1987). Nevertheless, as rank increases the combustion properties become similar to those of vitrinite.

Although liptinite is deemed to be mainly reactive, interestingly, Crelling et al. (1992) found that the sporinite sub-macerals may also behave as unreactive during combustion. The results shown that although sporinite appeared very reactive initially, at temperatures above volatile ignition, it became the least reactive maceral. This conclusion was drawn after looking at the char burning profiles obtained during the study. High char burnout temperatures and the lowest maximum rate of weight loss were given by the sporinite. This behaviour was assumed to be due to its greater yield of volatile matter and low ignition temperature during pyrolysis.

According to a recent investigation (Milligan et al., 1997), some of the material evolved during pyrolysis of the liptinitic material may react with the surface of the other materials, or may enhance fluidity leading to agglomeration of particles.

2.5.5.3 *Inertinite*

It should be emphasised that by considering the inertinite group as one entity, the very different behaviour of the individual macerals within the inertinite group is very often disregarded (Thomas et al., 1989b). The different sub-macerals within this maceral group can exhibit more significant differences in chemical composition than those from the other maceral groups and, therefore, slight differences in their behaviour during combustion may be expected. This fact has increased the interest of coal researchers in assessing the behaviour of inertinite macerals during pyrolysis and combustion.

Disagreements regarding the reactivity of inertinite macerals are clear from the literature. Subdivision of the group into 'reactive' and 'unreactive' components on the basis of their reflectance values with respect to the vitrinite maceral was intended to clarify these discrepancies. Schapiro et al. (1961), for example, adopted a reflectance of 2.2% to differentiate between fusible and non-fusible inertinite. Conversely, by studying a wide variety of coals, Jones et al. (1985b) reported that there was a fairly well defined reflectance level below which inertinite became fluid during pyrolysis. This boundary was found to be coal dependent and increased with rank from 1.3% to 1.8% for coals of vitrinite random reflectance ranging from 0.5-1.2%. Furthermore, it should be highlighted that the overall reactivity of inertinite is affected not only by its chemical composition but also by its morphological properties, such as particle size, fineness of texture, specific area, pore size distribution, fluid permeability and mode of association with other macerals (Shibaoka et al., 1987).

The char particles generated from inertinite during pyrolysis depend upon the reflectance of the inertinite sub-maceral and range from solid type chars to open chars of different morphology and properties. For instance, inertinite can give crassispheres showing development of anisotropy (Tsai, 1987), unfused char with little or no porosity (Jones et al., 1985a), or vesicular and rounded particles (Goodarzi and Murchinson, 1978). Quantities of high-density chars in combustion residue can be related to petrographic properties including infusible

inertinite content and percentage of microlithotypes of high inertinite content (Bailey et al., 1990).

Although the poor combustion characteristics of a coal are sometimes attributed to a high inertinite concentration, variation of rank is also significant (Lee and Whaley, 1983). When dealing with low and medium reflectance inertinite macerals, using a laser microreactor as heating source in air, Thomas et al. (1989b) found that the produced char exhibited swelling, plasticity and fusion. This char type appears mostly as thin walled in the lower rank coals (<5 μ m thick) with few instances of unfused chars from inertinite of high reflectance. Similarly, Skoruska (1987) found that char particles obtained from the reactive inertinite macerals are mainly of irregular shape, usually elongated, with long, tight and parallel pores. Their morphologies indicate limited fluidity during pyrolysis.

By conducting experiments in both a fluidised bed and a drop tube furnace, Vleeskens and Nandi (1986) found that there was a general trend towards increasing unburnt coal during combustion with increasing inertinite content of coal. Not only high inertinite content but also oxidised vitrinite content was deemed to be responsible for this tendency. Similarly, other workers found that some inertinite-rich coals gave char particles that were predominantly of the same or smaller size than the original coal and denser (Cai et al., 1997). The morphology of these chars was described as being solid with angular edges, showing a dearth of fluidity during char formation and no development of anisotropy. From samples of broadly similar carbon content, relative reactivity of inertinite-rich chars was found to be greater than that of some vitrinitic chars (Borrego et al., 1997; Cai et al., 1997). This behaviour was assumed by Borrego et al. (1997) to be due to the disordered structure of some inertinites, although oxidised vitrinite could also have played a part.

Vleeskens and Nandi (1986) found that low reflectance semifusinite was more reactive than other inertinite macerals owing to its fluidity during combustion which leads to the formation of highly porous chars. By using a laser beam rather than conventional combustion apparatus, Shibaoka et al. (1989a) reported similar

results. High reflectance semifusinite, however, has been deemed to be one of the least reactive macerals among this group, due most likely, to its aromatic nature (Crelling et al., 1992). This specific, high reflectance sub-maceral has a lower porosity in relation to lower ranked inertinite and, therefore, it is less likely to swell and fluidise, even under high heating rates (Vleeskens and Nandi 1986).

2.5.6 Particle Size Effects

It is well known that particle size affects the behaviour of coal during combustion in different ways (Carpenter, 1988; Lester, 1994). Microscopic analysis, for instance, has shown that maceral disproportionation can occur during the grinding of pulverised coal sized fractions of inertinite-rich, low-rank bituminous coals (Jones et al., 1985a). The cause of size segregation is because of differences in grindability between macerals. In low-rank coals vitrinite is harder to grind than inertinite.

The largest particles of low-rank bituminous coals have been found to be enriched in vitrinite by 10-20% compared with the parent coal, whereas inertinite was concentrated in the smaller particles (Jones et al., 1985a). Therefore, the former coal particles have a higher volatile yield than the average for the coal and will yield less char on pyrolysis. It has been found, however, that the relative grindability of macerals can reverse at higher rank (Unsworth et al., 1991). Consequently, concentration of vitrinite in smaller size fractions would be expected for such coals. Those findings suggest that when dealing with pulverised coal the effect of maceral segregation on coal combustion must be considered rather than just the effect of particle size itself.

The particle size distribution of the pulverised coal affects burnout directly as particle lifetime increases with increasing feed coal particle size (Unsworth et al., 1991).

2.5.7 Mineral Effects

The mineral matter associated with coal includes a wide range of minerals, the most abundant forms being clay, quartz, carbonates, pyrite, marcasite and other forms of oxides. Some minerals are easily liberated by milling and can therefore be removed by beneficiation processes (Skorupska and Marsh, 1989). However, the mineral matter that is associated with the organic structure of the coal remains after beneficiation. It can be analysed and detected microscopically and by chemical analysis techniques in order to determine its effects on the whole combustion process of coal.

Depending upon the physical properties of mineral matter during pyrolysis it may alter the chemical and thermal behaviour of char, particularly when phase changes are involved (Smoot and Smith, 1985). For example, decomposition of clay hydrates, carbonates and sulphides may delay the rise in temperature of the coal particle and hence its ignition (Vleeskens and Nandi, 1986). Several studies (Solomon et al., 1986; Best et al., 1987) have shown that higher reactivity of lower rank coals/chars can be associated with the catalytic effect of minerals. The composition and amount of mineral matter can also influence the particle break-up process and hence the particle size of the char (Skorupska, 1987). A portion of the mineral matter can sometimes be emitted with the volatiles (Smoot and Smith, 1985).

Mineral matter in the form of salt can act as a catalyst and hence may affect the final reactivity of the char (Pullen, 1984), especially at low reaction temperatures (Skorupska and Marsh, 1989). The dispersion of calcium, for instance, has been shown to be one of the most important factors influencing char reactivity (Carpenter and Skorupska, 1993). The presence of calcium chloride may increase the reactivity of lignite char when the oxidation rate of char is controlled by chemical kinetics. However, when mass transport is the main process controlling the combustion rate of the char, this compound does not have any considerable effect on char reactivity (Serageldin and Pan, 1986).

CHAPTER 3 EXPERIMENTAL

3.1 Coal Sample Preparation

3.1.1 Origin of Samples

A total of thirteen coals were used in the course of this research. The samples were supplied by Powergen UK plc, Carbones del Guasare (Venezuela), and Inspectorate de Colombia and Carbones del Caribe (Colombia). Of the thirteen coals, eleven are from South America (seven from Colombia and four from Venezuela), one from North America (Ashland), and the other from the UK (Thoresby). The North American coal, as well as the British coal, were included for comparative purposes for the initial experiments in the DTF and the CTF experiments, respectively. Figure 3.1 shows the location of the South American coals. The criteria for choosing these coals include their availability, their combustion potential, and their actual or future potential marketing as thermal coals.

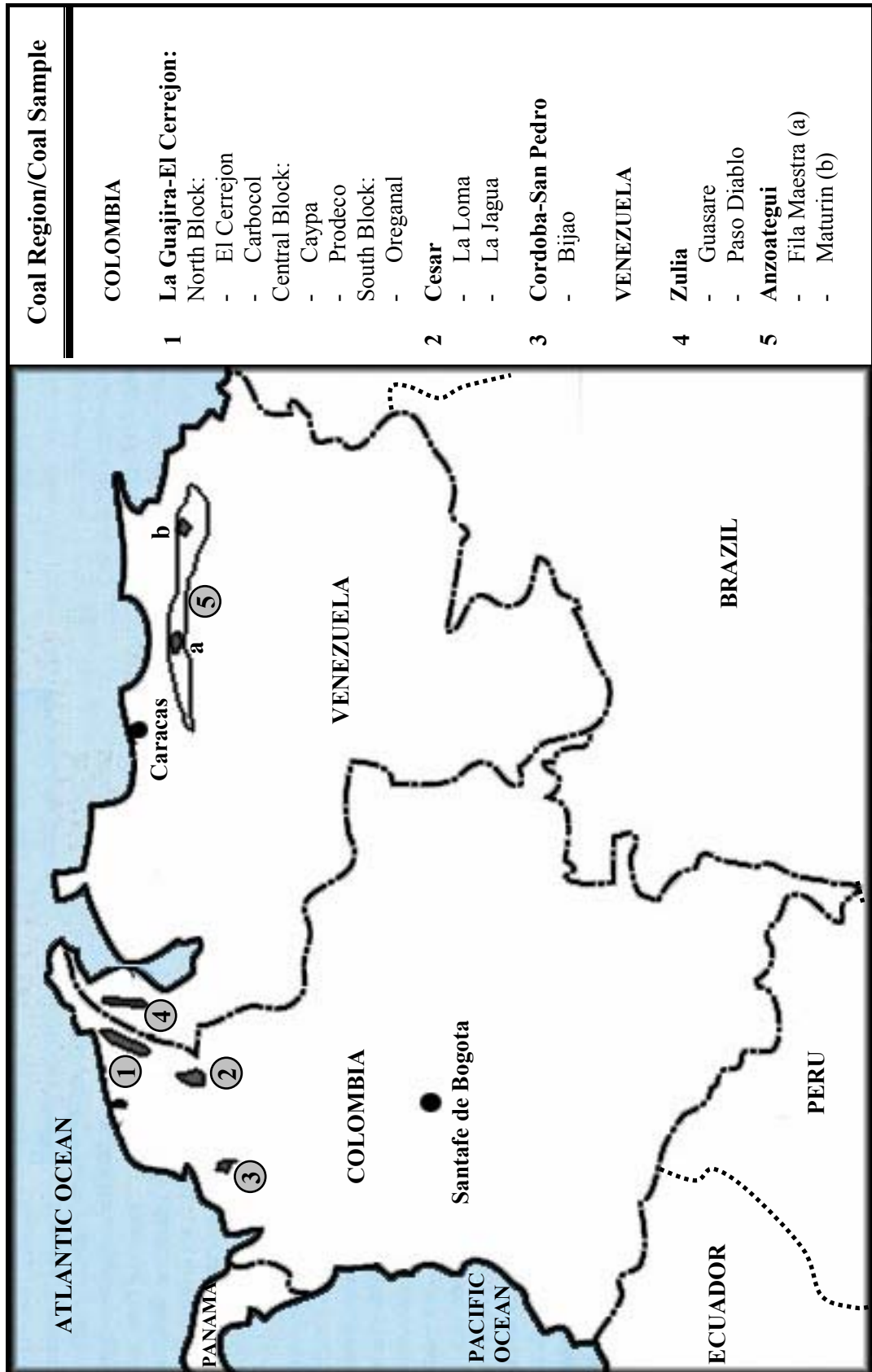
3.1.2 Screening

For the CTF experiments, coals were sourced by Powergen UK plc who arranged for contract grinding of the samples. Therefore, only the screening procedure regarding the DTF experiments will be discussed in this section.

3.1.2.1 Wet Sieving

Size fractions of 53-75 μm , 106-125 μm and 150-180 μm were produced from the pf samples of each coal by wet screening on a wet sieve cascade. The fractions were filtered in a vacuum filter device and were then air dried. The sieving procedure was performed using standard sieves conforming to British

Figure 3.1 Location of the South American coal samples used in this study



Standard 410. Those samples obtained as lumps (> 212 mm) were ground to pf size, prior to sieving, using a mechanical jaw crusher. The 53-75 μm and the 106-125 μm fractions were used for the initial experiments in the DTF, whereas all size fractions were used in the re-firing experiments.

3.1.2.2 *Alpine Jet Sieve*

An Alpine Air Jet sieve was used for further elimination of fines from the three size fractions. This equipment allows suction to be maintained on the under side of modified Endecott sieves while allowing a rotating finger to blow a thin jet air back through the sieve. This thin jet of air releases coal particles stuck on the surface of the sieve, hence agitates the sieving process and decreases the time required for a particular size range to be obtained. Figure 3.2 shows a photograph of the Alpine Air Jet sieve. Samples were stored in sealable plastic bags while not in use.

3.2 Coal Sample Characterisation

The coal fractions were characterised using standard techniques such as proximate and ultimate analysis, and maceral and rank analysis as well as image analysis and intrinsic reactivity by means of thermo-gravimetric analysis. The characterisation procedures are described in the following sub-sections.

3.2.1 Proximate Analysis

Coal fractions were analysed using a Stanton Redcroft STA 1000 thermo-gravimetric analyser (TGA) in order to determine their moisture content, volatile matter, fixed carbon and ash content. The analysis procedure developed, closely simulates the general standard method for the proximate test (British Standard 1016-104.3, 1998). The analyser is equipped with a single arm facility which allows up to 200 mg of sample to be loaded into the sample cup. Figure 3.3 shows a photograph of the TGA apparatus.

Figure 3.2 The Alpine Air Jet Sieve



Figure 3.3 The Stanton Redcroft STA 1000 thermo-gravimetric analyser



Approximately 150 mg of sample were loaded into the sample cup of the analyser. Two replicates of each fraction were analysed in order to provide an estimate of the repeatability of the analysis. Under the conditions at which the analysis was performed, this weight was found to give a repeatability of $\pm 1\%$ for the determination of ash and less than $\pm 0.8\%$ for volatiles and moisture content.

The program developed involves the heating of the sample through a sequence of ramps as follows.

- (1) Heat from ambient temperature to 120°C at $50^{\circ}\text{Cmin}^{-1}$
- (2) Hold at 120°C for 5 minutes
- (3) Heat from 120°C to 920°C at $50^{\circ}\text{Cmin}^{-1}$
- (4) Hold at 920°C for 10 minutes
- (5) Cool from 920°C to 820°C at $50^{\circ}\text{Cmin}^{-1}$
- (6) Hold at 820°C for 45 minutes

The gas supply for devolatilisation was nitrogen at a flow of 50 ccmin^{-1} . This was changed to air after devolatilisation to allow combustion char residue. A plot of weight loss and temperature against time is produced during the analysis. Figure 3.4 shows an example of this plot in which the different stages in the decomposition of the coal have been highlighted.

3.2.2 Elemental Analysis

Elemental analysis (carbon, hydrogen, nitrogen, and sulphur) of the coal fractions was carried out using a Leco 600 CHNS analyser. Approximately 100 mg of each fraction were used for the analysis. A photograph of the analyser is shown in Figure 5.

Figure 3.4 TGA curve showing proximate analysis of coal

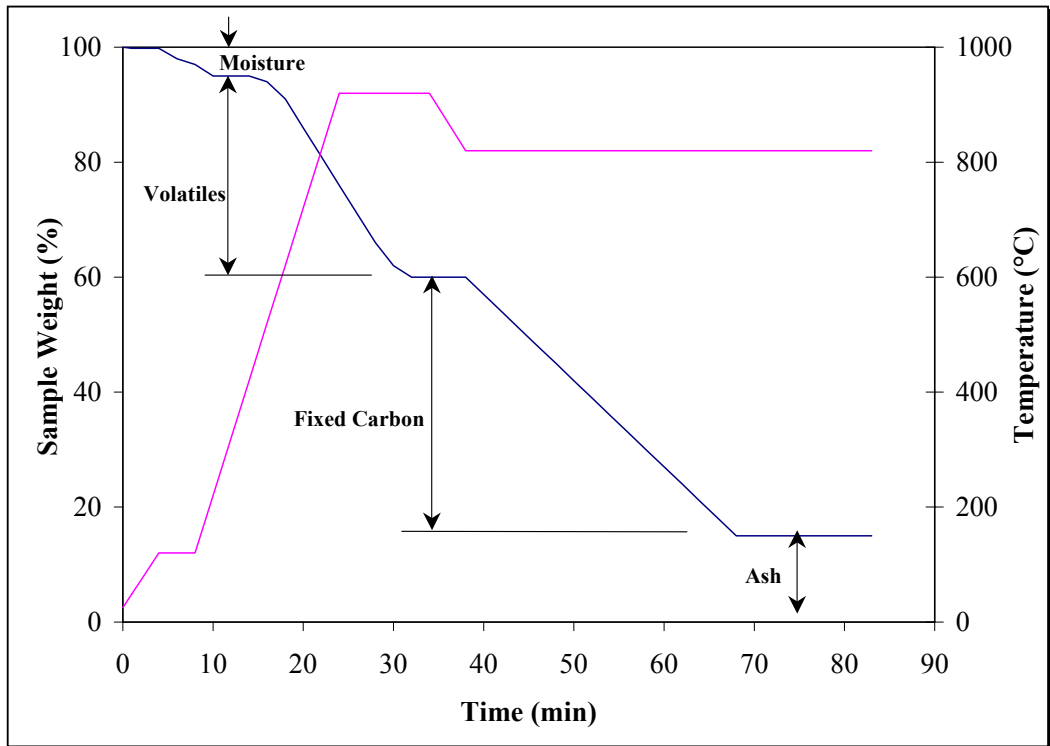


Figure 3.5 The Leco 600 CHNS analyser



3.2.3 Petrographic Characterisation

3.2.3.1 Sample Preparation

Coal blocks for point count and image analysis were produced by mounting the coal fractions in polished resin. The blocks were made by mixing a powdered dental epoxy resin called Simplex Rapid with the coal sample in a proportion of 2:5 by weight respectively. The mixture was then wetted with several drops of methyl methacrylate. The block was finally moulded by using either a Pressi Mecapress C or a Struers Prontopress-2 mounting presses (Figure 3.6). The block was subjected to a temperature of 150°C and a pressure of 250 kPa for about 15 minutes, followed by a cooling time of 3 minutes.

3.2.3.2 Polishing Procedure

For grinding and polishing the surface of the particulate block a Struers Pedemat Rotapol polisher was used (Figure 3.7). The aim was to reduce the amount of scratches on the surface of the coal block. Firstly, the surface of the block was ground using water-resistant silicon carbide paper of grit sizes 500 and 1200, for a period of one minute respectively. Then, polishing was carried out on a separate plate using one-micron alumina suspension on synthetic silk for one minute. The final polishing was performed by means of 0.04 µm colloidal silica suspension. Up to six blocks can be polished at once and each has a force of 30 N applied to it from above, via individual extendible pressure feet.

3.2.3.3 The Microscope

The microscope used for petrographic as well as image analysis of coal and char samples was a Leitz Ortholux II POL-BK. Figure 3.8 shows the microscope with a fluorescent attachment on the left hand side. For all the different analyses, a 32x magnification oil-immersion lens and non-fluorescing oil from Leitz are used. The eyepiece of the microscope has a 10x magnification lens.

Figure 3.6 The Pressi Mecapress C and Struers Prontopress-2 mounting presses



Figure 3.7 The Struers Pedemat Rotapol polisher



Figure 3.8 The Leitz Ortholux II POL-BK microscope



3.2.3.4 *Maceral Analysis*

For maceral analysis, a semi-automatic stage which was connected to a Swift point counting device was fitted to the microscope. 500 separate maceral points were counted for each analysis with stage movements of $1/3$ mm in accordance with British Standard 6127:3 (1981).

The polished coal block was placed under the lens of the microscope on the mobile stage and the maceral lying under the cross hairs of the microscope was identified. Only the three main maceral groups were recorded, with the exception of inertinite which was split into fusinite and semifusinite. The number of counts

recorded was converted automatically by the point counter to a proportion by volume of the total.

3.2.3.5 *Vitrinite Reflectance Measurements*

For the vitrinite reflectance determination, a Leitz photometer was used which was calibrated using Leitz light standards. A manual stage was fitted to the microscope, allowing the operator to move to any particular position on the block. 100 measurements of reflectance of any homogeneous and smooth vitrinite area that fell under the cross-hair was recorded. The mean value of the measurements represents the random mean vitrinite reflectance (VR_o) and is an indication of the rank of the coal sample. Two separate analyses of each sample were performed and the mean VR_o values reported.

The photometer was standardised using a glass prism light standard from Leitz with a nominal reflectivity value in oil of 1.24%. The calibration of the photometer system was subsequently verified by using a sapphire light standard with a nominal reflectance index of 0.54%. This value was closer to the mean vitrinite reflectance value of most of the coal samples. After each measurement, the standards were placed back under the lens in order to check for variations in the reference line.

3.2.4 Image Analysis

3.2.4.1 *The Image Analyser*

The system used to perform image analysis of the coal and char is called an IBAS 2000 Image Analyser manufactured by the Kontron Image Associates. The system is based on a 386 host processor connected to a hardwired image processor which captures images under the microscope via a high resolution Hamamatsu C2400-SIT black and white video camera. The on-line image from the camera may be displayed on a RGB monitor. The software for the IBAS system allows the user to interact via a keyboard, digitiser and a VGA monitor. An auto-stage

fitted under the microscope and connected to the IBAS allows a running program to move the stage automatically using the appropriate software command. Figure 3.9 shows the IBAS image analyser.

Figure 3.9 The IBAS 2000 Image Analyser



3.2.4.2 The Reactivity Assessment Program

By using the image analyser system, fifty images consisting of 512x512 pixels were captured for each coal fraction. Each pixel was then assigned a grey scale value ranging from 0 to 255 depending upon its reflectance. From the captured images, the coals were characterised using the Reactivity Assessment Program (RAP). This rapid analysis, which was developed at Nottingham by Lester (1994) and Cloke et al, (1995), makes the fundamental assumption that the behaviour of a maceral is associated primarily with its reflectance and not its type.

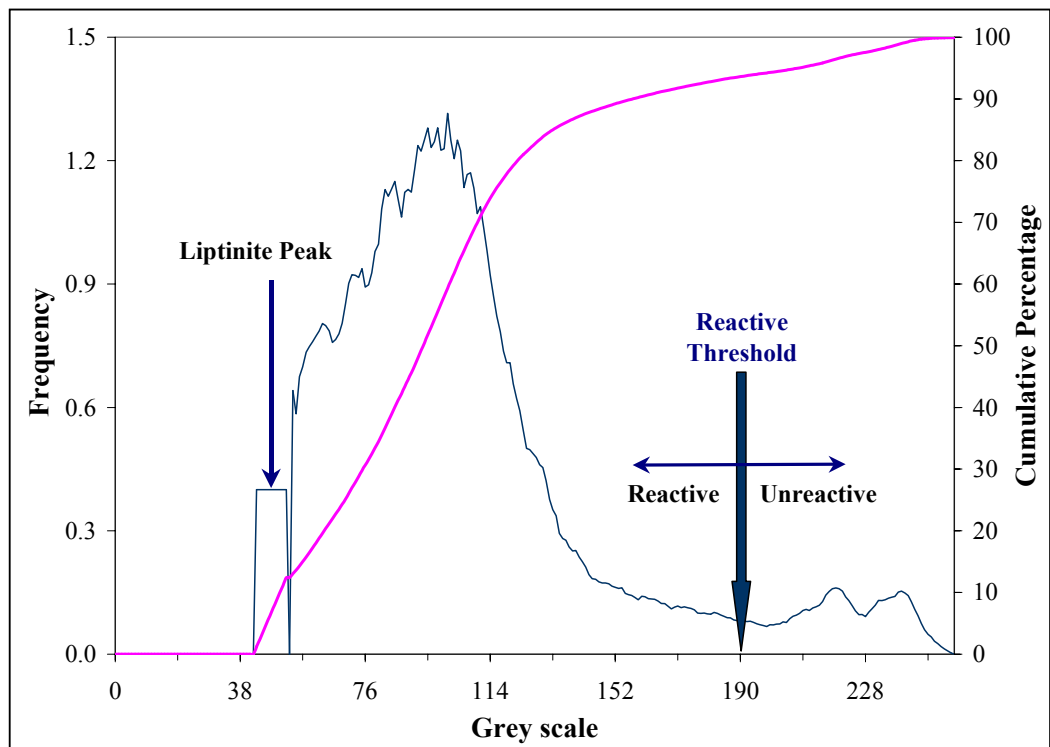
The main objective of the RAP analysis is to determine the ‘% unreactives’ i.e. the cumulative percentage of material that lies above a specific reflectance threshold. The determination of this boundary is arbitrary and it has been found to be dependent on the rank of the coal (Lester, 1994; Cloke et al., 1997a). A grey scale value of 190 have been chosen so that material above this is deemed to be

inert whilst the material below the threshold is considered reactive. This value has been determined experimentally using a wide range of world coals (Lester et al., 1995; Gilfillan, 1999). The cumulative percentage of material lying below the threshold is known as the ‘reactive number’.

As mentioned in section 3.2.3.5, a sapphire light standard was used to standardise the light levels of the camera and microscope. The captured image of the light standard also acts as a light filter, which allows each image to be corrected for light variations over the image field.

Figure 3.10 shows a typical grey scale histogram plot generated using the RAP. The histogram starts with the synthetic liptinite column at the left-hand side. The percentage of liptinite is taken from the point counting analysis for each fraction and substituted for a peak due to resin overlapping. The thicker line in the profile represents the cumulative percentage curve of the histogram over the grey scale range.

Figure 3.10 A typical reflectance histogram of coal



3.3 The Drop Tube Furnace

3.3.1 Description of Rig

A Drop Tube Furnace (DTF) system, which was developed at Powergen UK plc, was used to produce reasonable quantities of char under similar conditions to those of industrial pulverised fuel combustors at a power station. The main components of the system include a fuel feeder, a work tube and probe, ancillary equipment for gas supply and flow regulation, a product collector, a gas filter, temperature monitoring and other data measuring devices. A brief description of each of the components is given in the subsequent sub-sections. A schematic representation of the system and a photograph of the main working area of the rig are shown in Figures 3.11 and 3.12 respectively.

This particular DTF apparatus is able to achieve heating rates of the order of 10^4 to 10^5 K.s⁻¹, a maximum temperature of 1400°C, and oxygen levels can be regulated to simulate the atmosphere found during full-scale combustion. The average operating temperature is determined by changing the temperature setting of the oven. The residence time of the particles in the high temperature region of the DTF is estimated by considering, the separation between the feeder and collector probes, and the temperature and flow rate of the gas. The composition of the carrier gas can be predetermined using air and nitrogen cylinders. A cyclone device at the end of the collector probe allows the char material to be separated from any gaseous volatiles that may still remain in the carrier gas. In the DTF, a temperature of 1300°C, a residence time of 100-200 ms and a carrier gas of 1 % oxygen in nitrogen have been used to reproduce the conditions experienced by coal in the initial stage of combustion.

3.3.1.1 Gas Supply

The atmosphere for the DTF experiments is provided by high-pressure air and nitrogen cylinders using standard regulator valves. A small flow of nitrogen is

fed directly into the feeder assembly (see section 3.3.1.2). The main inlet stream to the system is monitored using an oxygen analyser to enable the desired inlet concentration to be achieved.

Figure 3.11 Schematic of the Drop Tube Furnace

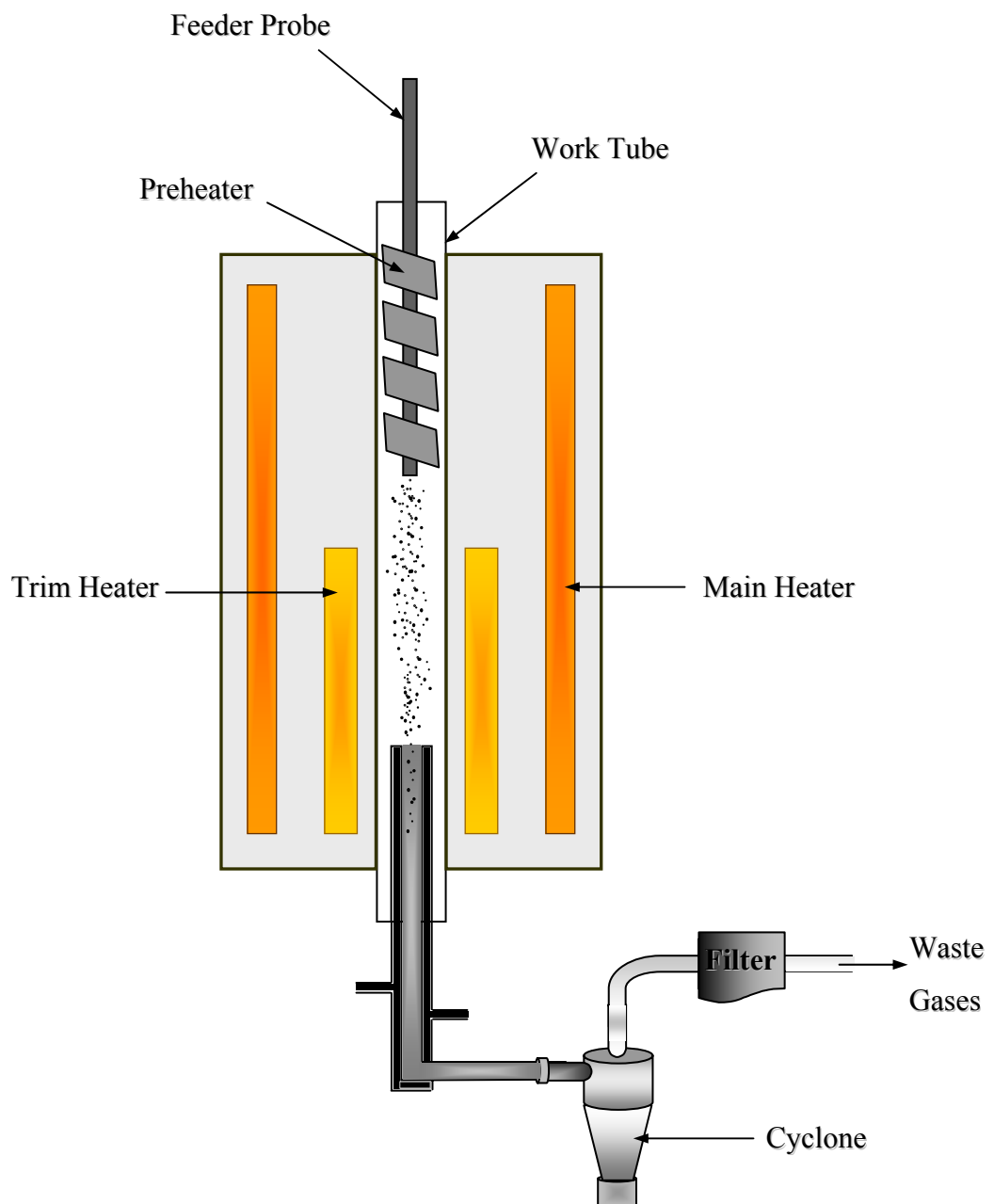


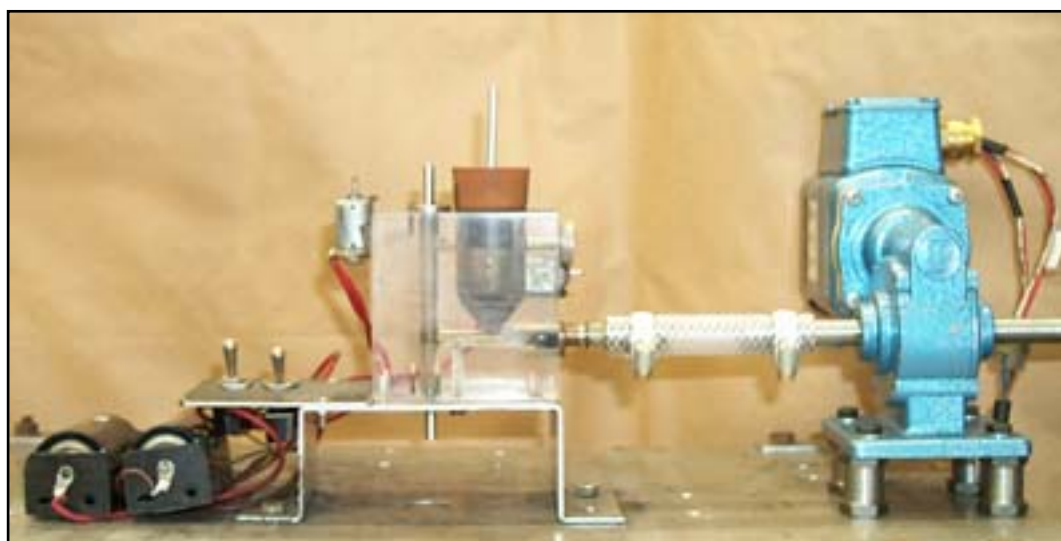
Figure 3.12 The main working are of the Drop Tube Furnace



3.3.1.2 Feeder System

A specially designed feeder system, made in the Chemical Engineering workshop at Nottingham University, was utilised to provide a steady flow rate throughout each experiment. Figure 3.13 shows a photograph of the feeder. The same system was used in the work of Lester (1994), Aquino (1999), and Gilfillan (1999). The coal is placed in a hopper and falls onto a rotating screw thread and is carried into a vertical tube where the coal falls under gravity and is swept into the DTF with a nitrogen stream of 1 lmin^{-1} . In order to provide a fluidised movement of the coal sample, a combination of battery-driven motors with eccentric weights was used to vibrate the assembly and prevent hold-up of the coal in the hopper. A modification of the original configuration of the motors was done to allow, not only horizontal, but also vertical movements of the system. This increased the feed rate of the sample and did not allow the sample to grip the edges of the internal hopper. Feed rates varied considerably depending upon the coal sample and particle size and were in the range 5 to 10 grams per hour.

Figure 3.13 The screw feeder system of the Drop Tube Furnace



3.3.1.3 Heating System and Controls

The heating system of the DTF consists of three separate heaters as shown in Figure 3.11. Firstly a preheater is fitted which heats the gases as they enter at the top of the apparatus and is essentially a coiled carbon graphite plate wrapped round the feeder probe. Secondly, the major source of heating is provided by the main heater which consists of four carbon graphite rods at each corner of the DTF. Finally, a trim heater is fitted which compensates for the effect of the large water cooled collector probe that causes a drop in temperature near the bottom of the DTF. The temperature in each heater is measured via two Pt/Rh (13%) thermocouples, positioned at right angles to the reaction tube.

3.3.1.4 Reaction Tube and Probes

The work tube, where the combustion of the coal sample takes place, is a 2 metre ceramic tube with an internal diameter of 50 mm, and a wall thickness of 5 mm. Both the feeder and collector probes are made of stainless steel, hence the need for water cooling when operating at high temperatures ($>600^{\circ}\text{C}$). Cooling is provided by an internal closed circuit system that contains 60 litres of water. The coolant recirculates from a chiller unit at about $5\text{--}6\text{ lmin}^{-1}$, through the control unit and a fine filter. The flow is divided between both probes, and is then fed back to the chiller unit.

3.3.1.5 Filter System

The gas filter system contains a circular piece of filter paper and a pad of fibreglass. These were found to be effective in removing tar and particulate matter from the exit gases before they were passed to the fume cupboard. Two filters were used in a parallel arrangement enabling operation to continue whilst one or other of the filters was being changed. The filter paper and the fibreglass from the filters are changed when saturated with waste tar and soot. The frequency of these changes depends on the DTF operating conditions and on the type of carbonaceous material being passed through the DTF system.

The pump in the system has been configured to extract gas from its own exhaust, as well as gas from inside the DTF. By altering the valve on the pump bypass the suction from the DTF may be increased or decreased, as required, during the experiments. The gas outlet flow rate should be approximately 1 lmin^{-1} greater than the total inlet flow. The pump has its own filters and these should be checked regularly and cleaned as necessary.

3.3.2 Drop Tube Furnace Experiments

For the initial experiments, two size fractions, 53-75 and 106-125 μm for three Colombian coals, were passed through the DTF operating at three different temperatures: 1000, 1150, and 1300°C. The residence time in the active length of the reactor was approximately 200 ms, with an oxygen concentration of 1% and a coal feed rate of 0.1 to 0.15 gmin^{-1} approximately. In order to assess the repeatability of the DTF two replicates at 1150°C were carried out. This initial study was undertaken to investigate possible effects of the operating temperature, particle size and coal type on char characteristics during combustion.

The second part of the DTF study was a large scale investigation. Six additional South American coals and one from USA were fired. The chars were prepared under the same conditions as those used in the initial experiments. The effects of particle size and DTF temperature on the devolatilisation of the coal and the morphological nature and intrinsic reactivity of the chars were investigated.

3.3.3 DTF Re-firing Experiments

The third part of the study involved the re-firing of six of the coals over a series of different residence times on the DTF in order to provide a relative comparison of the combustion rates of each coal. For these experiments, three size fractions of each coal were used (53-75, 106-125, and 150-180 μm). The samples were passed through the DTF, operating at 1300°C in a 1% oxygen in nitrogen atmosphere with a residence time of 200 ms. The coal and the chars (collected at the bottom of the cyclone), were carefully weighed. Ash content of the coals and

chars, together with the weight of coal fed and char collected, enable the collection efficiency of the process to be determined. This is known as the ash tracer method. Each char, so obtained, was re-fired in the DTF, again at 1300°C, over a series of different residence times (200, 400 and 600 ms), in an atmosphere containing 5% oxygen in nitrogen. The samples were carefully weighed as before.

3.4 The 1 MW Combustion Test Facility

3.4.1 Description of Rig

The purpose of this equipment is to simulate the time/temperature history that the coal and flue gas would see in a full size furnace under controlled and realistic conditions. The CTF includes all the necessary features to ensure maximum similarity with the process encountered in real furnaces.

The facility is capable of assessing:

- (1) Fuel quality effects on combustion and related equipment,
- (2) The characteristics of novel fuels,
- (3) Combustion equipment performance, and
- (4) The effectiveness of pollution control techniques.

The system is designed for a thermal input of 1 MW. Initial operation is with a single burner, but provision is in place for inclusion of up to four burners to enable closer simulation of multi-burners systems. The CTF was constructed in such a way as to allow flexibility in the choice of fuel as well as the position from which samples can be taken. Thus, the furnace may be fired using pulverised fuel, residual fuel, oil, Orimulsion, natural gas, or gas oil, with provision for unconventional fuels.

The CTF is provided with extensive, cooled, wall-mounted slagging panels, extensive probing and sampling ports, and gas analysis equipment.

Comprehensive computerised data-logging and processing equipment makes the facility ideally suited to the development of sophisticated test programmes. A schematic of the CTF showing the numerous sample ports is presented in Figure 3.14.

The temperature of the flue gases is conditioned by a water-cooled refractory-lined combustion chamber and convection duct, air-cooled ducting, and two water spray units. Operation of the apparatus is similar to that of a full-sized boiler with the exception that no steam is raised.

3.4.2 Combustion Experiments

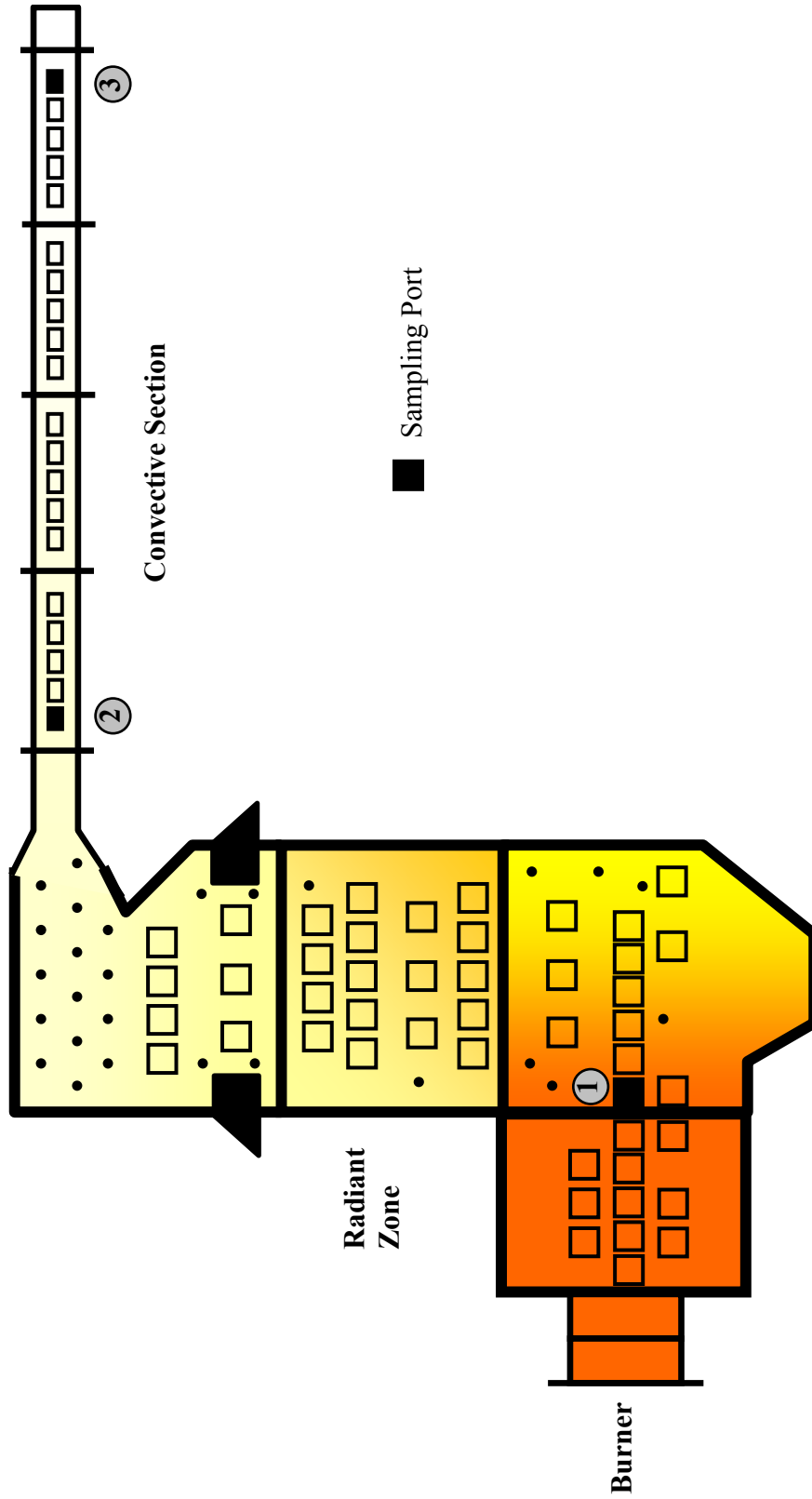
The main aim of the CTF work was to evaluate the effect of particle size distribution of a coal with its combustion burnout performance. Intermediate chars were obtained using sampling ports at various locations along the CTF. The three ports that were used are indicated in Figure 3.14. Since the CTF was installed, experience has been gained that established certain ports as the most suitable for obtaining particles such as char or fly ash. Port one samples relate to the chars that have just undergone pyrolysis, and are just entering the first stage of combustion.

Two coals were selected for these experiments, Carbocol, a sample from the El Cerrejon coal mine in Colombia, and a British coal, Thoresby, for comparative purposes. Five samples of different grind specifications for each coal were fired under the following test condition: 15% Over Fire Air, 1% oxygen.

3.5 Char Characterisation

The changes in the characteristics of the char produced during the course of this work were assessed using a number of different techniques including loss-on-ignition, intrinsic reactivity analysis, and manual and automatic image analysis.

Figure 3.14 Schematic of the 1 MW Combustion Test Facility



3.5.1 Loss-on-Ignition Test

A measurement of the loss-on-ignition of the samples obtained from the DTF was performed in the TGA analyser. The test of heating 10-12 mg of char sample in air to 820°C for one hour. Weight changes were assumed to be as a result of the remaining carbonaceous material present in the samples. The analysis of the samples from the 1 MW rig were carried out in a muffle furnace by staff at the Powergen Technology Centre of Powergen UK plc.

3.5.2 Microscopic Analysis

3.5.2.1 Char Block Preparation

Char blocks needed to be prepared before microscopic analysis were carried out. Originally this was done in a similar way as that for the coal samples. In this case, a reduction in pressure and temperature was required because of the fragility of the char walls. In spite of this, the mounting procedure produced blocks which showed a considerable amount of char particle fracture. Consequently, a new mounting method was developed which considerably reduced this problem. In this case, a liquid polyester resin was utilised. The resin called Estratil 2195 was provided by Cray Valley Ltd (Spain). The procedure for the preparation of the char blocks is as follows:

Methyl-ethyl-ketone (MEK), at 50% w/w, is added to the resin in a proportion of 6 parts by 100 parts of resin. The mixture so obtained is then stirred, and any air bubbles are removed by placing it in a desiccator which is connected to a vacuum pump. After this, 2 grams of resin are then mixed with 0.10 to 0.15 grams of char depending on the density of the char. This is done in a 25 mm diameter plastic mould by adding the resin first and then the char, followed by gently stirring to avoid char particle breakage. The air bubbles produced were evacuated in the same way as with the resin alone. Once set, pure resin was added on top of the dried layer to form a back to the block (9 to 10 g of resin approximately per block). The polishing of the blocks was performed in a similar way to that used

with the coal blocks, although extra force was applied via individual extendible pressure feet due to the greater hardness of the polyester resin.

3.5.2.2 Morphological Characterisation

Morphological characterisation of the individual char structures was performed by reflected light microscopy using the same equipment as for the maceral analysis of the coals samples. The char block is set on a semi-automatic stage coupled to a Swift point counting device. The selection of the particles was carried out by manual point counting on polished surfaces, individual particles being chosen when the cross hairs fell on the carbonaceous material. 250 morphological points were identified for each char block. The most important parameters considered in the determination of the different char types were wall thickness and basic char structure using the modified set of the ICCP classification system which was described in chapter 2 (section 2.5.2).

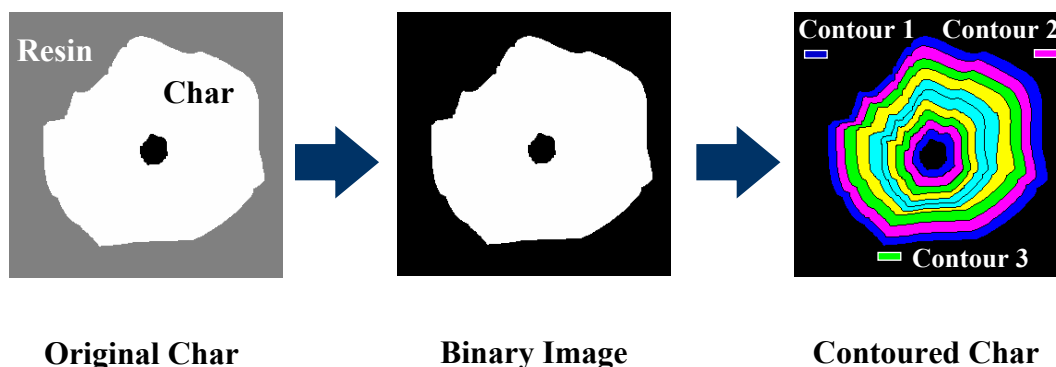
3.5.3 Image Analysis

A novel system for Automatic Char Analysis (ACA), developed at Nottingham (Lester, 1994; Cloke et al., 1997a,b), which allows the relative thickness of chars to be measured, was also used. The program was developed because manual analysis methods did not allow accurate evaluation of chars owing to the increased subjectivity involved during char analysis (Lester et al., 1996).

The program was developed using distance transform techniques. The char particles are singled out into binary images. The edges of any particle are given the grey scale number one. Any neighbouring white pixels are within the second contour, the row of pixels after this are then '3' and so on until the particle has been completely covered. The cumulative percent of char within five contours (ACA5) was taken as the most meaningful result. Since the thickness of the char material will affect burnout, whether mass transfer limited or not, ACA5 was thought to be a useful parameter. The distance transform mapping process is

schematically represented in Figure 3.15, where an idealised cenosphere char is used as an example.

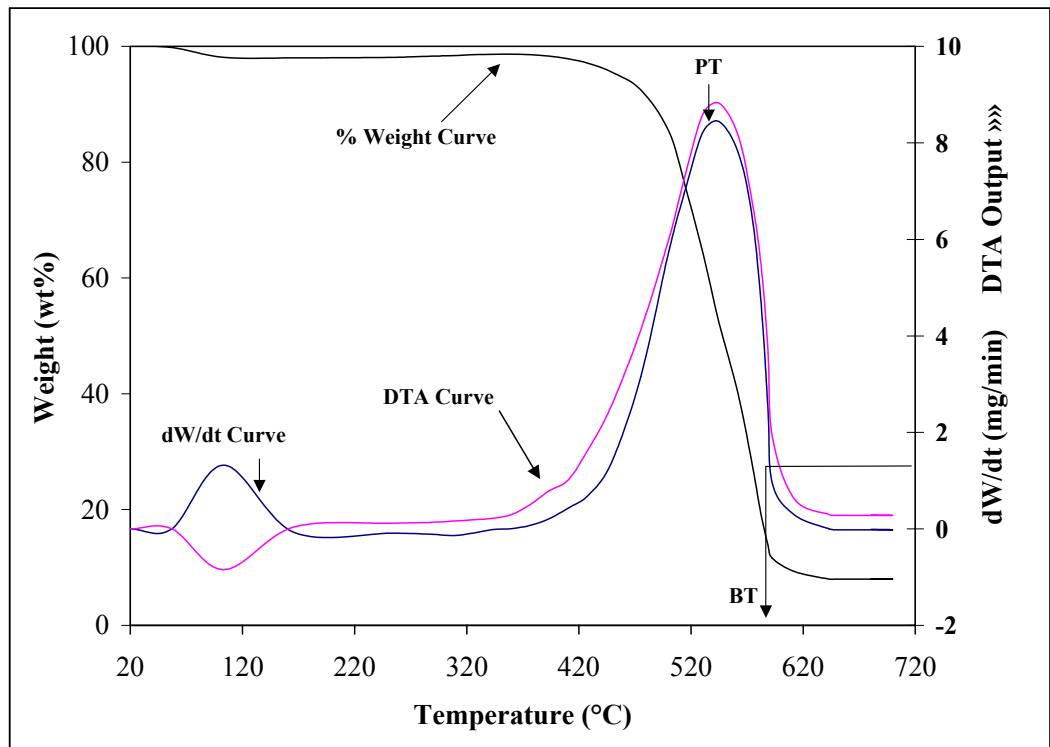
Figure 3.15 The distance transform mapping process



3.5.4 Intrinsic Reactivity Analysis

In order to determine the intrinsic reactivity of the char samples, a non-isothermal technique, which was described by Unsworth (1991), was used. For this purpose, 10 to 12 mg of ground char is loaded into the crucible of the TGA/DTA configuration system. The furnace is heated initially to 300°C at a constant heating rate of 50°Cmin⁻¹ in air, then at 15°Cmin⁻¹ up to around 800°C, depending upon the burnout behaviour of the char material. The TGA records the instantaneous sample mass for a given temperature. The resultant burning profile is a plot of the rate of weight loss against temperature and is shown in Figure 3.16.

Two main parameters were considered to assess the intrinsic reactivity of the char, the peak and burnout temperatures (PT, BT). The peak temperature is that where the burning rate is at a maximum and coincides with the peak on the DTA (Figure 3.16). The burnout temperature represents the temperature where sample oxidation is complete. This was taken as the point immediately before combustion ceases when the rate of weight loss is 1% per minute.

Figure 3.16 A typical burning profile from the intrinsic reactivity analysis

3.5.5 Scanning Electron Microscopy Analysis

An ISI Sx-30 scanning electron microscope was used to examine the coal fractions and chars. The samples were mounted onto double-sided carbon sticky stubs. The equipment used a Robinson backscatter electron detector and was run under an accelerating voltage of 30 kV.

CHAPTER 4 DROP TUBE FURNACE EXPERIMENTS

The first part of this chapter presents the results for the initial experiments performed in the Drop Tube Furnace (DTF) after the rig had been modified and some of its parts renovated or adjusted. Gas temperature profiles along the working tube were obtained before the DTF tests were conducted. Three Colombian coals and two size fractions were selected for this initial stage. The experiments were an attempt to investigate the changes that take place when coal particles are heated rapidly at high temperatures under a slightly oxidising atmosphere during the first 200 milliseconds. Additionally, the study was to act as an assessment of the repeatability of the DTF system.

In the second section of the chapter, the initial experimental design matrix was augmented by adding six additional South American coals and one from the USA. The American coal was selected for comparison purposes. The study was undertaken to investigate possible effects of the operating temperature, particle size and coal type on char characteristics during the combustion process.

4.1 Initial Drop Tube Furnace Experiments

Three vitrinite-rich coals from Colombia were selected for this initial study, on the basis of their different rank and location along the Caribbean region of the country. The first coal Bijao comes from Cordoba County, Caypa (CA) from the Central Cerrejon mine, in La Guajira County, and La Jagua (JA) from Cesar County. Bijao (BI) coal of lower rank, although, according to the ASTM coal classification system, along with the other two coals is ranked as high-volatile bituminous coal.

Since particle size is known to affect coal combustion behaviour, two different size fractions (53-75 and 106-125 μm) for each coal were used. These size ranges were used for two main reasons; firstly, pulverised fuel tends to block the screw

or weir feeder as well as the feeder probe of the DTF, when fines are present, and secondly, the presence of a wider size range would make it difficult to relate char properties to the original feed coal material since certain chars could be the result of coal particle fragmentation.

4.1.1 Coal Characterisation

Proximate and ultimate analysis data for each coal fraction are presented in Table 4.1, whilst Table 4.2 gives the results of the point count maceral analysis, rank, and % unreactives. The variations of volatile matter (VM), fixed carbon (FC), fuel ratio (FR), and carbon content with coal rank, as expressed by the vitrinite reflectance, clearly reflect the expected trends of increasing FR, FC and %C and decreasing VM with the increase of coal rank. Maceral composition of the coals indicates generally high vitrinite content (>84%) and low liptinite (<6%). Caypa and La Jagua both have similar proximate analyses but Caypa shows a slightly higher carbon content and higher vitrinite reflectance value. Another clear difference is that La Jagua coal exhibits a higher inertinite content in both semifusinite and fusinite sub-macerals. This explains the relatively high % unreactives value with respect to the other two coals.

Variations of coal properties with particle size for the coals used here will be discussed in section 4.2 and also in chapter 5 (section 5.1).

The vitrinite reflectance histograms of the coal fractions and the profiles from the Reactivity Assessment Program (RAP) analysis are given in Appendices A and B respectively. The RAP profiles take the form of frequency versus grey scale histograms. The % unreactives parameter, derived from the RAP profile, are given as figures in Table 4.2. Note that the RAP profile of each coal exhibits a rectangular peak at the low end of the reflectance range which corresponds to a synthetic liptinite peak (less than grey scale 55, although exact position is rank dependent). The liptinite concentration is taken from the point count analysis for each fraction and substituted for this peak. This substitution is necessary as the resin and liptinite have similar reflectance values and their respective peaks overlap (Cloke & Lester, 1994; Gilfillan, 1995). These liptinite peaks are barely

discernible for Caypa coal fractions due to the low concentration of liptinite maceral in this coal.

Table 4.1 Proximate and elemental analyses for the three coals

| Coal | Particle Size | Ash | VM | FC | FR | C | H | N | S | O ^a |
|--------------|---------------|-------|--------|--------|-------|--------|--------|--------|--------|----------------|
| | µm | (%db) | (%daf) | (%daf) | FC/VM | (%daf) | (%daf) | (%daf) | (%daf) | (%daf) |
| <i>Bijao</i> | 53-75 | 4.2 | 45.6 | 54.4 | 1.19 | 73.80 | 5.27 | 1.86 | 0.68 | 18.40 |
| | 106-125 | 4.1 | 45.2 | 54.8 | 1.21 | 73.82 | 5.42 | 1.78 | 0.63 | 18.35 |
| <i>Jagua</i> | 53-75 | 2.9 | 38.9 | 61.1 | 1.57 | 84.12 | 5.51 | 1.78 | 0.59 | 8.00 |
| | 106-125 | 2.5 | 39.2 | 60.8 | 1.55 | 84.36 | 5.61 | 1.79 | 0.58 | 7.65 |
| <i>Caypa</i> | 53-75 | 1.9 | 38.6 | 61.4 | 1.59 | 84.78 | 5.68 | 1.89 | 0.67 | 6.97 |
| | 106-125 | 2.2 | 38.9 | 61.1 | 1.57 | 85.43 | 5.76 | 1.86 | 0.64 | 6.31 |

^a by difference; VM=Volatile Matter; FC=Fixed Carbon; FR=Fuel Ratio (FC/VM); db=Dry Basis; daf=Dry, ash-free Basis.

Table 4.2 Petrographic and image analyses for the six coal fractions

| Coal | Particle Size | Rank | Maceral Content (vol%) | | | | U ₁₉₀ ^b |
|--------------|---------------|----------------------|------------------------|-----------|--------------|----------|-------------------------------|
| | µm | VRo (%) ^a | Vitrinite | Liptinite | Semifusinite | Fusinite | (vol%) |
| <i>Bijao</i> | 53-75 | 0.50 | 94.2 | 3.6 | 1.6 | 0.6 | 1.1 |
| | 106-125 | 0.50 | 90.8 | 6.0 | 2.6 | 0.6 | 1.1 |
| <i>Jagua</i> | 53-75 | 0.54 | 85.2 | 2.0 | 7.8 | 5.0 | 4.1 |
| | 106-125 | 0.53 | 84.2 | 2.4 | 10.2 | 3.2 | 4.5 |
| <i>Caypa</i> | 53-75 | 0.60 | 96.8 | 0.4 | 2.4 | 0.4 | 3.4 |
| | 106-125 | 0.59 | 95.2 | 0.4 | 3.6 | 0.8 | 3.6 |

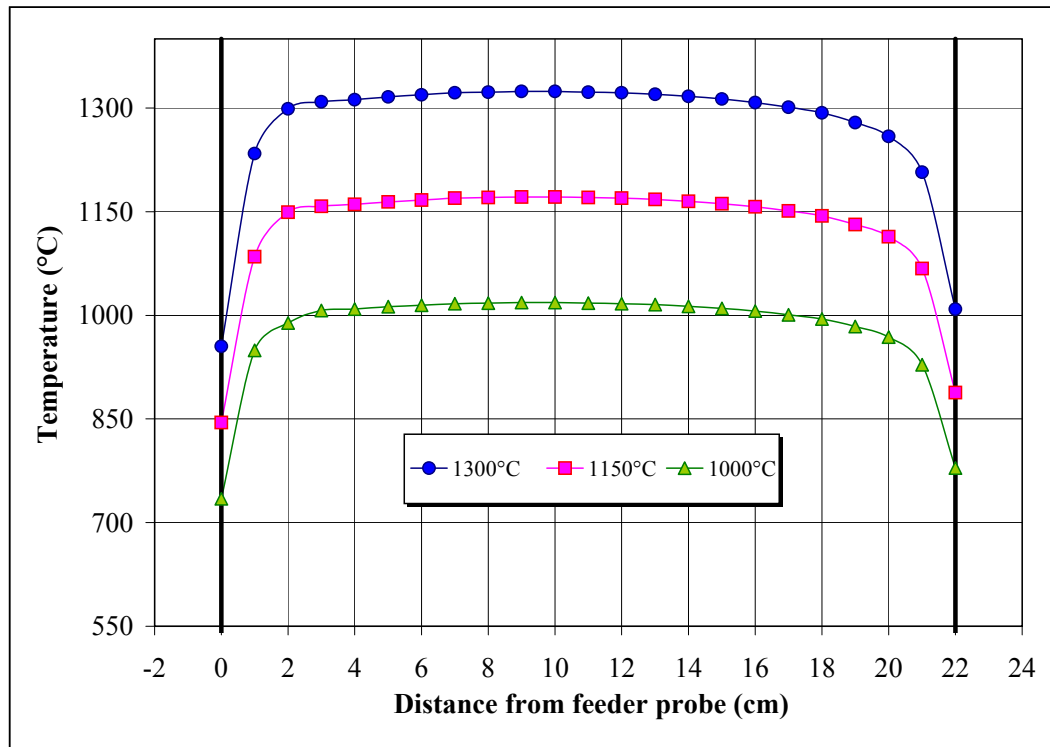
^a VRo = Mean Random Vitrinite Reflectance; ^b U₁₉₀ = % unreactives

The threshold used to calculate the percent of unreactive material is shown in the RAP profiles (grey scale 190). The S-like curves in each plot represent the cumulative percentage curve of the histogram over the grey scale range. The shape of this curve is characteristic of the reactivity of the coal (Cloke et al., 1997b). High-sided S-like curves generally denote coals with low inertinite figures and low variations in vitrinite reflectance. Long sloping curves are generally characteristic of coals which exhibit high semifusinite levels or contain mainly high-rank vitrinite. Blending of various coals may also produce sloped curves. The coals used in the initial experiments, for instance, all give steep curves due to their low variations in vitrinite reflectance and low semifusinite content.

4.1.2 Drop Tube Furnace Conditions

All chars were prepared at three different gas temperatures (1000, 1150, and 1300°C), with a residence time of 200 ms. It was envisaged that fundamental differences between char samples would be observed over this temperature range. The combustion process was completed at 1 atm and under a slightly oxidising atmosphere (1% oxygen in nitrogen). This was considered necessary to avoid contamination of the char samples with soot and condensed tars. In order to assess the repeatability of the system, two replicates at 1150°C were carried out. Only the mean value of the two replicates for each char parameter was reported. Ash repeatability between replicates was found to be within $\pm 1.7\%$ on a dry basis, whilst variations in peak and burnout temperatures were in the order of 1-3°C. This initial study was undertaken to investigate the possible effects of the operating temperature, particle size and coal type on char characteristics during combustion in the DTF.

Gas temperature profiles along the centre line of the working tube were obtained as a function of axial distance from the bottom of the feeder probe. Figure 4.1 shows the profiles obtained for the three different operating temperatures. It can be seen from the figure that high temperature gradients near both the feeder and collector probes, and a long isothermal zone were attained.

Figure 4.1 Temperature profiles along the reaction zone in the DTF

4.1.3 Char Collection Efficiency

The weight loss incurred in coal pyrolysis/combustion experiments is often measured to determine the extent of the reaction. However, the preparation of char at high temperature and under slightly oxidising atmospheres produces a complex mixture of tars, gases and soot, which make it practically impossible to perform a reliable mass balance by direct weighing. Therefore, an alternative method to determine char yield is necessary. This is usually carried out indirectly by the ‘ash tracer method’, which makes use of the ash associated with the coal as tracer (Xian et al., 1988). By knowing the ash content of the coal and that of the char collected in the cyclone after passing through the furnace, the collection efficiency can be calculated. A similar collection efficiency for each set of runs in the DTF would provide a way of assessing the repeatability of the experiments. For this reason the collection efficiency was determined for every sample by the formula given below (Badzioch et al., 1968):

$$\varepsilon (\%) = \frac{\text{Mass of Char Collected} \times A_{\text{char}}}{\text{Mass of Coal Feed} \times A_{\text{coal}}} \times 100 \quad (4.1)$$

Where ε is the collection efficiency and A_{coal} and A_{char} are the coal and char ash content respectively on a dry basis.

Table 4.3 Ash content of coals and chars

| Coal | Particle Size | Coal Ash Content (wt% db) | Char Ash Content (wt% db) | | |
|--------------|---------------|------------------------------|---------------------------|--------|--------|
| | μm | | 1000°C | 1150°C | 1300°C |
| <i>Bijao</i> | 53-75 | 4.2 | 9.90 | 11.64 | 13.42 |
| | 106-125 | 4.1 | 8.86 | 10.94 | 12.16 |
| <i>Jagua</i> | 53-75 | 2.9 | 5.86 | 7.06 | 7.94 |
| | 106-125 | 2.5 | 4.82 | 5.55 | 6.56 |
| <i>Caypa</i> | 53-75 | 1.9 | 4.15 | 4.94 | 5.56 |
| | 106-125 | 2.2 | 4.87 | 5.60 | 6.07 |

Table 4.4 Char yield and collection efficiency data for the three coals

| Coal | Particle Size | Char Yield (g/g of coal fed) | | | Collection Efficiency (%) | | |
|--------------|---------------|------------------------------|--------|--------|---------------------------|--------|--------|
| | μm | 1000°C | 1150°C | 1300°C | 1000°C | 1150°C | 1300°C |
| <i>Bijao</i> | 53-75 | 0.496 | 0.369 | 0.270 | 116.0 | 101.6 | 85.7 |
| | 106-125 | 0.461 | 0.401 | 0.299 | 100.6 | 108.0 | 89.7 |
| <i>Jagua</i> | 53-75 | 0.489 | 0.395 | 0.349 | 99.5 | 97.0 | 96.4 |
| | 106-125 | 0.466 | 0.371 | 0.347 | 91.0 | 83.3 | 92.2 |
| <i>Caypa</i> | 53-75 | 0.473 | 0.401 | 0.343 | 104.5 | 105.6 | 101.7 |
| | 106-125 | 0.472 | 0.418 | 0.359 | 102.6 | 104.4 | 97.3 |

Ash content of the coals and chars are presented in Table 4.3 whilst Table 4.4 gives the data for the mass of char collected and the collection efficiency for all

the samples. It can be seen from the tables that collection efficiency figures vary in accordance with changes in ash levels, particle size, and the operating temperature. At 1000°C, for instance, collection efficiency values were higher for the smaller size fraction. For 1150 and 1300°C the same trend was observed for Caypa and La Jagua coal samples but not Bijao. Collection efficiency values were all greater than 80% and in half of the cases greater than 100%. This problem highlights the deficiencies in the ash tracer method since any inaccuracies in the ash content of the coal or char will result in either unexpected high or low collection efficiencies. Inaccuracies and poor reproducibility that occur during indirect determinations of weight losses may arise for several reasons and they are discussed below.

When the ash content of the coal or char is low (as for the coals used here), a wide scatter of results can arise from even small analytical errors in the determination of ash. This is particularly serious when the amount of decomposition is small so that the change in the ash content may be too small to be detected (Carpenter, 1993). Nevertheless, the extent of devolatilisation of these particular coals during the pyrolysis experiment is high enough so that the error becomes less significant.

It was anticipated that at the operating conditions of the DTF in this study, in particular at the highest temperature, some ash volatilisation may be likely to take place. However, the residence time of the pyrolysing coal particles in these experiments is very low compared with the standard coal ashing method (British Standard, 1016-104.3, 1998). Therefore, the errors that might be introduced in the char yield determinations would be rather small as suggested by other workers (Thompson et al., 1993).

Coal particles undergoing pyrolysis may experience unexpected trajectories on expulsion of the volatiles in the reactor, which may cause different flow patterns (Carpenter, 1993). The particles may also become sticky, adhering to the walls of the reactor tube and the collector so that they cannot be recovered quantitatively. Even if the flow pattern were theoretically laminar, lighter particles in particular, may be lost in the gas flow. Additionally, the rapid thermal quenching experienced by the char particles may induce recondensation of volatiles on the

walls of the collector probe. Therefore, as the number of experiments increase, the amount of tar and soot residues builds up. Consequently, ash particles may adhere more readily to the surface. In order to reduce the chance of this occurring, the collector probe was cleaned after about ten grams of coal had been passed through the DTF. Note also that the cyclone used to collect char does not trap all of the particles passing through it, so collection efficiency may be lower than expected.

As can be seen from the previous discussion, the ash tracer method is not without some error. However, this method is very simple and the most widely used, and alternative methods are not always practical. As a result, the ash tracer method has been utilised throughout this study.

4.1.4 DTF Volatiles and R Factor

It is well known that the amount of volatiles emitted from coal under higher temperatures and heating rates can exceed the volatile matter measured in standard proximate analysis (Gibbins et al., 1991). Currently, a variety of test methods are used in research laboratories to measure volatiles release under rapid heating conditions. Experiments in drop-tube furnaces, and similar devices, have been found to simulate more closely the conditions encountered in real combustion processes, since the individual particles are dispersed in a gas stream during heating. Nevertheless, they experience the problem of having to recapture the particles for analysis. In practice, complete sample recovery is not possible and hence the measurements of volatile release in DTF experiments normally rely on the use of the ash tracer technique. As with the collection efficiency, by knowing the ash content of the coal (*A_{coal}*) and that of the char (*A_{char}*) on a dry basis, the DTF volatiles yield (*V_{DTF}*), can be estimated as follows:

$$V_{DTF} = \frac{100 \times (A_{char} - A_{coal})}{A_{char}} \quad (\% \text{ dry coal}) \quad (4.2)$$

$$V_{DTF} = \frac{10^4 \times (A_{char} - A_{coal})}{A_{char} \times (100 - A_{coal})} \quad (\% \text{ daf coal}) \quad (4.3)$$

Given the uncertainty associated with indirect weight loss determinations by using the ash tracer technique, it is usual practice to calculate the so-called R factor. The purpose of this factor is to compare the weight loss that occurs in a DTF with the coal's proximate volatile matter (VM). For practical purposes, the R factor under pf combustion conditions can provide the 'true' volatile release potential of different coals. The R factor may also be used as a qualitative indicator of the behaviour of a coal during rapid heating. It can be calculated as follows (Kimber and Gray, 1967):

$$R \text{ Factor} = \frac{\text{Weight loss of coal (\% daf)}}{\text{Proximate VM content of coal (\% daf)}} = \frac{V_{DTF} (\% \text{ daf})}{V_{coal} (\% \text{ daf})} \quad (4.4)$$

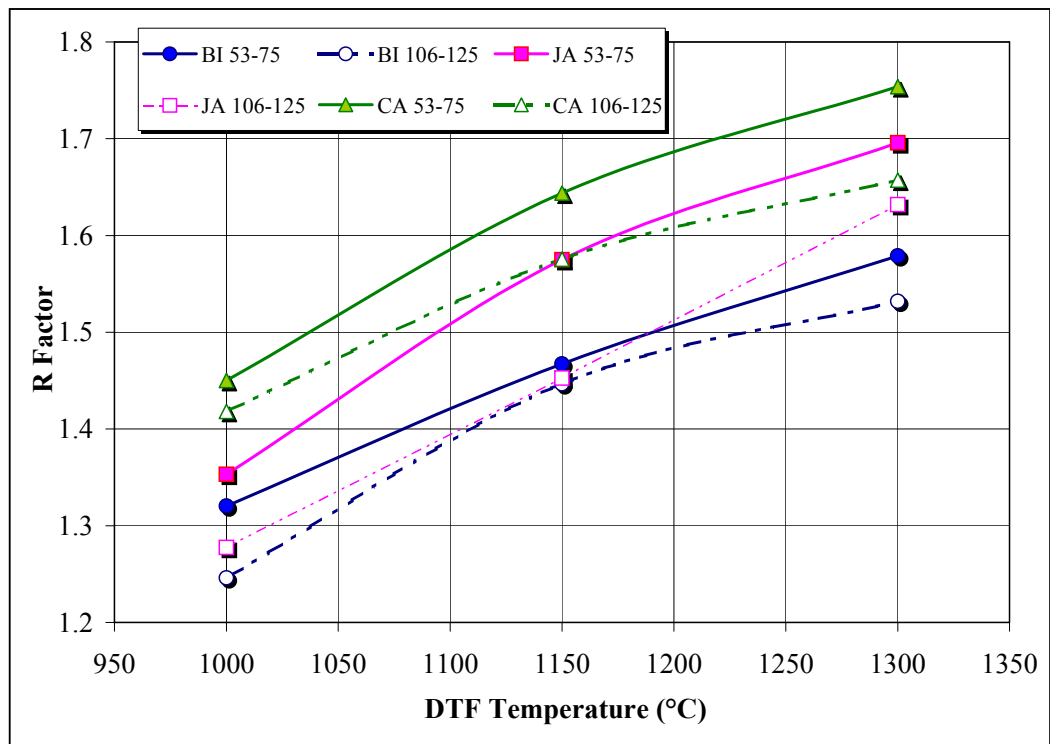
As can be seen, estimates of R factor make use of the ash tracer technique, and hence, clearly rely on ash analyses being undertaken for the coal feed and the product char.

Table 4.5 Proximate and DTF volatiles and R Factor data for the three coals and chars

| Coal | Particle size | Proximate Volatiles (wt% daf) | DTF Volatiles - V _{DTF} (wt% daf) | | | R factor | | |
|--------------|---------------|-------------------------------|--|--------|--------|----------|--------|--------|
| | µm | | 1000°C | 1150°C | 1300°C | 1000°C | 1150°C | 1300°C |
| <i>Bijao</i> | 53-75 | 45.3 | 59.8 | 66.4 | 71.5 | 1.32 | 1.47 | 1.58 |
| | 106-125 | 45.3 | 56.5 | 65.6 | 69.4 | 1.25 | 1.45 | 1.53 |
| <i>Jagua</i> | 53-75 | 38.7 | 52.4 | 61.0 | 65.7 | 1.35 | 1.57 | 1.70 |
| | 106-125 | 39.2 | 50.0 | 56.9 | 63.9 | 1.28 | 1.45 | 1.63 |
| <i>Caypa</i> | 53-75 | 38.5 | 55.8 | 63.3 | 67.5 | 1.45 | 1.64 | 1.75 |
| | 106-125 | 38.9 | 55.2 | 61.4 | 64.5 | 1.42 | 1.58 | 1.66 |

DTF volatiles data (expressed on a dry, ash-free basis) and R factor values for the coal fractions are presented in Table 4.5. Figure 4.2 shows the change in the R factor, for the six coal fractions as a function of the DTF operating temperature. It is apparent from the data and figures that R factor (and hence DTF volatiles) increases as the DTF operating temperature rises, independent of coal type. This would be expected, since the higher the temperature a coal is exposed to, the greater the chance of residual volatiles being emitted (Lester et al., 1995; Kimber and Gray, 1967; Gibbins et al., 1991). There is also an increase of R factor with increasing coal rank (Caypa>La Jagua>Bijao). However, La Jagua gave lower DTF volatiles content than Caypa even though the proximate volatiles of both coals are fairly similar. This confirms the inadequacy of standard proximate volatiles to characterise or predict coal's rapid heating behaviour.

Figure 4.2 A plot of R Factor as a function of operating temperature and particle size for the three coals



As far as particle size is concerned, the 106-125 μm fraction tends to give lowest R factor values which indicates that these particles require a longer time in the furnace at higher temperatures before they will emit more volatiles than that

detected using standard proximate analysis. An explanation for this might be that the surface area per gram of coal would be lower and pore length higher for this fraction, thus making loss of volatiles more difficult.

4.1.5 Char Intrinsic Reactivity

Table 4.6 shows the intrinsic reactivity data for the char samples. A plot for each reactivity parameter (PT and BT), as a function of both particle size and the operating temperature, are presented in Figure 4.3 and Figure 4.4 respectively. Char burning profiles, derived from the intrinsic reactivity analysis, are given in Appendix C. The profiles take the form of DTA output (μVmg^{-1}) as a function of temperature.

Table 4.6 Intrinsic reactivity data of chars as a function of temperature and particle size

| Coal | Particle Size | Peak Temperature (°C) | | | Burnout Temperature (°C) | | |
|--------------|---------------|-----------------------|--------|--------|--------------------------|--------|--------|
| | μm | 1000°C | 1150°C | 1300°C | 1000°C | 1150°C | 1300°C |
| <i>Bijao</i> | 53-75 | 384 | 442 | 474 | 535 | 537 | 544 |
| | 106-125 | 392 | 444 | 478 | 540 | 545 | 560 |
| <i>Jagua</i> | 53-75 | 503 | 535 | 590 | 552 | 584 | 626 |
| | 106-125 | 516 | 562 | 600 | 554 | 604 | 646 |
| <i>Caypa</i> | 53-75 | 502 | 541 | 594 | 547 | 579 | 635 |
| | 106-125 | 505 | 567 | 627 | 560 | 612 | 670 |

The most obvious feature is that the intrinsic reactivity decreases (higher PT and BT values) as the operating temperature increases. For Bijao coal the increase in BT is not as significant as the increase in PT as can be seen from the plots (Figures 4.3 and 4.4). The 106-125 μm fraction gave higher PT and BT values

Figure 4.3 Peak temperature as a function of coal particle size and DTF operating temperature

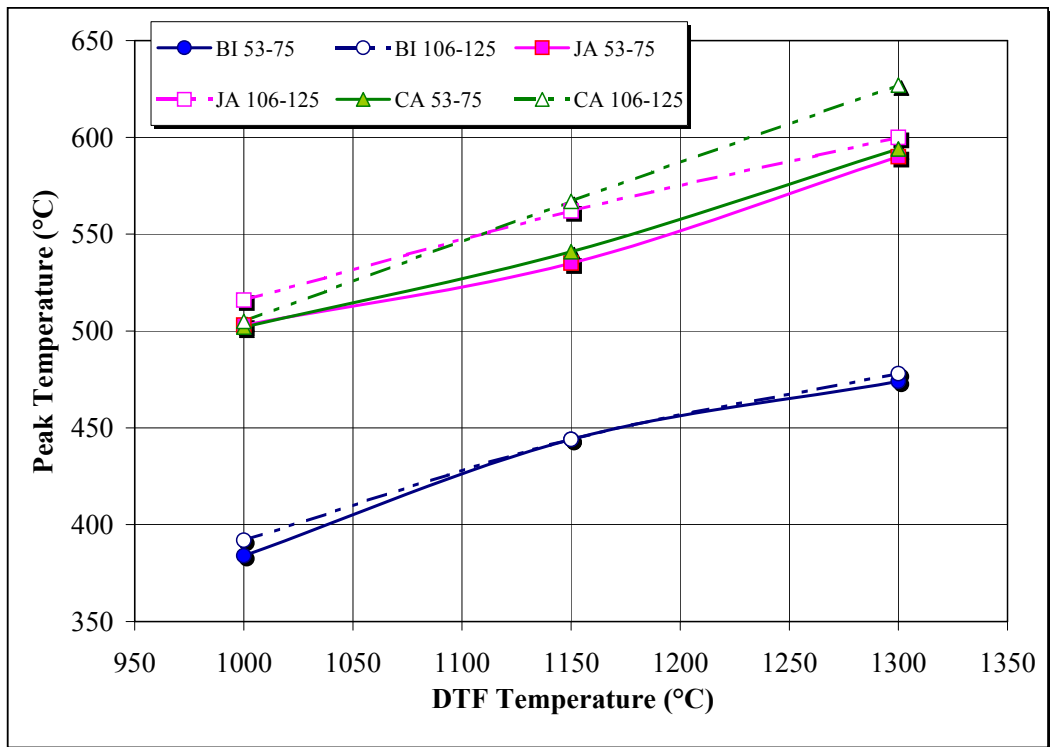
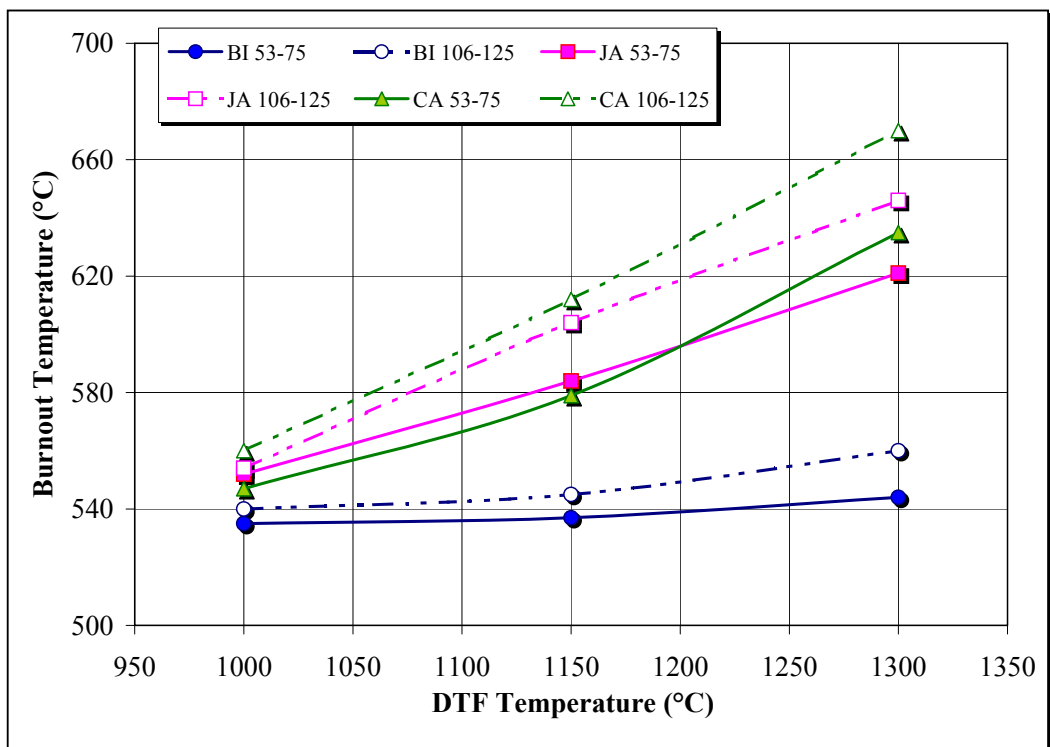


Figure 4.4 Burnout temperature as a function of coal particle size and DTF operating temperature



than the 53-75 μm fraction. However, these differences are more significant for Caypa and La Jagua at 1150 and 1300°C for BT. It is clear from the results that Bijao coal exhibits higher intrinsic reactivity, whilst there are little differences in the figures between La Jagua and Caypa.

4.1.6 Optical and Automatic Image Analyses of Chars

The manual char analysis reveals that the characteristics of the initial coal material has a significant effect on the type and morphological properties of the char produced (Tables 4.7 to 4.9). The lower rank coal Bijao, for instance, produces predominantly network chars as shown in Figure 4.5. Caypa and La Jagua coals both tend to form mainly cenospheres, although La Jagua also produces a slightly higher percentage of fusinoid and solid char particles (see Figure 4.6 and figure 4.7 respectively). This can be explained by the higher inertinite content of La Jagua coal.

From the manual char analysis, it can be seen that the larger size fractions (II) give the thickest walled chars. These fractions gave consistently lower ACA5 values indicating thicker chars as shown in Figure 4.8. It was observed that when the operating temperature in the DTF was increased the amount of thin-walled chars increased quite substantially for coals Caypa and La Jagua regardless of the particle size. For Bijao the percentage of thin chars was already very high at 1000°C as indicated by the high ACA5 value.

Bijao which has the lowest % unreactive material, produced the highest ACA5 values followed by coal Caypa and La Jagua. This same trend was observed at the different temperatures of operation of the DTF, as shown in Figure 4.9, for all fractions. This leads to the conclusion that the % unreactives parameter derived from the grey-scale histogram, obtained by image analysis of the coal, provides a useful parameter for the prediction of coal combustion behaviour.

Table 4.7 Manual char analysis for the samples at 1000°C

| Coal | Particle Size (μm) | TS | CS | TN | CN | I | F/S |
|--------------|---------------------------------|------|------|------|------|-----|-----|
| <i>Bijao</i> | 53-75 | 0.0 | 1.1 | 51.5 | 45.9 | 1.3 | 0.2 |
| | 106-125 | 0.0 | 0.7 | 49.6 | 47.7 | 1.6 | 0.4 |
| <i>Jagua</i> | 53-75 | 25.7 | 39.4 | 5.3 | 15.8 | 7.9 | 5.9 |
| | 106-125 | 13.6 | 40.1 | 1.7 | 31.6 | 7.2 | 5.8 |
| <i>Caypa</i> | 53-75 | 42.3 | 52.3 | 0.5 | 2.4 | 1.1 | 1.5 |
| | 106-125 | 29.5 | 64.0 | 0.7 | 3.1 | 0.8 | 1.9 |

TS=Tenuisphere; CS=Crassisphere; TN=Tenuinetwork; CN=Crassinetwork; I=Inertoid; F/S=Fusinoid/Solid

Table 4.8 Manual char analysis for the samples at 1150°C

| Coal | Particle Size (μm) | TS | CS | TN | CN | I | F/S |
|--------------|---------------------------------|------|------|------|------|-----|-----|
| <i>Bijao</i> | 53-75 | 0.5 | 0.5 | 63.5 | 34.4 | 0.8 | 0.4 |
| | 106-125 | 0.4 | 0.3 | 56.1 | 41.2 | 1.6 | 0.4 |
| <i>Jagua</i> | 53-75 | 41.3 | 29.0 | 3.3 | 15.1 | 6.6 | 4.9 |
| | 106-125 | 28.6 | 33.9 | 1.3 | 24.6 | 6.4 | 5.3 |
| <i>Caypa</i> | 53-75 | 63.4 | 30.7 | 0.5 | 3.2 | 0.9 | 1.5 |
| | 106-125 | 47.6 | 46.2 | 0.7 | 3.2 | 0.8 | 1.6 |

Table 4.9 Manual char analysis for the samples at 1300°C

| Coal | Particle Size (μm) | TS | CS | TN | CN | I | F/S |
|--------------|---------------------------------|------|------|------|------|-----|-----|
| <i>Bijao</i> | 53-75 | 0.7 | 0.1 | 75.2 | 22.7 | 0.9 | 0.4 |
| | 106-125 | 0.5 | 0.3 | 58.4 | 39.1 | 1.3 | 0.4 |
| <i>Jagua</i> | 53-75 | 56.8 | 18.6 | 1.3 | 14.3 | 5.2 | 3.8 |
| | 106-125 | 43.5 | 27.7 | 0.8 | 17.6 | 5.6 | 4.8 |
| <i>Caypa</i> | 53-75 | 84.5 | 9.4 | 0.4 | 3.9 | 0.6 | 1.2 |
| | 106-125 | 66.2 | 27.7 | 0.7 | 3.2 | 0.7 | 1.5 |

Figure 4.5 Scanning Electron Micrograph showing typical network structure of Bijao chars

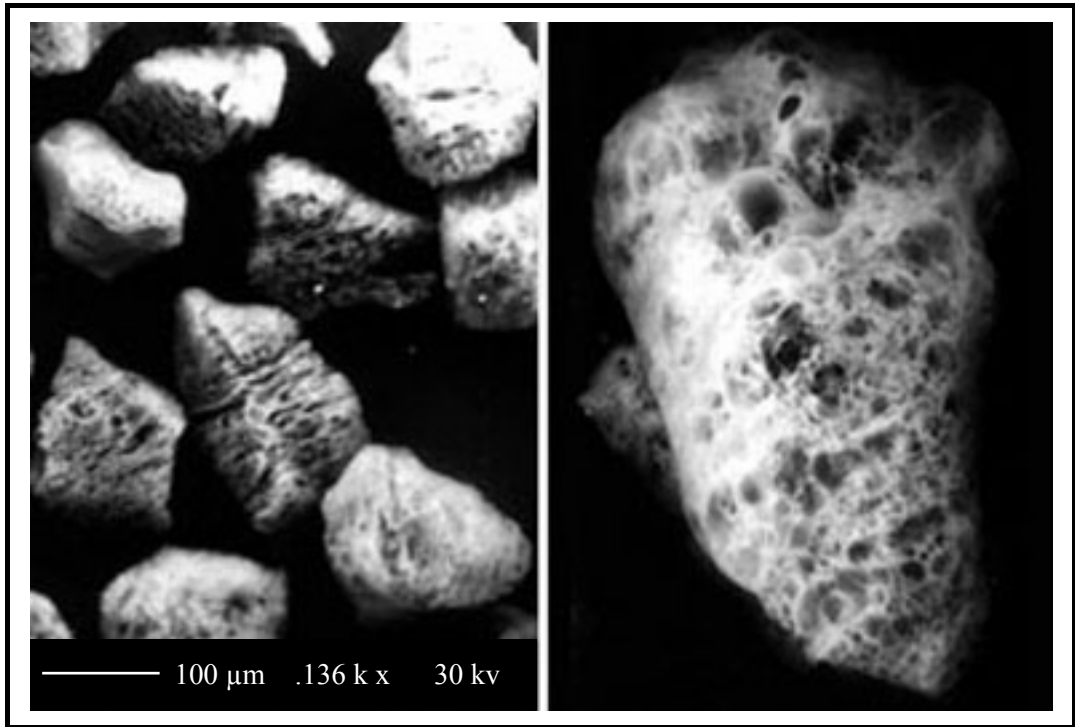


Figure 4.6 Scanning Electron Micrograph showing cenospheres from Caypa chars

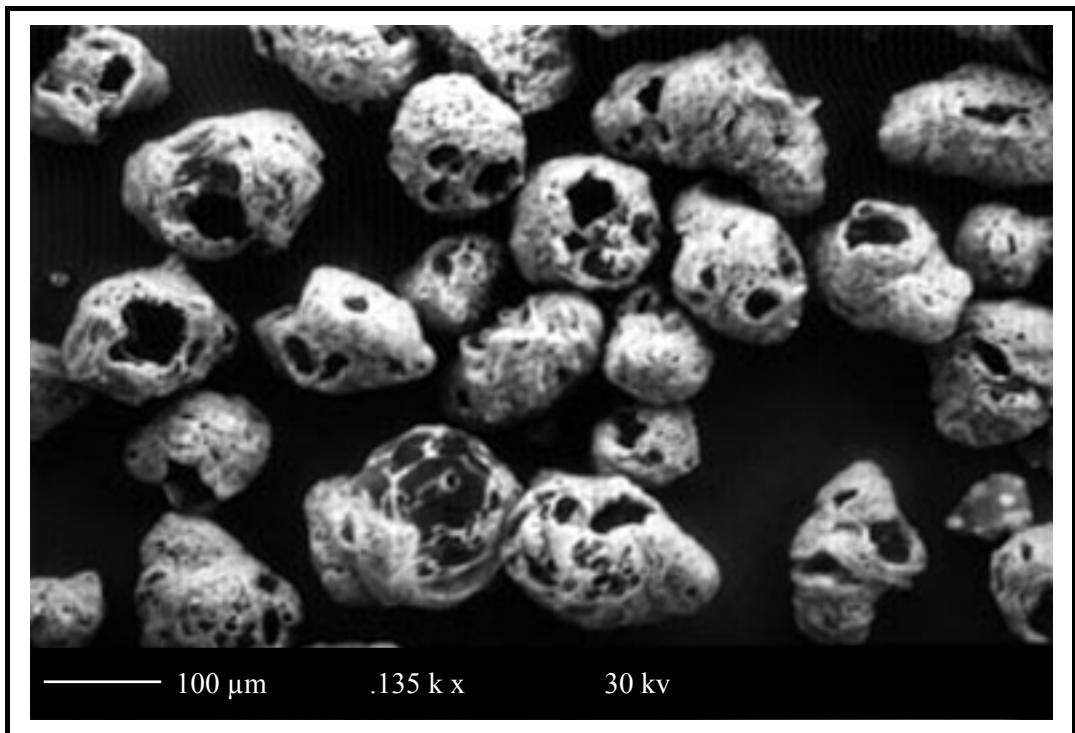


Figure 4.7 Scanning Electron Micrograph showing cenospheres and fusinoid chars in La Jagua

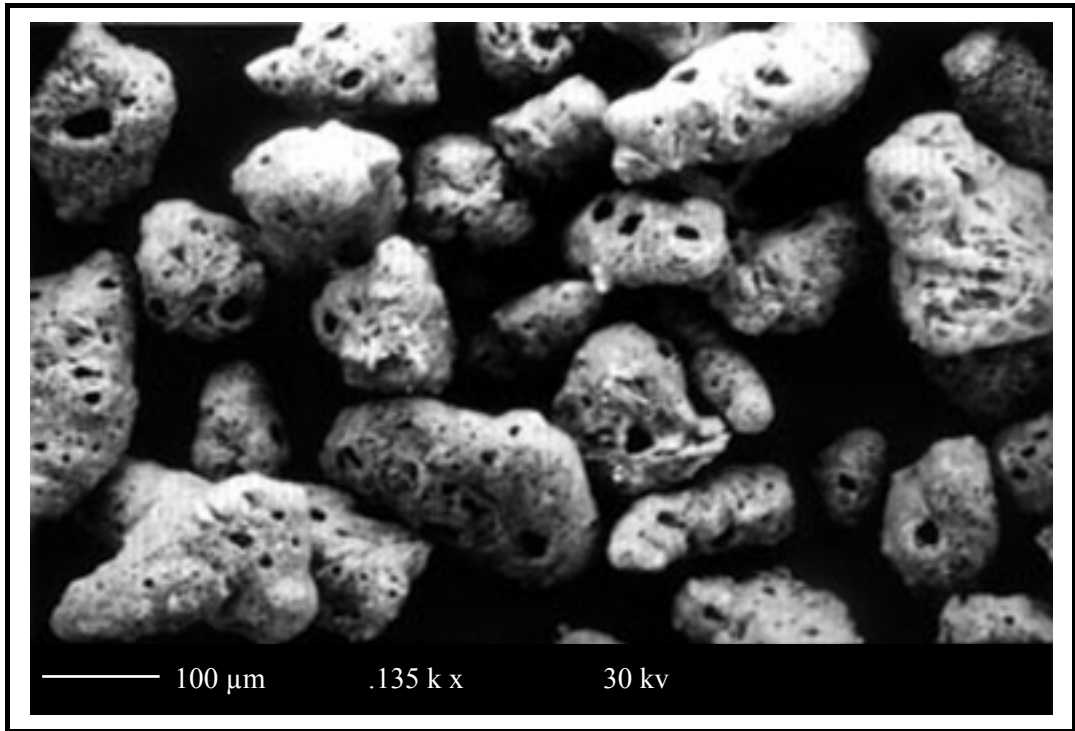


Figure 4.8 Changes in ACA5 as a function of temperature and particle size

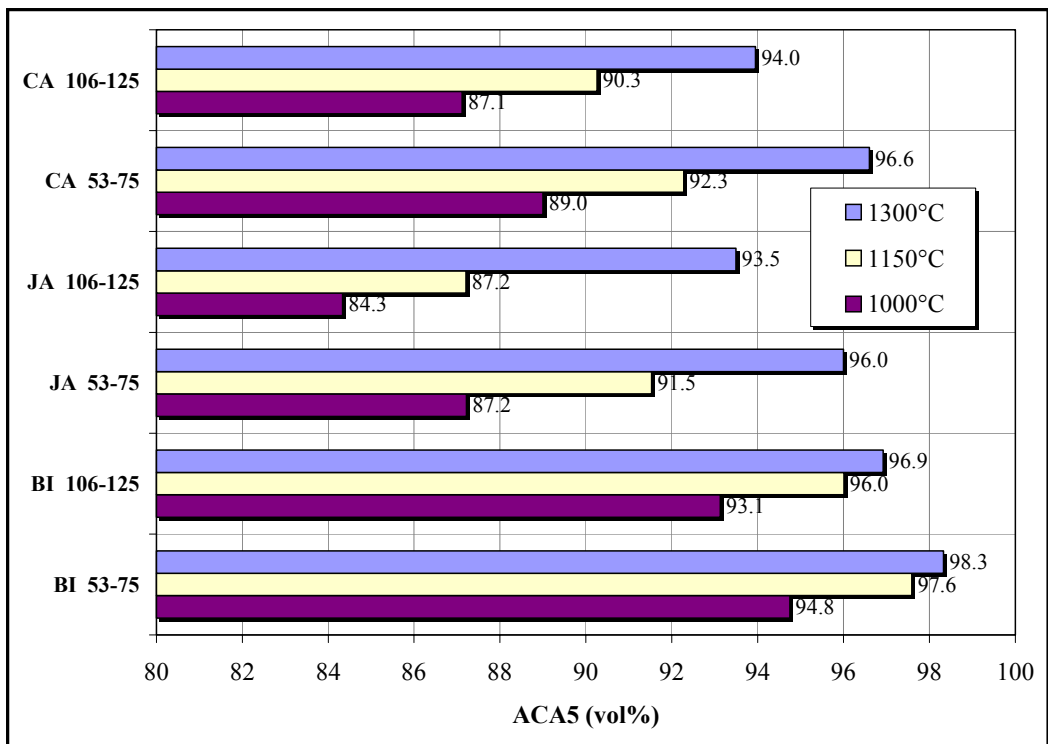
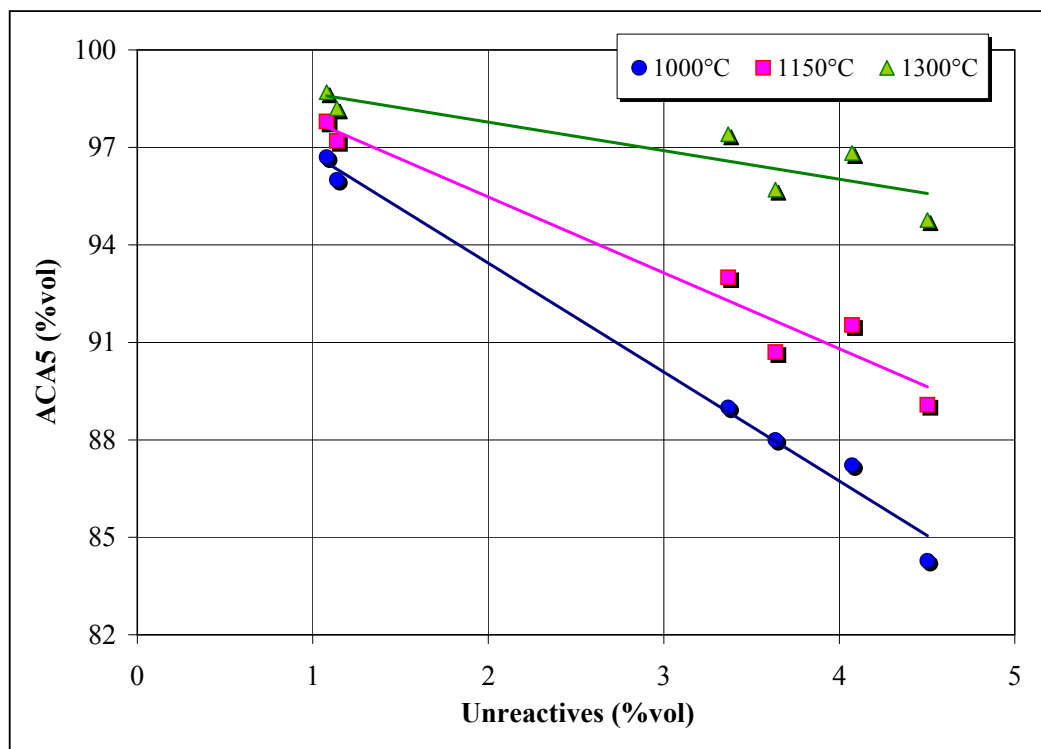


Figure 4.9 A plot of ACA5 against % unreactives

4.2 Further Drop Tube Furnace Experiments

As mentioned in the introduction of the chapter, the second part of the DTF study was a larger scale investigation. This involved the pyrolysis of six additional South American coals and one from the USA. The study was undertaken to investigate the behaviour of the different coals during pyrolysis when changing the operating temperature in the DTF and the particle size of the coals. The morphological nature and the intrinsic reactivity of the remaining chars were also investigated along with the volatiles yield and ash content of the chars.

4.2.1 Proximate and Ultimate Analysis of Coals

Proximate analysis data for the various coal fractions (determined by thermogravimetric analysis) is shown in Table 4.10. The data is presented on a dry, and dry, ash-free bases. Coals have been ordered by rank (expressed as the random vitrinite reflectance). Note that the fuel ratio parameter, i.e. fixed

carbon/volatile matter content (dry, ash-free basis), has also been recorded in the table for each sample. The fuel ratio shows a clear increase with rank and ranges from 1.21 for the low rank Colombian coal, Bijao, up to 1.87 for the higher rank American coal, Ashland.

Table 4.10 Proximate analysis data for the coal fractions

| Coal/Fraction ^a | | Moisture | Dry Basis (wt%) | | | Dry, ash-free basis (wt%) | | Fuel Ratio |
|--|-----------|----------|-----------------|-----------------|------|---------------------------|------|------------|
| | | (wt%) | VM ^b | FC ^c | Ash | VM | FC | FC/VM |
| <i>Bijao</i> <i>(BI)</i> | <i>I</i> | 7.9 | 43.4 | 52.4 | 4.2 | 45.3 | 54.7 | 1.21 |
| | <i>II</i> | 6.2 | 43.5 | 52.5 | 4.1 | 45.3 | 54.7 | 1.21 |
| <i>Fila Maestra</i> <i>(FM)</i> | <i>I</i> | 5.4 | 41.7 | 52.5 | 5.9 | 44.3 | 55.7 | 1.26 |
| | <i>II</i> | 5.0 | 41.5 | 52.3 | 6.2 | 44.2 | 55.8 | 1.26 |
| <i>La Loma</i> <i>(LO)</i> | <i>I</i> | 5.1 | 38.6 | 56.8 | 4.6 | 40.5 | 59.5 | 1.47 |
| | <i>II</i> | 4.8 | 38.8 | 56.8 | 4.4 | 40.6 | 59.4 | 1.46 |
| <i>Oreganal</i> <i>(OR)</i> | <i>I</i> | 4.2 | 37.6 | 58.7 | 3.7 | 39.1 | 60.9 | 1.56 |
| | <i>II</i> | 4.0 | 38.0 | 59.5 | 2.5 | 39.0 | 61.0 | 1.56 |
| <i>La Jagua</i> <i>(JA)</i> | <i>I</i> | 3.3 | 37.6 | 59.5 | 2.9 | 38.7 | 61.3 | 1.58 |
| | <i>II</i> | 3.2 | 38.2 | 59.3 | 2.5 | 39.2 | 60.8 | 1.55 |
| <i>El Cerrejon</i> <i>(CE)</i> | <i>I</i> | 3.4 | 37.1 | 58.5 | 4.5 | 38.8 | 61.2 | 1.58 |
| | <i>II</i> | 3.3 | 37.7 | 58.8 | 3.5 | 39.1 | 60.9 | 1.56 |
| <i>Caypa</i> <i>(CA)</i> | <i>I</i> | 2.4 | 37.8 | 60.4 | 1.9 | 38.5 | 61.5 | 1.60 |
| | <i>II</i> | 2.3 | 38.1 | 59.7 | 2.2 | 38.9 | 61.1 | 1.57 |
| <i>Paso Diablo</i> <i>(PD)</i> | <i>I</i> | 2.3 | 36.2 | 58.9 | 4.9 | 38.0 | 62.0 | 1.63 |
| | <i>II</i> | 2.1 | 37.3 | 60.0 | 2.7 | 38.3 | 61.7 | 1.61 |
| <i>Maturin</i> <i>(MA)</i> | <i>I</i> | 1.3 | 34.8 | 61.1 | 4.1 | 36.3 | 63.7 | 1.76 |
| | <i>II</i> | 1.0 | 35.2 | 61.1 | 3.7 | 36.6 | 63.4 | 1.73 |
| <i>Ashland</i> <i>(AL)</i> | <i>I</i> | 1.6 | 31.2 | 58.3 | 10.5 | 34.9 | 65.1 | 1.87 |
| | <i>II</i> | 1.3 | 33.1 | 57.8 | 9.2 | 36.4 | 63.6 | 1.75 |

^aI=53-75 μ m, II=106-125 μ m; ^bVM=Volatile Matter; ^cFC=Fixed Carbon.

Volatile matter is known to decrease (and fixed carbon increases) progressively with increasing coal rank (Unsworth, 1991; Van Krevelen, 1993). Clearly from the data in Table 4.10, this general trend can be observed. Volatile matter contents range from 45.3 (%dry, ash-free basis) for Bijao to 34.9 (%dry, ash-free basis) for Ashland. Further to this, the 106-125 μm coal fractions tend to exhibit higher volatile matter contents than the 53-75 μm fractions. These variations are, however, within the experimental error of the analysis (0.8%) for all the coals, other than Ashland, where an increase is clearly evident with increasing particle size.

Bijao and Fila Maestra fractions contain higher moisture contents than the other coal fractions, whilst Maturin and Ashland exhibit the lowest figures. This is consistent with the observation that inherent moisture content decreases with rank (Unsworth et al., 1991). Most of the coals have a very low ash content (lower than 5%) excluding the Venezuelan coal Fila Maestra (~6%) and the American coal (~10%).

Elemental analysis (ultimate analysis) of the coal fractions is shown in Table 4.11. The data consists of percentage by weight of carbon, hydrogen, nitrogen and sulphur. Oxygen is calculated by difference and all data is on a dry, ash-free basis. A general trend can be identified from this data. The carbon content increases with rank, whilst the oxygen content shows a decrease. All the coals contain very small amounts of sulphur (less than 1%).

4.2.2 Petrographic Characterisation of Coals

Petrographic analysis for the twenty coal fractions, including maceral analysis and rank (random vitrinite reflectance, VRo) is given in Table 4.12. The data is provided on a volume/volume, mineral matter-free basis. The vitrinite reflectance histograms of the samples are shown in Appendix A.

From the maceral analysis results, it can be concluded that all the South American coals in this study are rich in vitrinite with low concentrations of liptinite. The North American coal, Ashland, is also a vitrinite-rich coal although its liptinite

content is relatively higher in comparison with the South American coals. The results show a significant variation in maceral composition from 68.5-96.8% for vitrinite, 0.4-14.3% for liptinite, 0.4-10.2% for semifusinite, and 0.4-12.6% for fusinite.

Table 4.11 Ultimate analysis data for the coal fractions

| Coal/Fraction | | C | H | N | S | O |
|---------------------|-----------|-----------|-----------|-----------|-----------|-----------|
| | | (wt% daf) |
| <i>Bijao</i> | <i>I</i> | 73.80 | 5.27 | 1.86 | 0.68 | 18.40 |
| | <i>II</i> | 73.82 | 5.42 | 1.78 | 0.63 | 18.35 |
| <i>Fila Maestra</i> | <i>I</i> | 76.81 | 5.67 | 2.01 | 0.87 | 14.63 |
| | <i>II</i> | 78.19 | 5.77 | 2.03 | 0.85 | 13.16 |
| <i>La Loma</i> | <i>I</i> | 78.79 | 5.42 | 1.72 | 0.64 | 13.42 |
| | <i>II</i> | 78.37 | 5.42 | 1.84 | 0.69 | 13.68 |
| <i>Oreganal</i> | <i>I</i> | 82.23 | 5.49 | 1.82 | 0.63 | 9.83 |
| | <i>II</i> | 81.97 | 5.54 | 1.81 | 0.61 | 10.06 |
| <i>La Jagua</i> | <i>I</i> | 84.12 | 5.51 | 1.78 | 0.59 | 8.00 |
| | <i>II</i> | 84.36 | 5.61 | 1.79 | 0.58 | 7.65 |
| <i>El Cerrejon</i> | <i>I</i> | 84.23 | 5.53 | 1.83 | 0.68 | 7.73 |
| | <i>II</i> | 83.80 | 5.58 | 1.83 | 0.65 | 8.14 |
| <i>Caypa</i> | <i>I</i> | 84.78 | 5.68 | 1.89 | 0.67 | 6.97 |
| | <i>II</i> | 85.43 | 5.76 | 1.86 | 0.64 | 6.31 |
| <i>Paso Diablo</i> | <i>I</i> | 86.12 | 5.65 | 1.90 | 0.82 | 5.51 |
| | <i>II</i> | 86.53 | 5.76 | 1.90 | 0.74 | 5.07 |
| <i>Maturin</i> | <i>I</i> | 87.02 | 5.83 | 1.83 | 0.70 | 4.62 |
| | <i>II</i> | 87.41 | 5.77 | 1.83 | 0.66 | 4.33 |
| <i>Ashland</i> | <i>I</i> | 87.77 | 5.60 | 1.90 | 0.83 | 3.91 |
| | <i>II</i> | 88.91 | 5.71 | 1.85 | 0.78 | 2.75 |

Table 4.12 Petrographic Analysis of the coal fractions

| Coal/Fraction | Rank | Maceral Content (vol%) | | | | U ₁₉₀ | |
|---------------------|-----------|------------------------|-----------|-----------|--------------|------------------|--------|
| | | VRo (%) | Vitrinite | Liptinite | Semifusinite | Fusinite | (vol%) |
| <i>Bijao</i> | <i>I</i> | 0.50 | 94.2 | 3.6 | 1.6 | 0.6 | 1.1 |
| | <i>II</i> | 0.50 | 90.8 | 6.0 | 2.6 | 0.6 | 1.1 |
| <i>Fila Maestra</i> | <i>I</i> | 0.50 | 95.6 | 2.6 | 0.6 | 1.2 | 1.7 |
| | <i>II</i> | 0.51 | 95.4 | 3.4 | 0.4 | 0.8 | 2.3 |
| <i>La Loma</i> | <i>I</i> | 0.51 | 95.6 | 0.4 | 3.6 | 0.4 | 2.2 |
| | <i>II</i> | 0.53 | 96.8 | 0.2 | 2.6 | 0.4 | 2.8 |
| <i>Oreganal</i> | <i>I</i> | 0.53 | 91.8 | 0.8 | 1.8 | 5.6 | 3.3 |
| | <i>II</i> | 0.55 | 91.2 | 1.8 | 0.8 | 6.2 | 3.2 |
| <i>La Jagua</i> | <i>I</i> | 0.54 | 85.2 | 2.0 | 7.8 | 5.0 | 4.1 |
| | <i>II</i> | 0.53 | 84.2 | 2.4 | 10.2 | 3.2 | 4.5 |
| <i>El Cerrejon</i> | <i>I</i> | 0.56 | 90.8 | 2.4 | 3.4 | 3.4 | 3.3 |
| | <i>II</i> | 0.59 | 90.6 | 1.6 | 3.2 | 4.6 | 3.9 |
| <i>Caypa</i> | <i>I</i> | 0.60 | 96.8 | 0.4 | 2.4 | 0.4 | 3.4 |
| | <i>II</i> | 0.59 | 95.2 | 0.4 | 3.6 | 0.8 | 3.6 |
| <i>Paso Diablo</i> | <i>I</i> | 0.64 | 88.8 | 2.4 | 2.0 | 6.8 | 5.5 |
| | <i>II</i> | 0.61 | 88.0 | 2.8 | 2.4 | 6.8 | 6.0 |
| <i>Maturin</i> | <i>I</i> | 0.74 | 88.0 | 2.0 | 3.0 | 7.0 | 5.9 |
| | <i>II</i> | 0.71 | 86.8 | 1.2 | 2.6 | 9.4 | 7.0 |
| <i>Ashland</i> | <i>I</i> | 0.76 | 78.8 | 7.5 | 4.2 | 9.5 | 6.3 |
| | <i>II</i> | 0.75 | 68.5 | 14.3 | 4.6 | 12.6 | 8.4 |

From the maceral analysis data in Table 4.12, it is possible to identify some general trends. It is clearly evident that vitrinite often concentrates in the smaller size fractions. Although this may not always be the case, the behaviour of vitrinites during grinding is a possible explanation for this. Vitrinites are

characterised by their high degree of brittleness, and so, during grinding, they fracture and splinter easily to form very small fragments which are concentrated in the fines (Stach et al., 1982). Conversely, liptinites shows a tendency to concentrate in the larger fractions. This fractionation behaviour of liptinites has been observed in other coals (Thompson et al., 1993), and can be attributed to their toughness and resistance to crack formation, which may impede fragmentation during grinding (Stach et al., 1982).

Fusinite is known to be denser and harder than the other macerals, however, it is much more brittle and, therefore, it is likely to concentrate in the lowest size fractions (Stach et al., 1982). However, fusinite may become harder when impregnated with minerals, and as a result will be found mostly in the larger size fractions. Semifusinite exhibits properties which range between those of vitrinite and fusinite but mineral impregnations are less likely to occur. From the petrographic analysis data in Table 4.12, both inertinite sub-macerals fusinite and semifusinite do not show a definite trend with particle size.

In terms of rank, small variations in the figures are reported between the two size fractions. The results indicate that all are bituminous coals. From the vitrinite reflectance histograms it was observed that most of the coals gave a normal or '*quasi-normal*' distribution which is characteristic of an unblended coal sample.

4.2.3 Image Analysis of Coals

The grey scale histograms of the coal fractions, as derived from the RAP analysis, are shown Appendix B. The profiles take the form of frequency versus grey scale histograms. The % unreactives figures for each fraction are given in Table 4.12.

From the grey scale histograms, it is possible to tentatively assign various peaks to the major maceral groups. Nevertheless, the exact position of these peaks is rank dependent, and there can be a considerable degree of overlap, particularly between vitrinite and semifusinite. For instance, for the lowest ranked coals, Bijao, Fila Maestra, and La Loma, the liptinite peaks lie below grey level 38, whilst for the subsequent coals in the rank series (Oreganal, La Jagua, El Cerrejon, Caypa, and

Paso Diablo), this grey level boundary is around 45. For the higher ranked coals (Maturin and Ashland), the liptinite peak is moderately higher (approximately 55). The vitrinite peaks lie between the liptinite boundary and a maximum grey level on the range of 100-120 for most of the coals, excluding the higher ranked coals Paso Diablo, Maturin, and Ashland, where the boundaries are approximately 140, 160, and 175 respectively. Regarding inertinite, one or more distinctive peaks can be distinguished beyond a grey level of 210 for all of the coals, and this can be assigned to semifusinite (specially that of high reflectance), fusinite, and mineral matter.

The cumulative percentage curve of the histograms of La Jagua, Oreganal, Caypa, Bijao, El Cerrejon, and La Loma, appear to be rather steep indicating low variation in vitrinite reflectance and low levels of semifusinite. Paso Diablo, Ashland and Maturin show relatively large amounts of material with a grey scale greater than 190 and are clearly different from the other coals. These differences may be manifested in combustion performance and in the pyrolysed chars that are formed.

4.2.4 Drop Tube Furnace Conditions

All chars were prepared at the same conditions used in the previous section, i.e. three different gas temperatures (1000, 1150, and 1300°C), a residence time of 200 ms, and a slightly oxidising atmosphere (1% oxygen in nitrogen).

4.2.5 Char Collection Efficiency

Ash content of the coals and chars are given in Table 4.13 whereas Table 4.14 contains data on the char yields and the collection efficiency for all the samples. A variation of collection efficiency in accordance with changes in ash levels, particle size, and the operating temperature can be seen from the tables. As in the previous section, collection efficiency values were all greater than 80% and in some cases greater than 100%. Generally speaking, a decrease in collection efficiency occurs with increasing particle size. This is more apparent at 1000°C where collection efficiency values were all higher for the smaller size fraction.

There is also a general trend of decreasing collection efficiency with increasing the DTF operating temperature for most of the coals. It is not clear why larger particles tend to give lower collection efficiencies, although it is most likely associated with the way these particles behave inside the hot zone before they are collected.

Table 4.13 Ash content of coal and chars

| Coal | Particle Size | Coal Ash Content | Char Ash Content (wt% db) | | |
|---------------------|---------------|------------------|---------------------------|--------|--------|
| | μm | (wt% db) | 1000°C | 1150°C | 1300°C |
| <i>Bijao</i> | 53-75 | 4.2 | 9.90 | 11.64 | 13.42 |
| | 106-125 | 4.1 | 8.86 | 10.94 | 12.16 |
| <i>Fila Maestra</i> | 53-75 | 5.9 | 13.29 | 14.79 | 16.42 |
| | 106-125 | 6.2 | 13.08 | 14.52 | 15.82 |
| <i>La Loma</i> | 53-75 | 4.6 | 10.07 | 11.14 | 14.01 |
| | 106-125 | 4.4 | 9.14 | 10.36 | 12.01 |
| <i>Oreganal</i> | 53-75 | 3.7 | 8.32 | 9.06 | 9.96 |
| | 106-125 | 2.5 | 5.56 | 6.35 | 6.98 |
| <i>La Jagua</i> | 53-75 | 2.9 | 5.86 | 7.06 | 7.94 |
| | 106-125 | 2.5 | 4.82 | 5.55 | 6.56 |
| <i>El Cerrejon</i> | 53-75 | 4.5 | 9.36 | 11.03 | 12.54 |
| | 106-125 | 3.5 | 7.42 | 8.33 | 9.56 |
| <i>Caypa</i> | 53-75 | 1.9 | 4.15 | 4.94 | 5.56 |
| | 106-125 | 2.2 | 4.87 | 5.60 | 6.07 |
| <i>Paso Diablo</i> | 53-75 | 4.9 | 9.28 | 10.66 | 11.54 |
| | 106-125 | 2.7 | 5.42 | 6.24 | 7.07 |
| <i>Maturin</i> | 53-75 | 4.1 | 7.90 | 9.46 | 10.43 |
| | 106-125 | 3.7 | 7.07 | 7.78 | 8.91 |
| <i>Ashland</i> | 53-75 | 10.5 | 17.81 | 19.95 | 21.92 |
| | 106-125 | 9.2 | 15.23 | 16.02 | 17.83 |

Table 4.14 Char yield and collection efficiency results

| Coal | Particle Size | Char Yield (g/g of coal fed) | | | Collection Efficiency (%) | | |
|---------------------|---------------|------------------------------|--------|--------|---------------------------|--------|--------|
| | µm | 1000°C | 1150°C | 1300°C | 1000°C | 1150°C | 1300°C |
| <i>Bijao</i> | 53-75 | 0.496 | 0.369 | 0.270 | 116.0 | 101.6 | 85.7 |
| | 106-125 | 0.461 | 0.401 | 0.299 | 100.6 | 108.0 | 89.7 |
| <i>Fila Maestra</i> | 53-75 | 0.431 | 0.364 | 0.317 | 97.6 | 91.8 | 88.8 |
| | 106-125 | 0.430 | 0.396 | 0.333 | 90.8 | 92.9 | 85.1 |
| <i>La Loma</i> | 53-75 | 0.471 | 0.343 | 0.290 | 104.0 | 83.6 | 89.1 |
| | 106-125 | 0.448 | 0.382 | 0.316 | 92.7 | 89.7 | 86.0 |
| <i>Oreganal</i> | 53-75 | 0.503 | 0.384 | 0.337 | 112.6 | 93.7 | 90.2 |
| | 106-125 | 0.453 | 0.346 | 0.329 | 101.4 | 88.4 | 92.6 |
| <i>La Jagua</i> | 53-75 | 0.489 | 0.395 | 0.350 | 99.5 | 97.0 | 96.5 |
| | 106-125 | 0.466 | 0.371 | 0.347 | 91.0 | 83.3 | 92.2 |
| <i>El Cerrejon</i> | 53-75 | 0.499 | 0.384 | 0.349 | 104.4 | 94.8 | 97.8 |
| | 106-125 | 0.470 | 0.373 | 0.358 | 100.3 | 89.4 | 98.5 |
| <i>Caypa</i> | 53-75 | 0.473 | 0.401 | 0.343 | 104.5 | 105.6 | 101.7 |
| | 106-125 | 0.472 | 0.418 | 0.359 | 102.6 | 104.4 | 97.3 |
| <i>Paso Diablo</i> | 53-75 | 0.504 | 0.436 | 0.413 | 95.7 | 95.0 | 97.6 |
| | 106-125 | 0.467 | 0.423 | 0.367 | 92.4 | 96.4 | 94.9 |
| <i>Maturin</i> | 53-75 | 0.475 | 0.433 | 0.438 | 91.4 | 99.9 | 111.5 |
| | 106-125 | 0.454 | 0.438 | 0.404 | 86.6 | 92.0 | 97.1 |
| <i>Ashland</i> | 53-75 | 0.541 | 0.461 | 0.435 | 91.4 | 87.1 | 90.3 |
| | 106-125 | 0.548 | 0.468 | 0.418 | 90.9 | 81.7 | 81.2 |

4.2.6 DTF Volatiles and R Factor

Proximate and DTF volatiles data along with R factor values for the coal and char fractions are given in Table 4.15. Plots of the R factors versus the DTF operating temperature were produced for each size fraction and they are shown in Figures 4.10 and 4.11. It can be seen from the tables and figures that the R factors and DTF volatiles increase with increasing DTF temperature. In most cases, the R factors were correspondingly higher for the smaller particle size. However, Oreganal and Paso Diablo did not follow this trend.

It is evident from these results that a coal that is exposed to high temperatures and heating rates will emit more volatiles than that determined by standard proximate analysis and this agrees with the findings of other researchers (Gibbins et al., 1991; Thompson et al., 1993). In effect, these particular coals emitted approximately 20% to 47% more volatiles at 1000°C, from 29% to 64% at 1150°C, and from 47% to 75% at 1300°C. The variation in R factor serves to demonstrate the inadequacy of the proximate volatile matter as a suitable indicator of the behaviour of coal during rapid heating.

4.2.7 Char Intrinsic Reactivity

The intrinsic reactivity results for all the char samples are given in Table 4.16. Char burning profiles, as derived from the intrinsic reactivity analysis, are presented in Appendix C. The profiles take the form of DTA output (μVmg^{-1}) as a function temperature, and are provided for each coal fraction as a function of DTF temperature.

4.2.7.1 Peak Temperature

Plots of the peak temperature data as a function of the DTF operating temperature for both the smaller, and the coarser fractions, are presented in Figures 12 and 13, respectively. It is clearly evident from the graphs that char reactivity decreases as the operating temperature increases, independently of particle size, and coal type. With the exception of the American coal Ashland, there is an increase in PT with

coal rank. Bijao, La Loma, and Fila Maestra show high reactivity (low PT values), whilst Paso Diablo and Maturin exhibit high PTs. El Cerrejon is the clear exception since it exhibits higher reactivity than La Jagua. However, it is well known that char intrinsic reactivity is not only affected by the rank of the parent coal, but also by its chemical composition and maceral content.

Table 4.15 Proximate and DTF volatiles and R factor data for the ten coals and chars

| Coal | Particle size | Proximate Volatiles (wt% daf) | DTF Volatiles (wt% daf) | | | R factor | | |
|---------------------|---------------|-------------------------------|-------------------------|--------|--------|----------|--------|--------|
| | µm | | 1000°C | 1150°C | 1300°C | 1000°C | 1150°C | 1300°C |
| <i>Bijao</i> | 53-75 | 45.3 | 59.8 | 66.4 | 71.5 | 1.32 | 1.47 | 1.58 |
| | 106-125 | 45.3 | 56.5 | 65.6 | 69.4 | 1.25 | 1.45 | 1.53 |
| <i>Fila Maestra</i> | 53-75 | 44.3 | 59.3 | 64.1 | 68.3 | 1.34 | 1.45 | 1.54 |
| | 106-125 | 44.2 | 56.1 | 61.1 | 64.9 | 1.27 | 1.38 | 1.47 |
| <i>La Loma</i> | 53-75 | 40.5 | 57.3 | 61.9 | 70.7 | 1.42 | 1.53 | 1.75 |
| | 106-125 | 40.6 | 54.1 | 60.0 | 66.2 | 1.33 | 1.48 | 1.63 |
| <i>Oreganal</i> | 53-75 | 39.1 | 57.4 | 61.3 | 65.1 | 1.47 | 1.57 | 1.67 |
| | 106-125 | 39.0 | 56.8 | 62.4 | 66.1 | 1.45 | 1.60 | 1.69 |
| <i>La Jagua</i> | 53-75 | 38.7 | 52.4 | 61.0 | 65.7 | 1.35 | 1.57 | 1.70 |
| | 106-125 | 39.2 | 50.0 | 56.9 | 63.9 | 1.28 | 1.45 | 1.63 |
| <i>El Cerrejon</i> | 53-75 | 38.8 | 54.7 | 62.2 | 67.3 | 1.41 | 1.60 | 1.74 |
| | 106-125 | 39.1 | 55.1 | 60.4 | 65.9 | 1.41 | 1.55 | 1.69 |
| <i>Caypa</i> | 53-75 | 38.5 | 55.8 | 63.3 | 67.5 | 1.45 | 1.64 | 1.75 |
| | 106-125 | 38.9 | 55.2 | 61.4 | 64.5 | 1.42 | 1.58 | 1.66 |
| <i>Paso Diablo</i> | 53-75 | 38.0 | 49.8 | 57.0 | 60.6 | 1.31 | 1.50 | 1.59 |
| | 106-125 | 38.3 | 50.9 | 57.7 | 63.0 | 1.33 | 1.51 | 1.64 |
| <i>Maturin</i> | 53-75 | 36.3 | 50.1 | 59.1 | 63.3 | 1.38 | 1.63 | 1.75 |
| | 106-125 | 36.6 | 49.4 | 54.3 | 60.6 | 1.35 | 1.48 | 1.66 |
| <i>Ashland</i> | 53-75 | 34.9 | 45.6 | 52.7 | 58.0 | 1.31 | 1.51 | 1.66 |
| | 106-125 | 36.4 | 43.8 | 47.0 | 53.4 | 1.20 | 1.29 | 1.47 |

Table 4.16 Char intrinsic reactivity data as a function of temperature and particle size

| Coal | Particle Size | Peak Temperature (°C) | | | Burnout Temperature (°C) | | |
|---------------------|---------------|-----------------------|--------|--------|--------------------------|--------|--------|
| | µm | 1000°C | 1150°C | 1300°C | 1000°C | 1150°C | 1300°C |
| <i>Bijao</i> | 53-75 | 384 | 444 | 474 | 535 | 537 | 544 |
| | 106-125 | 392 | 444 | 478 | 540 | 545 | 560 |
| <i>Fila Maestra</i> | 53-75 | 419 | 483 | 515 | 495 | 533 | 558 |
| | 106-125 | 426 | 483 | 532 | 540 | 542 | 564 |
| <i>La Loma</i> | 53-75 | 401 | 459 | 536 | 530 | 562 | 573 |
| | 106-125 | 426 | 492 | 545 | 560 | 565 | 585 |
| <i>Oreganal</i> | 53-75 | 458 | 530 | 566 | 535 | 577 | 607 |
| | 106-125 | 474 | 538 | 571 | 560 | 585 | 619 |
| <i>La Jagua</i> | 53-75 | 503 | 535 | 590 | 552 | 584 | 621 |
| | 106-125 | 516 | 562 | 600 | 554 | 604 | 646 |
| <i>El Cerrejon</i> | 53-75 | 457 | 514 | 577 | 539 | 577 | 627 |
| | 106-125 | 469 | 540 | 577 | 553 | 591 | 630 |
| <i>Caypa</i> | 53-75 | 502 | 541 | 594 | 547 | 579 | 635 |
| | 106-125 | 505 | 567 | 627 | 560 | 612 | 670 |
| <i>Paso Diablo</i> | 53-75 | 507 | 547 | 612 | 565 | 600 | 641 |
| | 106-125 | 511 | 557 | 629 | 579 | 611 | 695 |
| <i>Maturin</i> | 53-75 | 503 | 543 | 618 | 563 | 607 | 650 |
| | 106-125 | 508 | 550 | 623 | 573 | 613 | 656 |
| <i>Ashland</i> | 53-75 | 461 | 532 | 546 | 562 | 607 | 624 |
| | 106-125 | 476 | 564 | 577 | 567 | 622 | 637 |

Figure 4.10 A plot of R Factor as a function of operating temperature for the 53-75 μm char fractions

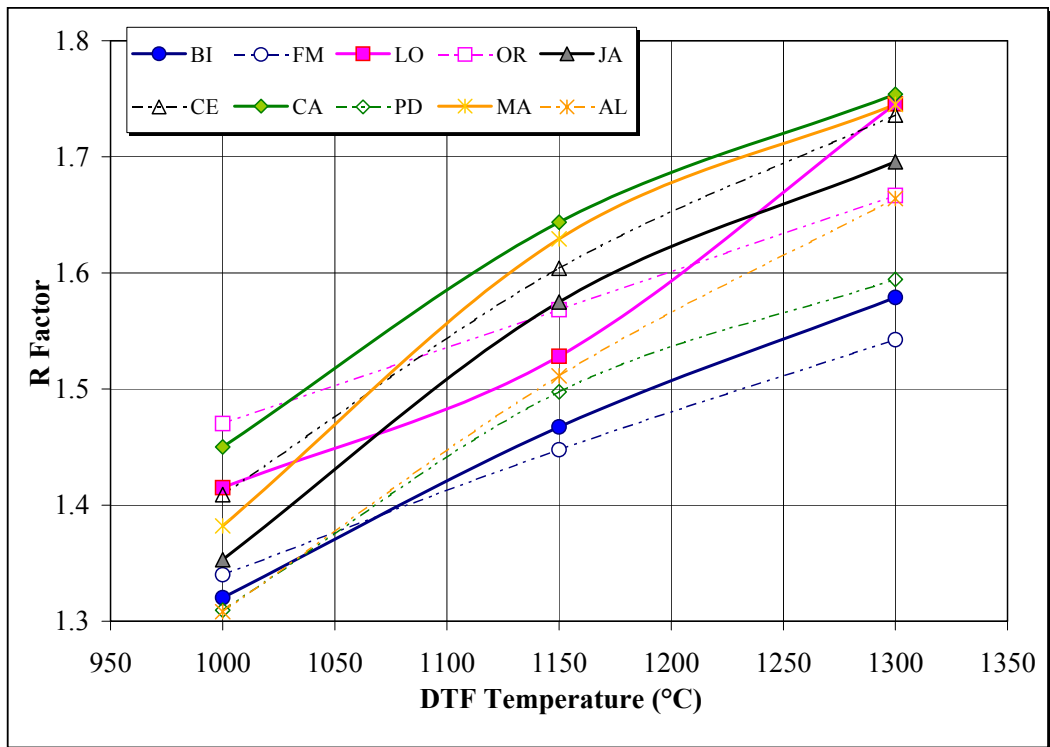


Figure 4.11 A plot of R Factor as a function of operating temperature for the 106-125 μm char fractions

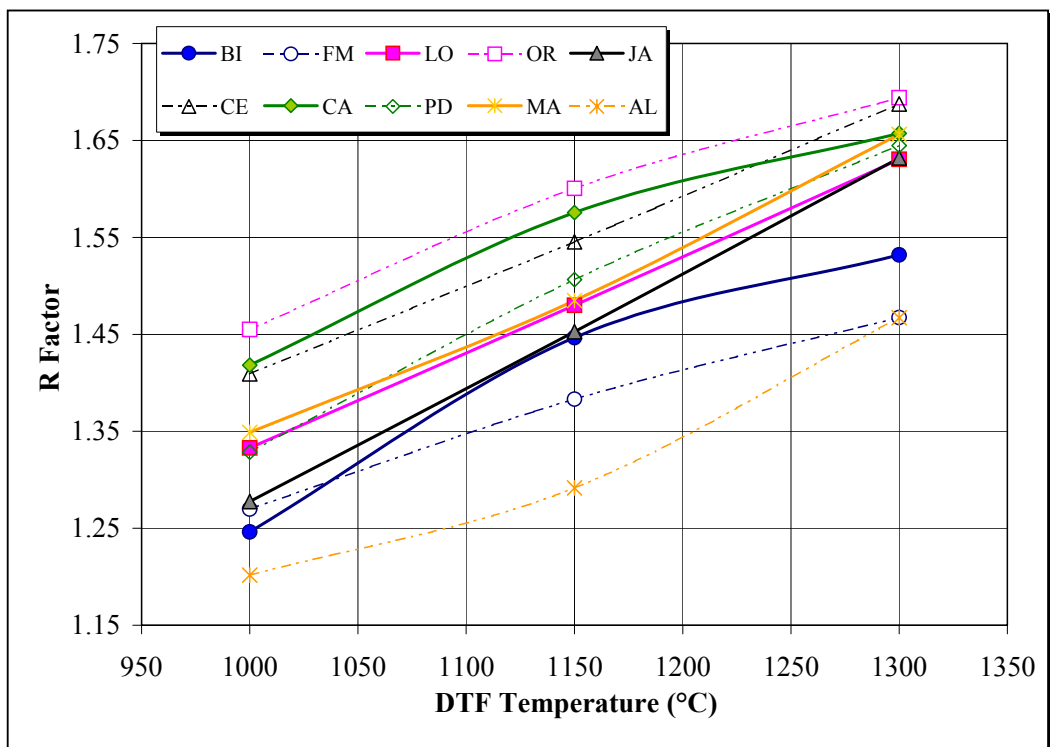


Figure 4.12 A Plot of peak temperature as a function of the DTF operating temperature for the 53-75 μm char fractions

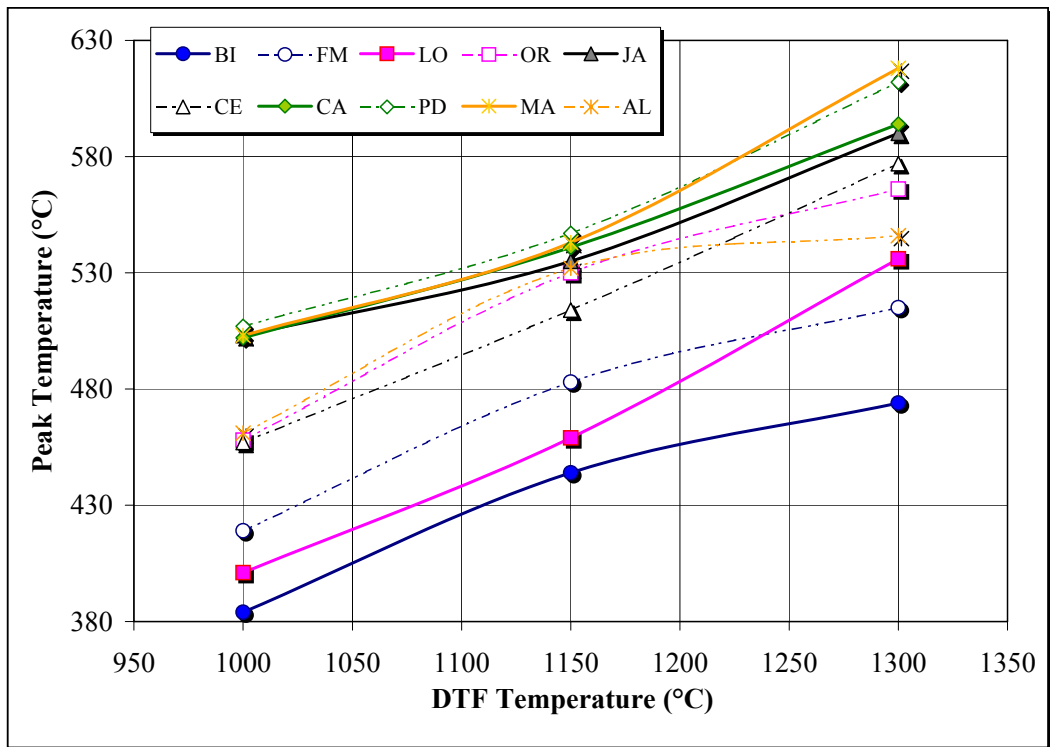


Figure 4.13 A Plot of peak temperature as a function of the DTF operating temperature for the 106-125 μm char fractions

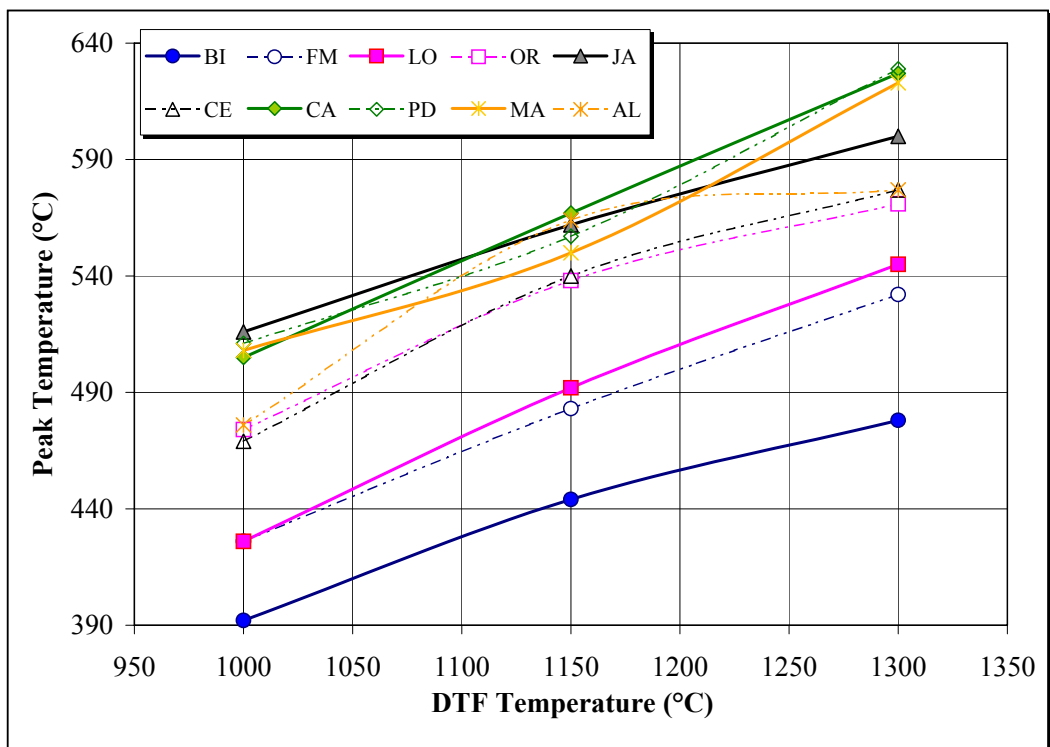


Figure 4.14 A Plot of burnout temperature as a function of the DTF operating temperature for the 53-75 μm char fractions

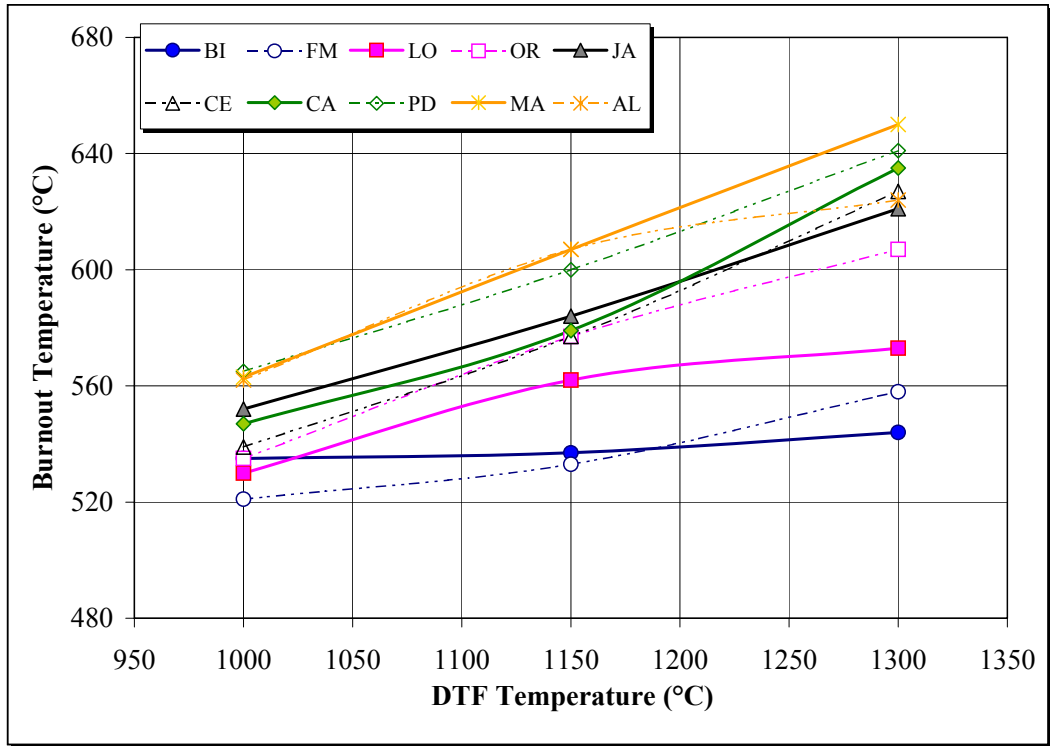
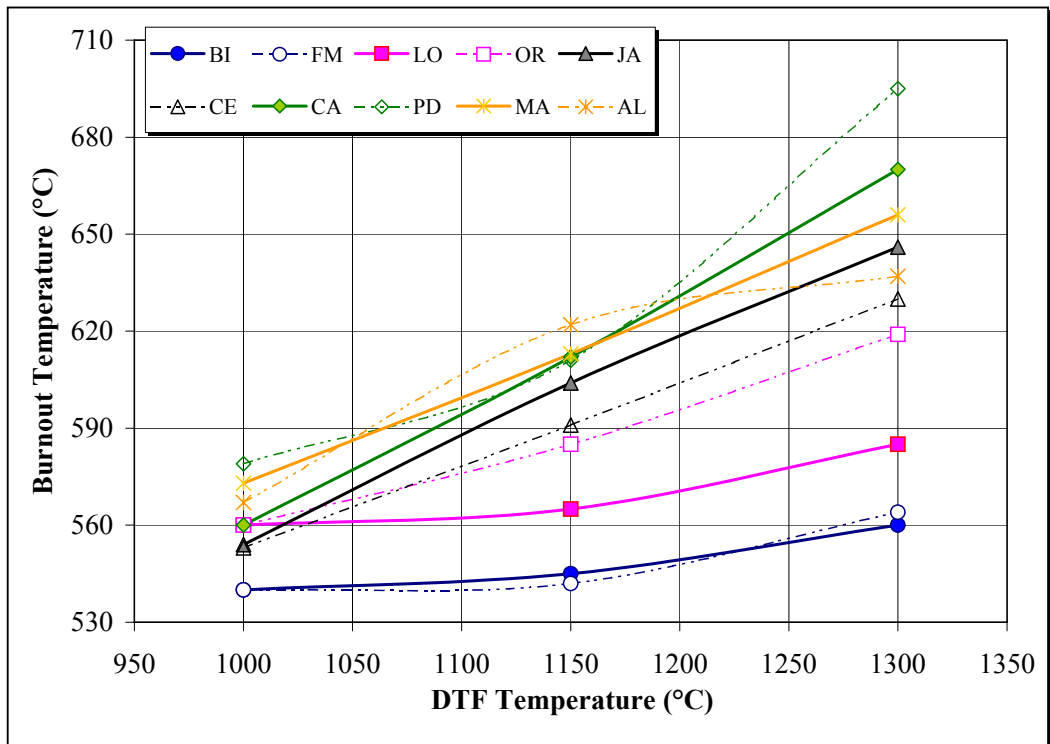


Figure 4.15 A Plot of burnout temperature as a function of the DTF operating temperature for the 106-125 μm char fractions



Overall, the 106-125 μm fractions gave higher PTs than the 53-75 μm fractions. Nevertheless, these differences are not very significant (do not exceed 8°C) for Bijao and Maturin under any condition. Ashland is the only coal where the PT values for the 106-125 μm fraction is significantly higher than the values for the smaller fraction at any given condition. For some coals, the effect of particle size is influenced by the temperature of operation of the DTF. For La Loma, Oreganal, La Jagua, and El Cerrejon the effect of particle size is more pronounced at the lowest temperatures (1000°C, or 1150°C, or both). Conversely, for the remaining coals (Fila Maestra, Caypa and Paso Diablo), the particle size effect is more evident as the DTF temperature increases (only at 1300°C for Fila Maestra).

From the plots (Figures 12 and 13), it can be seen that all the South American coals show a gradual increase in PT with increasing DTF temperature. These differences vary from 71°C to 14°C, and from 88°C down to 13°C, for the smaller and the coarser fractions respectively. For the USA coal (Ashland), the increase in PT from 1000°C to 1150°C is considerably higher than that from 1150°C to 1300°C.

4.2.7.2 *Burnout Temperature*

Figure 4.14 shows a plot of the burnout temperature as a function of the DTF operating temperature for the 53-75 μm fractions. Similarly, a plot for the 106-125 μm fractions is presented in Figure 4.15. The results are similar to those of the peak temperature, i.e. char reactivity decreases (BT increases) as the operating temperature increases, independently of particle size, and coal type.

As with the PT, the lower rank coals (Bijao, La Loma, and Fila Maestra) gave the lowest BT values, indicating high reactivity. Further to this, little variations of BT with increasing DTF temperature was observed for these coals. The higher rank coals, such as Caypa, Paso Diablo, Maturin, and to some extent Ashland, all tend to give higher BTs, indicating lower reactivity.

The spread of results is, generally, smaller than for PT for the char samples pyrolysed at 1000°C, particularly for the 106-125 μm fractions. This indicates that the burnout of the most inert fraction of char within any of these samples,

takes place at similar temperatures. With increasing DTF operating temperature, however, the spread of results increases as can be seen in Figures 4.14 and 4.15. Thus, for the 106-125 μm fractions, BT values range only from 540 to 579°C at a DTF temperature of 1000°C, from 542 to 622°C at 1150°C, and from 560 to 695°C at 1300°C.

4.2.8 Optical Morphology and Automatic Analysis of Chars

All the samples were analysed for optical morphology using reflected light microscopy. The most important parameters considered in the determination of the different char types were wall thickness, and basic char structure, using a modified version of Bailey's char morphology system, which has been explained in chapter 2 (section 2.5.2). Tables 4.17 to 4.19 show the results of the manual char analysis for the samples produced in the DTF at 1000°C, 1150°C, and 1300°C respectively. Previous work in this laboratory suggested grouping all thin-walled chars together (tenuispheres and tenuinetworks), all thick-walled chars together (crassispheres and crassinetworks), and combining inertoid and solid with fusinoid chars as solids (Lester, 1994, Gilfillan, 1999). This facilitates the interpretation and discussion of the data, which is summarised in Table 4.20.

Automatic char analysis was performed on all the char samples. The results obtained are presented in Table 4.21, and are presented as relative char wall thicknesses (ACA5). This parameter is the cumulative percentage of char material covered by five contours as described in chapter 3 (section 3.5.3). ACA5 was taken as the most meaningful result, since the thickness of the char material may be used to provide an indication of burnout potential during actual combustion, whether mass transfer limited or not. For thin-walled chars, most of the material is effectively enclosed by five contours whereas thick-walled chars require more contours, and even more for the solid chars (fusinoid and inertoid chars included). High ACA5 values are hence associated with high concentrations of thin-walled chars and low values of ACA5 with a high percentage of thick-walled and solid chars.

Table 4.17 Manual char analysis results for the samples at 1000°C

| Coal | Particle Size | Char Type Composition (vol%) ^a | | | | | |
|---------------------|-------------------|---|------|------|------|-----|-----|
| | (μm) | TS | CS | TN | CN | I | F/S |
| <i>Bijao</i> | 53-75 | 0.0 | 1.1 | 51.5 | 45.9 | 1.3 | 0.2 |
| | 106-125 | 0.0 | 0.7 | 49.6 | 47.7 | 1.6 | 0.4 |
| <i>Fila Maestra</i> | 53-75 | 8.9 | 12.4 | 26.5 | 50.1 | 1.1 | 1.0 |
| | 106-125 | 4.5 | 16.7 | 20.3 | 56.1 | 1.0 | 1.4 |
| <i>La Loma</i> | 53-75 | 18.7 | 33.5 | 15.7 | 29.8 | 1.3 | 1.0 |
| | 106-125 | 8.4 | 19.8 | 19.7 | 49.3 | 1.3 | 1.5 |
| <i>Oreganal</i> | 53-75 | 28.7 | 31.5 | 12.5 | 24.3 | 2.1 | 0.9 |
| | 106-125 | 19.8 | 38.4 | 9.8 | 28.7 | 1.8 | 1.5 |
| <i>La Jagua</i> | 53-75 | 25.7 | 45.4 | 5.8 | 18.8 | 2.2 | 2.1 |
| | 106-125 | 13.6 | 46.6 | 1.7 | 33.5 | 2.2 | 2.4 |
| <i>El Cerrejon</i> | 53-75 | 33.1 | 40.5 | 4.9 | 18.4 | 2.0 | 1.1 |
| | 106-125 | 20.1 | 50.0 | 2.2 | 23.5 | 1.9 | 2.3 |
| <i>Caypa</i> | 53-75 | 42.3 | 52.3 | 0.5 | 2.4 | 1.1 | 1.4 |
| | 106-125 | 29.5 | 64.0 | 0.7 | 3.1 | 0.8 | 1.9 |
| <i>Paso Diablo</i> | 53-75 | 35.3 | 37.2 | 5.1 | 17.2 | 1.9 | 3.3 |
| | 106-125 | 5.4 | 53.6 | 0.3 | 34.1 | 2.8 | 3.8 |
| <i>Maturin</i> | 53-75 | 15.6 | 45.0 | 0.0 | 32.9 | 2.6 | 3.9 |
| | 106-125 | 5.5 | 45.1 | 0.0 | 42.7 | 2.3 | 4.4 |
| <i>Ashland</i> | 53-75 | 17.3 | 38.5 | 3.2 | 35.0 | 4.1 | 1.9 |
| | 106-125 | 12.8 | 42.8 | 2.3 | 33.5 | 5.4 | 3.2 |

^aTS=Tenuisphere; CS=Crassisphere; TN=Tenuinetwork; CN=Crassinetwork; I=Inertoid; F/S=Fusinoid/Solid

Table 4.18 Manual char analysis results for the samples at 1150°C

| Coal | Particle Size | Char Type Composition (vol%) ^a | | | | | |
|---------------------|-------------------|---|------|------|------|-----|-----|
| | (μm) | TS | CS | TN | CN | I | F/S |
| <i>Bijao</i> | 53-75 | 0.5 | 0.5 | 63.5 | 34.4 | 0.8 | 0.3 |
| | 106-125 | 0.4 | 0.3 | 56.1 | 41.2 | 1.6 | 0.4 |
| <i>Fila Maestra</i> | 53-75 | 24.5 | 7.0 | 34.6 | 32.0 | 1.0 | 0.9 |
| | 106-125 | 7.7 | 15.8 | 25.5 | 48.8 | 1.0 | 1.2 |
| <i>La Loma</i> | 53-75 | 28.5 | 20.2 | 22.2 | 26.4 | 1.4 | 1.3 |
| | 106-125 | 6.2 | 9.7 | 34.8 | 46.7 | 1.3 | 1.3 |
| <i>Oreganal</i> | 53-75 | 50.6 | 15.8 | 14.6 | 16.1 | 2.0 | 0.9 |
| | 106-125 | 27.2 | 31.9 | 13.5 | 24.5 | 1.6 | 1.3 |
| <i>La Jagua</i> | 53-75 | 48.8 | 29.0 | 3.3 | 15.1 | 2.4 | 1.4 |
| | 106-125 | 27.2 | 43.5 | 1.3 | 24.6 | 2.2 | 1.2 |
| <i>El Cerrejon</i> | 53-75 | 49.5 | 24.3 | 6.1 | 17.7 | 1.4 | 1.0 |
| | 106-125 | 25.6 | 50.2 | 3.7 | 16.6 | 1.7 | 2.2 |
| <i>Caypa</i> | 53-75 | 63.4 | 30.7 | 0.3 | 3.5 | 0.8 | 1.3 |
| | 106-125 | 46.2 | 47.6 | 0.5 | 3.2 | 0.8 | 1.7 |
| <i>Paso Diablo</i> | 53-75 | 38.6 | 27.6 | 6.3 | 23.2 | 1.7 | 2.6 |
| | 106-125 | 8.0 | 63.4 | 0.1 | 22.4 | 2.0 | 4.1 |
| <i>Maturin</i> | 53-75 | 23.2 | 45.1 | 0.0 | 26.5 | 2.0 | 3.2 |
| | 106-125 | 12.9 | 43.7 | 0.0 | 37.8 | 1.9 | 3.7 |
| <i>Ashland</i> | 53-75 | 19.8 | 41.2 | 2.8 | 30.8 | 4.0 | 1.4 |
| | 106-125 | 13.7 | 47.1 | 2.2 | 28.8 | 4.7 | 3.5 |

^aTS=Tenuisphere; CS=Crassisphere; TN=Tenuinetwork; CN=Crassinetwork; I=Inertoid; F/S=Fusinoid/Solid

Table 4.19 Manual char analysis results for the samples at 1300°C

| Coal | Particle Size | Char Type Composition (vol%) ^a | | | | | |
|---------------------|-------------------|---|------|------|------|-----|-----|
| | (μm) | TS | CS | TN | CN | I | F/S |
| <i>Bijao</i> | 53-75 | 0.7 | 0.1 | 75.2 | 22.7 | 0.9 | 0.4 |
| | 106-125 | 0.5 | 0.3 | 58.4 | 39.1 | 1.1 | 0.6 |
| <i>Fila Maestra</i> | 53-75 | 28.9 | 7.8 | 35.9 | 25.9 | 0.8 | 0.7 |
| | 106-125 | 22.3 | 13.2 | 27.8 | 35.1 | 1.0 | 0.6 |
| <i>La Loma</i> | 53-75 | 37.7 | 15.4 | 34.5 | 11.1 | 0.8 | 0.5 |
| | 106-125 | 5.3 | 8.4 | 48.1 | 36.7 | 1.1 | 0.4 |
| <i>Oreganal</i> | 53-75 | 58.1 | 9.9 | 14.7 | 14.8 | 1.8 | 0.7 |
| | 106-125 | 35.4 | 22.4 | 14.3 | 25.2 | 1.7 | 1.0 |
| <i>La Jagua</i> | 53-75 | 56.8 | 19.7 | 4.4 | 15.6 | 1.8 | 1.7 |
| | 106-125 | 30.2 | 54.3 | 1.6 | 11.3 | 2.0 | 0.6 |
| <i>El Cerrejon</i> | 53-75 | 60.7 | 18.9 | 4.9 | 13.4 | 1.2 | 0.9 |
| | 106-125 | 30.5 | 49.0 | 4.8 | 12.7 | 1.6 | 1.4 |
| <i>Caypa</i> | 53-75 | 74.5 | 19.4 | 0.4 | 3.9 | 0.6 | 1.2 |
| | 106-125 | 66.2 | 27.7 | 0.7 | 3.2 | 0.7 | 1.5 |
| <i>Paso Diablo</i> | 53-75 | 48.4 | 20.1 | 6.2 | 21.4 | 1.5 | 2.4 |
| | 106-125 | 15.9 | 52.5 | 0.3 | 26.4 | 1.5 | 3.4 |
| <i>Maturin</i> | 53-75 | 38.3 | 39.1 | 0.5 | 17.6 | 1.8 | 2.7 |
| | 106-125 | 20.2 | 32.3 | 0.0 | 42.4 | 1.7 | 3.4 |
| <i>Ashland</i> | 53-75 | 23.7 | 40.9 | 2.7 | 27.9 | 3.8 | 1.0 |
| | 106-125 | 16.2 | 45.8 | 2.0 | 29.4 | 5.5 | 1.1 |

^aTS=Tenuisphere; CS=Crassisphere; TN=Tenuinetwork; CN=Crassinetwork; I=Inertoid; F/S=Fusinoid/Solid

Table 4.20 Summary of manual char analysis at the three DTF temperatures

| Coal | Particle Size | 1000°C | | | 1150°C | | | 1300°C | | |
|---------------------|-------------------|-------------|--------------|--------|-------------|--------------|--------|-------------|--------------|--------|
| | (μm) | Thin Walled | Thick Walled | Solids | Thin Walled | Thick Walled | Solids | Thin Walled | Thick Walled | Solids |
| <i>Bijao</i> | 53-75 | 51.5 | 47.0 | 1.5 | 64.0 | 34.9 | 1.1 | 75.9 | 22.8 | 1.3 |
| | 106-125 | 49.6 | 48.4 | 2.0 | 56.5 | 41.5 | 2.0 | 58.9 | 39.4 | 1.7 |
| <i>Fila Maestra</i> | 53-75 | 35.4 | 62.5 | 2.1 | 59.1 | 39.0 | 1.9 | 64.8 | 33.7 | 1.5 |
| | 106-125 | 24.8 | 72.8 | 2.4 | 33.2 | 64.6 | 2.2 | 50.1 | 48.3 | 1.6 |
| <i>La Loma</i> | 53-75 | 34.4 | 63.3 | 2.3 | 50.7 | 46.6 | 2.7 | 72.2 | 26.5 | 1.3 |
| | 106-125 | 28.1 | 69.1 | 2.8 | 41.0 | 56.4 | 2.6 | 53.4 | 45.1 | 1.5 |
| <i>Oreganal</i> | 53-75 | 41.2 | 55.8 | 3.0 | 65.2 | 31.9 | 2.9 | 72.8 | 24.7 | 2.5 |
| | 106-125 | 29.6 | 67.1 | 3.3 | 40.7 | 56.4 | 2.9 | 49.7 | 47.6 | 2.7 |
| <i>La Jagua</i> | 53-75 | 31.5 | 64.2 | 4.3 | 52.1 | 44.1 | 3.8 | 61.2 | 35.3 | 3.5 |
| | 106-125 | 15.3 | 80.1 | 4.6 | 28.5 | 68.1 | 3.4 | 31.8 | 65.6 | 2.6 |
| <i>El Cerrejon</i> | 53-75 | 38.0 | 58.9 | 3.1 | 55.6 | 42.0 | 2.4 | 65.6 | 32.3 | 2.1 |
| | 106-125 | 22.3 | 73.5 | 4.2 | 29.3 | 66.8 | 3.9 | 35.3 | 61.7 | 3.0 |
| <i>Caypa</i> | 53-75 | 42.8 | 54.7 | 2.5 | 63.7 | 34.2 | 2.1 | 74.9 | 23.3 | 1.8 |
| | 106-125 | 30.2 | 67.1 | 2.7 | 46.7 | 50.8 | 2.5 | 66.9 | 30.9 | 2.2 |
| <i>Paso Diablo</i> | 53-75 | 40.4 | 54.4 | 5.2 | 44.9 | 50.8 | 4.3 | 54.6 | 41.5 | 3.9 |
| | 106-125 | 5.7 | 87.7 | 6.6 | 8.1 | 85.8 | 6.1 | 16.2 | 78.9 | 4.9 |
| <i>Maturin</i> | 53-75 | 15.6 | 77.9 | 6.5 | 23.2 | 71.6 | 5.2 | 38.8 | 56.7 | 4.5 |
| | 106-125 | 5.5 | 87.8 | 6.7 | 12.9 | 81.5 | 5.6 | 20.2 | 74.7 | 5.1 |
| <i>Ashland</i> | 53-75 | 20.5 | 73.5 | 6.0 | 22.6 | 72.0 | 5.4 | 26.4 | 68.8 | 4.8 |
| | 106-125 | 15.1 | 76.3 | 8.6 | 15.9 | 75.9 | 8.2 | 18.2 | 75.2 | 6.6 |

Table 4.21 Automatic char analysis data as a function of DTF temperature

| Coal | Particle Size | ACA5 (vol%) | | |
|---------------------|-------------------|-------------|--------|--------|
| | (μm) | 1000°C | 1150°C | 1300°C |
| <i>Bijao</i> | 53-75 | 94.8 | 97.6 | 98.3 |
| | 106-125 | 93.1 | 96.0 | 96.9 |
| <i>Fila Maestra</i> | 53-75 | 92.2 | 94.5 | 97.0 |
| | 106-125 | 88.5 | 91.3 | 95.2 |
| <i>La Loma</i> | 53-75 | 90.2 | 93.4 | 96.3 |
| | 106-125 | 87.4 | 90.5 | 93.3 |
| <i>Oreganal</i> | 53-75 | 88.5 | 91.5 | 94.4 |
| | 106-125 | 87.5 | 90.2 | 93.2 |
| <i>La Jagua</i> | 53-75 | 87.2 | 91.5 | 96.0 |
| | 106-125 | 84.3 | 87.2 | 93.5 |
| <i>El Cerrejon</i> | 53-75 | 88.7 | 91.3 | 95.6 |
| | 106-125 | 84.3 | 89.3 | 92.6 |
| <i>Caypa</i> | 53-75 | 89.0 | 92.3 | 96.6 |
| | 106-125 | 87.1 | 90.3 | 94.0 |
| <i>Paso Diablo</i> | 53-75 | 76.3 | 84.3 | 90.1 |
| | 106-125 | 73.9 | 78.9 | 86.1 |
| <i>Maturin</i> | 53-75 | 77.5 | 84.0 | 89.6 |
| | 106-125 | 73.4 | 80.0 | 86.4 |
| <i>Ashland</i> | 53-75 | 74.7 | 82.6 | 87.4 |
| | 106-125 | 69.6 | 77.9 | 83.6 |

From examination of the data in Tables 4.17 to 4.20, it is clear that the morphological properties and concentration of certain type of chars, is dependent on the characteristics of the parent coal. Bijao and Fila Maestra, the lower rank coals, for instance, tend to produce predominantly network chars. The other coals (excluding La Loma) tend to give cenospheric chars (more than 50%). At least 93% of the chars produced by Caypa coal are cenospheric and this is related to the very high vitrinite content of this coal (~95%). La Loma, in contrast, produced a combination of networks and cenospheres, due primarily to the lower rank vitrinite and maceral association observed during point count maceral analysis and vitrinite reflectance measurements. Despite the fact that all the coals used in this study are all vitrinite-rich coals, variations in char morphology were evident. This demonstrates that it is impossible to assign any one char type to a single maceral group. It is apparent that vitrinite, in fact, generates a wide range of char types depending on the rank of the parent coal and on the maceral association within the coal. Furthermore, some studies (Bend et al., 1992) suggest that cenosphere formation is linked to the inherent caking/non-caking propensity of coals. Generally, caking propensity has been found to be more typical of high volatile and medium volatile bituminous coals. Conversely, vitrinite-rich sub-bituminous and low rank coals in general are normally considered non-caking and tend to generate a greater proportion of network chars.

From the data in Table 4.20, it can be observed that the operating temperature has an effect on the amount of thin and thick-walled chars generated. It is clearly evident that the higher the temperature, the greater the amount of thin-walled chars and the lower the concentration of thick-walled chars. Plots of ACA5 values versus DTF operating temperature are shown in Figures 4.16 and 4.17 for the 53-75 μm fraction and the 106-125 μm fraction respectively. The increase in ACA5 values with increasing DTF temperature is in agreement with the manual char data. A trend of increasing solid chars with decreasing temperature was also noticed, although these variations are less apparent due to the very low proportions of these types of chars. The higher rank coals (Maturin, Paso Diablo, and Ashland) exhibit a higher proportion of thick-walled chars and solids, and gave consistently lower ACA5 values (Table 4.21).

Figure 4.16 A Plot of ACA5 against DTF temperature for the 53-75 μm char fractions

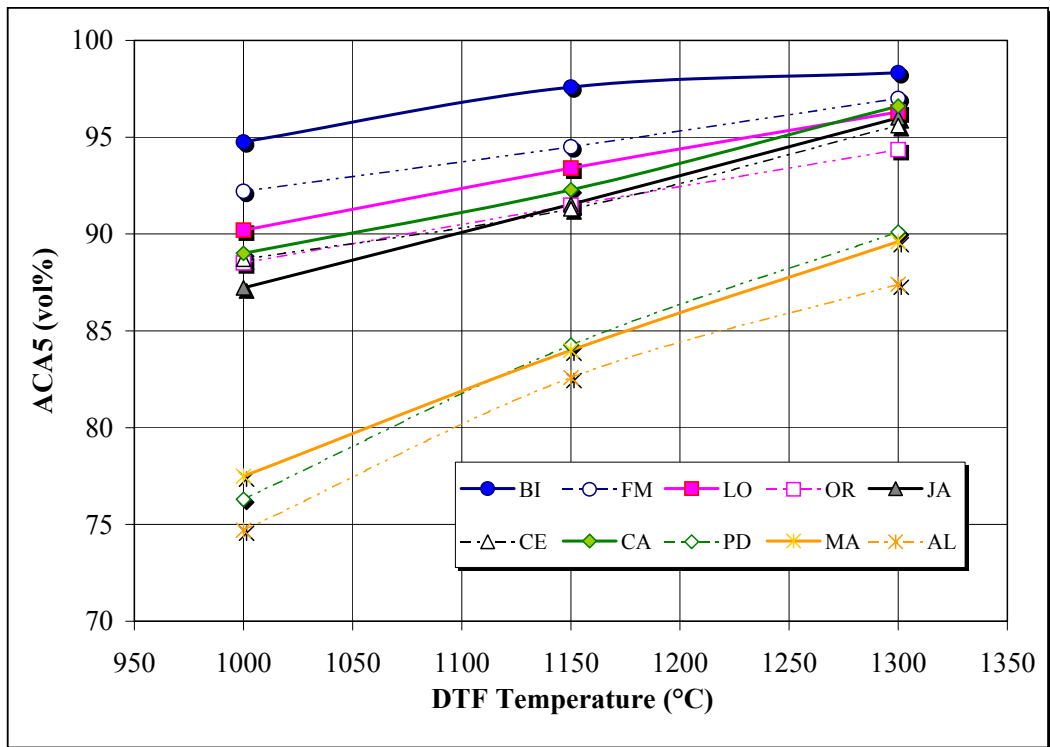
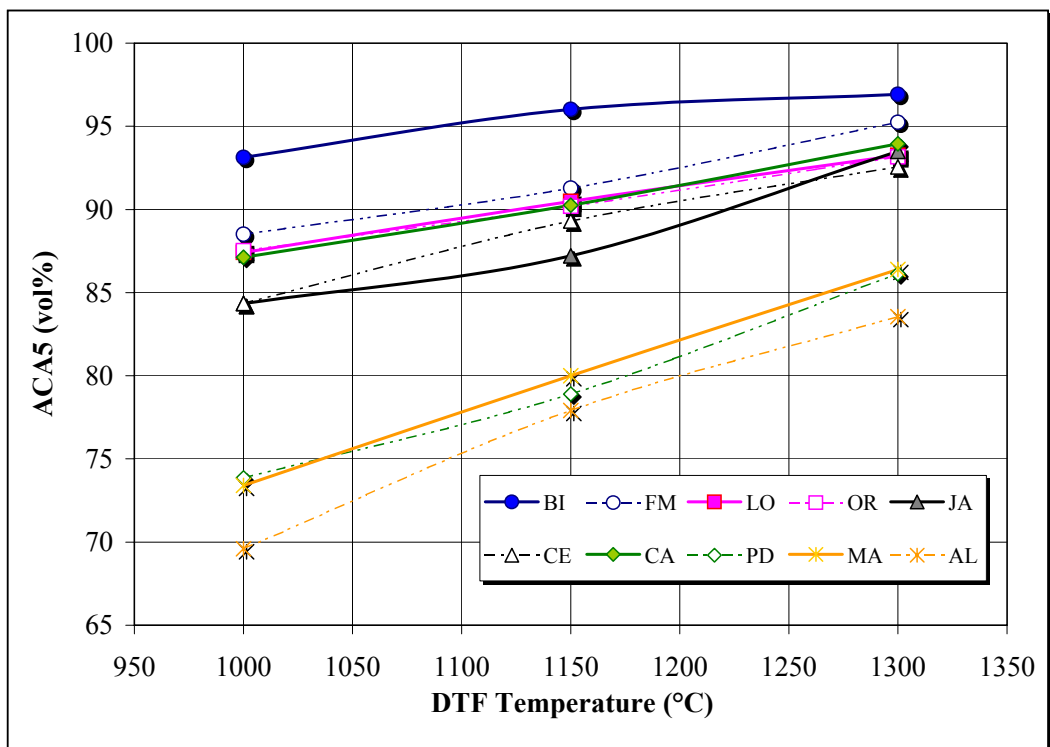


Figure 4.17 A Plot of ACA5 against DTF temperature for the 106-125 μm char fractions



It can be seen from the manual char analysis results (Tables 4.17 to 4.20) that the larger fractions gave the thickest walled chars (crassinetworks, crassispheres, and solids). This is in agreement with data obtained from the automatic char analysis (Table 4.21).

4.2.9 Correlation of Char Properties and DTF Volatiles with Coal Characteristics

Multiple linear regressions were performed in order to compare the results of the char properties and DTF volatiles with some of the characteristics of the parent coals. Linear regression simply means that the functional relationship between the dependent variable (a char property, for instance) and the independent variables (coal properties) can be expressed by a linear equation or, in other words, a sum of terms including the error:

$$y = b_0 + b_1 x_1 + b_2 x_2 + \dots + b_i x_i + \text{error} \quad (4.5)$$

In this equation y represents the dependent variable, x_1, x_2, \dots, x_i , the independent variables and $b_0, b_1, b_2, \dots, b_i$, the parameters or coefficients of the model.

The F-statistic, which is based on the F-distribution, is normally used to determine whether there is a linear relationship between the dependent variable and the independent variables (Aiken and West, 1991; Montgomery, 1997). A confidence level of 95% is normally selected in order to allow definite statements to be made in the presence of statistical error. The remaining 5% represents the probability of erroneously concluding that there is a relationship among the variables. The term "Alpha" is used in the F-statistic to account for this error on a fractional level so that in this particular case Alpha (α) is equal to 0.05. There is a relationship between the variables if the F-observed statistic is greater than the F-critical value. The F-critical value can be obtained by referring to a table of F-critical values which appear in standard statistics textbooks. A table of the percentage points of the F-distribution for a confidence level of 95% ($\alpha = 0.05$) have been reproduced from the book by Draper and Harry (1998) and is presented in Appendix D. Note

that the F-distribution depends on two separate degrees of freedom which are abbreviated as ν_1 and ν_2 . They can be calculated as follows; $\nu_1 = k$ and $\nu_2 = n - (k + 1)$, where k is the number of independent variables in the regression analysis and n is the number of data points.

The coefficient of multiple determination R^2 is used almost universally to judge a regression analysis. R^2 , when multiplied by 100, represents the percentage of the total variation in the data which can be explained by the fitted regression equation. The coefficient of determination is an extremely useful indicator even if there are no absolute rules about how large it should be (Vinod and Ullah, 1981). For the regressions carried out in this study a confidence level of 95% was selected. Both the F-observed statistic and the coefficient of determination were estimated to evaluate the variance and significance of the regressions. These values appear in the table of the correlation results. The F values are highlighted when the regression is found to be significant.

4.2.9.1 Automatic Char Analysis

Maceral composition is known to affect the combustion propensity of coals. Correlation of the char automatic analysis data (ACA5) against maceral analysis and particle size have been performed. This has been done using multiple linear regression. The results shows that there is some correlation between maceral analysis and the ACA5 parameter with R^2 values of 0.80, 0.79, and 0.85, with increasing DTF temperature. The plot obtained for the correlation at 1300°C is shown in Figure 4.18, where a wide spread of the data can be seen. This is mainly due to the variations of the reflectance of macerals in different coals, in particular, vitrinite with rank. Subsequently, when rank is included in the correlation, as mean random vitrinite reflectance, as shown in Figure 4.19 again for a DTF temperature of 1300°C, the correlation is significantly improved with R^2 value of 0.90, 0.87, and 0.91 with increasing DTF temperature. This demonstrates the important effect of rank on the structure of the coal, where the varying structure of vitrinite with rank is now taken into account. However, inertinites also vary in reflectance and this is accounted for by using the grey scale histogram. This is discussed below.

Figure 4.18 Actual values of ACA5 against predicted values following linear regression with maceral content - DTF temp.: 1300°C

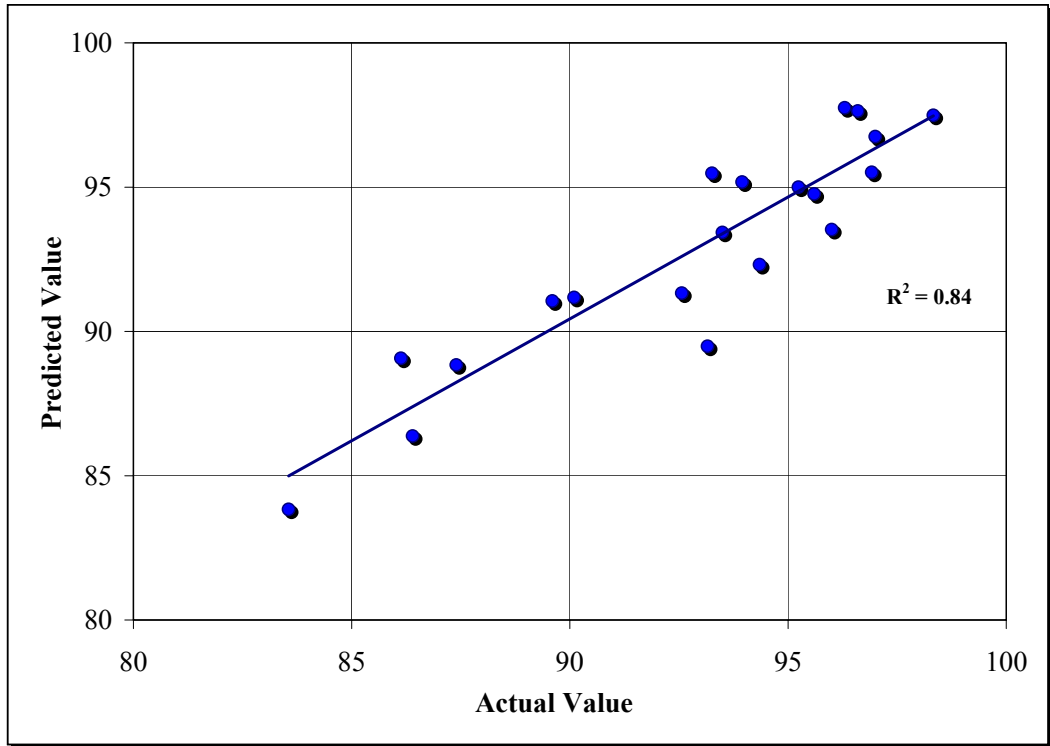
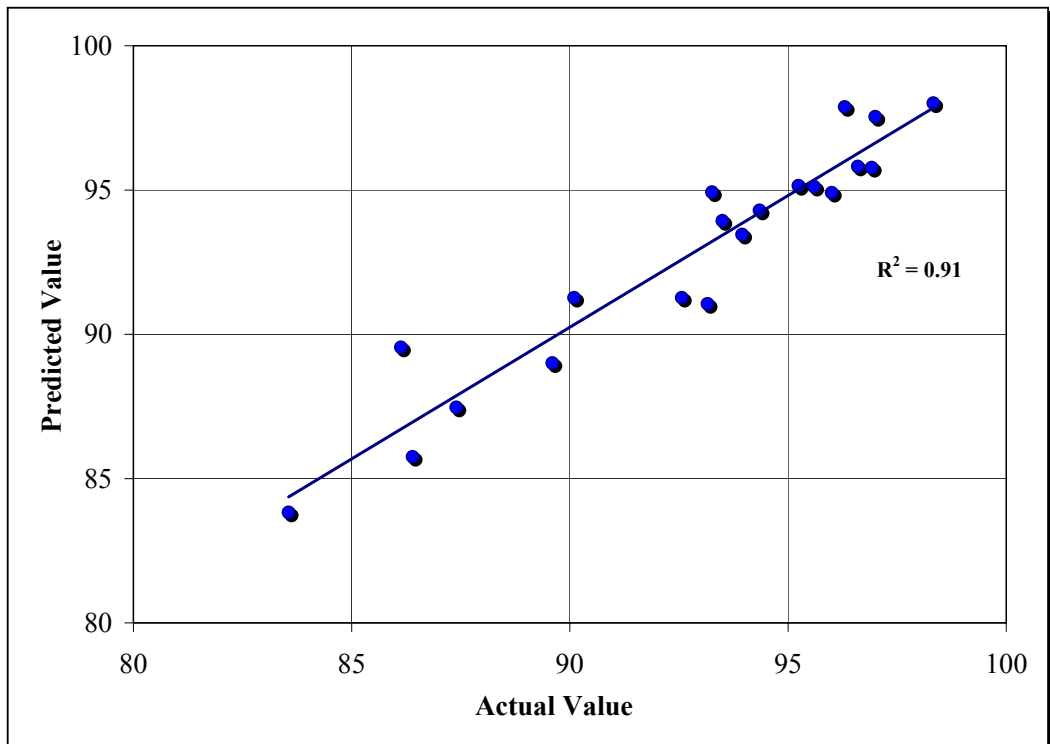
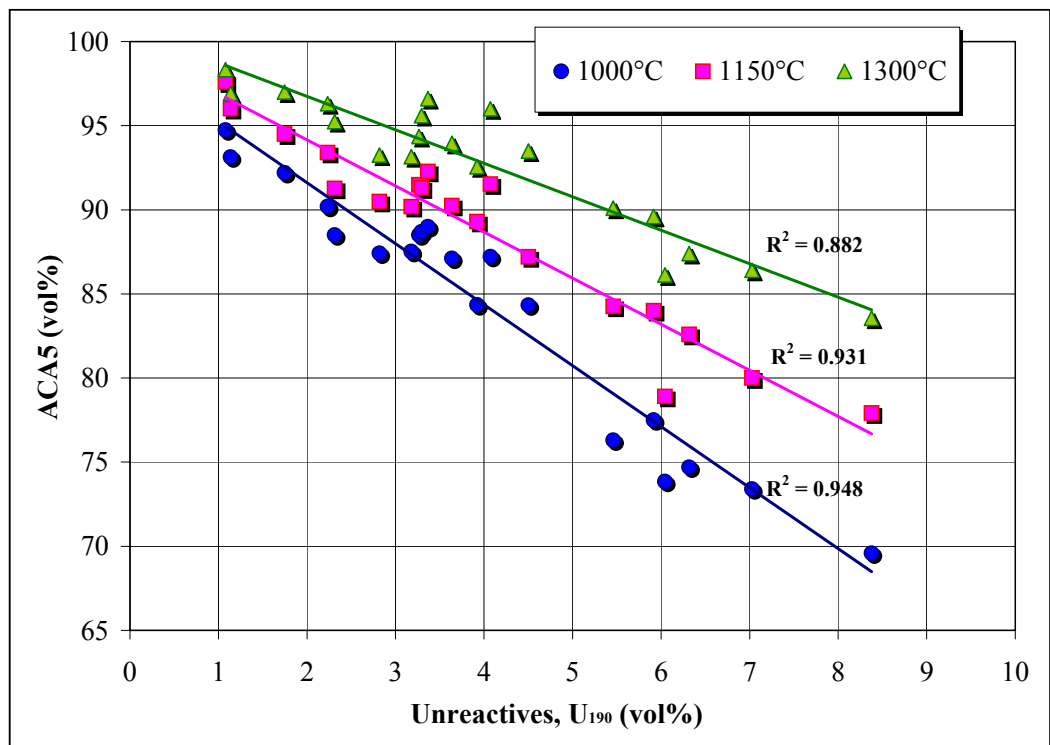


Figure 4.19 Actual values of ACA5 against predicted values following linear regression with maceral content and rank - DTF temp.: 1300°C



Previous work in this laboratory has shown that the % unreactives of coal correlates well with the burnout potential of coals from different origins (Cloke et al., 1997a & b). Essentially, this represents a split between coal material which will burn effectively and that which will be unreactive or more inert during combustion. This parameter makes no distinction as to the source of the inert or reactive material in terms of maceral type. Instead, an objective measure is obtained which accounts for differences in maceral reactivity due to its reflectance (or grey scale value).

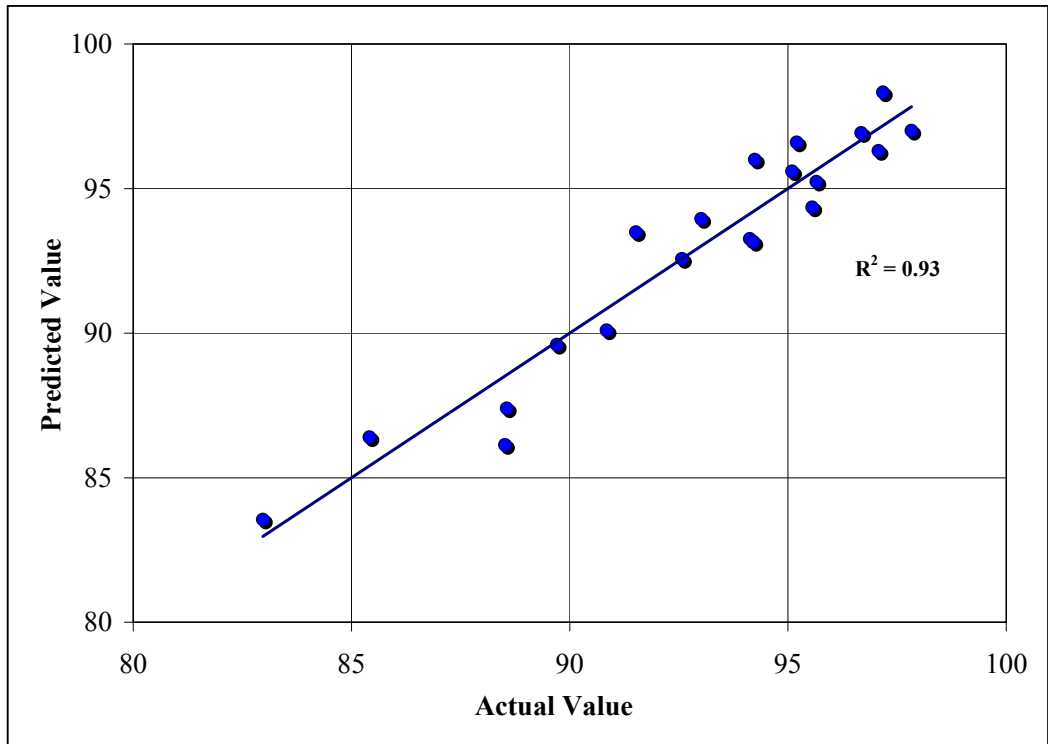
Figure 4.20 A Plot of ACA5 against % unreactive as a function of DTF temperature



Following the aforementioned approach, automatic char analysis data (ACA5) may be correlated with the % unreactives. Plots of this data have been obtained and are given as a function of DTF temperature in Figure 4.20. A good linear correlation between ACA5 and % unreactives is obtained, independently of DTF temperature, with R^2 ranging from 0.88 to 0.95. Note that the particle size effect has not been accounted for in these correlations. When the particle size effect is taken into account, by performing a multiple linear regression, a slightly

improvement in the correlations is achieved with R^2 values ranging from 0.90 to 0.95. It is clear from the correlations that coals with high % unreactives figures produces thicker walled chars.

Figure 4.21 Actual values of ACA5 against predicted values following linear regression with image analysis, grey scale histograms- DTF temp.: 1300°C



In a more recent work (Clove et al, 1997d) in this laboratory, FTIR data has been successfully correlated with percentages of certain bands of the grey scale histogram. It was necessary to consider the whole histogram since the % unreactives threshold ignores part of the coal which may be contributing to the FTIR data. By taking into account this novel approach, correlation of the automatic char analysis with bands of the grey scale histogram has been carried out. These bands are represented by the percentage below [50], the percentage above [210] and the percentages in-between, sub-divided into 40 grey scale units, i.e. between [50] and [90], [90] and [130], and so forth. The value [50] represents mainly the liptinite content which has been inserted into the histograms. As explained in section 4.2.3 the liptinite boundary for the coals fluctuates from approximately [38] to [55] grey scale units, so a value of [50] will take account of

all the liptinite and part of the low reflectance vitrinite or nearly all of the liptinite. The percentage of coal material obtained at each of the above cut-off points is given in Table 4.22. The correlation of ACA5 values with the grey scale histogram gave much better correlations ($R^2 \geq 0.93$) than with macerals plus rank, and quite similar results to those with % unreactives alone. A plot of the ACA5 predicted values versus actual values is shown in Figure 4.21, for a DTF temperature of 1300°C. A summary of the correlation results is given in Table 4.23.

4.2.9.2 DTF Volatiles and Char Intrinsic Reactivity

In a similar way as with automatic char analysis, the DTF volatiles and the intrinsic reactivity data (PT and BT) has been correlated with maceral content alone, maceral content and rank, and the grey scale histogram of the coals. The results are summarised in Table 4.23. According to the results, it is evident that the grey scale histogram can predict the intrinsic reactivity of the chars and the high temperature volatiles released during pyrolysis of the coals. Correlation coefficients were found to range from 0.83 to 0.93 and from 0.90 to 0.94, respectively. The % unreactives alone is only able to predict the DTF volatiles released but not the intrinsic reactivity of the chars.

The grey scale (reflectance) of the coal particles is a good measure of their reactivity, irrespective of maceral type. The RAP profile accounts for both maceral type and reflectance, and assumes that macerals with the same grey scale level have the same reactivity. This is supported by the data presented here, where linear regression of char properties with grey scale produce good correlation coefficients. This is reinforced by the improvement in the correlations when rank is included in the correlation with maceral content. The improvement is related, evidently, to the inclusion of the variation of vitrinite structure with rank. The RAP analysis takes this stage further by including the variation in reflectance for all the macerals. Therefore, the results indicate that the RAP analysis provides a simple and objective technique to predict the combustion behaviour of coals.

Table 4.22 Percentage of material at different grey scale bands on grey scale histograms of the coals

| Coal | Particle Size | Grey Scale Bands | | | | | |
|---------------------|-------------------|------------------|---------|----------|-----------|-----------|------|
| | (μm) | <50 | [50-90] | [90-130] | [130-170] | [170-210] | >210 |
| <i>Bijao</i> | 53-75 | 28.29 | 61.12 | 7.75 | 1.59 | 0.34 | 0.92 |
| | 106-125 | 22.31 | 51.32 | 16.95 | 7.60 | 0.92 | 0.90 |
| <i>Fila Maestra</i> | 53-75 | 17.03 | 65.50 | 10.63 | 4.36 | 1.17 | 1.30 |
| | 106-125 | 16.61 | 62.23 | 11.78 | 5.98 | 1.74 | 1.67 |
| <i>La Loma</i> | 53-75 | 14.88 | 74.46 | 5.49 | 2.20 | 1.16 | 1.81 |
| | 106-125 | 19.14 | 69.85 | 4.91 | 2.40 | 1.45 | 2.25 |
| <i>Oreganal</i> | 53-75 | 9.45 | 78.48 | 6.44 | 1.83 | 1.00 | 2.80 |
| | 106-125 | 6.86 | 75.53 | 11.54 | 2.30 | 1.09 | 2.69 |
| <i>La Jagua</i> | 53-75 | 12.64 | 69.75 | 8.57 | 3.83 | 2.08 | 3.14 |
| | 106-125 | 6.21 | 67.12 | 17.06 | 3.89 | 1.99 | 3.74 |
| <i>El Cerrejon</i> | 53-75 | 11.18 | 73.94 | 8.83 | 2.12 | 1.13 | 2.80 |
| | 106-125 | 7.29 | 72.47 | 13.53 | 2.22 | 1.16 | 3.32 |
| <i>Caypa</i> | 53-75 | 6.89 | 74.08 | 12.63 | 2.26 | 1.34 | 2.81 |
| | 106-125 | 4.42 | 69.52 | 19.40 | 2.35 | 1.33 | 2.98 |
| <i>Paso Diablo</i> | 53-75 | 7.12 | 55.83 | 26.26 | 4.34 | 2.19 | 4.26 |
| | 106-125 | 6.20 | 53.39 | 28.29 | 5.01 | 2.47 | 4.64 |
| <i>Maturin</i> | 53-75 | 1.28 | 40.29 | 43.94 | 6.36 | 3.92 | 4.20 |
| | 106-125 | 1.60 | 28.03 | 52.84 | 8.14 | 4.16 | 5.23 |
| <i>Ashland</i> | 53-75 | 9.92 | 35.72 | 38.33 | 7.73 | 3.61 | 4.69 |
| | 106-125 | 10.24 | 26.19 | 41.18 | 11.60 | 3.99 | 6.80 |

Table 4.23 Coefficients of determination and F values results from the regressions of char properties and DTF volatiles with coal characteristics

| Dependent Variables | DTF Temp. | Independent Variables ^a | | | | | | | |
|---------------------|-----------|------------------------------------|--------------|-----------------------------|--------------|----------------------------|---------------|-----------------------------------|--------------|
| | | Maceral Content ^b | | Macerals +Rank ^c | | % unreactives ^d | | Grey-scale Histogram ^e | |
| | (°C) | R ² | F | R ² | F | R ² | F | R ² | F |
| ACA5 | 1000 | 0.80 | 12.09 | 0.90 | 20.02 | 0.95 | 162.78 | 0.95 | 33.55 |
| | 1150 | 0.79 | 11.61 | 0.87 | 15.52 | 0.95 | 156.17 | 0.94 | 28.23 |
| | 1300 | 0.84 | 16.33 | 0.91 | 24.41 | 0.91 | 89.60 | 0.93 | 44.71 |
| PT | 1000 | 0.65 | 5.46 | 0.71 | 5.64 | 0.50 | 8.67 | 0.83 | 9.18 |
| | 1150 | 0.65 | 5.49 | 0.70 | 5.32 | 0.62 | 13.67 | 0.92 | 20.42 |
| | 1300 | 0.65 | 5.58 | 0.74 | 6.58 | 0.48 | 7.96 | 0.90 | 16.64 |
| BT | 1000 | 0.69 | 6.55 | 0.80 | 9.60 | 0.76 | 26.51 | 0.83 | 9.18 |
| | 1150 | 0.76 | 9.55 | 0.88 | 17.33 | 0.81 | 35.81 | 0.93 | 25.66 |
| | 1300 | 0.61 | 4.67 | 0.71 | 5.79 | 0.59 | 12.06 | 0.88 | 13.46 |
| V _{DTF} | 1000 | 0.80 | 11.91 | 0.91 | 24.66 | 0.86 | 51.51 | 0.91 | 18.75 |
| | 1150 | 0.80 | 11.92 | 0.85 | 13.06 | 0.86 | 52.00 | 0.94 | 28.01 |
| | 1300 | 0.80 | 12.04 | 0.86 | 13.90 | 0.85 | 48.19 | 0.90 | 16.74 |

^aIncluding Mean Particle Size;^bv₁=5, v₂=14, F-critical=2.96; ^cv₁=6, v₂=13, F-critical=2.92;^dv₁=2, v₂=17, F-critical=3.59; ^ev₁=7, v₂=12, F-critical=2.91

CHAPTER 5 DTF CHAR RE-FIRING EXPERIMENTS

This chapter presents the results for the char re-firing experiments in the DTF. Six coals were re-fired over a series of different residence times in order to provide a relative comparison of the combustion rates of each coal. For these experiments, three size fractions for each coal were used in order to evaluate the effect of particle size in the re-firing process.

5.1 Coal Selection and Properties

Five Colombian coals which have been already used in the pyrolysis experiments were selected for the re-firing experiments. An additional coal sample from Venezuela (Guasare) was obtained and was included in the design matrix. This particular coal has been found to give burnout problems at power stations. The size fractions used were 53-75, 106-125, and 150-180 μm . For simplicity of discussion, these fractions are referred to as fractions I, II and III respectively.

5.1.1 Proximate and Ultimate Analysis

Proximate analysis data for the various coal fractions is shown in Table 5.1. The data is presented on a dry, and dry, ash-free bases. As in the previous chapter, coals have been ordered by rank, expressed as random vitrinite reflectance. Note that the fuel ratio, which has been recorded for each sample, shows a clear increase with rank and ranges from 1.16 for the low rank Colombian coal, Bijao, to 1.62 for the higher rank Venezuelan coal, Guasare. There is a slight decrease of the fuel ratio with particle size.

From examination of the data in Table 5.1, it can be seen that volatile matter tends to decrease with increasing coal rank, although little variation among La Jagua, El

Cerrejon, Caypa and Guasare can be noticed. A slight increase in volatile matter content with particle size was also observed.

Table 5.1 Proximate analysis data for the coal fractions

| Coal/Fraction | | Moisture | Dry Basis (wt%) | | | Dry, ash-free Basis (wt%) | | Fuel Ratio |
|---------------------------|------------|----------|-----------------|-----------------|-----|---------------------------|------|------------|
| | | (wt%) | VM ^a | FC ^b | Ash | VM | FC | FC/VM |
| <i>Bijao</i> | <i>I</i> | 7.9 | 43.4 | 52.4 | 4.2 | 45.3 | 54.7 | 1.21 |
| | <i>II</i> | 6.2 | 43.5 | 52.5 | 4.1 | 45.3 | 54.7 | 1.21 |
| | <i>III</i> | 6.2 | 44.3 | 51.5 | 4.2 | 46.2 | 53.8 | 1.16 |
| <i>La Loma</i> | <i>I</i> | 5.1 | 38.6 | 56.8 | 4.6 | 40.5 | 59.5 | 1.47 |
| | <i>II</i> | 4.8 | 38.8 | 56.8 | 4.4 | 40.6 | 59.4 | 1.46 |
| | <i>III</i> | 4.1 | 39.6 | 56.2 | 4.3 | 41.3 | 58.7 | 1.42 |
| <i>La Jagua</i> | <i>I</i> | 3.3 | 37.6 | 59.5 | 2.9 | 38.7 | 61.3 | 1.58 |
| | <i>II</i> | 3.2 | 38.2 | 59.3 | 2.5 | 39.2 | 60.8 | 1.55 |
| | <i>III</i> | 3.1 | 38.6 | 58.4 | 3.0 | 39.8 | 60.2 | 1.51 |
| <i>El Cerrejon</i> | <i>I</i> | 3.4 | 37.1 | 58.5 | 4.5 | 38.8 | 61.2 | 1.58 |
| | <i>II</i> | 3.3 | 37.7 | 58.8 | 3.5 | 39.1 | 60.9 | 1.56 |
| | <i>III</i> | 2.8 | 37.8 | 58.9 | 3.3 | 39.1 | 60.9 | 1.56 |
| <i>Caypa</i> | <i>I</i> | 2.4 | 37.8 | 60.4 | 1.9 | 38.5 | 61.5 | 1.60 |
| | <i>II</i> | 2.3 | 38.1 | 59.7 | 2.2 | 38.9 | 61.1 | 1.57 |
| | <i>III</i> | 2.1 | 38.5 | 59.7 | 1.8 | 39.2 | 60.8 | 1.55 |
| <i>Guasare</i> | <i>I</i> | 2.8 | 35.6 | 57.4 | 7.0 | 38.2 | 61.8 | 1.62 |
| | <i>II</i> | 2.1 | 36.1 | 57.3 | 6.6 | 38.6 | 61.4 | 1.59 |
| | <i>III</i> | 1.6 | 36.5 | 57.0 | 6.5 | 39.0 | 61.0 | 1.56 |

^a VM=Volatile Matter; ^b FC=Fixed Carbon

There is a decrease in moisture content with coal rank, with Caypa and Guasare exhibiting the lowest figures, Bijao and La Loma the highest, and La Jagua and El Cerrejon very similar values. The moisture content also decreases with increasing particle size. All coals have a very low ash content (less than 7%) with Guasare exhibiting the highest figures.

Table 5.2 Ultimate analysis data for the coal fractions

| Coal/Fraction | | C | H | N | S | O |
|---------------------------|------------|-----------|-----------|-----------|-----------|-----------|
| | | (wt% daf) |
| <i>Bijao</i> | <i>I</i> | 73.80 | 5.27 | 1.86 | 0.68 | 18.40 |
| | <i>II</i> | 73.83 | 5.42 | 1.78 | 0.63 | 18.35 |
| | <i>III</i> | 73.75 | 5.34 | 1.79 | 0.63 | 18.49 |
| <i>La Loma</i> | <i>I</i> | 78.79 | 5.42 | 1.72 | 0.64 | 13.42 |
| | <i>II</i> | 78.37 | 5.42 | 1.84 | 0.69 | 13.68 |
| | <i>III</i> | 79.23 | 5.55 | 1.77 | 0.65 | 12.81 |
| <i>La Jagua</i> | <i>I</i> | 84.12 | 5.51 | 1.78 | 0.59 | 8.00 |
| | <i>II</i> | 84.36 | 5.61 | 1.79 | 0.58 | 7.65 |
| | <i>III</i> | 84.35 | 5.62 | 1.81 | 0.60 | 7.62 |
| <i>El Cerrejon</i> | <i>I</i> | 84.23 | 5.53 | 1.83 | 0.68 | 7.73 |
| | <i>II</i> | 83.80 | 5.58 | 1.83 | 0.65 | 8.14 |
| | <i>III</i> | 83.52 | 5.56 | 1.85 | 0.65 | 8.41 |
| <i>Caypa</i> | <i>I</i> | 84.78 | 5.68 | 1.89 | 0.67 | 6.97 |
| | <i>II</i> | 85.43 | 5.76 | 1.86 | 0.64 | 6.31 |
| | <i>III</i> | 85.04 | 5.73 | 1.86 | 0.65 | 6.71 |
| <i>Guasare</i> | <i>I</i> | 86.78 | 5.70 | 1.90 | 0.76 | 4.86 |
| | <i>II</i> | 87.35 | 5.84 | 1.89 | 0.74 | 4.18 |
| | <i>III</i> | 87.07 | 5.78 | 1.93 | 0.76 | 4.45 |

Data from the elemental analysis of the coal fractions is shown in Table 5.2. The data consists of the percent composition of carbon, hydrogen, nitrogen, sulphur and oxygen (calculated by difference) on a dry, ash-free basis. As would be expected, there is a general trend of increasing carbon content with increasing rank. Similarly, oxygen content tends to decrease with coal rank. No definite trend for % C or % O can be seen with particle size. All the coals exhibit low sulphur contents (less than 0.8%).

5.1.2 Petrographic Characterisation

Petrographic analysis for the various coal fractions, including maceral analysis and rank is given in Table 5.3. The data is provided on a volume/volume, mineral matter-free basis. The vitrinite reflectance histograms of the samples are shown in Appendix B.

From the maceral analysis data in Table 5.3, it is possible to identify some general trends. It is evident that vitrinites concentrate in the smaller size fractions. Liptinites, on the contrary, show a tendency to concentrate in the larger size fractions. This fractionation behaviour of macerals has been observed in other coals (Thompson et al., 1993), and can be attributed to the behaviour of macerals during grinding as explained in the previous chapter (section 4.2.2). Fusinite and semifusinite, do not show a definite trend with particle size.

In terms of rank, small variation in the figures are reported between the three size fractions. From analysis of the vitrinite reflectance histograms in Appendix B, it was observed that most of the coals give a normal or '*quasi-normal*' distribution characteristic of an unblended coal sample.

5.1.3 Image Analysis

The grey scale histograms of the coal fractions, derived from the RAP analysis, are given in Appendix C. These profiles take the form of frequency versus grey

scale histograms. The % unreactives parameter (U_{190}), derived from the RAP profiles, are given in Table 5.3.

Table 5.3 Petrographic Analysis of the coal fractions

| Coal/Fraction | | Rank | Maceral Content (vol%) | | | | U_{190} |
|--------------------|------------|---------|------------------------|-----------|--------------|----------|-----------|
| | | VRo (%) | Vitrinite | Liptinite | Semifusinite | Fusinite | (vol%) |
| <i>Bijao</i> | <i>I</i> | 0.50 | 94.2 | 3.6 | 1.6 | 0.6 | 1.1 |
| | <i>II</i> | 0.50 | 90.8 | 6.0 | 2.6 | 0.6 | 1.1 |
| | <i>III</i> | 0.54 | 90.2 | 7.4 | 2.0 | 0.4 | 1.7 |
| <i>La Loma</i> | <i>I</i> | 0.51 | 95.6 | 0.4 | 3.6 | 0.4 | 2.2 |
| | <i>II</i> | 0.53 | 96.8 | 0.2 | 2.6 | 0.4 | 2.8 |
| | <i>III</i> | 0.54 | 92.8 | 2.4 | 3.2 | 1.6 | 3.1 |
| <i>La Jagua</i> | <i>I</i> | 0.54 | 85.2 | 2.0 | 7.8 | 5.0 | 4.1 |
| | <i>II</i> | 0.53 | 84.2 | 2.4 | 10.2 | 3.2 | 4.5 |
| | <i>III</i> | 0.56 | 83.2 | 2.8 | 8.4 | 5.6 | 4.5 |
| <i>El Cerrejon</i> | <i>I</i> | 0.56 | 90.8 | 2.4 | 3.4 | 3.4 | 3.3 |
| | <i>II</i> | 0.59 | 90.6 | 1.6 | 3.2 | 4.6 | 3.9 |
| | <i>III</i> | 0.60 | 85.4 | 4.6 | 4.2 | 5.8 | 4.8 |
| <i>Caypa</i> | <i>I</i> | 0.60 | 96.8 | 0.4 | 2.4 | 0.4 | 3.4 |
| | <i>II</i> | 0.59 | 95.2 | 0.4 | 3.6 | 0.8 | 3.6 |
| | <i>III</i> | 0.56 | 94.8 | 1.2 | 2.2 | 1.8 | 3.7 |
| <i>Guasare</i> | <i>I</i> | 0.66 | 90.0 | 1.6 | 5.2 | 3.2 | 4.5 |
| | <i>II</i> | 0.68 | 85.4 | 2.6 | 7.2 | 4.8 | 4.9 |
| | <i>III</i> | 0.71 | 83.6 | 4.4 | 6.6 | 5.4 | 5.5 |

From the grey scale histograms, it is possible to tentatively assign various peaks to the major maceral groups. The exact position of these peaks is rank dependent, and there can be a considerable degree of overlap, particularly between vitrinite and semifusinite. This has already been discussed in the previous chapter for all

the coal excluding Guasare. For this coal, the liptinite peak lies on a similar grey scale level as La Jagua, El Cerrejon, and Caypa, i.e. around 45. The vitrinite peaks lie between this grey level and approximately 130. Other distinctive peaks can be distinguished beyond a grey level of 230 and can be ascribed to high reflectance semifusinite, fusinite, and mineral matter. The cumulative percentage curves from the RAP profiles of the size fractions of this coal are all steep indicating low variation in vitrinite reflectance and a low level of semifusinite.

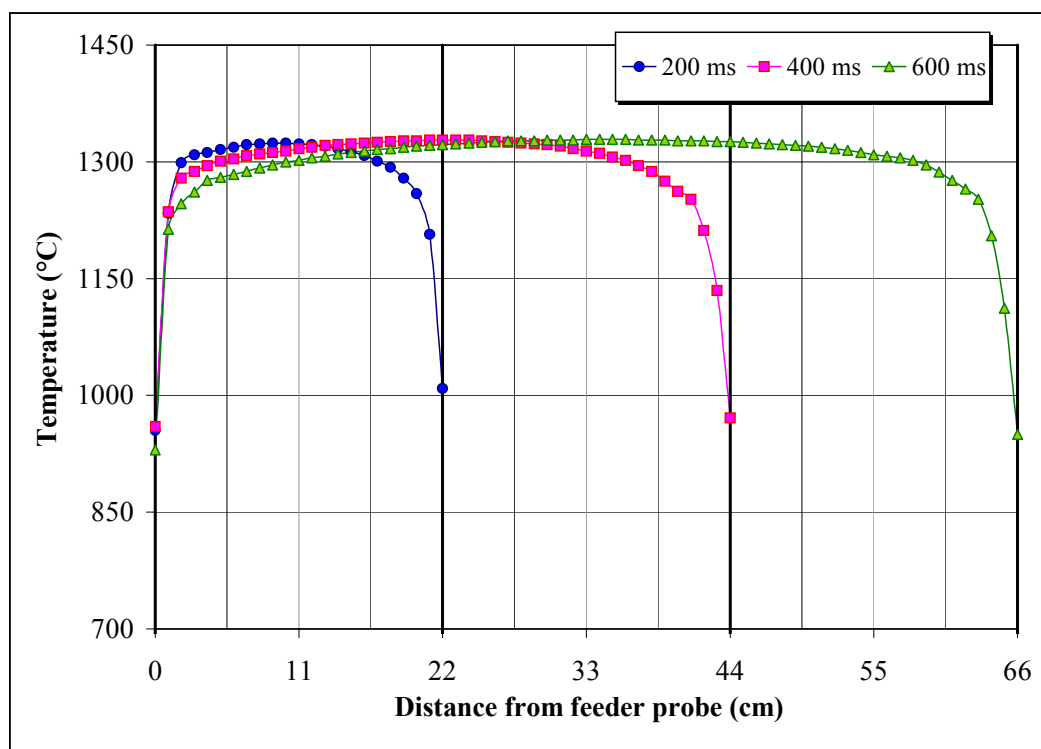
5.2 Drop Tube Furnace Conditions

The samples were initially pyrolysed in the DTF operating at 1300°C in order to allow extensive devolatilisation in all size fractions. The combustion process was completed at 1 atm and under a slightly oxidising atmosphere (1% oxygen in nitrogen), with a residence time of 200 ms. Again, a small amount of oxygen was considered necessary to avoid contamination of the char samples with soot and condensed tars. Twenty grams of each coal fraction were used during this initial stage, although two separate runs of ten grams each were carried out to avoid blockage of the collector probe. This means that two replicates for each sample were performed which enabled the repeatability of the system to be tested. The coal used and the chars obtained carefully weighed for ash tracer purposes. Each char was then re-fired in the DTF, again at 1300°C, over a series of different residence times (200, 400 and 600 ms), in an atmosphere containing 5% oxygen in nitrogen. In order to produce a reasonable amount of re-fired char for analysis, one to three grams of each pyrolysed char sample were utilised, depending on coal type, particle size, and residence time. The samples were carefully weighed, as before, to determine collection efficiencies.

Gas temperature profiles along the centre line of the working tube were obtained as a function of axial distance from the bottom of the feeder probe. Figure 5.1 shows the profiles obtained for the three different residence times. Note that the separation of the collector probe from the feeder probe varies with residence time since the gas flow is kept constant. It can be seen from the figure that high temperature gradients exist near the feeder and collector probes, and a long

isothermal zone was attained. Additionally, the results revealed that the temperature profile is independent of the position of the collector probe, which is inserted from the bottom of the reactor.

Figure 5.1 Temperature profiles as a function of residence time along the reaction zone in the DTF



5.3 Char Collection Efficiency

Ash contents of the coal fractions and chars produced in this study are given in Table 5.4, whilst Table 5.5 contains data on the char yields and the collection efficiencies. From analysis of this data, it can be seen that collection efficiency varies in accordance with changes in ash levels, particle size, and percentage of burnout. As in the previous chapter, collection efficiency values were all greater than 80% for the pyrolysed char samples and in only one case exceeds 100%. Generally speaking, a decrease in collection efficiency occurs with increasing residence time particularly for fractions I and II, although this trend is more evident for fraction I. Collection efficiency figures range from around 72-95% for a residence time of 200 ms, and fall to approximately 50-85% for 600 ms.

Fractions I and II tend to give a higher collection efficiency than fraction III for the pyrolysed chars and for the 200 ms re-fired chars. As the residence time is increased to 400 ms this trend tends to reverse, becoming more apparent at 600 ms with fraction III giving the highest collection efficiency (greater than 72%). The fact that larger particles tend to give high collection efficiency values as the residence time increases, is likely to be associated with the low burnout level of these fractions.

Table 5.4 Ash content of coal fractions and pyrolysed and re-fired chars

| Coal/Fraction | | Coal Ash Content | Char Ash Content (wt% db) | | | |
|--------------------|------------|------------------|---------------------------|----------------|--------|--------|
| | | (wt% db) | Pyrolysed Char | Re-fired Chars | | |
| | | | | 200 ms | 400 ms | 600 ms |
| <i>Bijao</i> | <i>I</i> | 4.2 | 13.59 | 51.30 | 88.02 | 100.00 |
| | <i>II</i> | 4.1 | 11.91 | 29.61 | 61.81 | 97.96 |
| | <i>III</i> | 4.2 | 10.11 | 22.09 | 42.90 | 79.15 |
| <i>La Loma</i> | <i>I</i> | 4.6 | 14.04 | 45.65 | 83.87 | 100.00 |
| | <i>II</i> | 4.4 | 11.91 | 29.31 | 56.47 | 97.77 |
| | <i>III</i> | 4.3 | 10.66 | 23.05 | 41.76 | 82.29 |
| <i>La Jagua</i> | <i>I</i> | 2.9 | 8.03 | 16.18 | 42.71 | 95.00 |
| | <i>II</i> | 2.5 | 6.35 | 12.04 | 22.99 | 52.92 |
| | <i>III</i> | 3.0 | 6.47 | 11.07 | 19.67 | 34.96 |
| <i>El Cerrejon</i> | <i>I</i> | 4.5 | 12.69 | 24.66 | 45.13 | 92.27 |
| | <i>II</i> | 3.5 | 8.96 | 18.15 | 26.47 | 39.44 |
| | <i>III</i> | 3.3 | 7.30 | 13.36 | 19.74 | 32.54 |
| <i>Caypa</i> | <i>I</i> | 1.9 | 5.57 | 11.62 | 31.38 | 94.38 |
| | <i>II</i> | 2.2 | 5.99 | 10.95 | 19.31 | 38.32 |
| | <i>III</i> | 1.8 | 4.33 | 8.19 | 13.31 | 24.17 |
| <i>Guasare</i> | <i>I</i> | 7.0 | 17.96 | 27.93 | 49.68 | 93.34 |
| | <i>II</i> | 6.6 | 15.27 | 20.73 | 27.59 | 40.68 |
| | <i>III</i> | 6.5 | 12.68 | 15.97 | 19.58 | 29.79 |

Table 5.5 Char yield and collection efficiency for the pyrolysed and re-fired chars

| Coal/Fraction | | Char Yield (g/g of feed) | | | | Collection Efficiency (%) | | | |
|--------------------|------------|--------------------------|--------|--------|--------|---------------------------|--------|--------|--------|
| | | char | 200 ms | 400 ms | 600 ms | char | 200 ms | 400 ms | 600 ms |
| <i>Bijao</i> | <i>I</i> | 0.282 | 0.224 | 0.115 | 0.071 | 90.6 | 84.5 | 74.6 | 52.3 |
| | <i>II</i> | 0.311 | 0.345 | 0.152 | 0.080 | 91.3 | 85.7 | 78.6 | 65.9 |
| | <i>III</i> | 0.363 | 0.362 | 0.188 | 0.095 | 88.3 | 79.1 | 79.9 | 74.0 |
| <i>La Loma</i> | <i>I</i> | 0.293 | 0.247 | 0.118 | 0.071 | 90.1 | 80.3 | 70.4 | 50.6 |
| | <i>II</i> | 0.331 | 0.303 | 0.156 | 0.077 | 89.3 | 74.6 | 73.8 | 63.0 |
| | <i>III</i> | 0.324 | 0.334 | 0.199 | 0.093 | 80.7 | 72.4 | 78.1 | 72.1 |
| <i>La Jagua</i> | <i>I</i> | 0.332 | 0.444 | 0.145 | 0.055 | 92.6 | 89.5 | 77.2 | 65.2 |
| | <i>II</i> | 0.337 | 0.426 | 0.217 | 0.081 | 86.7 | 80.7 | 78.7 | 67.7 |
| | <i>III</i> | 0.397 | 0.467 | 0.262 | 0.141 | 85.7 | 79.9 | 79.7 | 76.3 |
| <i>El Cerrejon</i> | <i>I</i> | 0.335 | 0.449 | 0.216 | 0.093 | 94.9 | 87.2 | 76.7 | 68.0 |
| | <i>II</i> | 0.366 | 0.432 | 0.288 | 0.178 | 94.2 | 87.6 | 85.2 | 78.5 |
| | <i>III</i> | 0.404 | 0.451 | 0.297 | 0.192 | 88.3 | 82.5 | 80.4 | 85.6 |
| <i>Caypa</i> | <i>I</i> | 0.337 | 0.455 | 0.139 | 0.038 | 100.2 | 94.8 | 78.4 | 63.8 |
| | <i>II</i> | 0.362 | 0.502 | 0.272 | 0.128 | 96.9 | 91.8 | 87.5 | 82.0 |
| | <i>III</i> | 0.404 | 0.477 | 0.287 | 0.147 | 95.2 | 90.1 | 88.0 | 82.1 |
| <i>Guasare</i> | <i>I</i> | 0.382 | 0.554 | 0.295 | 0.120 | 98.1 | 86.1 | 81.6 | 62.5 |
| | <i>II</i> | 0.422 | 0.613 | 0.430 | 0.275 | 97.0 | 83.3 | 77.8 | 73.2 |
| | <i>III</i> | 0.497 | 0.664 | 0.489 | 0.323 | 97.0 | 83.6 | 75.5 | 75.8 |

5.4 DTF Volatiles and R Factor

Table 5.6 contains data on proximate and DTF volatiles figures along with R factor values for the coal fractions and the pyrolysed chars. Plots of the DTF volatiles and R factors versus mean particle size for each coal are shown in Figures 5.2 and 5.3 respectively. It can be seen from the tables and figures that R

factor and DTF volatiles decrease with increasing particle size. This indicates that the coarser particles require a longer time in the DTF system to emit their volatile matter. An explanation for this might be transport limitations within particles (Suuberg et al., 1979). The coarsest particles would have a lower surface area per unit weight and a higher pore length, which make loss of volatiles more difficult.

Table 5.6 Proximate and DTF volatiles and R factor data for the coals and the pyrolysed chars

| Coal/Fraction | | Proximate Volatiles | DTF Volatiles | R Factor |
|--------------------|------------|---------------------|---------------|----------|
| | | (wt% daf) | (wt% daf) | |
| <i>Bijao</i> | <i>I</i> | 45.3 | 71.9 | 1.59 |
| | <i>II</i> | 45.3 | 68.7 | 1.52 |
| | <i>III</i> | 46.2 | 61.4 | 1.33 |
| <i>La Loma</i> | <i>I</i> | 40.5 | 70.7 | 1.75 |
| | <i>II</i> | 40.6 | 65.8 | 1.62 |
| | <i>III</i> | 41.3 | 62.5 | 1.51 |
| <i>La Jagua</i> | <i>I</i> | 38.7 | 66.1 | 1.71 |
| | <i>II</i> | 39.2 | 62.7 | 1.60 |
| | <i>III</i> | 39.8 | 55.4 | 1.39 |
| <i>El Cerrejon</i> | <i>I</i> | 38.8 | 67.8 | 1.75 |
| | <i>II</i> | 39.1 | 63.4 | 1.62 |
| | <i>III</i> | 39.1 | 56.1 | 1.44 |
| <i>Caypa</i> | <i>I</i> | 38.5 | 67.6 | 1.76 |
| | <i>II</i> | 38.9 | 64.0 | 1.64 |
| | <i>III</i> | 39.2 | 58.6 | 1.50 |
| <i>Guasare</i> | <i>I</i> | 38.2 | 65.6 | 1.72 |
| | <i>II</i> | 38.6 | 60.5 | 1.57 |
| | <i>III</i> | 39.0 | 52.1 | 1.34 |

Figure 5.2 A plot of DTF volatiles as a function of particle size for each coal

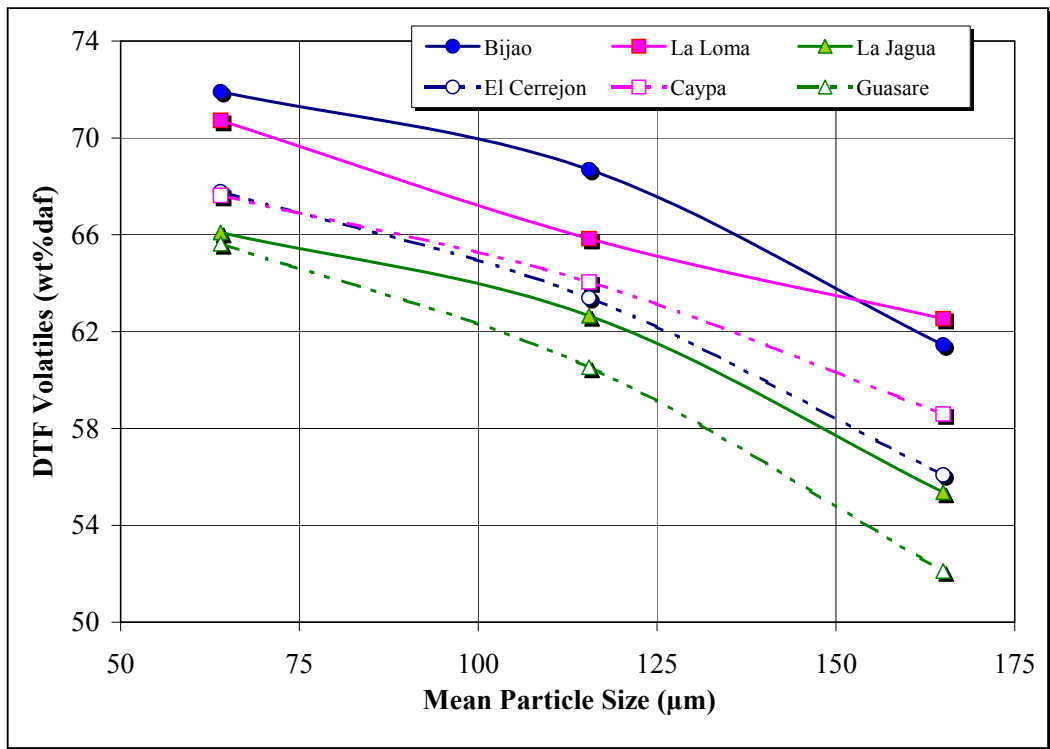
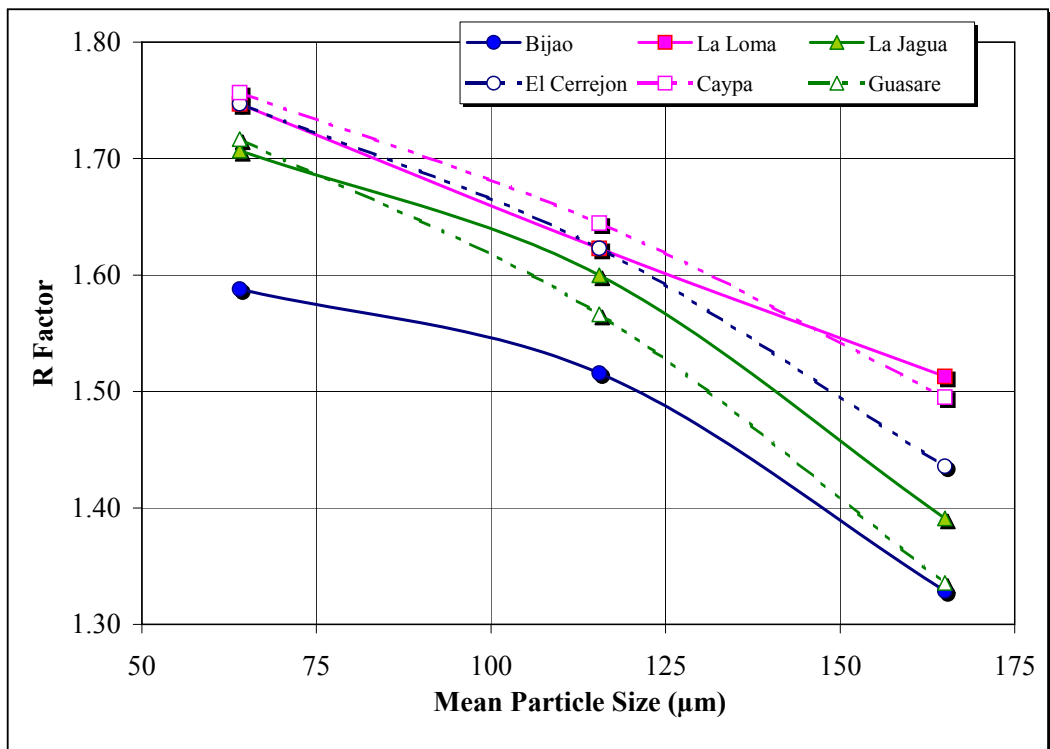


Figure 5.3 A plot of R Factor versus particle size for each coal



Once again, these results serve to demonstrate that a coal which is exposed to high temperatures and heating rates emits more volatiles than that obtained during standard proximate analysis. In fact, the coals used in this study emitted from 33% to 76% more volatiles (R factor values of 1.33 to 1.76 respectively).

5.5 Properties of the Pyrolysed Char

5.5.1 Char Intrinsic Reactivity

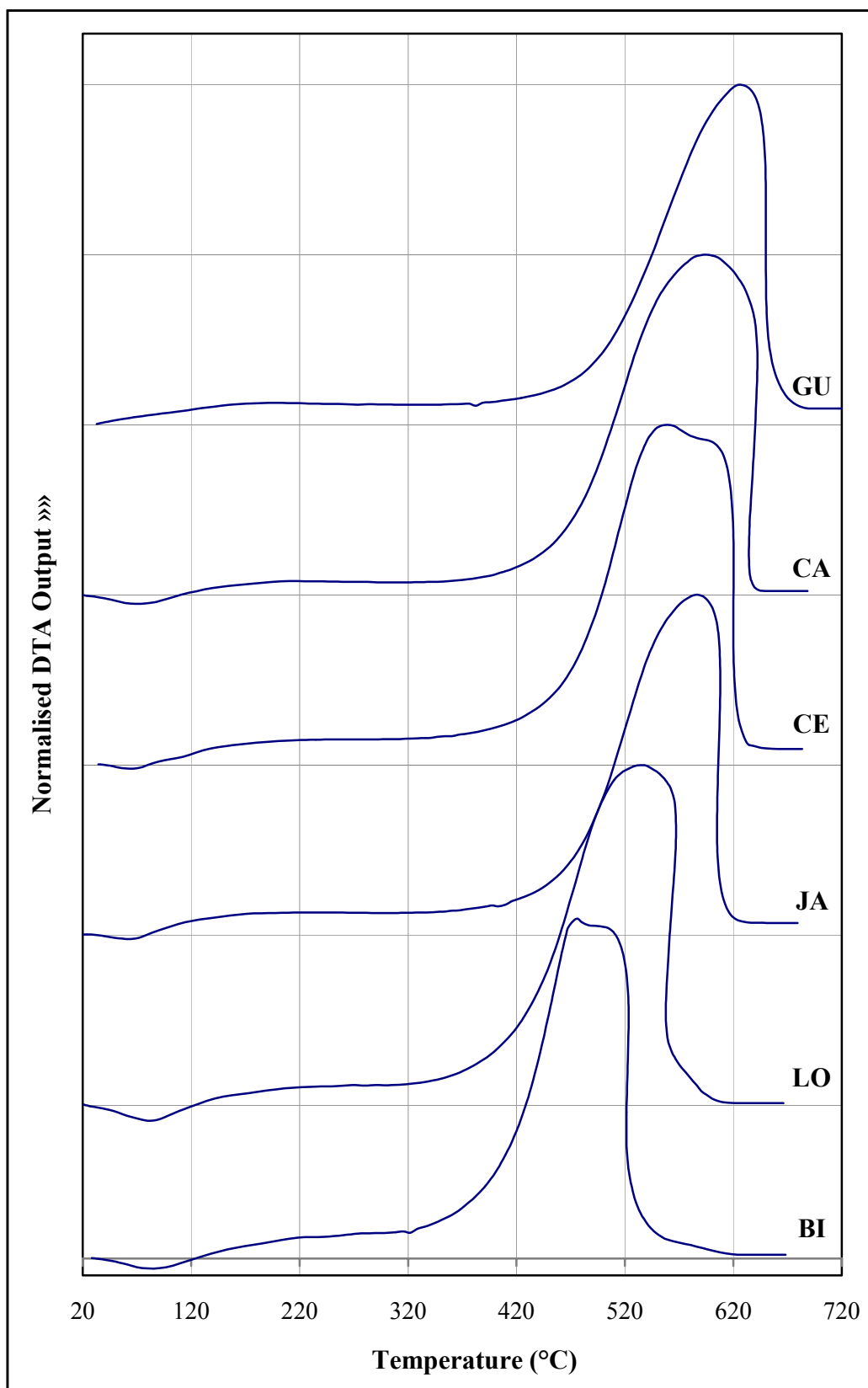
The intrinsic reactivity results for all the pyrolysed char samples are given in Table 5.7. Char burning profiles, as derived from the intrinsic reactivity analysis, are presented in Appendix E. The profiles take the form of DTA output as a function of temperature. The DTA output ($\mu\text{V}\cdot\text{mg}^{-1}$) was normalised to the maximum value, i.e. the value given by the curve when reaching the maximum rate of weight loss. This was necessary to facilitate the interpretation of profiles, particularly when comparing pyrolysed char burning profiles with those of the re-fired chars or from different coals. Appendix E presents the burning profiles of the pyrolysed char for each coal as a function of particle size. Additionally, Figure 5.4 shows the burning profiles of the fraction I chars in order to assess the effect of coal rank. Plots of PT and BT as a function of mean particle size are given in Figures 5.5 and 5.6 respectively.

The most evident feature from Table 5.7 and Figures 5.5 and 5.6 is that intrinsic reactivity decreases (PT and BT increase) with particle size. The increase in PTs is not as significant as the increase in BTs. Generally speaking, there is an increase of PT and BT with coal rank as shown in Figure 5.4. El Cerrejon is the only exception, since it exhibits lower PTs than La Jagua, although the BT values are higher. A possible explanation for this is that the burning profiles of El Cerrejon chars tend to give a main peak followed by a wide shoulder (fraction I and II) or a wide peak (fraction III). This indicates that the most reactive material of El Cerrejon char reacts very quickly but the inert fraction left after reaching the maximum rate of weight loss takes a longer time to complete burnout. The chars

derived from Bijao coal fractions also tend to give a main peak follow by a shoulder.

Table 5.7 Intrinsic reactivity data for the pyrolysed chars as a function of particle size

| Coal/Fraction | | Peak Temperature | Burnout Temperature |
|--------------------|------------|------------------|---------------------|
| | | (°C) | (°C) |
| <i>Bijao</i> | <i>I</i> | 480 | 550 |
| | <i>II</i> | 486 | 554 |
| | <i>III</i> | 503 | 568 |
| <i>La Loma</i> | <i>I</i> | 535 | 575 |
| | <i>II</i> | 545 | 586 |
| | <i>III</i> | 546 | 596 |
| <i>La Jagua</i> | <i>I</i> | 587 | 619 |
| | <i>II</i> | 593 | 625 |
| | <i>III</i> | 597 | 645 |
| <i>El Cerrejon</i> | <i>I</i> | 563 | 631 |
| | <i>II</i> | 574 | 631 |
| | <i>III</i> | 594 | 646 |
| <i>Caypa</i> | <i>I</i> | 595 | 635 |
| | <i>II</i> | 630 | 669 |
| | <i>III</i> | 642 | 669 |
| <i>Guasare</i> | <i>I</i> | 626 | 668 |
| | <i>II</i> | 631 | 670 |
| | <i>III</i> | 637 | 676 |

Figure 5.4 DTA burning profiles for the 53-75 μm fraction pyrolysed chars

BI=Bijao; LO=La Loma; JA=La Jagua; CE=El Cerrejon; CA=Caypa; GU=Guasare

Figure 5.5 A plot of peak temperature as a function of mean particle size for the pyrolysed chars

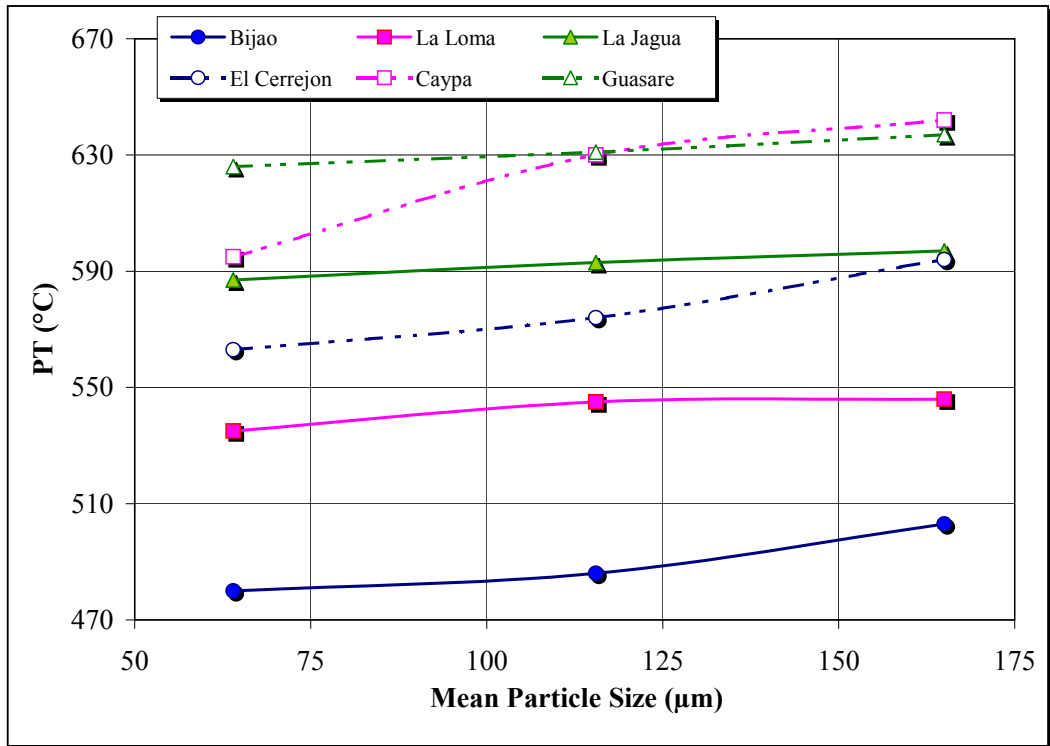
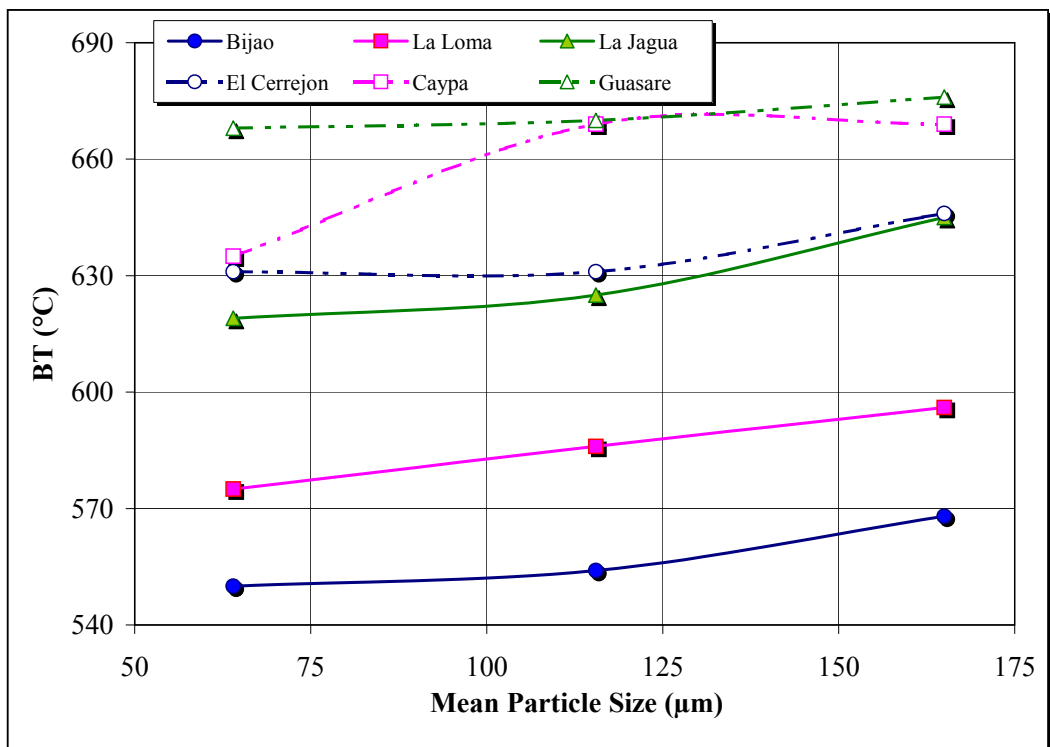


Figure 5.6 A plot of burnout temperature as a function of mean particle size for the pyrolysed chars



From analysis of the profiles in Appendix E, some differences in the effect of particle size can be seen for different coals. Guasare, for instance, shows little variation in the profiles and hence very similar PTs and BTs, as shown in Table 5.7. For Bijao and El Cerrejon chars, the profiles of fraction I and II are very similar but that of fraction III gives higher PT and BT values. For La Jagua, similar variations can be seen, although there is only a significant difference in BT values. Caypa shows the greatest differences in the profiles as a function of particle size. All the three fractions show significant differences in PT values. However, BT values for fractions II and III are identical and far higher than that of fraction I.

5.5.2 Optical Morphology and Automatic Analysis

The results for the manual and automatic char analysis are given in Table 5.8. The data consists of the different char types derived from the ICCP char classification system and the relative wall thickness parameter (ACA5). A summary of the manual char analysis which consists of thin-walled, thick-walled and solid chars, is shown in Table 5.9. In addition, tenuispheres and crassispheres have been group together as cenospheres, and crassinetworks and tenuinetworks as networks. These two categories were included in Table 5.9.

The results related to fraction I and II of the five Colombian coals are very similar to the data obtained in the previous chapter. Therefore, since this data has already been discussed, only the trends related to the inclusion of the new fraction (III) will be addressed here along with the results for the Venezuelan coal.

For Bijao and La Loma coals, which have the lowest rank of the coals tested, tenuinetworks comprise most of the thin-walled or low-density chars. For the rest of the coals, tenuispheres are the dominant low-density, thin-walled char type. It can be seen from Table 5.9 that the greater the particle size, the lower the proportion of thin-walled chars. This is in agreement with data obtained from the automatic char analysis i.e. ACA5 decreases with increasing particle size.

Guasare coal, as most vitrinite-rich bituminous coals, tends to produce mainly cenospheric chars. Tenuispheres make up most of the cenosphere population for fraction I. Fraction II and III, however, tend to give thicker walled chars (crassispheres) and, consistently, lower ACA5 values.

Table 5.8 Manual and automatic char analysis results

| Coal/Fraction | | ACA5 | Char Type Composition (vol%) ^a | | | | | |
|--------------------|------------|--------|---|------|------|------|-----|-----|
| | | (vol%) | TS | CS | TN | CN | I | F/S |
| <i>Bijao</i> | <i>I</i> | 98.5 | 0.5 | 0.1 | 77.1 | 21.3 | 0.5 | 0.5 |
| | <i>II</i> | 97.0 | 0.5 | 0.2 | 55.9 | 41.9 | 0.9 | 0.6 |
| | <i>III</i> | 93.4 | 0.0 | 0.1 | 36.8 | 61.3 | 1.2 | 0.6 |
| <i>La Loma</i> | <i>I</i> | 96.4 | 37.4 | 18.9 | 34.1 | 8.3 | 0.8 | 0.5 |
| | <i>II</i> | 93.6 | 8.9 | 11.3 | 46.1 | 32.1 | 0.7 | 0.9 |
| | <i>III</i> | 91.9 | 0.2 | 17.9 | 31.3 | 48.9 | 0.8 | 0.9 |
| <i>La Jagua</i> | <i>I</i> | 95.2 | 60.2 | 22.4 | 6.9 | 8.3 | 1.3 | 0.9 |
| | <i>II</i> | 92.6 | 33.2 | 47.6 | 1.6 | 14.5 | 2.4 | 0.7 |
| | <i>III</i> | 88.7 | 13.6 | 56.5 | 3.2 | 22.1 | 2.4 | 2.2 |
| <i>El Cerrejon</i> | <i>I</i> | 95.3 | 63.2 | 23.4 | 7.3 | 4.1 | 1.4 | 0.6 |
| | <i>II</i> | 92.9 | 35.7 | 44.3 | 6.4 | 11.4 | 1.2 | 1.0 |
| | <i>III</i> | 88.8 | 10.7 | 61.8 | 4.0 | 18.2 | 1.9 | 3.4 |
| <i>Caypa</i> | <i>I</i> | 96.3 | 77.9 | 15.7 | 0.2 | 4.8 | 0.4 | 1.0 |
| | <i>II</i> | 93.8 | 55.9 | 36.9 | 0.4 | 5.2 | 0.5 | 1.1 |
| | <i>III</i> | 89.9 | 14.6 | 70.5 | 0.0 | 10.6 | 1.3 | 3.0 |
| <i>Guasare</i> | <i>I</i> | 91.1 | 62.7 | 29.8 | 1.4 | 3.4 | 1.5 | 1.2 |
| | <i>II</i> | 89.5 | 24.8 | 65.5 | 0.9 | 5.7 | 2.0 | 1.1 |
| | <i>III</i> | 85.6 | 13.3 | 69.2 | 0.2 | 10.2 | 2.9 | 4.2 |

^aTS=Tenuisphere; CS=Crassisphere; TN=Tenuinetwork; CN=Crassinetwork; I=Inertoid; F/S=Fusinoid/Solid

Table 5.9 Summary of the manual char analysis results

| Coal/Fraction | | Proportion of Char Type (vol%) | | | | |
|--------------------|------------|--------------------------------|--------------|--------|-------------|----------|
| | | Thin Walled | Thick Walled | Solids | Cenospheres | Networks |
| <i>Bijao</i> | <i>I</i> | 77.6 | 21.4 | 1.0 | 0.6 | 98.4 |
| | <i>II</i> | 56.4 | 42.1 | 1.5 | 0.7 | 97.8 |
| | <i>III</i> | 36.8 | 61.4 | 1.8 | 0.1 | 98.1 |
| <i>La Loma</i> | <i>I</i> | 71.5 | 27.2 | 1.3 | 56.3 | 42.4 |
| | <i>II</i> | 55.0 | 43.4 | 1.6 | 20.2 | 78.2 |
| | <i>III</i> | 31.5 | 66.8 | 1.7 | 18.1 | 80.2 |
| <i>La Jagua</i> | <i>I</i> | 67.1 | 30.7 | 2.2 | 82.6 | 15.2 |
| | <i>II</i> | 34.8 | 62.1 | 3.1 | 80.8 | 16.1 |
| | <i>III</i> | 16.8 | 78.6 | 4.6 | 70.1 | 25.3 |
| <i>El Cerrejon</i> | <i>I</i> | 70.5 | 27.5 | 2.0 | 86.6 | 11.4 |
| | <i>II</i> | 42.1 | 55.7 | 2.2 | 80.0 | 17.8 |
| | <i>III</i> | 14.7 | 80.0 | 5.3 | 72.5 | 22.2 |
| <i>Caypa</i> | <i>I</i> | 78.1 | 20.5 | 1.4 | 93.6 | 5.0 |
| | <i>II</i> | 56.3 | 42.1 | 1.6 | 92.8 | 5.6 |
| | <i>III</i> | 14.6 | 81.1 | 4.3 | 85.1 | 10.6 |
| <i>Guasare</i> | <i>I</i> | 64.1 | 33.2 | 2.7 | 92.5 | 4.8 |
| | <i>II</i> | 25.7 | 71.2 | 3.1 | 90.3 | 6.6 |
| | <i>III</i> | 13.5 | 79.4 | 7.1 | 82.5 | 10.4 |

5.5.3 Correlation of DTF Volatiles and Char Properties with Coal Characteristics

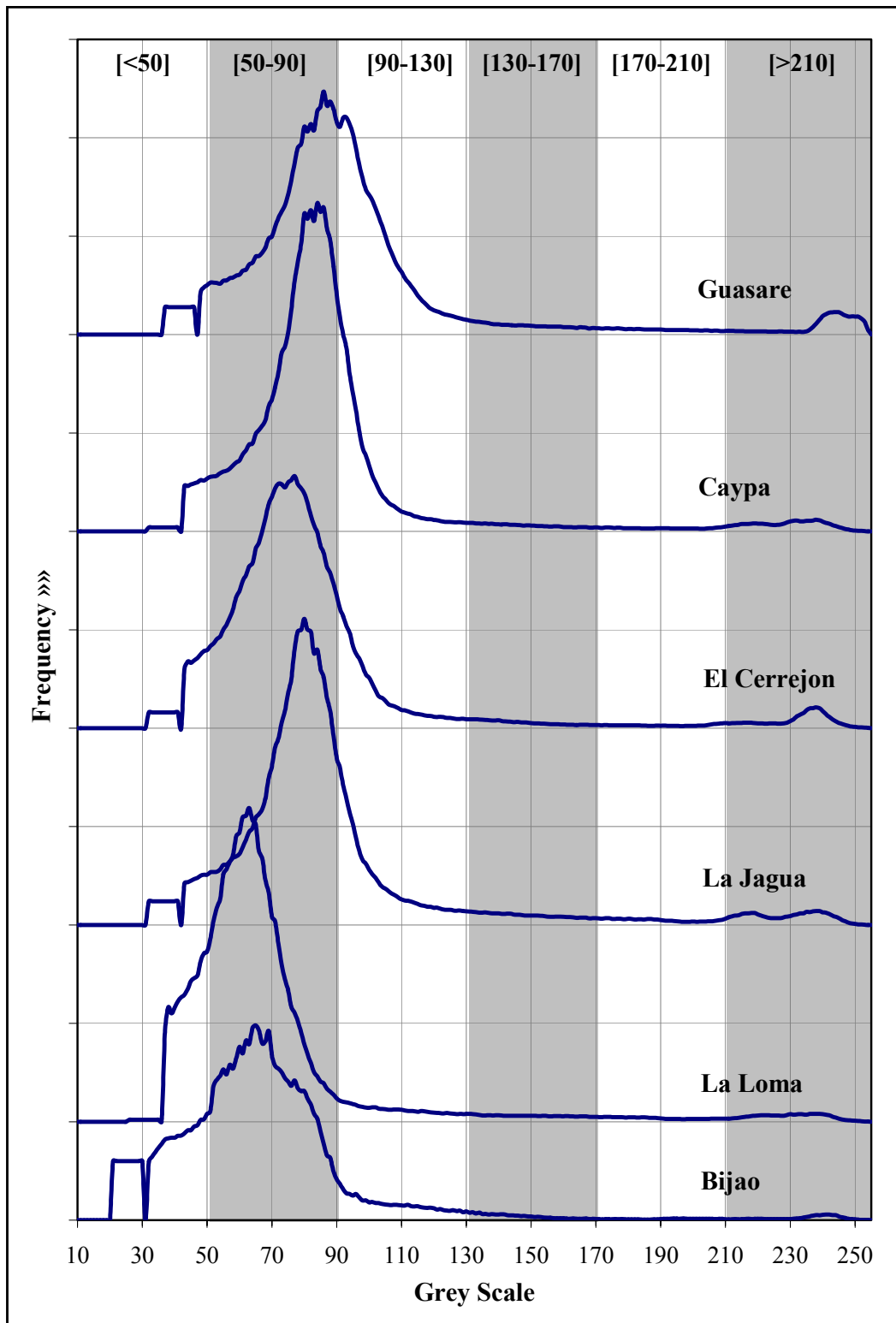
In a similar way as in chapter 4, correlation of the DTF volatiles and char properties such as PT, BT and ACA5 against some coal properties have been performed. The coal properties or independent variables considered were maceral content, maceral content and rank, and bands of the grey scale histograms. This was done by means of multiple linear regressions where the mean particle size of

the parent coal has been considered as an additional independent variable. The way in which the grey scale histogram of the coal was subdivided into different grey scale bands was explained in chapter 4, section 4.2.9.1. The percentage of the coal material covered by the different grey scale bands is given in Table 5.10 for all the coal fractions. Figure 5.7 shows the different grey scale bands for the 106-125 fraction for each coal.

Table 5.10 Percentage of coal material at different grey scale bands

| Coal/Fraction | | Grey Scale Bands | | | | | |
|--------------------|------------|------------------|---------|----------|-----------|-----------|------|
| | | <50 | [50-90] | [90-130] | [130-170] | [170-210] | >210 |
| <i>Bijao</i> | <i>I</i> | 28.29 | 61.12 | 7.75 | 1.59 | 0.34 | 0.92 |
| | <i>II</i> | 22.31 | 51.32 | 16.95 | 7.60 | 0.92 | 0.90 |
| | <i>III</i> | 27.13 | 64.47 | 5.19 | 1.38 | 0.55 | 1.29 |
| <i>La Loma</i> | <i>I</i> | 14.88 | 74.46 | 5.49 | 2.20 | 1.16 | 1.81 |
| | <i>II</i> | 19.14 | 69.85 | 4.91 | 2.40 | 1.45 | 2.25 |
| | <i>III</i> | 22.56 | 68.43 | 3.72 | 1.65 | 0.83 | 2.81 |
| <i>La Jagua</i> | <i>I</i> | 12.64 | 69.75 | 8.57 | 3.83 | 2.08 | 3.14 |
| | <i>II</i> | 6.21 | 67.12 | 17.06 | 3.89 | 1.99 | 3.74 |
| | <i>III</i> | 7.09 | 70.14 | 12.57 | 4.28 | 2.20 | 3.72 |
| <i>El Cerrejon</i> | <i>I</i> | 11.18 | 73.94 | 8.83 | 2.12 | 1.13 | 2.80 |
| | <i>II</i> | 7.29 | 72.47 | 13.53 | 2.22 | 1.16 | 3.32 |
| | <i>III</i> | 10.23 | 68.25 | 13.32 | 2.66 | 1.18 | 4.35 |
| <i>Caypa</i> | <i>I</i> | 6.89 | 74.08 | 12.63 | 2.26 | 1.34 | 2.81 |
| | <i>II</i> | 4.42 | 69.52 | 19.40 | 2.35 | 1.33 | 2.98 |
| | <i>III</i> | 7.80 | 79.06 | 7.40 | 1.55 | 0.84 | 3.36 |
| <i>Guasare</i> | <i>I</i> | 5.47 | 74.53 | 12.04 | 2.64 | 1.57 | 3.75 |
| | <i>II</i> | 4.29 | 51.46 | 34.52 | 3.67 | 2.02 | 4.04 |
| | <i>III</i> | 6.31 | 52.57 | 30.87 | 3.64 | 2.01 | 4.59 |

Figure 5.7 Grey scale histograms for the 106-125 μm coal fractions showing the different grey scale bands



The correlation results are summarised in Table 5.11. According to this data, some correlation between maceral analysis and the dependent variables exists particularly with DTF Volatiles ($R^2=0.91$) and ACA5 ($R^2=0.82$). When the rank was included in the regressions, the correlations remarkably improved with R^2 values greater than 0.84. Once again, the regressions against the grey scale histogram gave, in general, better correlation coefficients ($R^2>0.91$).

Table 5.11 Correlation coefficients and F values results from the regressions of the pyrolysed char properties with coal characteristics

| Dependent Variables | Independent Variables ^a | | | | | |
|------------------------|------------------------------------|--------------|---------------------------------|--------------|-----------------------------------|--------------|
| | Maceral Content ^b | | Macerals plus Rank ^c | | Grey-Scale Histogram ^d | |
| | R ² | F | R ² | F | R ² | F |
| <i>V_{DTF}</i> | 0.91 | 25.14 | 0.96 | 48.98 | 0.95 | 29.75 |
| <i>PT</i> | 0.63 | 4.45 | 0.85 | 11.68 | 0.91 | 16.52 |
| <i>BT</i> | 0.59 | 3.71 | 0.84 | 10.49 | 0.93 | 19.60 |
| <i>ACA5</i> | 0.82 | 11.79 | 0.93 | 27.80 | 0.94 | 26.84 |

^aIncluding Mean Particle Size;

^b $v_1=5$, $v_2=12$, F-critical=3.11; ^c $v_1=6$, $v_2=11$, F-critical=3.09; ^d $v_1=7$, $v_2=10$, F-critical=3.14

5.6 Properties of the Re-Fired Chars

5.6.1 Char Reactivity and Burnout

Coal combustion is hardly ever completed in practical pf combustion systems and a small proportion of the fuel is emitted from the boiler as partially burnt char. This is normally named unburnt carbon and typically accounts for approximately 0.5% within the range 0.2-1.0%, compared with unburnt fuel levels of approximately 0.1% for oil and virtually nil for gas (Unsworth et al., 1991; Singer, 1981). Basically the unburnt carbon can be defined as the weight percentage of dry, ash-free coal that is not burnt in the furnace. In this work, unburnt carbon will be referred to as unburnt combustible. The amount of

unburnt combustible depends on coal type, boiler design and operating conditions. The combustion burnout performance of a coal is of considerable commercial importance. Unburnt combustible represent a direct loss in thermal efficiency and the performance of electrostatic dust collection equipment can be seriously damaged by high levels of carbon in ash.

The reactivity of pf coal char has been widely studied because of its importance in the combustion process. The efficiency of char combustion within the DTF system may be measured by the proportion of combustible remaining within the re-fired char residue. This can be easily calculated if the ash content of the feed coal and that of the char product are known. It is assumed that the ash is inert in the system and the mass of ash in the feed coal equals the mass of the ash product. The re-fired char residue is the result of the burnout of a previously pyrolysed char, therefore, unburnt combustible can be determined either relative to the pyrolysed char or to the feed coal. Since most of the volatile matter is released during high temperature pyrolysis, the unburnt combustible figures relative to the pyrolysed char would comprise the percentage of fixed carbon remaining. Unburnt combustible determination relies on the ash tracer technique, and can be estimated as follows:

(1) Relative to the pyrolysed char:

$$\text{Unburnt Combustible (wt\%)} = \frac{100 \times A_P \times (100 - A_R)}{A_R \times (100 - A_P)} \quad (5.1)$$

(2) Relative to the feed coal:

$$\text{Unburnt Combustible (wt\%)} = \frac{100 \times A_C \times (100 - A_P)}{A_P \times (100 - A_C)} \quad (5.2)$$

Where A_C , A_P and A_R are the ash content of the parent coal, the pyrolysed and the re-fired chars, respectively, on a dry basis.

Frequently, the efficiency of combustion is measured by the burnout level of the char sample relative to the parent coal. That is, the percentage of the combustible matter in the feed coal which has been devolatilised or burnt out after pyrolysis and re-firing. According to its definition, the burnout level of a coal can be easily calculated by simply subtracting the percentage of unburnt combustible in the char from 100%.

Table 5.12 contains the results of the unburnt combustible for the re-fired chars relative to both the pyrolysed char and to the parent coal. For the re-fired chars at 600 ms, unburnt combustible levels of the coal studied range from zero to 16.4% indicating that the majority of the original coal particles have completely burnt out in the presence of oxygen. The data shows the highly reactive nature of Bijao and La Loma, where the burnout is significantly higher than for any of the other coals. In fact, the unburnt combustible figures for the re-fired chars at 200 ms of these two coals range from around 15% for fraction III, approximately 10% for fraction II, and only 5% for fraction I.

The data obtained confirms the importance of particle size on burnout. The average proportion of unburnt combustible in the chars range from 0.2 to 12.2% for fraction I, from 3.7 to 17% for fraction II, and from 6.2 to 22.5% for the coarsest coal fraction III. It is also notable that differences occur between coals with Guasare showing the poorest combustible conversion efficiency and Bijao and La Loma the best. Since chars derived from low rank coals are more porous than chars from higher rank coals, this offers an explanation of why chars from low rank coals are generally more reactive than those from higher rank coals.

As mentioned in chapter 4, previous work in this laboratory has shown that the % unreactives correlates well with burnout potential of coals (Cloke et al., 1997a & b). Following this approach, plots of unburnt combustible data against % unreactives have been obtained and are shown in Figures 5.8 to 5.10 for the 200 ms, 400 ms and 600 ms samples, respectively.

Table 5.12 Unburnt combustible and burnout results for the re-fired chars

| Coal/Fraction | | Unburnt Combustible ^a (wt% daf) | | | Unburnt Combustible ^b (wt% daf) | | |
|--------------------|------------|---|--------|--------|---|--------|--------|
| | | 200 ms | 400 ms | 600 ms | 200 ms | 400 ms | 600 ms |
| <i>Bijao</i> | <i>I</i> | 14.93 | 2.14 | 0.00 | 4.19 | 0.60 | 0.00 |
| | <i>II</i> | 32.13 | 8.35 | 0.28 | 10.06 | 2.62 | 0.09 |
| | <i>III</i> | 39.68 | 14.97 | 2.96 | 15.30 | 5.77 | 1.14 |
| <i>La Loma</i> | <i>I</i> | 19.44 | 3.14 | 0.00 | 5.69 | 0.92 | 0.00 |
| | <i>II</i> | 32.61 | 10.42 | 0.31 | 11.14 | 3.56 | 0.11 |
| | <i>III</i> | 39.81 | 16.63 | 2.57 | 14.91 | 6.23 | 0.96 |
| <i>La Jagua</i> | <i>I</i> | 45.26 | 11.72 | 0.46 | 15.34 | 3.97 | 0.16 |
| | <i>II</i> | 49.53 | 22.71 | 6.03 | 18.50 | 8.48 | 2.25 |
| | <i>III</i> | 55.54 | 28.22 | 12.86 | 24.79 | 12.60 | 5.74 |
| <i>El Cerrejon</i> | <i>I</i> | 44.39 | 17.67 | 1.22 | 14.30 | 5.69 | 0.39 |
| | <i>II</i> | 44.37 | 27.33 | 15.11 | 16.24 | 10.00 | 5.53 |
| | <i>III</i> | 51.10 | 32.03 | 16.33 | 22.44 | 14.07 | 7.17 |
| <i>Caypa</i> | <i>I</i> | 44.88 | 12.90 | 0.35 | 14.53 | 4.18 | 0.11 |
| | <i>II</i> | 51.84 | 26.64 | 10.26 | 18.64 | 9.58 | 3.69 |
| | <i>III</i> | 50.79 | 29.51 | 14.21 | 21.03 | 12.22 | 5.88 |
| <i>Guasare</i> | <i>I</i> | 56.48 | 22.17 | 1.56 | 19.41 | 7.62 | 0.54 |
| | <i>II</i> | 68.88 | 47.27 | 26.27 | 27.19 | 18.66 | 10.37 |
| | <i>III</i> | 76.46 | 59.65 | 34.24 | 36.61 | 28.56 | 16.40 |

^a Relative to the pyrolysed char; ^b Relative to the parent coal

Figure 5.8 Unburnt combustible against % unreactives for the 200 ms re-fired chars

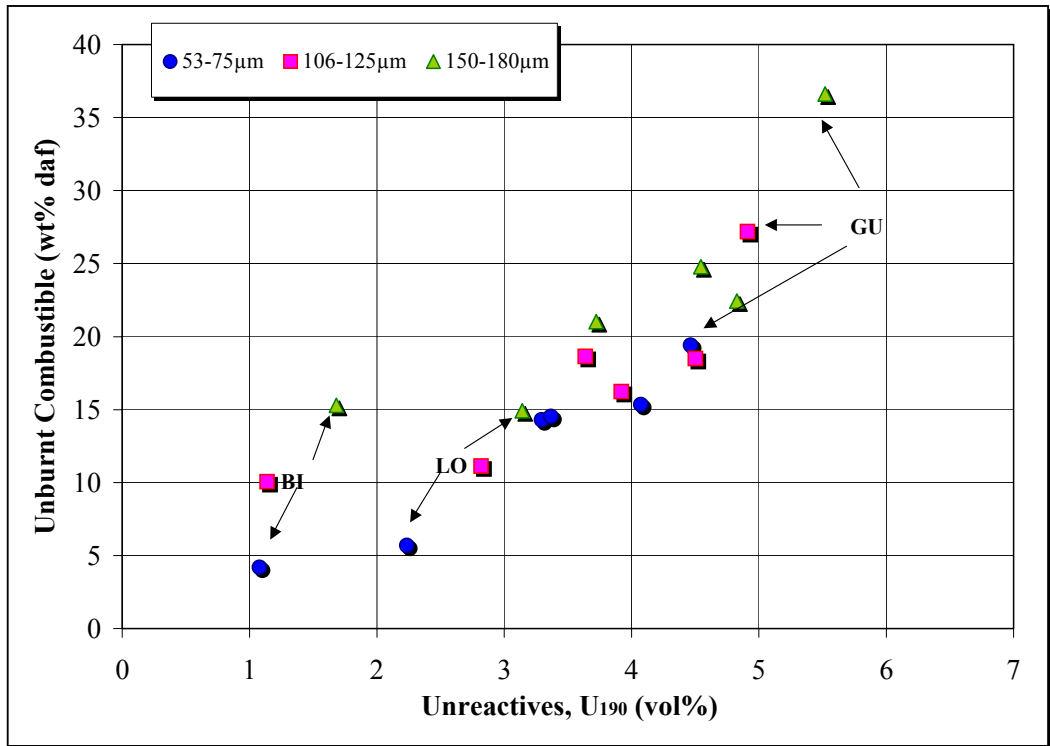


Figure 5.9 Unburnt combustible against % unreactives for the 400 ms re-fired chars

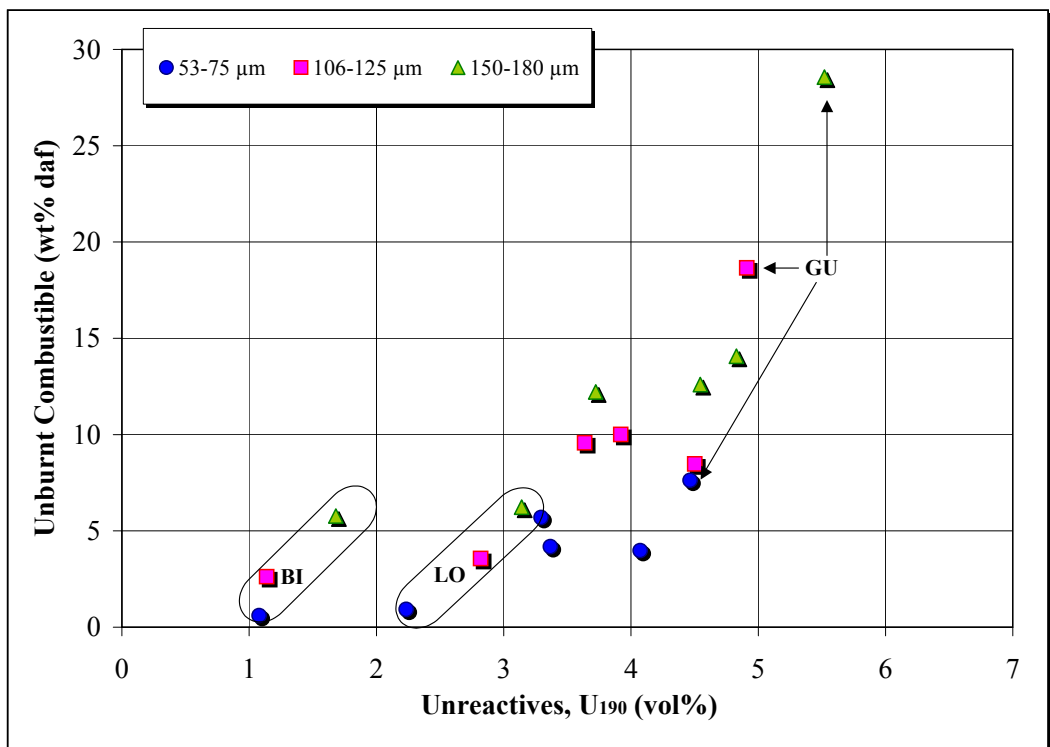
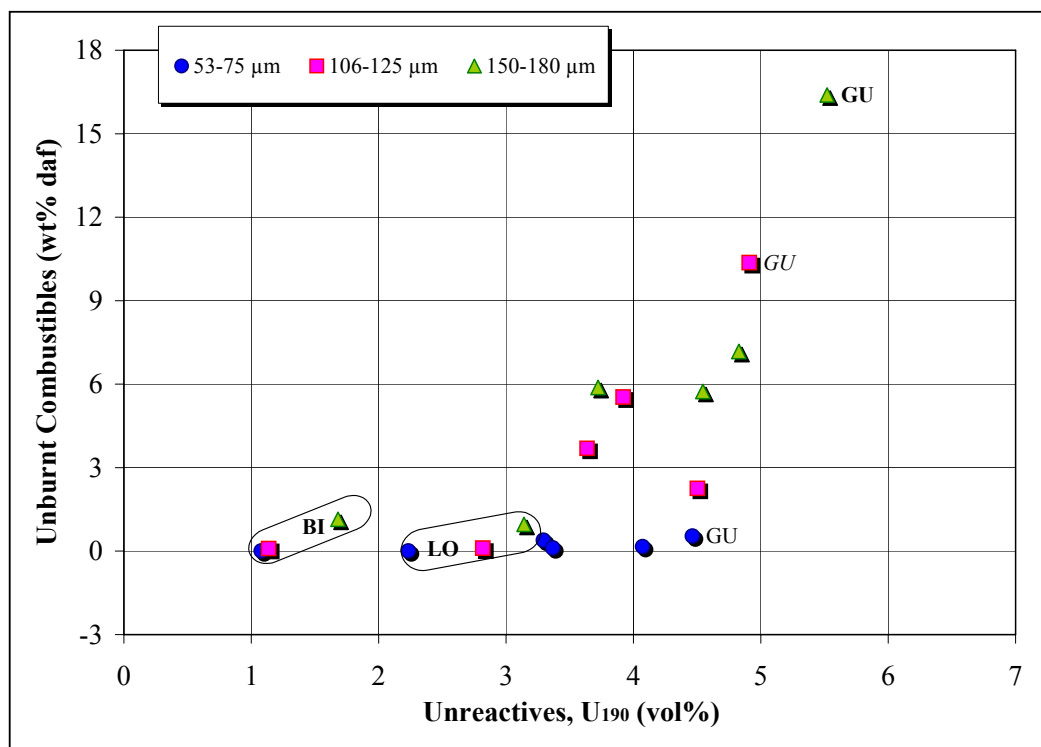


Figure 5.10 Unburnt combustible against % unreactives for the 600 ms re-fired chars



From examination of the previous figures and the data in Table 5.12, it can be seen that fractions II and III of Guasare coal appear to burnout slowly. Fraction I does not show poor burnout implying that particle size considerably affects the burnout behaviour of this particular coal. This means that the percentage of combustible in ash will increase significantly for Guasare if it is not properly milled before combustion.

The combustible burnout data of the re-fired chars was compared with the automatic char analysis of the pyrolysed char in order to determine whether there was any correlation. A plot of unburnt combustible for the 400 ms re-fired chars against ACA5 for all the coal fractions is given in Figure 5.11. It shows a general trend of decreasing unburnt combustible with increasing ACA5. It can be noticed from the plot that Guasare does not reveal any unusual behaviour. This confirms the usefulness of high temperature pyrolysis char as a predictor of burnout behaviour. The poor burnout performance of Guasare is clearly due to the

formation of thicker walled chars during pyrolysis (mainly cenospheric chars) and this agrees with the finding of Cloke et al. (1997a).

In a similar way as with automatic char analysis data, a plot of unburnt combustible for the 400 ms re-fired char against peak temperature of the pyrolysed char was produced (Figure 5.12). The graph shows a general trend of increasing unburnt combustible with decreasing intrinsic reactivity (increasing PT). The clear outlier from the trend is Guasare which shows a higher-than-expected percentage of unburnt combustible. Only fractions II and III of this coal appear to burn out slower than expected. Fraction I does not show poor burnout and this is in agreement with the prediction of the % unreactives parameter as discussed above. It can be concluded that particle size considerably affects the burnout behaviour of Guasare coal. The better prediction of unburnt combustible from the ACA5 parameter suggests that the initial char morphology is the most important controlling factor in the final combustion performance of the char. However, the intrinsic reactivity of the initial char also plays a part.

Figure 5.11 Relation between unburnt combustible of the 400 ms re-fired chars and the automatic char analysis of the pyrolysed chars

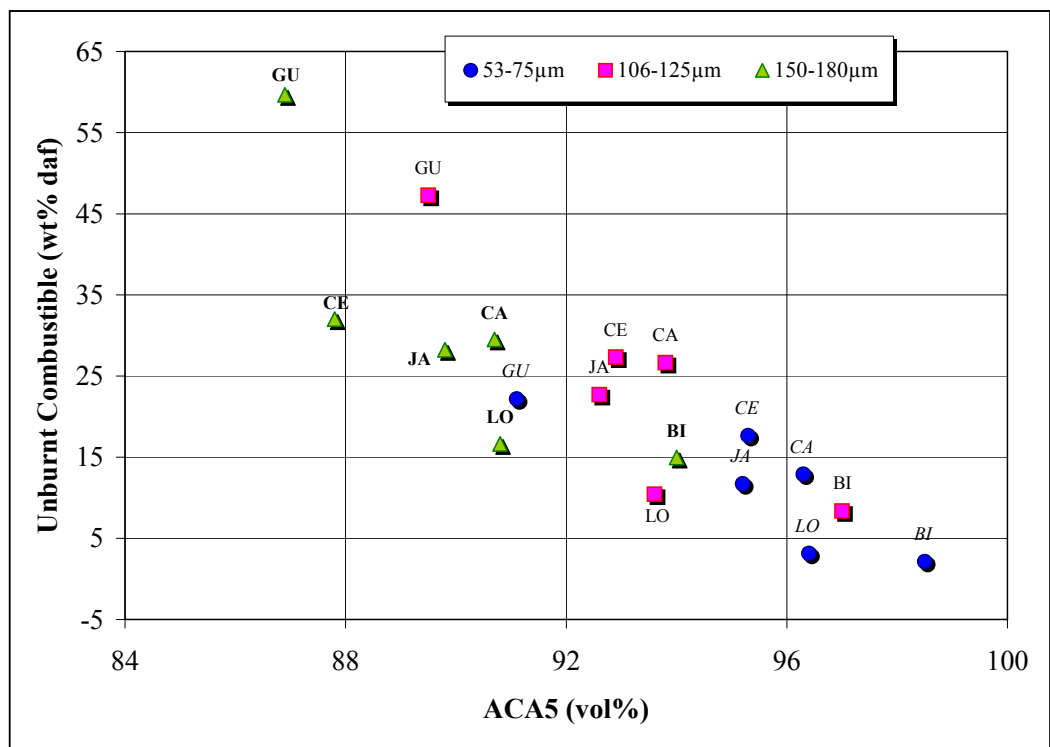
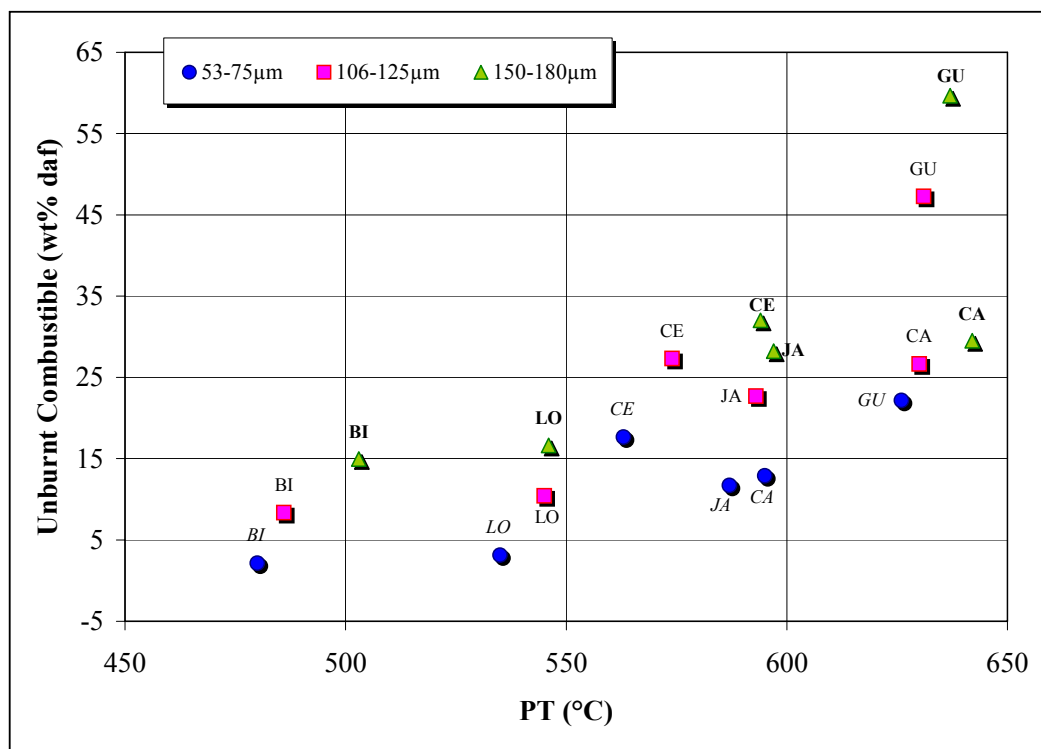


Figure 5.12 Relation between unburnt combustible of the 400 ms re-fired chars and the peak temperature of the pyrolysed chars



5.6.2 Char Intrinsic Reactivity

Table 5.13 contains the intrinsic reactivity data for the re-fired chars. The DTA burning profiles are presented in Appendix F as a function of particle size at each different residence time. The DTA output was normalised as explained in section 5.5.1.

The results obtained suggest that the intrinsic reactivity, as measured by the BT, decreases with increasing burnout, i.e. with increasing residence time. However, as the residence time increases, most of the chars from the same parent coal appear to change very little as far as PT is concerned. This implies that during the initial stage of the TGA analysis, the rate at which a char particle burns is practically independent of degree of burnout. In many cases, a slight decrease of PT with increasing burnout was observed. It is expected that diffusion of oxygen into the char particle has a smaller influence on a char which has achieved greater

Table 5.13 Char intrinsic reactivity data as a function of temperature and particle size

| Coal/Fraction | | Peak Temperature (°C) | | | Burnout Temperature (°C) | | |
|---------------------------|------------|-----------------------|--------|--------|--------------------------|--------|--------|
| | | 200 ms | 400 ms | 600 ms | 200 ms | 400 ms | 600 ms |
| <i>Bijao</i> | <i>I</i> | 569 | 563 | 551 | 601 | 638 | 650 |
| | <i>II</i> | 552 | 572 | 573 | 596 | 606 | 640 |
| | <i>III</i> | 550 | 564 | 578 | 595 | 603 | 613 |
| <i>La Loma</i> | <i>I</i> | 572 | 579 | 573 | 615 | 635 | 660 |
| | <i>II</i> | 569 | 584 | 599 | 616 | 636 | 656 |
| | <i>III</i> | 577 | 580 | 585 | 628 | 635 | 649 |
| <i>La Jagua</i> | <i>I</i> | 597 | 595 | 597 | 638 | 641 | 658 |
| | <i>II</i> | 609 | 602 | 599 | 656 | 658 | 660 |
| | <i>III</i> | 611 | 608 | 605 | 670 | 670 | 670 |
| <i>El Cerrejon</i> | <i>I</i> | 630 | 619 | 620 | 679 | 681 | 685 |
| | <i>II</i> | 632 | 624 | 622 | 682 | 685 | 690 |
| | <i>III</i> | 634 | 636 | 635 | 690 | 694 | 707 |
| <i>Caypa</i> | <i>I</i> | 618 | 611 | 616 | 638 | 677 | 680 |
| | <i>II</i> | 645 | 641 | 630 | 680 | 709 | 715 |
| | <i>III</i> | 647 | 647 | 637 | 690 | 720 | 724 |
| <i>Guasare</i> | <i>I</i> | 636 | 632 | 622 | 680 | 704 | 706 |
| | <i>II</i> | 638 | 646 | 635 | 680 | 711 | 711 |
| | <i>III</i> | 648 | 650 | 639 | 701 | 715 | 715 |

burnout. The chars with higher burnout exhibit more open pores which are accessible for gas phase transport so that the reactive material remaining in the char will burn very effectively and may, therefore, give similar, or even lower, PT values than chars with less burnout.

A general trend of increasing PT and BT values for La Jagua, El Cerrejon, Caypa and Guasare chars with increasing particle size can be observed from Appendix E and Table 5.13. Bijao shows the opposite trend, particularly with BT values. For La Loma chars, no definite trend of intrinsic reactivity with particle size is observed and this appears to vary with burnout. Thus, char of different size, although from the same coal, are intrinsically different. Not only must maceral segregation effects be considered, but also the intrinsic size dependence on particle size may need to be taken into account. Hence, some caution is necessary when reactivity data obtained on a single char size range is applied to a total coal.

Overall, there is an increase of intrinsic reactivity (PT and BT), with increasing coal rank. Figure 5.13 shows the DTA burning profiles of the 400 ms re-fired chars in which this general trend can be observed. It can also be seen from the figure that the higher the rank of the coal char the broader the burning profile. Since chars from low rank coals are generally more porous than chars from higher rank coals, this may be an explanation of why chars from low rank coals are generally more reactive than those from higher rank coals. Variations in char reactivity can be further related to catalytic effects of trace minerals in the char. This is, however, beyond the scope of this study.

5.6.3 Scanning Electron Microscope Examination

Scanning electron microscope (SEM) photographs of the parent coal (fraction II), the pyrolysed and the 400 ms re-fired chars were obtained to identify any changes in external appearance which may have occurred during pyrolysis and char re-firing. The SEM photograph for the various coal/char samples (fraction II) are presented in Figures 5.14 to 5.19, whereas Table 5.14 gives a brief description of the visual examination features of the pyrolysed and re-fired chars.

Figure 5.13 DTA burning profiles for the 400 ms re-fired chars (Fraction II)

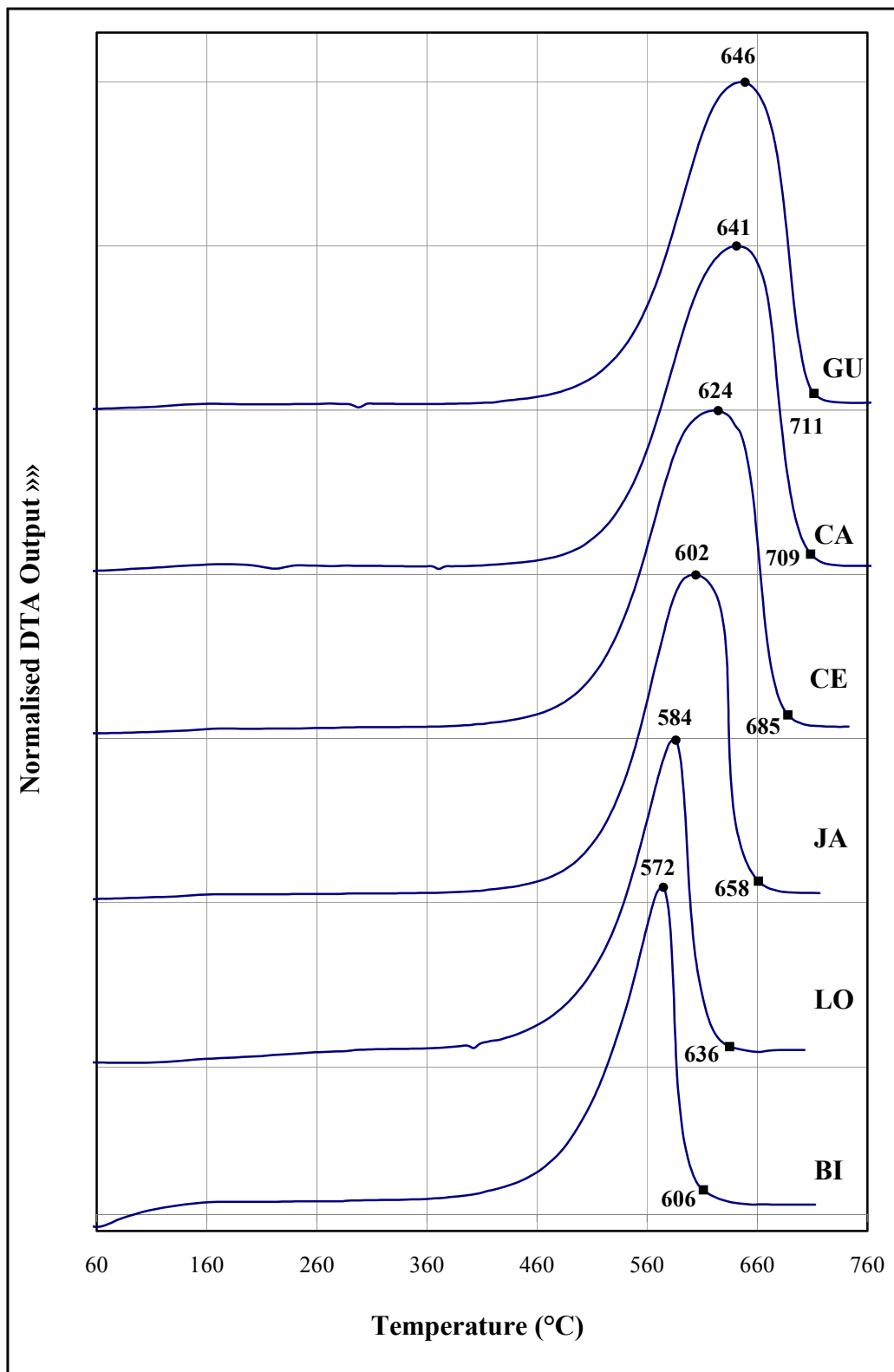


Table 5.14 External appearance of pyrolysed and re-fired chars, fraction II

| Coal | Morphology and External Appearance | |
|--------------------|---|---|
| | Pyrolysed Char | Re-fired Char @ 400 ms |
| <i>Bijao</i> | Chars which exhibit fissure-type macropores and an extended network of micropores. Discrete particles, mostly intact, and with irregular to subangular appearance. | Char with a network-like structure, some are solid with some degree of porosity, and others are fragmented. Mineral inclusions and high ash level. |
| <i>La Loma</i> | Similar to Bijao although the fissure-type micropores are not evident. Discrete particles, elongated with subangular to oblate appearance and few spherical. | Similar to Bijao although the remaining solid particles are more spherical. |
| <i>La Jagua</i> | Chars that have many large vesicles. Discrete particles, mainly spherical to subspherical in appearance, typical of cenospheric chars. | Cenospheres with different burnout level; some very lacy. Most of the particles are intact. Mineral inclusions and ash associated with the particles. |
| <i>El Cerrejon</i> | Some chars exhibit large vesicles others extended network of micropores. Discrete particles, mostly spherical, few irregular and others subangular and oblate in appearance. | Similar to La Jagua, although the cenospheres exhibit, generally, less burnout. Very little fragmentation. |
| <i>Caypa</i> | Similar to La Jagua although some particles show larger vesicles and a higher degree of swelling. Discrete particles, spherical in appearance typical of high vitrinite bituminous coals. | Cenospheres with different stages of burnout as El Cerrejon and La Jagua although most particles have larger vesicles and are more rounded in shape. |
| <i>Guasare</i> | Similar to La Jagua and Caypa. Discrete particles, mainly spherical in appearance. Some particles appear to be larger than those from the coal. | Cenospheres with different burnout level. Some chars exhibit a high percentage of mineral matter. |

Figure 5.14 SEM photomicrograph of Bijao coal/chars, fraction II

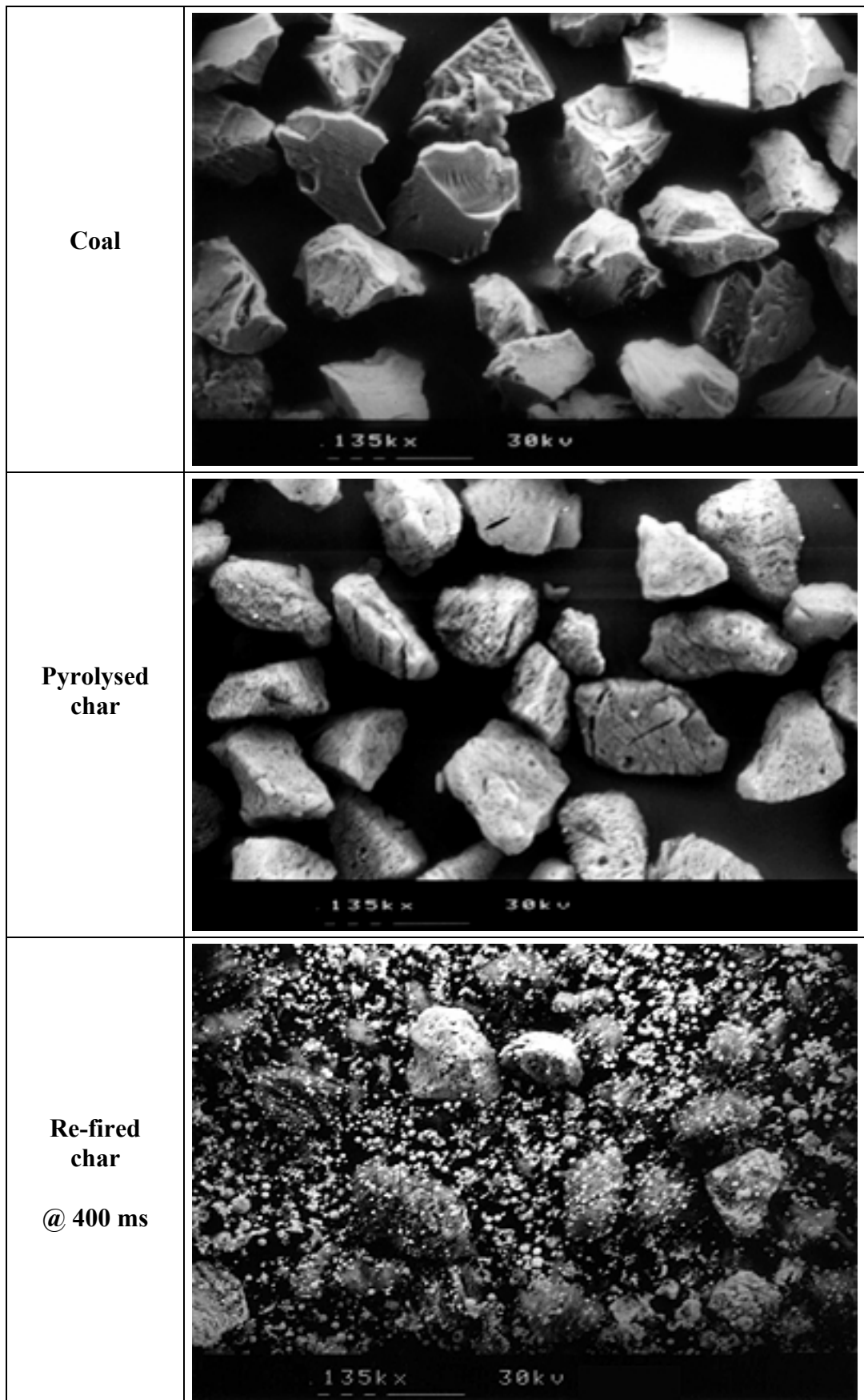


Figure 5.15 SEM photomicrograph of La Loma coal/chars, fraction II

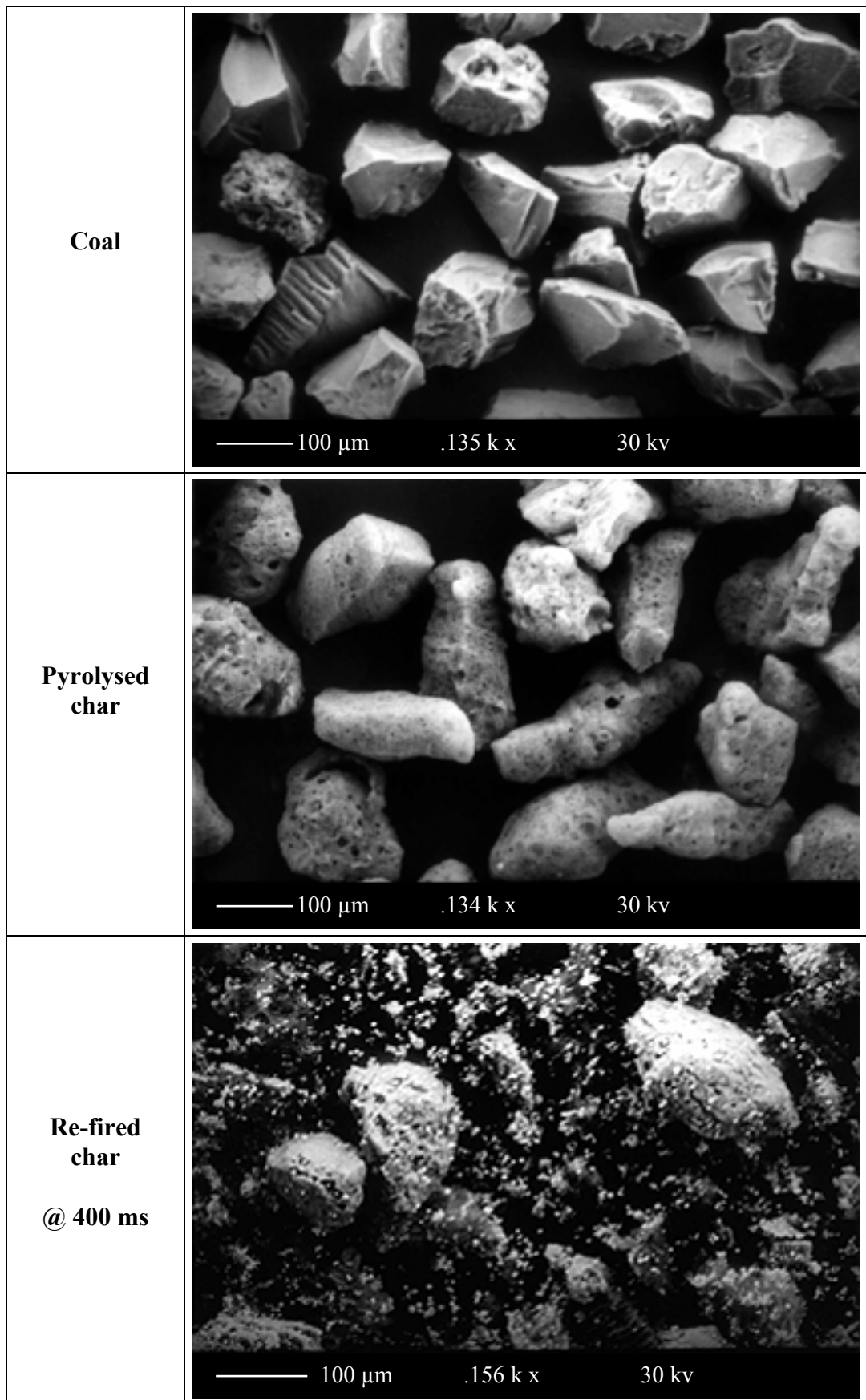


Figure 5.16 SEM photomicrograph of La Jagua coal/chars, fraction II

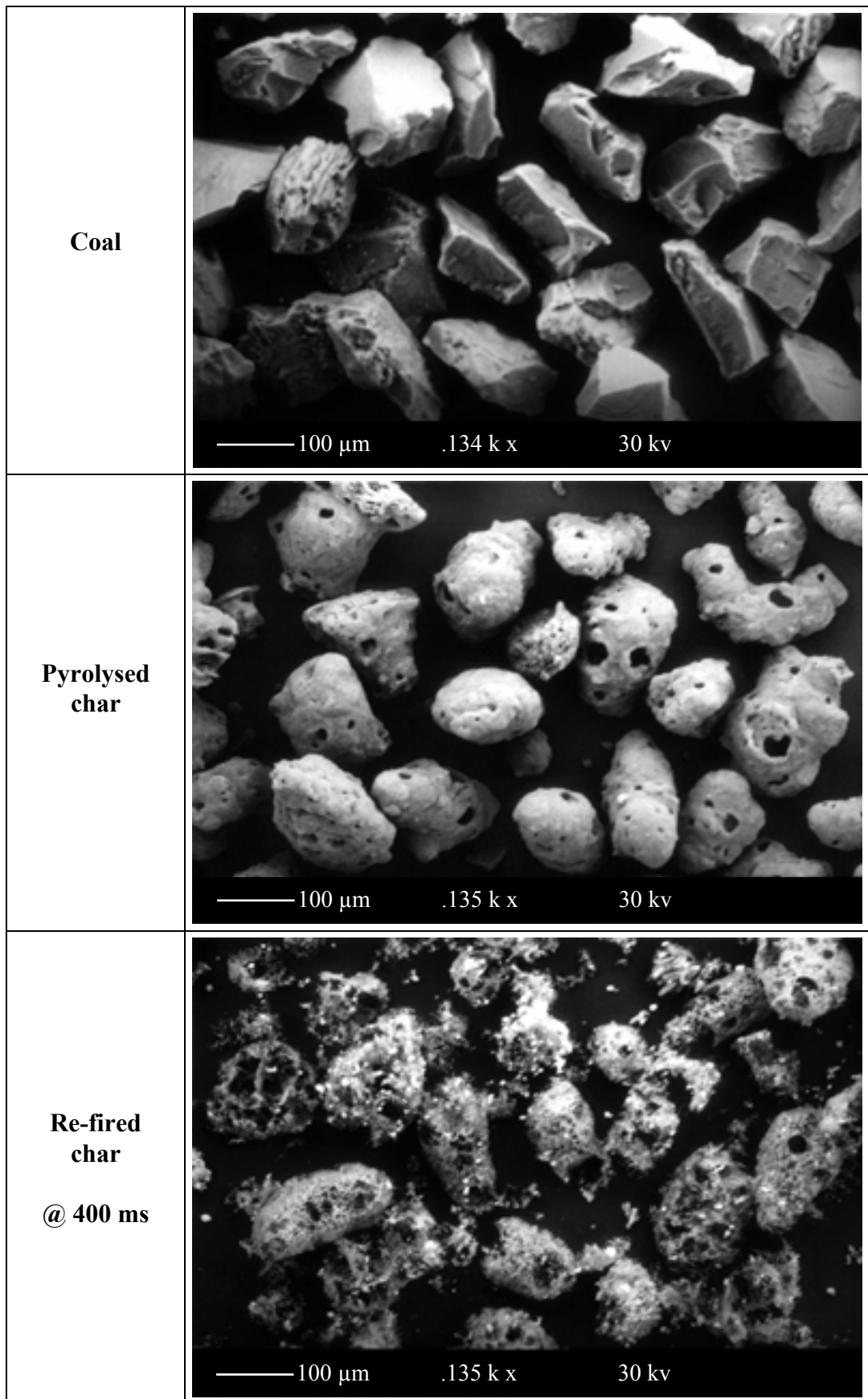


Figure 5.17 SEM photomicrograph of El Cerrejon coal/chars, fraction II

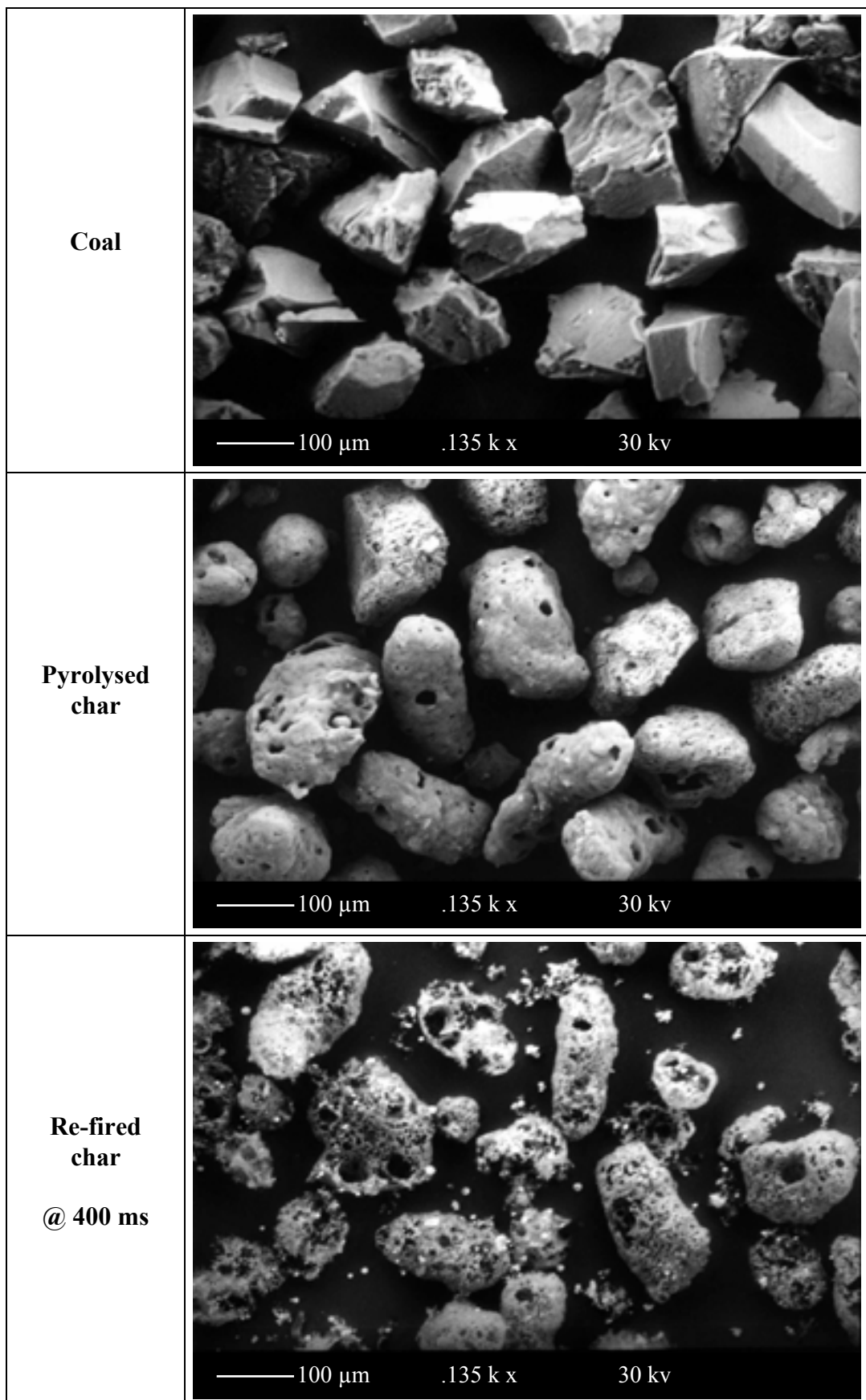


Figure 5.18 SEM photomicrograph of Caypa coal/chars, fraction II

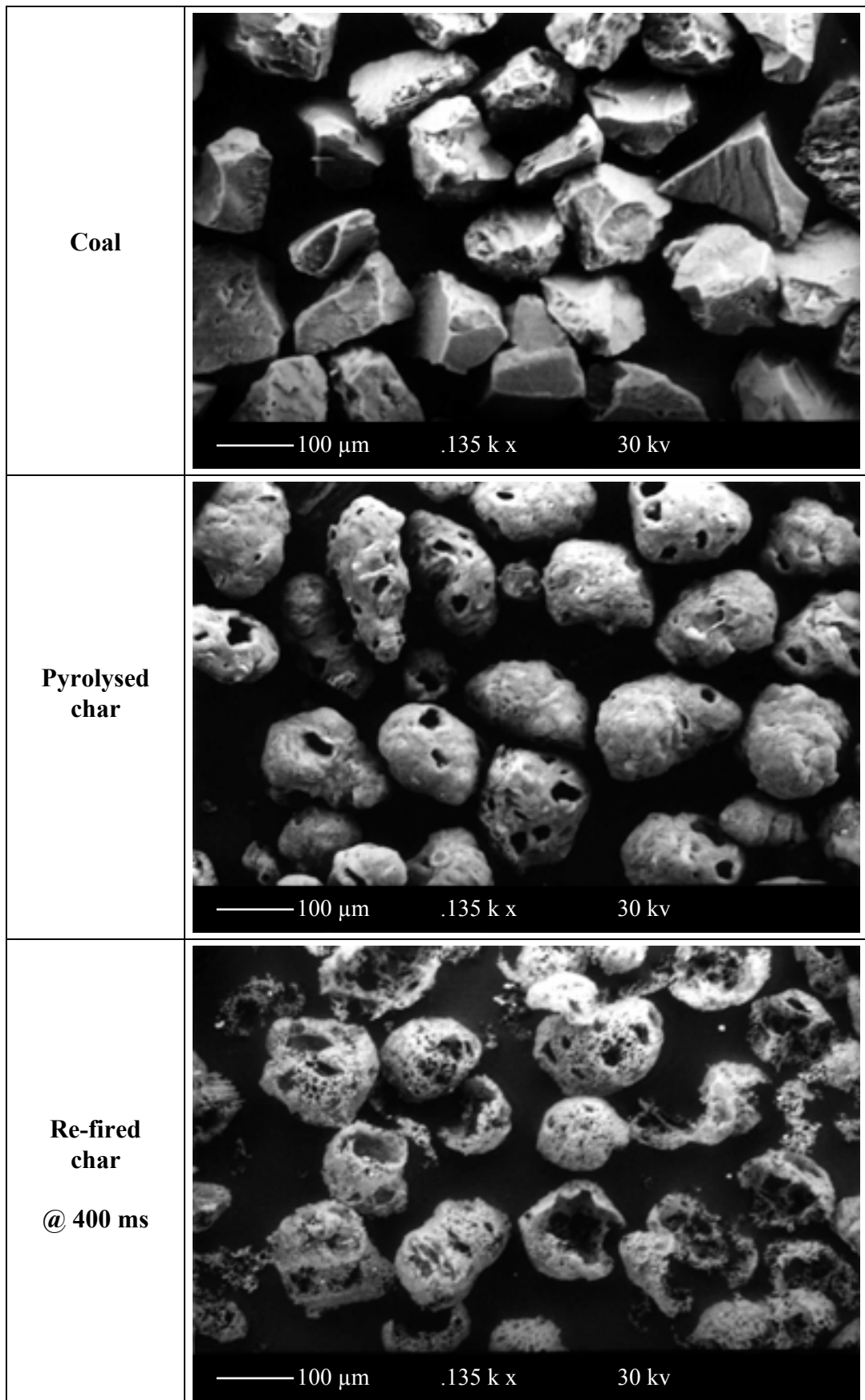
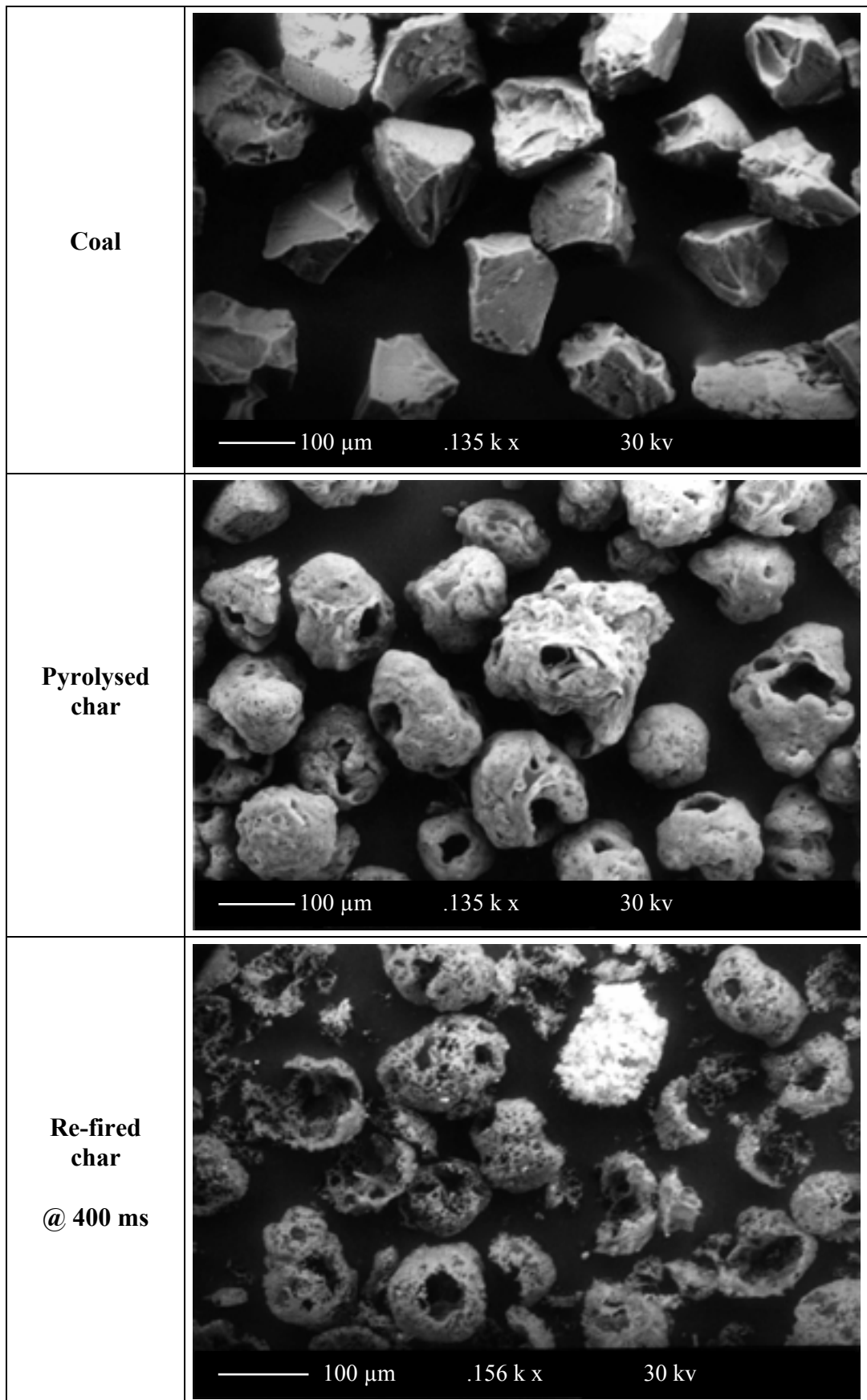


Figure 5.19 SEM photomicrograph of Guasare coal/chars, fraction II



Bijao and La Loma coal changed very little in shape and size after pyrolysis. Most of the particles from the other coals were angular and elongated in shape but became rounded or spherical as they softened during pyrolysis. The stronger chemical cross-linkage of hydrocarbon chains in the low rank coals prevents them from fusing properly in the furnace, so that they have limited ability to form spherical chars (Bailey et al., 1990). Instead, these coals devolatilise without caking, by releasing volatiles from many enlarged pores to form networks. The Guasare photographs do not offer any morphological explanation as to its poor burnout, since it is clearly able to form open chars. Although most of the chars produced by this coal during pyrolysis are mostly cenospheric, their high values of ACA5 indicate that these chars are thick and will therefore require more time to complete burnout.

5.1.1 Correlation of Re-fired Char Properties with Coal Characteristics

Correlations between unburnt combustibles and the intrinsic reactivity data of the re-fired chars with maceral content, maceral content and rank, and bands of the grey scale histograms have been performed. The mean particle size of the parent coal has been considered as an additional independent variable. The percentage of the coal material covered by the different grey scale bands has been presented in Table 5.10 for all the coal fractions.

The correlation data is presented in Table 5.15 as a function of residence time. The coefficients of determination R^2 and the F-observed values along with the F-critical values have been included. According to the results, a weak correlation between maceral analysis and the dependent variables can be observed in most cases as explained by the low R^2 and F values. When the rank is taken into account in the regressions, the correlations improved with R^2 values greater than 0.75. The unburnt combustible of the samples obtained at 200 and 400 ms gave the best correlations as shown by their high R^2 (0.96 and 0.91 respectively). The correlation for the unburnt combustible of the samples at 600 ms is not as good due mostly to the higher error involved in the ash determinations as the burnout level increases. The fact that fraction I of Bijao and La Loma gave virtually

100% burnout when re-fired at 600 ms suggests that these samples could have completed burnt out in less time. Once again, the best regressions are achieved when correlating the dependent variables against the bands of the grey scale histogram. Coefficients of determination are all greater than 0.86 and F values at least three times greater than the F-critical values.

Table 5.15 Correlation coefficients and F Values results from the regressions of char properties with coal characteristics

| Dependent Variables | Residence Time | Independent Variables ^a | | | | | |
|----------------------|----------------|------------------------------------|-------------|---------------------------------|--------------|-----------------------------------|--------------|
| | | Maceral Content ^b | | Macerals plus Rank ^c | | Grey-Scale Histogram ^d | |
| | ms | R ² | F | R ² | F | R ² | F |
| <i>U_C</i> | 200 | 0.69 | 5.75 | 0.96 | 43.15 | 0.92 | 17.43 |
| | 400 | 0.63 | 4.50 | 0.91 | 19.56 | 0.93 | 19.70 |
| | 600 | 0.59 | 3.71 | 0.80 | 7.91 | 0.87 | 10.82 |
| <i>PT</i> | 200 | 0.58 | 3.60 | 0.77 | 6.53 | 0.94 | 26.43 |
| | 400 | 0.54 | 3.07 | 0.80 | 7.89 | 0.93 | 20.57 |
| | 600 | 0.56 | 3.36 | 0.80 | 7.83 | 0.87 | 10.33 |
| <i>BT</i> | 200 | 0.70 | 6.03 | 0.81 | 8.59 | 0.92 | 18.31 |
| | 400 | 0.53 | 2.93 | 0.79 | 7.35 | 0.91 | 16.06 |
| | 600 | 0.53 | 2.94 | 0.75 | 6.08 | 0.86 | 9.30 |

^a Including Mean Particle Size;

^b $v_1=5$, $v_2=12$, F-critical= 3.11; ^c $v_1=6$, $v_2=11$, F-critical=3.09; ^d $v_1=7$, $v_2=10$, F-critical=3.14

CHAPTER 6 EXPERIMENTS IN THE 1MW RIG

6.1 Introduction

Owing to recent developments in milling technology, significant improvements in mill product quality are now achievable. This can, potentially, provide combustion efficiency improvements with associated reductions in combustible-in-ash levels, CO production, and particulate and gaseous emissions.

The performance of current pf milling plant is limited by the best practically attainable fineness from conventional equipment. This, however, does not necessarily indicate the optimal particle size distribution for a particular coal. By taking into consideration the potential improvements in mill product quality available through new classification technologies, a recent study has been carried out by Powergen UK plc, in collaboration with Nottingham University, to determine the effect of pf particle size distribution on coal burnout propensity. The programme of work is entitled “Combustion Test Facility testing to assess the effects of PF grind quality on combustion”. The study involved combustion tests on two different coals in the 1 MW combustion test facility rig (CTF) at Powergen Technology Centre.

In this work coals were sourced by Powergen UK plc who arranged for contract grinding of the coals and carried out combustion tests on their 1 MW CTF at Power Technology Centre, Ratcliffe-on-Soar, Nottingham. Powergen carried out particle-size analysis on the pf and proximate and ultimate analysis on all coals and char samples. Petrographic analysis of coals, morphology and reactivity of chars, and image analysis of coals and chars was carried out by the author at Nottingham University. All relevant results from this study are now presented.

For these tests, the coals selected were Carbocol (a sample from the El Cerrejon coal mine in Colombia), and a British coal, Thoresby, for comparative purposes. On some Figures and Tables, these coals will be referred as CAR and THO respectively. Each coal was milled to five different particle size distributions. The coals themselves were selected to be representative of extremes in fuel characteristics experienced by coal-importing utilities in Europe. Suitable milling contractors were selected and the coals were ground according to different grind specifications which are discussed in the next section.

6.2 Sample Preparation

The primary aim of the combustion tests undertaken on the CTF was to quantify the effect of particle size distribution on combustion performance. More specifically, it was intended that the tests assess the improvement in combustion performance that could be achieved by retrofitting commercially available “high performance” static or dynamic classifiers to existing plant. A poorly ground sample labelled COARSE was also tested to assess the impact of poor mill maintenance. These tests were compared with baseline results from the coals ground to a specification representative of the currently accepted standard for pf fineness ($> 70\%$ by mass $< 75 \mu\text{m}$, $< 1\%$ by mass $> 300 \mu\text{m}$).

Thus, the grinds specified for the combustion tests were intended to be representative of the products that would be produced by:

- (a) A typical power station mill equipped with a static classifier, in good condition, and operating according to the regular guidelines for mill performance (STD grind specification).
- (b) A standard mill fitted with a high performance static classifier (HPSTAT).
- (c) A standard mill fitted with a high performance dynamic classifier (HPDYN).
- (d) A typical power station mill equipped with a static classifier, in poor condition and giving the worst performance that could reasonably be expected on plant labelled BAD.

Comparison of the required specifications and the predictions for the mill product showed that the HPSTAT and the HPDYN distributions could be accurately replicated particularly for the particle size range of greater than 100 μm . The STD and BAD specifications could not be accurately reproduced. It was predicted that the mill would produce too small a proportion of particles in the $>150 \mu\text{m}$ size fraction. Therefore, two additional grinds, designated COARSE and FINE were defined, which would produce the desired STD and BAD grinds when blended. The STD blend was produced from equal proportions of each coal (50:50), whilst the BAD grind was obtained from a 70:30 blend.

The specifications for the size distribution, as shown in Table 6.1, were based on typical plant data and manufacturers' claims. The COARSE and FINE grinds specifications have also been included in this Table.

Table 6.1 Size distribution specifications for combustion tests

| Size Fraction | COARSE | BAD | STD | HPSTAT | HPDYN | FINE |
|-----------------------|---------------|------------|------------|---------------|--------------|-------------|
| (μm) | (wt %) | (wt %) | (wt %) | (wt %) | (wt %) | (wt %) |
| <i>>300</i> | 20 | 2 | 1 | 0.2 | Trace | Trace |
| <i>150-300</i> | | 14 | 8 | 4.8 | 1 | |
| <i>75-150</i> | 30 | 24 | 21 | 24 | 16 | 10 |
| <i><75</i> | 50 | 60 | 70 | 71 | 83 | 90 |

The $>150 \mu\text{m}$ size fraction is believed to be the most significant in determining combustible-in-ash levels. The $<75 \mu\text{m}$ size fraction is not thought to have a significant impact on combustible-in-ash levels, and is mainly thought to be important for flame stability, particularly when firing low-volatile coals. Hence, discrepancies between the desired grind specifications and those predicted/produced for the smaller size fractions were not expected to significantly affect the tests.

The particle size distribution of each grind for the two coals is presented below in Table 6.2. These results were obtained by dry sieving control samples supplied by the contract grinder.

The required grind specifications were well reproduced for the HPSTAT, HPDYN and FINE grinds. The COARSE was not as well produced (slightly fine). As a result it was envisaged that the BAD grind would be better replicated by an 80:20 blend of the COARSE and FINE grinds.

Table 6.2 Summary of results of the grinding and blending

| Grind | Sample | Percentage (wt%) | | | |
|---------------|---------------|--------------------|-----------------------|----------------------|-------------------|
| | | >300 μm | 150-300 μm | 75-150 μm | <75 μm |
| <i>FINE</i> | Specification | Trace | | 10 | 90 |
| | Thoresby | 0 | 0.3 | 12.4 | 87.3 |
| | Carbocol | 0 | 0.2 | 12.1 | 87.7 |
| <i>HPDYN</i> | Specification | Trace | 1 | 16 | 83 |
| | Thoresby | 0 | 1.3 | 17.1 | 81.6 |
| | Carbocol | 0 | 1.0 | 19.2 | 79.8 |
| <i>HPSTAT</i> | Specification | 0.2 | 4.8 | 24 | 71 |
| | Thoresby | 0.4 | 7.6 | 23.4 | 68.6 |
| | Carbocol | 0.4 | 7.8 | 28.8 | 63 |
| <i>STD</i> | Specification | 1 | 8 | 21 | 70 |
| | Thoresby | 4.2 | 17.4 | 21.0 | 57.4 |
| | Carbocol | 1.6 | 10.2 | 22.6 | 65.6 |
| <i>BAD</i> | Specification | 2 | 14 | 24 | 60 |
| | Thoresby | 3.6 | 14.4 | 21.0 | 61.0 |
| | Carbocol | 2.1 | 13.2 | 24.1 | 60.6 |
| <i>COARSE</i> | Specification | 20 | | 30 | 50 |
| | Thoresby | 3.8 | 19.4 | 23.4 | 53.4 |
| | Carbocol | 1.1 | 13.5 | 28.4 | 57.0 |

It can be seen from Table 6.2 that significantly coarser grinds than expected were produced for the STD grind of both coals. Most significantly, the fraction of particles $>150\ \mu\text{m}$ was higher than specification, particularly for Thoresby coal. As far as the BAD grind is concerned, the required size distribution was well replicated for both coals. For both STD and BAD grinds, analysis of samples taken throughout the day showed that blending was consistent.

6.3 Coal Properties

The coals used in this study were selected to be representative of extremes in fuel characteristics experienced by coal-importing utilities in Europe. From the beginning of the project it was intended to fully characterise the different coal grinds. However, due to financial constraints and from the analysis of the combustion test results, the characterisation of some of the different coal grinds could not be performed. Additionally, due to fuel shortage, the COARSE grind of Thoresby coal was not tested and, therefore, analyses of this sample were not carried out.

Proximate analysis data for the various coal grinds is presented in Table 6.3. The results are presented on a dry, and dry-ash-free basis and include the fuel ratio for each grind. It can be seen that small changes occur in fuel ratio and ash content between the grinds. Carbocol exhibits higher volatile matter content (therefore, lower fuel ratio) and lower ash content than Thoresby.

Data from the elemental analysis of the coal grinds is shown in Table 6.4. The data consists of the percent composition of carbon, hydrogen, nitrogen, sulphur and oxygen (calculated by difference) on a dry-ash-free basis. Note that only the HPSTAT grind of Carbocol coal was analysed. It can be seen from the Table that both coals exhibit similar carbon and hydrogen content. Thoresby has a slightly higher nitrogen content and a very high sulphur content (over 2%) and consequently lower oxygen content compared to Carbocol. This could have an impact on NO_x and SO_x emissions during combustion.

Table 6.3 Proximate analysis data for the coal grinds

| Coal/Grind | Moisture | Dry Basis (wt%) | | | Dry, ash-free basis (wt%) | | Fuel Ratio |
|--------------------------|----------|-----------------|-----------------|------|---------------------------|------|------------|
| | (wt%) | VM ^a | FC ^b | Ash | VM | FC | FC/VM |
| <i>FINE</i> | 2.5 | 30.1 | 49.9 | 20.0 | 37.6 | 62.4 | 1.66 |
| <i>HPDYN</i> | 2.5 | 30.3 | 49.7 | 20.0 | 37.8 | 62.2 | 1.64 |
| THO <i>HPSTAT</i> | 2.5 | 30.8 | 50.6 | 18.7 | 37.8 | 62.2 | 1.64 |
| <i>STD</i> | 3.0 | 30.6 | 50.4 | 19.0 | 37.8 | 62.2 | 1.65 |
| <i>BAD</i> | 3.0 | 30.1 | 50.2 | 19.7 | 37.5 | 62.5 | 1.67 |
| <i>HPDYN</i> | 3.6 | 37.0 | 53.7 | 9.2 | 40.8 | 59.2 | 1.45 |
| CAR <i>HPSTAT</i> | 3.9 | 37.1 | 53.8 | 9.1 | 40.8 | 59.2 | 1.45 |
| <i>STD</i> | 5.3 | 37.5 | 54.4 | 8.1 | 40.8 | 59.2 | 1.45 |
| <i>BAD</i> | 4.8 | 37.6 | 54.1 | 8.3 | 41.0 | 59.0 | 1.44 |

^a VM=Volatile Matter; ^b FC=Fixed Carbon

Table 6.4 Ultimate analysis data for the coal grinds

| Coal/Grind | C | H | N | S | O |
|--------------------------|-----------|-----------|-----------|-----------|-----------|
| | (wt% daf) |
| <i>FINE</i> | 83.39 | 5.81 | 1.84 | 2.27 | 6.69 |
| <i>HPDYN</i> | 82.59 | 5.95 | 1.81 | 2.28 | 7.37 |
| THO <i>HPSTAT</i> | 83.30 | 5.83 | 1.92 | 2.26 | 6.70 |
| <i>STD</i> | 82.18 | 5.63 | 1.79 | 2.48 | 7.92 |
| <i>BAD</i> | 84.25 | 5.68 | 1.86 | 2.44 | 5.78 |
| CAR <i>HPSTAT</i> | 82.09 | 5.65 | 1.68 | 0.81 | 9.762 |

Petrographic analysis for the various coal grinds, including, maceral analysis and rank is given in Table 6.5. The data is provided on a volume/volume, mineral-matter-free basis. The vitrinite reflectance histograms of the samples are shown

in Figures 6.1 and 6.2 for Thoresby and Carbocol coal grinds respectively. In order to elucidate the differences in vitrinite reflectance among the grinds, the histograms are presented in a continuous-scale plot.

The maceral analysis results indicate that both coals are rich in vitrinite with Carbocol containing more than 90% and Thoresby around 80%. The liptinite and inertinite content of Thoresby is higher by comparison with Carbocol. The maceral composition of the different grinds of the two coals does not vary considerably. Vitrinite tends to concentrate in the finest grinds (FINE, HPDYN and HPSTAT) whereas liptinite and inertinite concentrate in the coarsest grinds. In terms of rank, little variation in mean random vitrinite reflectance was observed. Thoresby is a coal of higher rank (0.75%) than Carbocol (0.60%).

Table 6.5 Petrographic Analysis of the coal grinds

| Coal/Grind | Rank | Maceral Content (vol%) | | | U ₁₉₀ | |
|------------|---------------|------------------------|-----------|------------|------------------|-----|
| | VRo (%) | Vitrinite | Liptinite | Inertinite | (vol%) | |
| THO | <i>FINE</i> | 0.73 | 81.1 | 8.2 | 10.7 | 4.7 |
| | <i>HPDYN</i> | 0.77 | 79.6 | 8.4 | 12.0 | 5.2 |
| | <i>HPSTAT</i> | 0.76 | 79.8 | 8.2 | 12.0 | 5.5 |
| | <i>STD</i> | 0.75 | 79.4 | 8.5 | 12.1 | 6.2 |
| | <i>BAD</i> | 0.76 | 79.0 | 9.0 | 12.0 | 6.0 |
| CAR | <i>FINE</i> | 0.59 | 93.8 | 0.8 | 5.4 | 3.2 |
| | <i>HPDYN</i> | 0.59 | 92.4 | 0.8 | 6.8 | 3.4 |
| | <i>HPSTAT</i> | 0.56 | 91.6 | 0.8 | 7.6 | 3.5 |
| | <i>STD</i> | 0.60 | 91.4 | 1.0 | 7.6 | 3.5 |
| | <i>BAD</i> | 0.59 | 91.2 | 1.2 | 7.6 | 3.8 |
| | <i>COARSE</i> | 0.60 | 90.1 | 1.6 | 8.3 | 4.2 |

From examination of the vitrinite reflectance plots of Carbocol (Figure 6.2) it is clearly evident that the BAD and STD grinds are the result of a blend. Two distinctive peaks can be noticed in the plots which can be ascribed to the FINE and COARSE grind respectively. For Thoresby coal no significant differences in the vitrinite reflectance plots can be distinguished among grinds as shown in Figure 6.1.

The grey scale histograms of Thoresby and Carbocol coal grinds, derived from the RAP analysis, are given in Figure 6.3 and Figure 6.4 respectively. These profiles take the form of frequency versus grey scale. The % unreactives parameter, derived from the RAP profiles, are given in Table 6.5. It can be seen from the histograms that the liptinite peak lies below grey level 50 (slightly lower for Carbocol due to its lower rank). The vitrinite peak lies between this boundary to a grey level of around 100 for Carbocol and 120 for Thoresby. This is in agreement with the vitrinite reflectance histograms which show the broader range in vitrinite reflectance for Thoresby. A distinctive peak beyond a grey level of 230 can be distinguished from the grey scale histograms and this is attributed to high reflectance inertinite and mineral matter. This peak contributes the most to the % unreactives parameter. Since this peak is slightly higher for Thoresby coal, this offers an explanation for its higher % unreactives.

6.4 Test Programme

Testing was undertaken on Powergen's 1 MW Combustion Test Facility (CTF) at Ratcliffe-on-Soar, Nottingham. Both coals were fired at each grind specification under the following test conditions: 15% over-fire Air, 1% excess oxygen. As explained earlier, the COARSE grind of Thoresby could not be tested due to fuel shortage. For each of the grinds tested, extractive wet sampling of char was taken from three different points along the system, i.e. a sample at the burner region (Port 1) and two samples in the convective pass (Ports 2 and 3). Figure 3.16 shows a schematic of the CTF rig showing these ports. Since the CTF was built, experience has been gained that established these particular ports as the most suitable for obtaining representative samples from the combustion process.

Samples from Port 1 resemble chars that have just undergone pyrolysis and are just entering the first stage of combustion.

Figure 6.1 Vitrinite reflectance histograms of Thoresby coal grinds

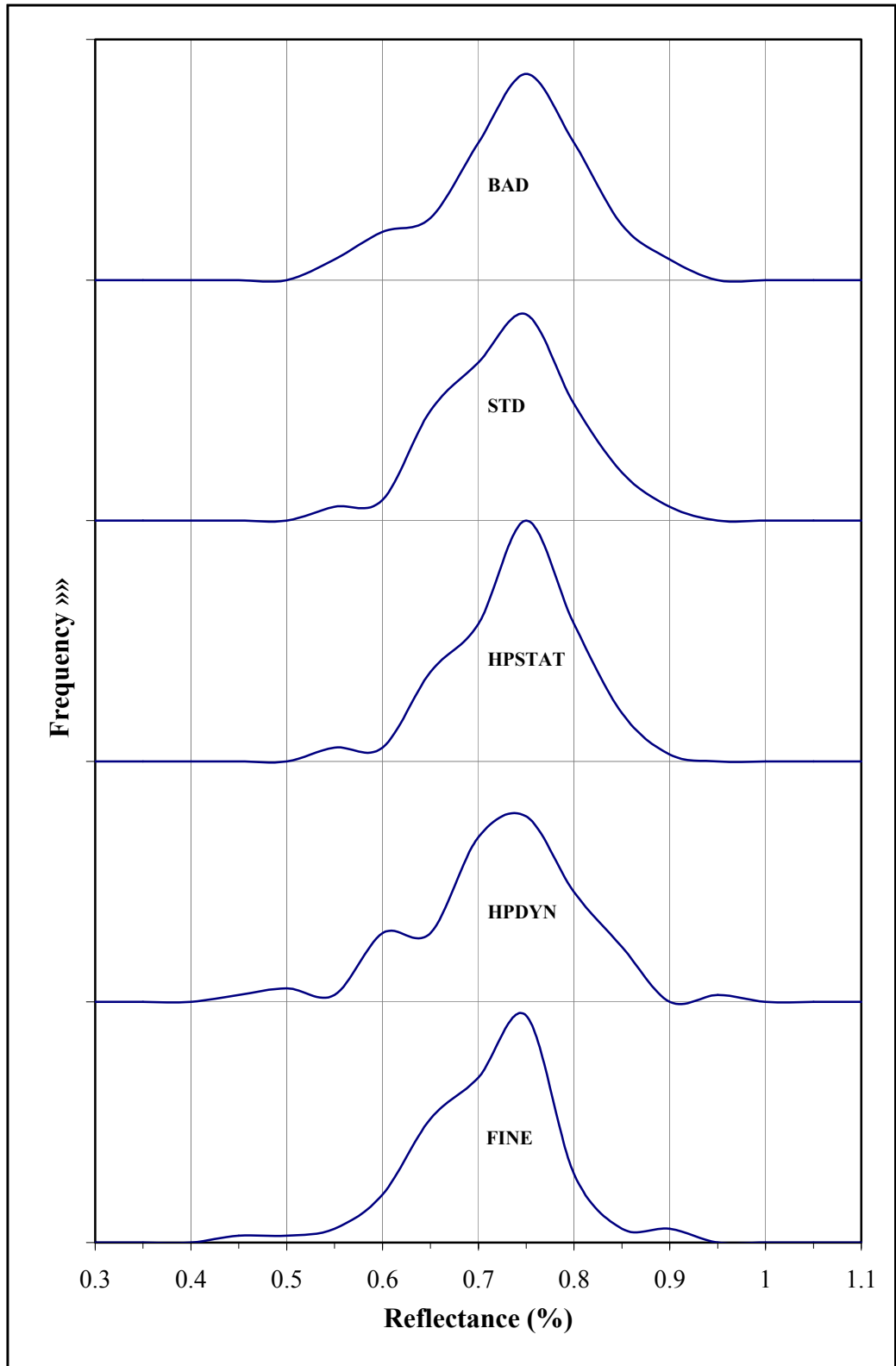


Figure 6.2 Vitrinite reflectance histograms of Carbocol coal grinds

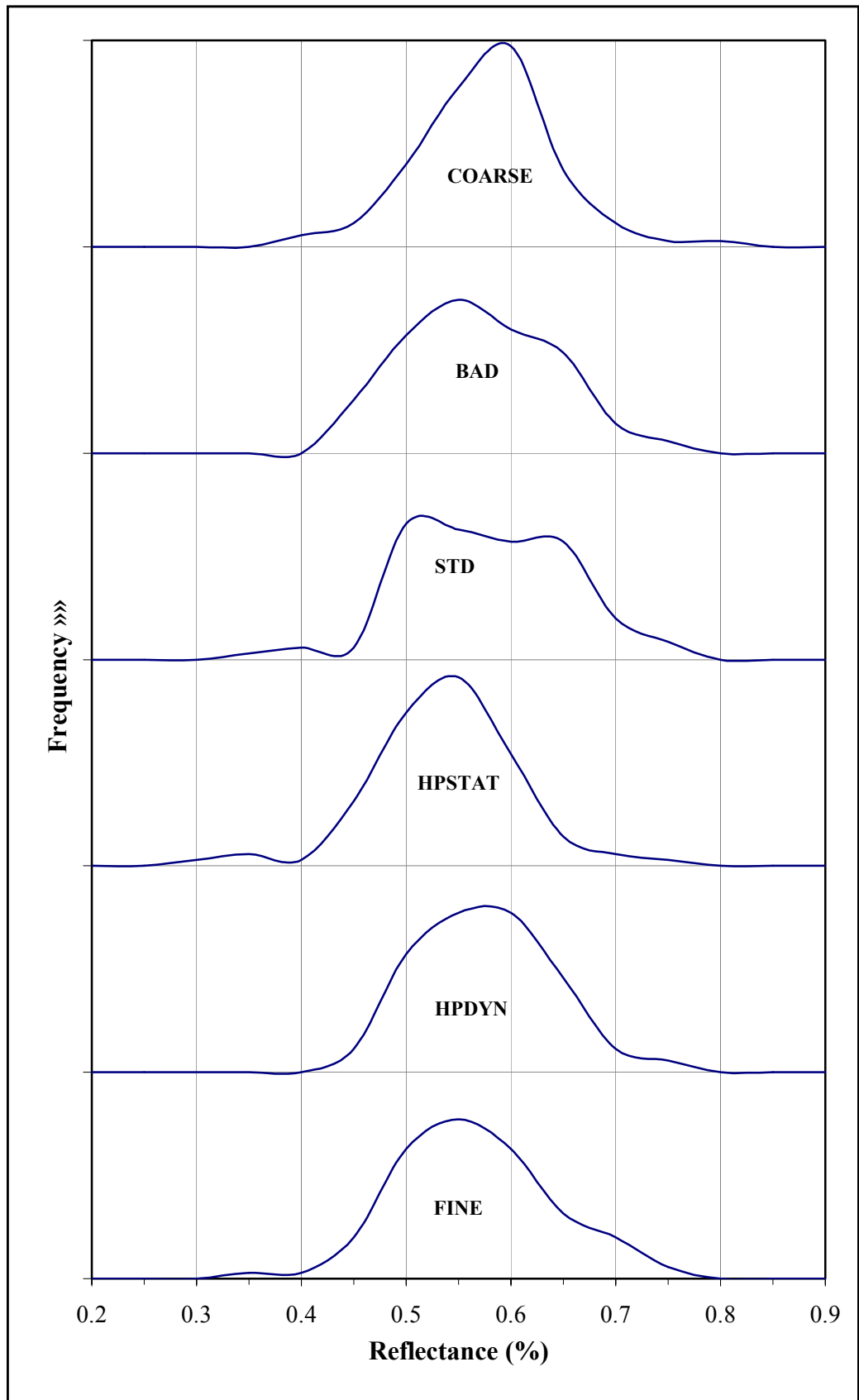


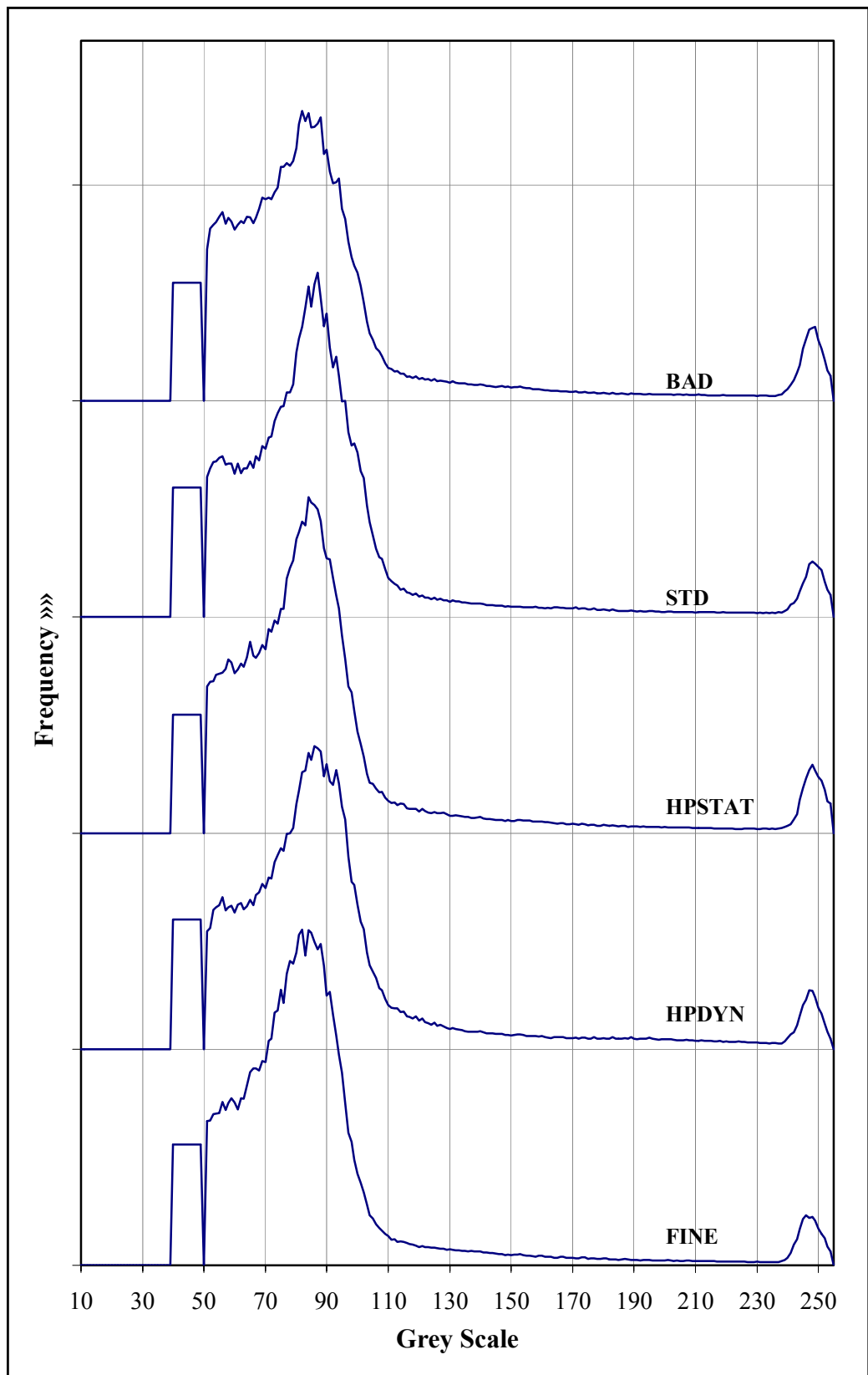
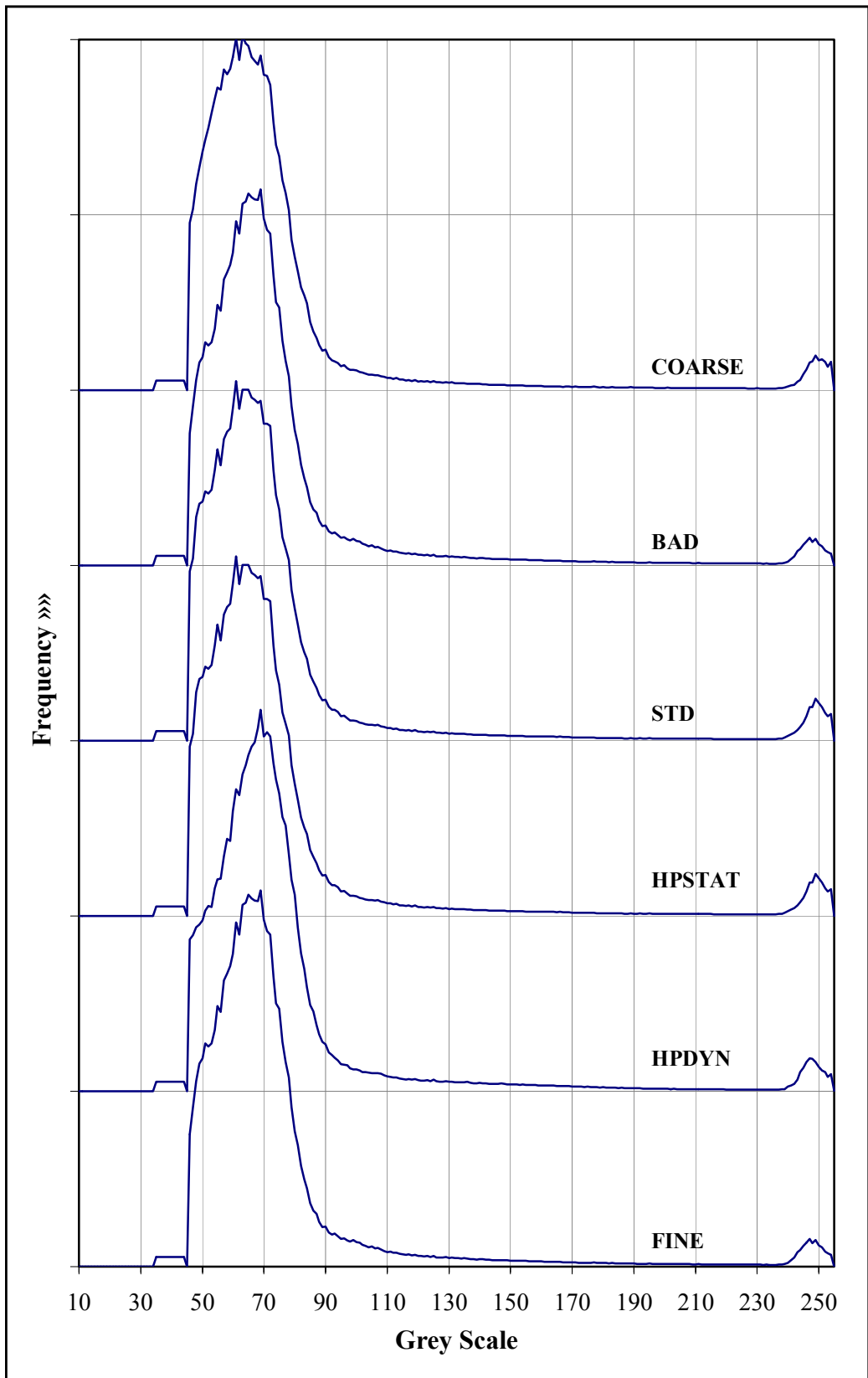
Figure 6.3 Grey scale histograms of Thoresby coal grinds

Figure 6.4 Grey scale histograms of Carbocol coal grinds

Apart from the aforementioned test programme, the project at Powergen involved the firing of the same samples at 1.5, 2.5 and 4% excess oxygen with and without over-fire air. Additionally, back-end gas analysis for NO, SO₂, O₂ and CO were carried out for all conditions. However, this was not part of the collaboration programme between the company and Nottingham University and these results will not be discussed.

Table 6.6 Intrinsic reactivity data for the chars obtained at Port 1

| Coal/Grind | >150 μm | Peak Temperature | Burnout Temperature | |
|-----------------|--------------------|------------------------|------------------------|-----|
| | (wt%) | ($^{\circ}\text{C}$) | ($^{\circ}\text{C}$) | |
| <i>Thoresby</i> | <i>FINE</i> | 1.4 | 571 | 655 |
| | <i>HPDYN</i> | 2.0 | 571 | 672 |
| | <i>HPSTAT</i> | 8.0 | 570 | 680 |
| | <i>STD</i> | 21.6 | 572 | 689 |
| | <i>BAD</i> | 18.0 | 570 | 693 |
| <i>Carbocol</i> | <i>FINE</i> | 1.0 | 576 | 651 |
| | <i>HPDYN</i> | 2.2 | 576 | 658 |
| | <i>HPSTAT</i> | 8.2 | 577 | 660 |
| | <i>STD</i> | 11.8 | 575 | 660 |
| | <i>BAD</i> | 16.2 | 575 | 657 |
| | <i>COARSE</i> | 20.4 | 576 | 665 |

6.5 Properties of the Chars from the Near-Burner Region

6.5.1 Intrinsic Reactivity

The intrinsic reactivity results for all the char samples from the near-burner region (Port 1) are given in Table 6.6. The results are given as a function of the weight percentage of coal particles above 150 μm , the size fraction believed to impact

most on unburnt combustible formation. Char burning profiles, as derived from the intrinsic reactivity analysis, are presented in Figure 6.5 and Figure 6.6 for Thoresby and Carbocol grinds respectively. As in the previous chapter, the DTA output ($\mu\text{V}\cdot\text{mg}^{-1}$) was normalised to the value of maximum rate of weight loss, as this facilitates the interpretation of the profiles.

The most evident feature from the data in Table 6.6 is that the peak temperature parameter is fairly similar for all the char grinds. This suggests that fineness, within the range of grind size tested, has no significant effect on peak temperature for both coals. The DTA burning profiles in Figures 6.6. and 6.7 clearly show this similarity among the grinds. In contrast, burnout temperature (BT) shows a tendency to increase with increasing fraction of particles above $150\ \mu\text{m}$ and this is shown in Figure 6.7. This increase is more apparent for Thoresby chars. An additional plot of BT as a function of % unreactives was obtained (Figure 6.8). A general trend of decreasing intrinsic reactivity with increasing % unreactives can be observed from the plot. Once again, this trend is more evident for Thoresby chars.

6.5.2 Automatic Char Analysis

Automatic char analysis was carried out for all the char samples. The results obtained are presented in Table 6.7, and are given as relative char wall thickness (ACA5). High ACA5 values are associated with high concentration of thin-walled chars and low values of ACA5 to high percentage of thick-walled and solid chars. In the results from previous chapters, variations of ACA5 figures with % unreactives as well as particle size were observed. Therefore, plots of ACA5 against both % unreactives and the percentage of material above $150\ \mu\text{m}$ were produced for both coals and are given in Figures 6.9 and 6.10 respectively. Note that the % unreactives and the percentage of coal material above $150\ \mu\text{m}$ have been included in the results (Table 6.7). According to the results and plots, the grinds with the lowest % unreactives material produced the highest ACA5 values irrespective of the coal. Consistently, a decrease of ACA5 figures with decreasing fineness of the coal grind can be noticed in Figure 6.10.

Figure 6.5 DTA burning profiles for Thoresby chars from Port 1

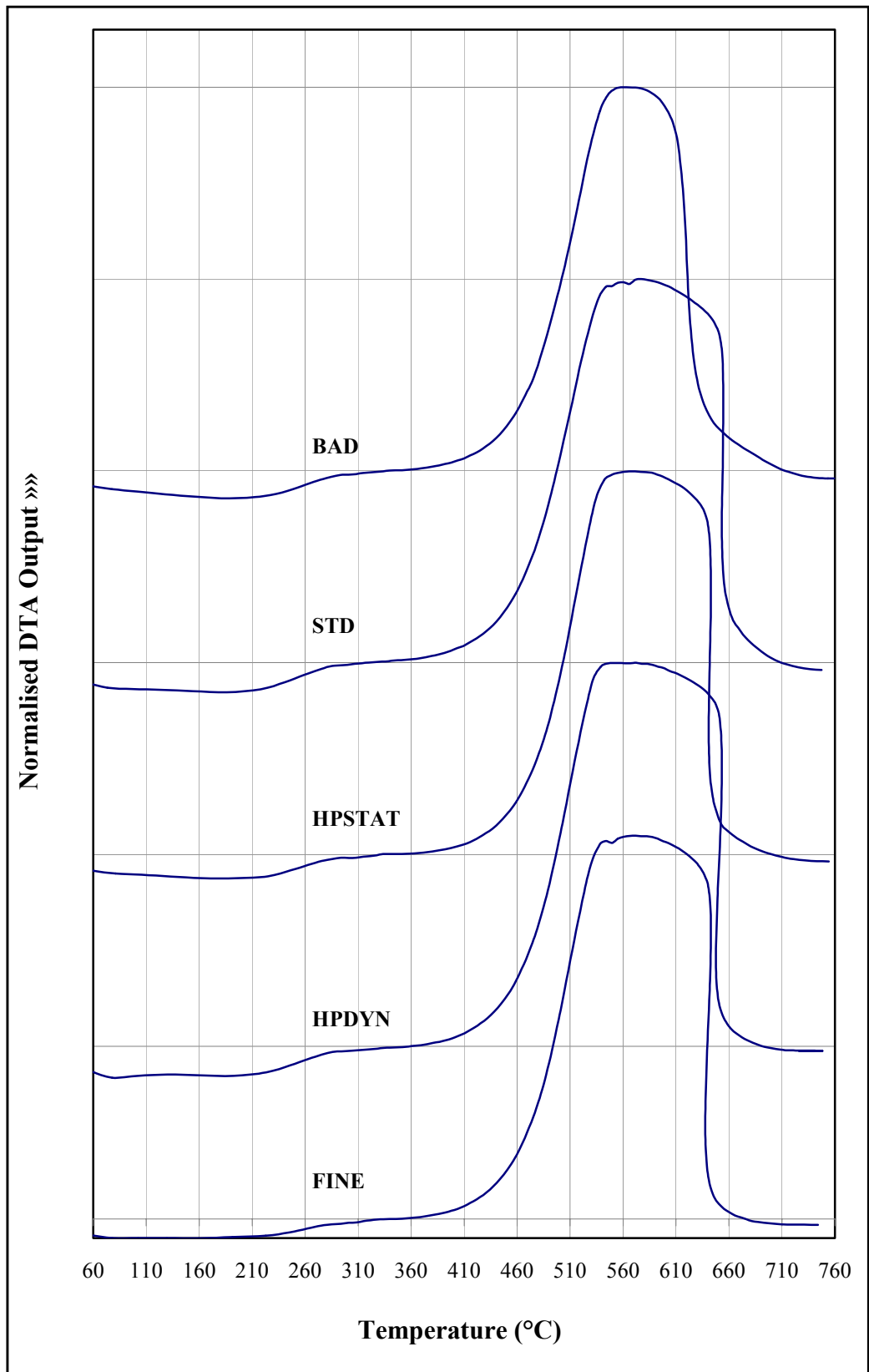


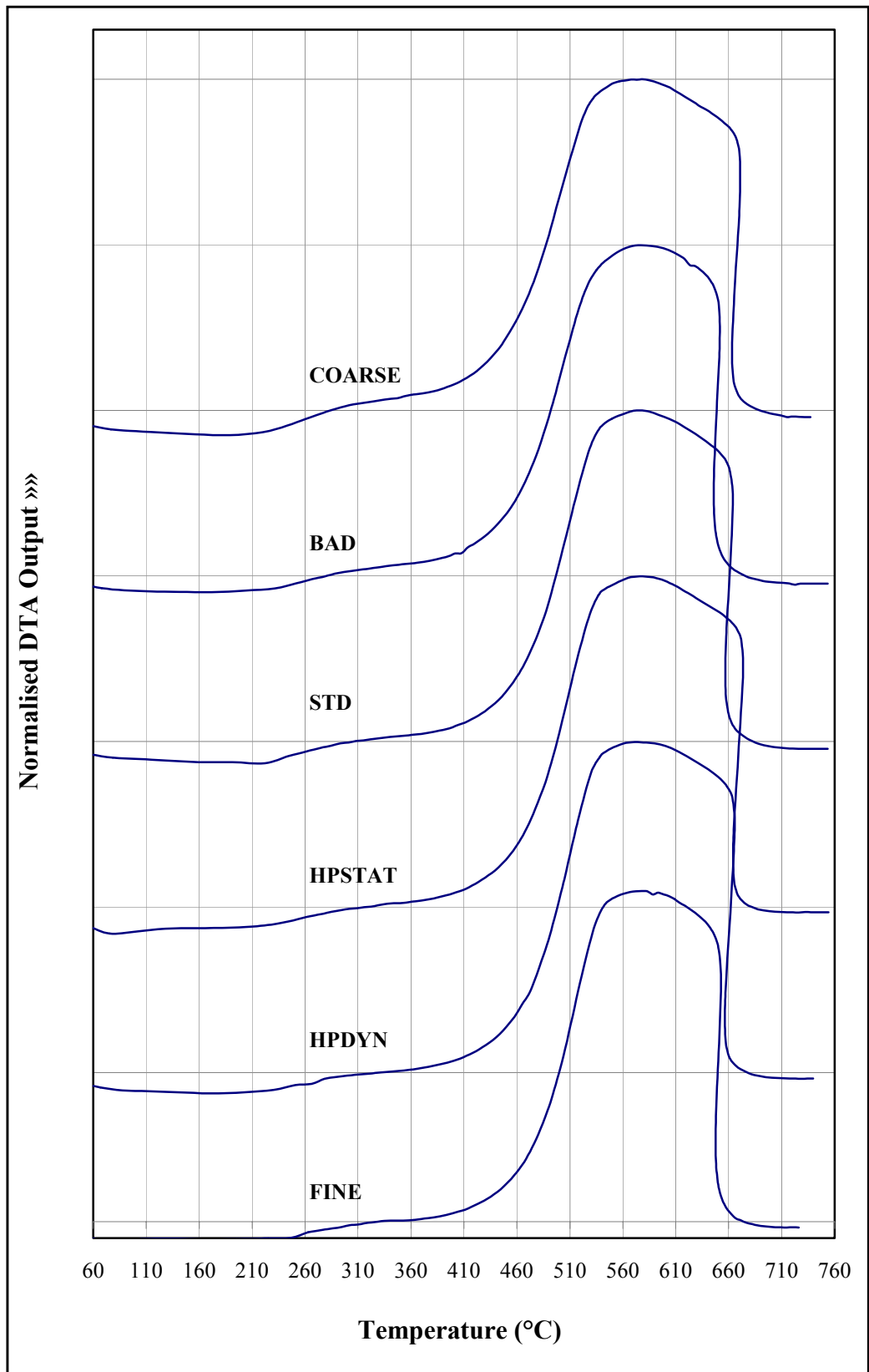
Figure 6.6 DTA burning profiles for Carbocol chars from Port 1

Figure 6.7 A plot of BT as a function of percentage of particles above 150µm for chars from Port 1

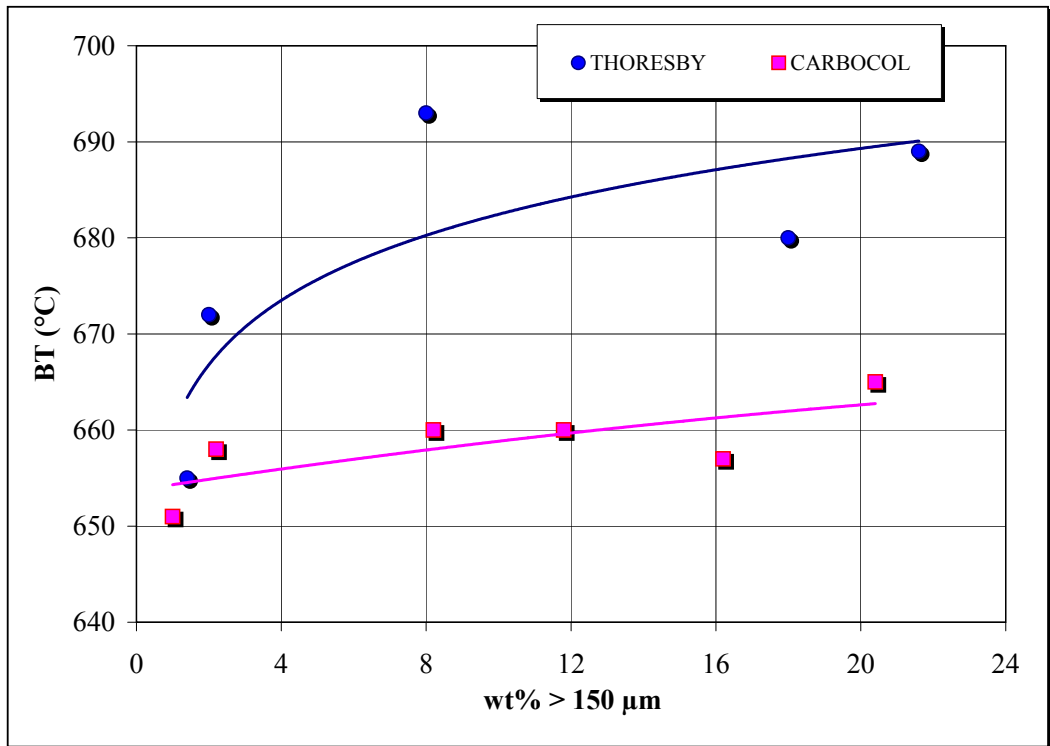


Figure 6.8 A plot of BT against % unreactives for chars from Port 1

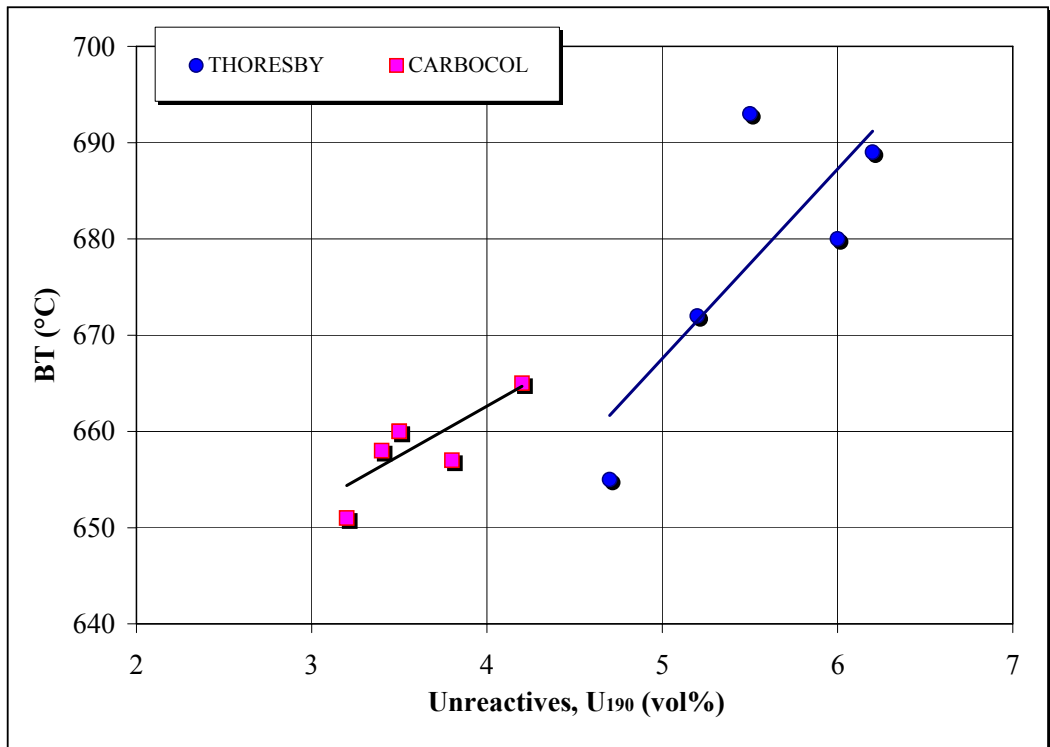


Table 6.7 Automatic char analysis data for the char from Port 1

| Coal/Grind | >150 μm | % unreactives | ACA5 | |
|-----------------|--------------------|---------------|--------|------|
| | (wt%) | (vol%) | (vol%) | |
| Thoresby | <i>FINE</i> | 1.4 | 4.7 | 83.5 |
| | <i>HPDYN</i> | 2.0 | 5.2 | 82.3 |
| | <i>HPSTAT</i> | 8.0 | 5.5 | 79.4 |
| | <i>STD</i> | 21.6 | 6.2 | 73.7 |
| | <i>BAD</i> | 18.0 | 6.0 | 78.8 |
| Carbocol | <i>FINE</i> | 1.0 | 3.2 | 89.4 |
| | <i>HPDYN</i> | 2.2 | 3.4 | 88.9 |
| | <i>HPSTAT</i> | 8.2 | 3.5 | 85.6 |
| | <i>STD</i> | 11.8 | 3.5 | 87.5 |
| | <i>BAD</i> | 16.2 | 3.8 | 83.1 |
| | <i>COARSE</i> | 20.4 | 4.2 | 80.5 |

Figure 6.9 A plot of ACA5 against % unreactives for chars from Port 1

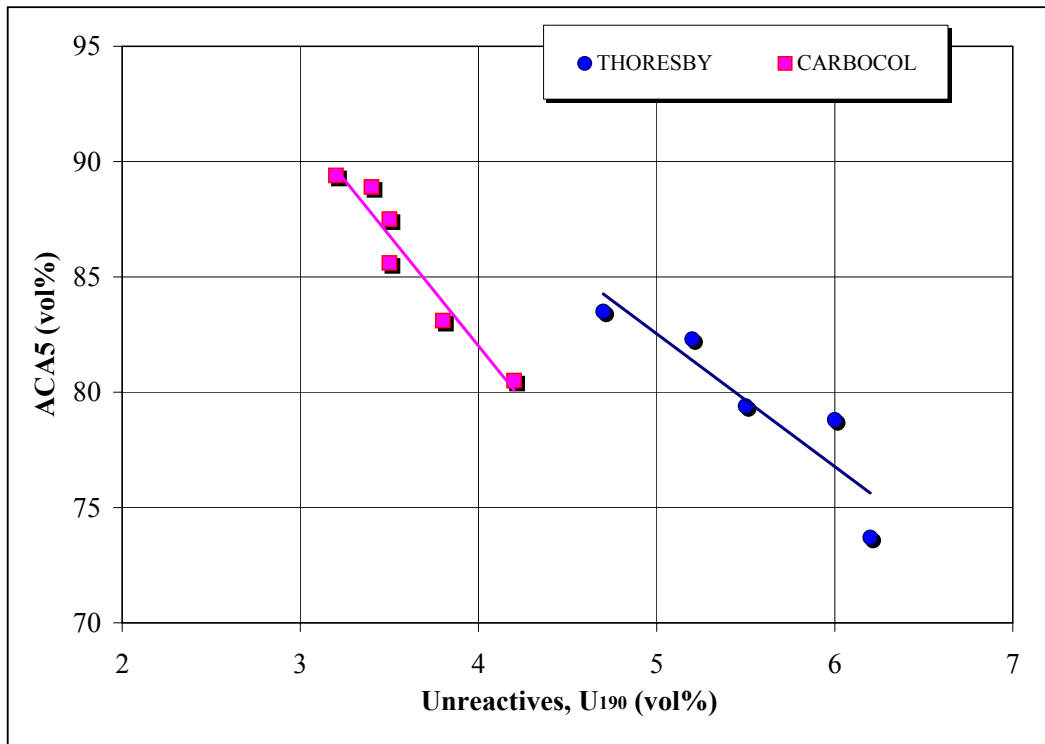
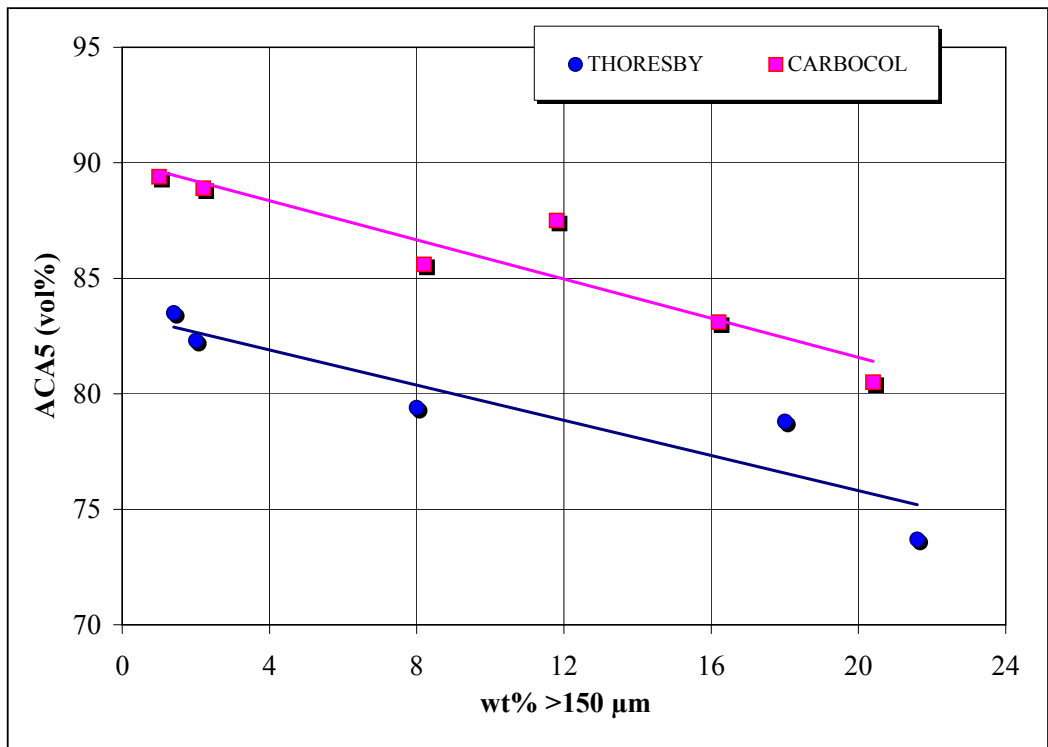


Figure 6.10 A plot of ACA5 against percentage of particles above 150 μ m for chars from Port 1



6.6 Properties of the Chars from the Convective section

6.6.1 Loss-on-Ignition and Unburnt Combustible

The two coals tested show significantly different behaviour in terms of the loss-on-ignition (LOI) and unburnt combustible (U_C) and this will be discussed separately. The results are presented in Table 6.8 and consist of the percentage of coal material above 150 μ m, the % unreactives, LOI and U_C for both ports at the convective section.

Unburnt combustible levels for the lower volatile coal Thoresby range from 1.22 to 4.13% at Port 2, and from 0.77 to 1.28% at Port 3. This indicates an overall combustion efficiency for this coal greater than 98.7%. Unburnt combustible has

been plotted against the percentage of particles above 150 μm , the fraction which has the most impact on unburnt combustible formation. This plot (Figure 6.11) indicates that the unblended coals behaved considerably differently to the blended coals, particularly when considering the results from Port 2. In another plot, in Figure 6.12, a similar behaviour of unburnt combustible against % unreactives can be seen.

Table 6.8 Loss-on-ignition and unburnt combustible data for chars from Ports 2 and 3

| Coal/Grind | >150 μm | U_{190}^a | LOI (wt%) | | U_C (wt%) ^b | |
|--------------------------|--------------------|-------------|-----------|--------|--------------------------|--------|
| | (wt%) | (vol%) | Port 2 | Port 3 | Port 2 | Port 3 |
| <i>FINE</i> | 1.4 | 4.7 | 7.16 | 3.62 | 1.93 | 0.94 |
| <i>HPDYN</i> | 2.0 | 5.2 | 7.60 | 4.17 | 2.06 | 1.09 |
| THO <i>HPSTAT</i> | 8.0 | 5.5 | 15.24 | 4.39 | 4.13 | 1.05 |
| <i>STD</i> | 21.6 | 6.2 | 6.28 | 5.18 | 1.57 | 1.28 |
| <i>BAD</i> | 18.0 | 6.0 | 4.75 | 3.06 | 1.22 | 0.77 |
| <i>FINE</i> | 1.0 | 3.2 | 15.62 | 8.72 | ND | ND |
| <i>HPDYN</i> | 2.2 | 3.4 | 10.99 | 7.67 | 1.26 | 0.85 |
| CAR <i>HPSTAT</i> | 8.2 | 3.5 | 17.91 | 8.86 | 2.17 | 0.97 |
| <i>STD</i> | 11.8 | 3.5 | 14.12 | 7.88 | 1.45 | 0.76 |
| <i>BAD</i> | 16.2 | 3.8 | 11.20 | 7.33 | 1.14 | 0.72 |
| <i>COARSE</i> | 20.4 | 4.2 | 16.10 | 7.86 | ND | ND |

^a U_{190} =% unreactives; ^b ND = Not Determined

Figure 6.11 A plot of unburnt combustible against percentage of particles above 150µm for Thoresby chars from Ports 2 and 3

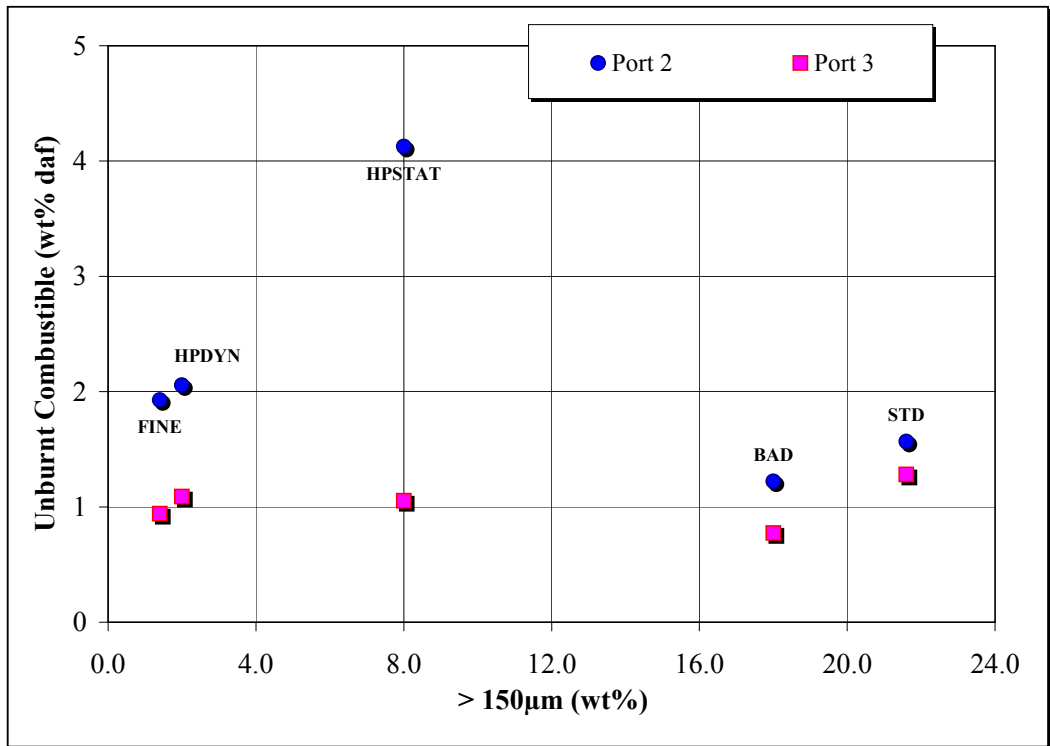
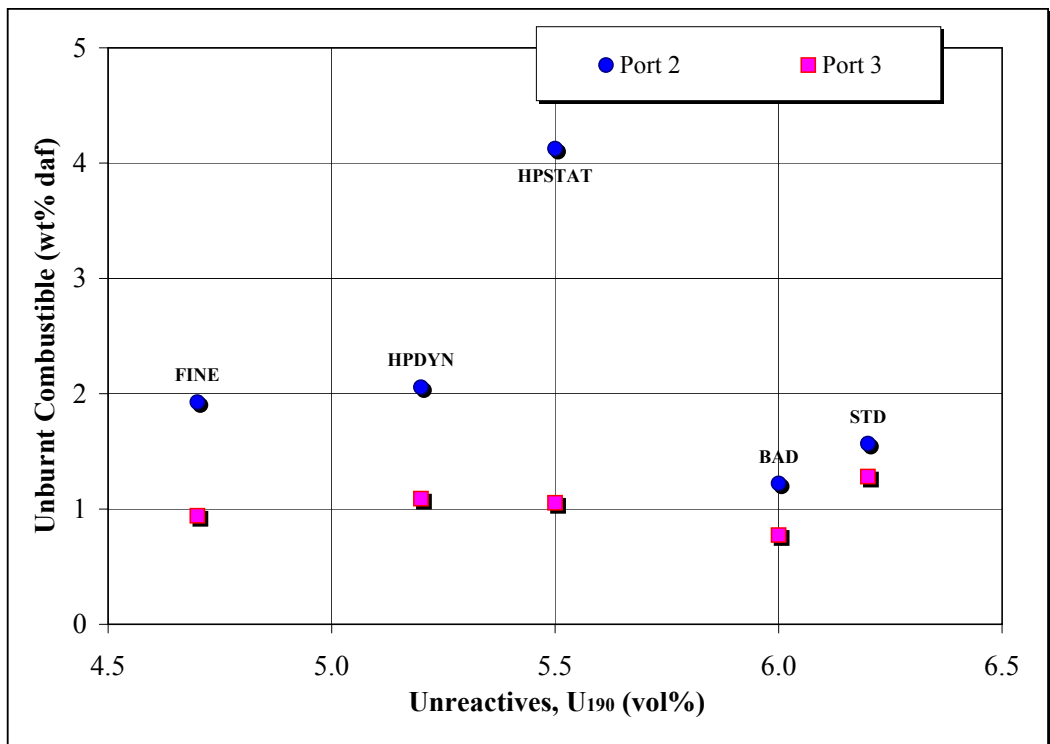


Figure 6.12 A plot of unburnt combustible against % unreactives for Thoresby chars from Ports 2 and 3



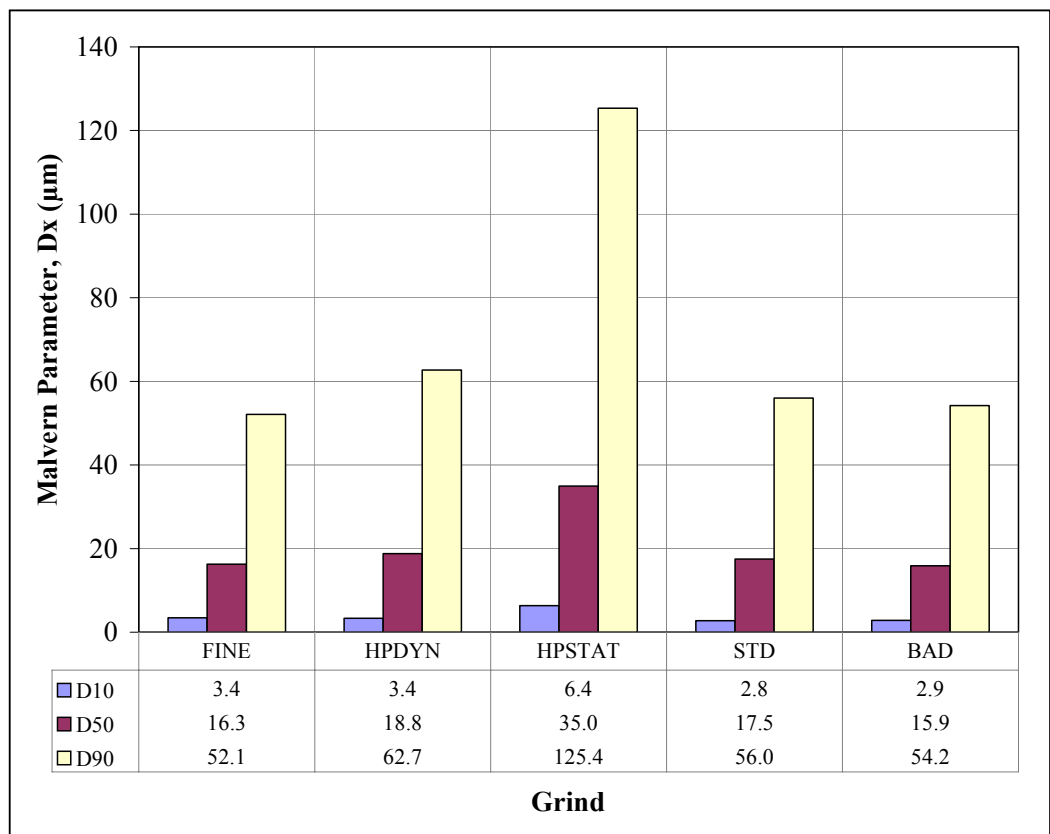
Across the range of tests, unburnt combustible levels tend to increase with increasing fraction of particles above 150 μm , for unblended grinds. This is an expected trend, and indicates that the installation of improved classification technology, leading to a finer product, will reduce combustible-in-ash levels. However, further data is required to determine the point of diminishing returns, where little reduction in combustible-in-ash levels is achieved for further improvements in grind quality (Hill et al., 2000).

The LOI and unburnt combustibles results for the blended coals are surprising, particularly for those at Port 2. The particle size distribution of the coals (section 6.2) shows the progressive decrease in overall particle fineness from the FINE grind through the BAD and COARSE blends. Results from the unblended coal would imply that further increases in unburnt combustible should have resulted from the combustion of the STD and BAD grinds. This was not the case, with the STD and BAD grinds producing unburnt combustible figures comparable with the FINE and HPDYN coals (Figure 6.11).

The unexpected behaviour of the blended coals was unclear. As a result, the Thoresby char samples from Port 2 were sized using a laser diffraction technique (Malvern), in order to find a possible explanation to this inconsistency. The Malvern sizing technique generates a particle size distribution profile of a sample on a volumetric basis. Three parameters are used to summarise the analysis – D10, D50 and D90. ‘D_x’ represents the largest particle diameter present in the smallest ‘x’ percent of the sample. Thus, the D10, D50 and D90 values represent the percentage of coal material with a maximum particle diameter of 10, 50, and 90 μm respectively. The results of the Malvern analysis for Thoresby chars at Port 2 are presented in Figure 6.13. The results revealed that the unblended grind (FINE, HPDYN, and HPSTAT) produced progressively larger chars. It would, therefore, be expected that the STD and BAD blended grinds would produce further increases in char size.

It would appear that, for the blended grinds, small chars were collected irrespective of the coarse particle content. This is not a feature of the extractive sampling technique. The possibility exists that coarser particles dropped out of suspension in the flue gas stream and were deposited on the floor of the convective pass. This would obviously lead to the sampling of smaller chars. Anecdotal information suggests that this phenomenon has been exhibited on the CTF in the past, although measured gas velocities of between 12 and 20 m/s in the convective pass suggest that particle fall out should not be a problem (Hill et al., 2000).

Figure 6.13 Comparison of Malvern size parameter for Thoresby chars from Port 2



Another possible explanation is that larger chars from the coarser grinds formed in the early stages of combustion fragment or deflagrate to form smaller particles that lead to improved burnout. Alternatively, the behaviour of these grinds may

be attributable to differences in properties of the fine and coarse particles produced during grinding. However, the maceral analysis and the % unreactives results of the different grinds do not show significant differences between the grinds. In fact, the % unreactives of the BAD and STD grinds is slightly higher than those of the unblended grinds which suggests poorer burnout of the blended grinds.

The testing of the COARSE grind would have determined if the unexpectedly low unburnt combustible level for the blended grinds are attributable to the blending, or attributable to an increase in increased mean particle size, but these tests were not possible due to shortage of coal.

The LOI and unburnt combustible results for the higher volatile coal Carbocol were presented in Table 6.8 along with the results for Thoresby. Unburnt combustible levels range from 1.14 to 2.17% at Port 2, and from 0.72 to 0.85% at Port 3. This indicates an overall combustion efficiency for this coal greater than 99.1%. It can be seen from the data that grind size has virtually no impact upon unburnt combustible levels. Improved particle fineness impacts on both volatile and char combustion. However, pilot scale combustion tests indicate that for higher volatile coals, the combustion of volatiles is enhanced, whereas for lower volatile coals, char combustion is enhanced. Carbocol is a fairly high volatile coal and, therefore, it could be expected that improved grind quality would have a minimal impact on combustible-in-ash.

6.6.2 Intrinsic Reactivity

Table 6.9 contains the data of the intrinsic reactivity results for the chars obtained at the convective section for both coals. The DTA burning profiles for Thoresby chars from Ports 2 and 3 are given in Figure 6.14 and Figure 6.15 respectively. Similar DTA burning profiles for Carbocol char samples are shown in Figure 6.16 and Figure 6.17. The intrinsic reactivity data has been plotted against the percentage of particles above 150 μ m and the graphs obtained are shown in Figure 6.18 and Figure 6.19 for Thoresby and Carbocol coals respectively.

The results for Thoresby follow a similar trend as with unburnt combustibles, i.e. a progressive decrease of reactivity with increasing the percentage of particles above 150 μ m. Results for Carbocol show a tendency of decreasing intrinsic reactivity with increasing fraction of particles above 150 μ m, particularly for the BT. It is very apparent that all the samples from Port 2 exhibit higher intrinsic reactivity (lower PTs and BTs values) than the samples from Port 3.

Table 6.9 Intrinsic reactivity data for the chars from Ports 2 and 3

| Coal/Grind | >150 μ m | Peak Temperature (°C) | | Burnout Temperature (°C) | | |
|-----------------|---------------|-----------------------|--------|--------------------------|--------|-----|
| | (wt%) | Port 2 | Port 3 | Port 2 | Port 3 | |
| <i>Thoresby</i> | <i>FINE</i> | 1.4 | 573 | 575 | 656 | 660 |
| | <i>HPDYN</i> | 2.0 | 577 | 580 | 675 | 677 |
| | <i>HPSTAT</i> | 8.0 | 590 | 591 | 702 | 705 |
| | <i>STD</i> | 21.6 | 586 | 589 | 692 | 693 |
| | <i>BAD</i> | 18.0 | 570 | 583 | 681 | 692 |
| <i>Carbocol</i> | <i>FINE</i> | 1.0 | 580 | 580 | 660 | 661 |
| | <i>HPDYN</i> | 2.2 | 572 | 578 | 665 | 670 |
| | <i>HPSTAT</i> | 8.2 | 573 | 581 | 665 | 670 |
| | <i>STD</i> | 11.8 | 582 | 585 | 674 | 681 |
| | <i>BAD</i> | 16.2 | 586 | 588 | 682 | 686 |
| | <i>COARSE</i> | 20.4 | 589 | 593 | 685 | 689 |

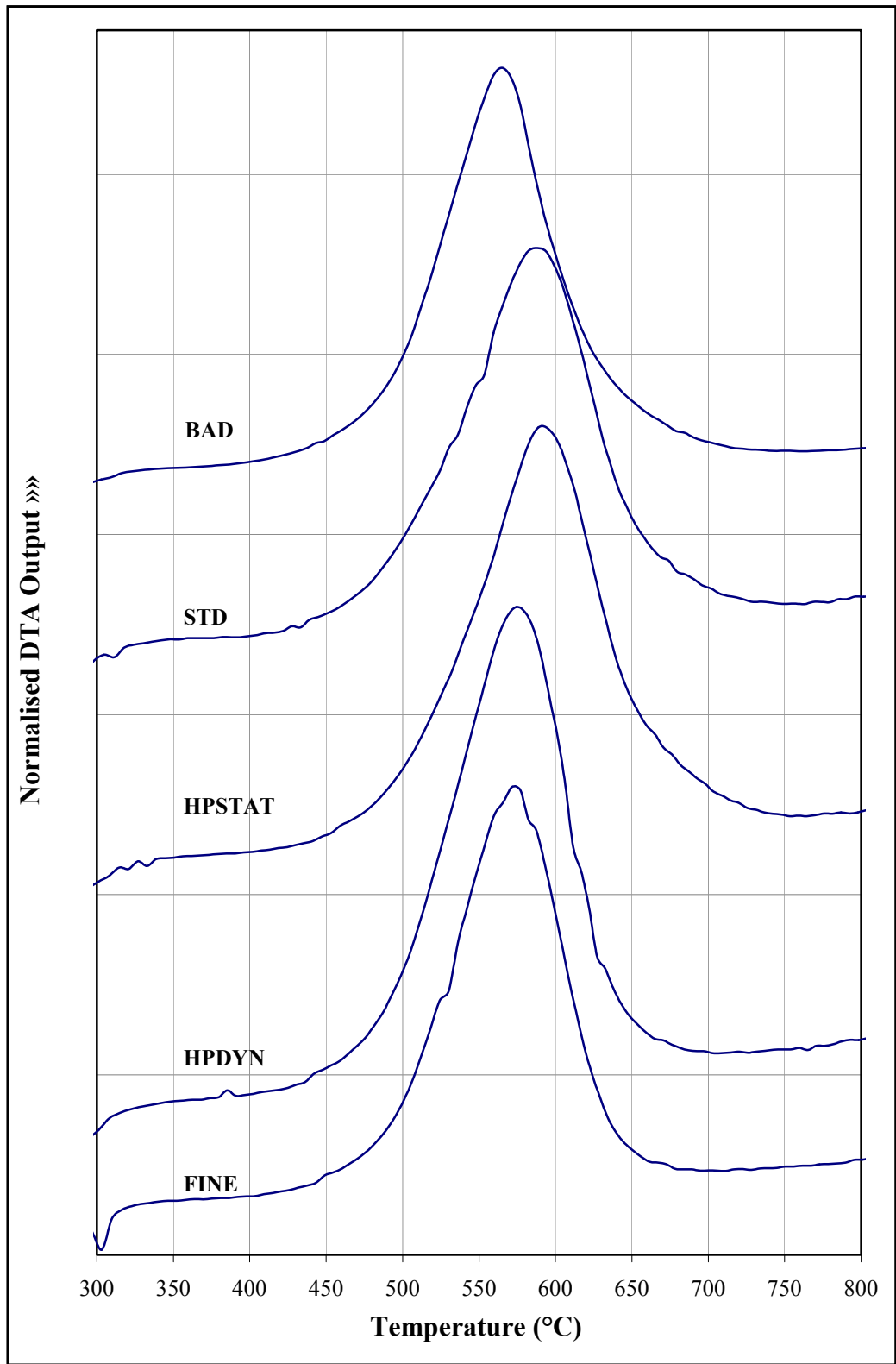
Figure 6.14 DTA burning profiles for Thoresby chars from Port 2

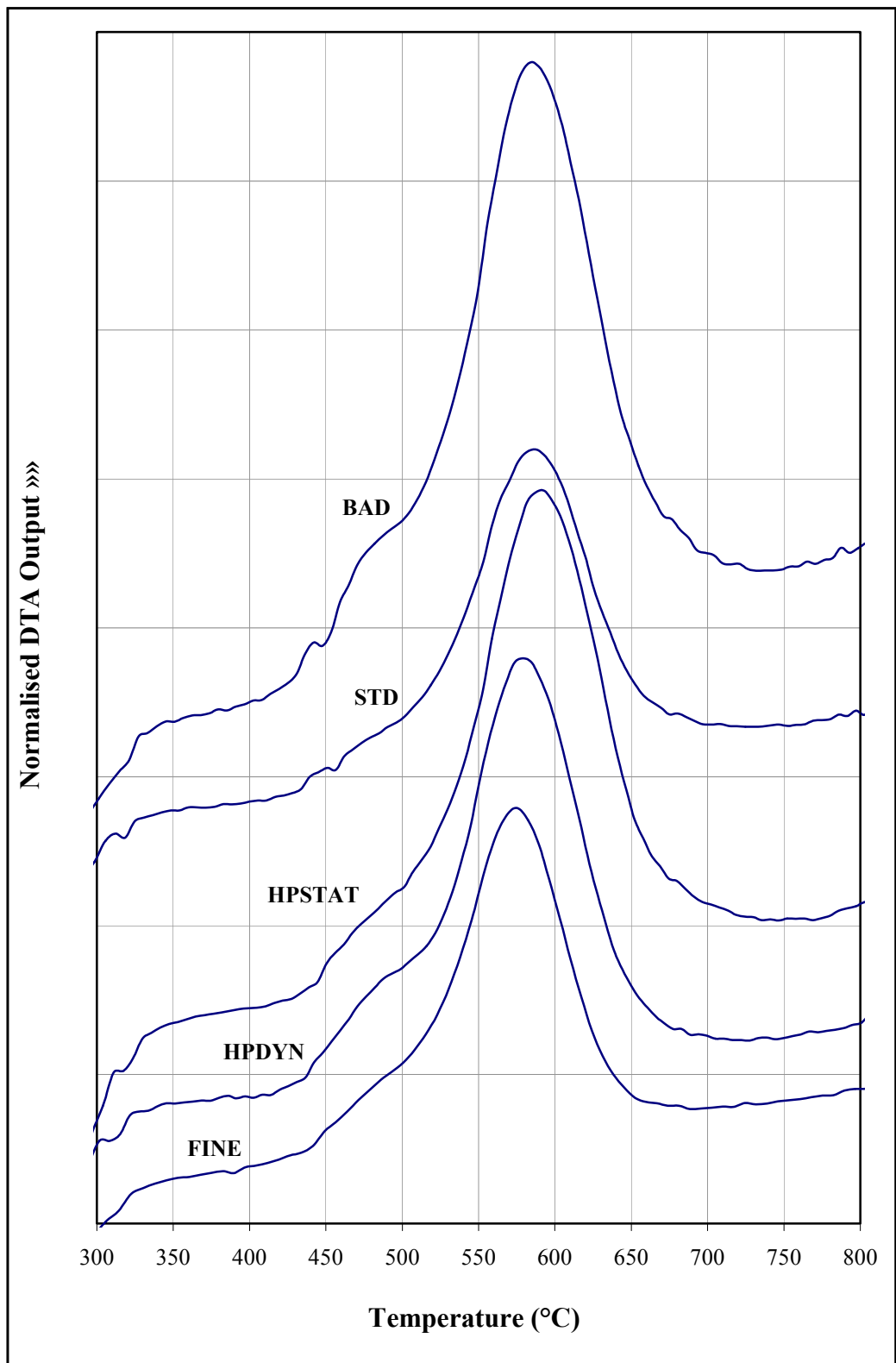
Figure 6.15 DTA burning profiles for Thoresby chars from Port 3

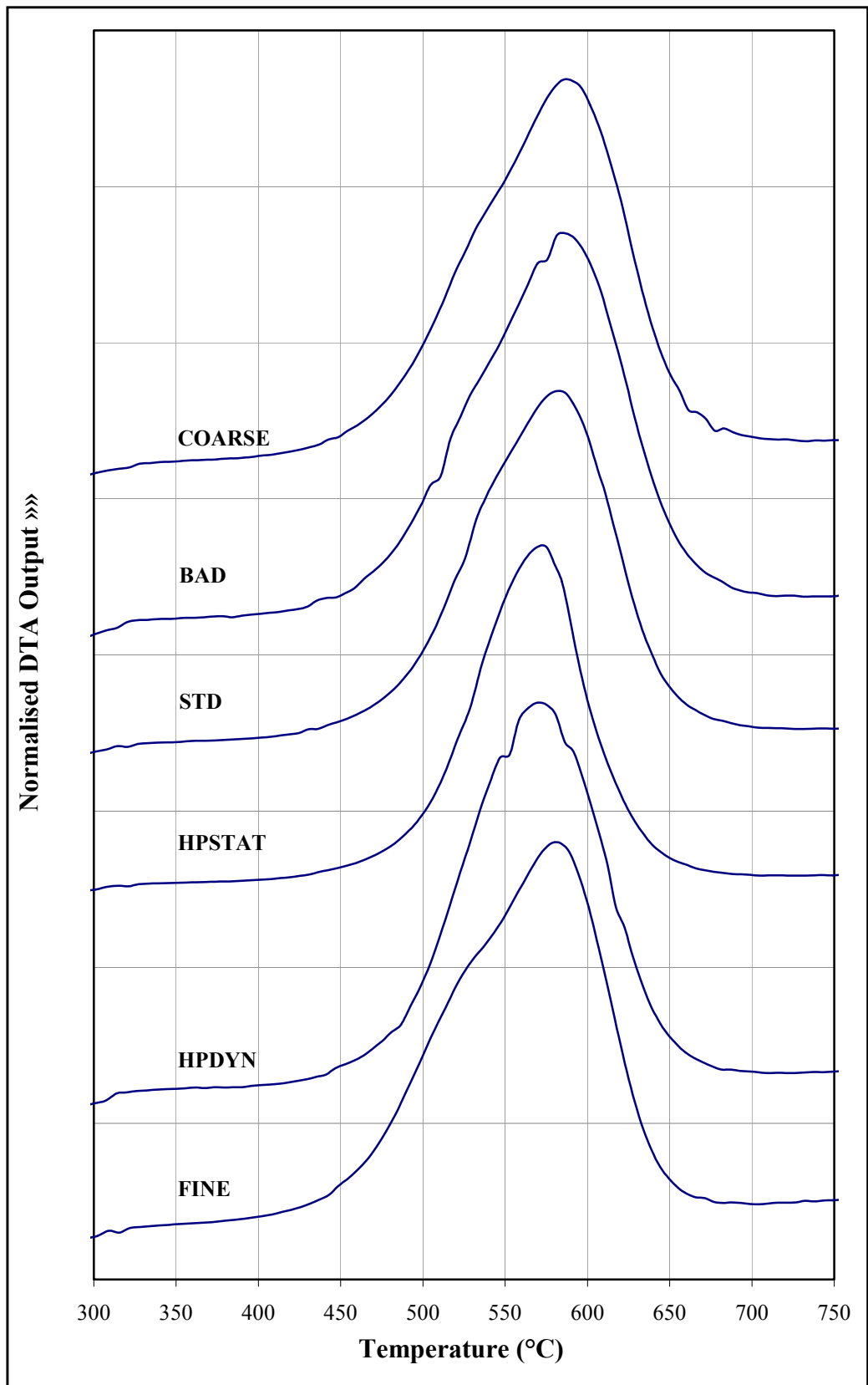
Figure 6.16 DTA burning profiles for Carbocol chars from Port 2

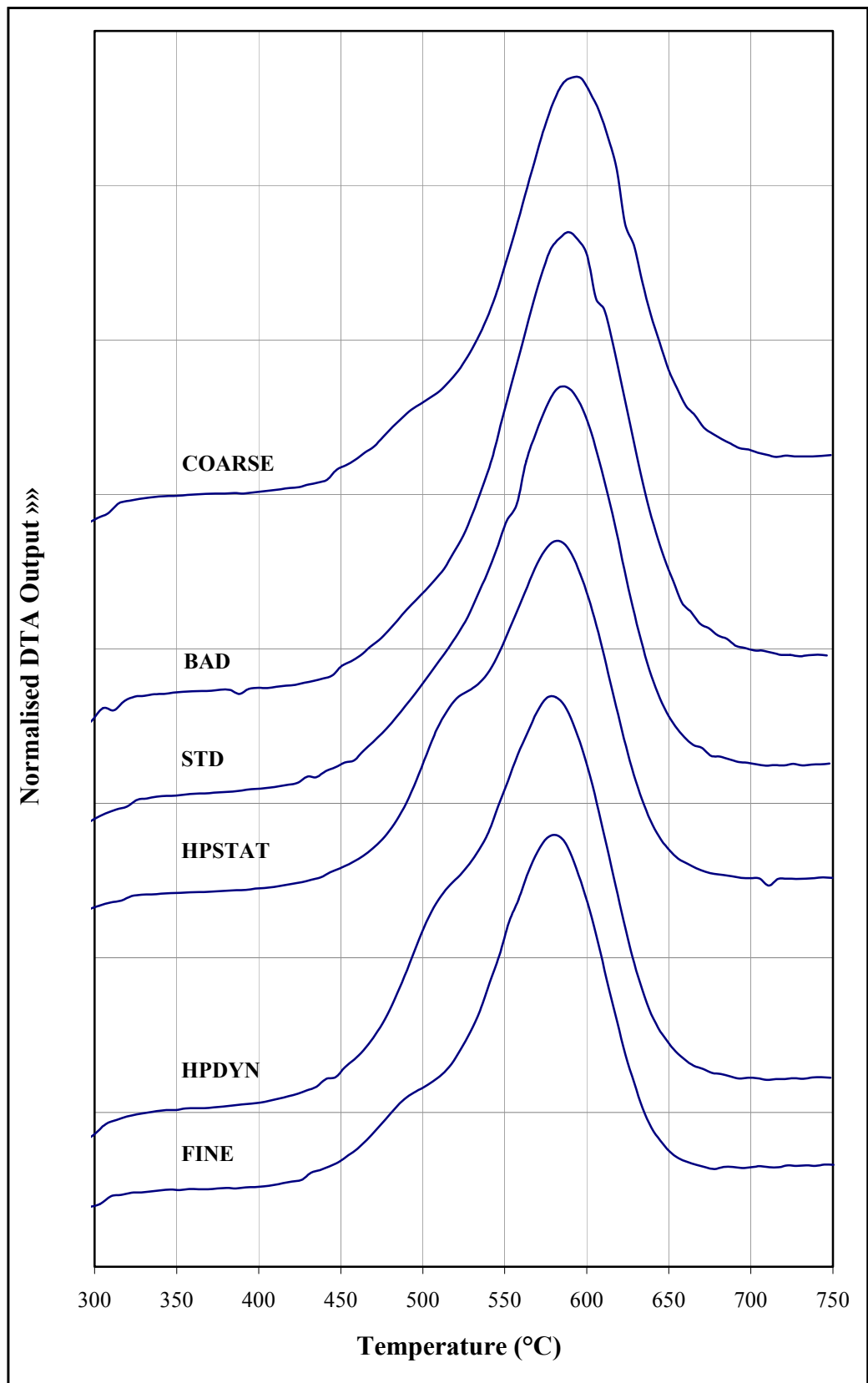
Figure 6.17 DTA burning profiles for Carbocol chars from Port 3

Figure 6.18 PT and BT data as a function of the percentage of particles above 150µm for Thoresby chars from Ports 2 and 3

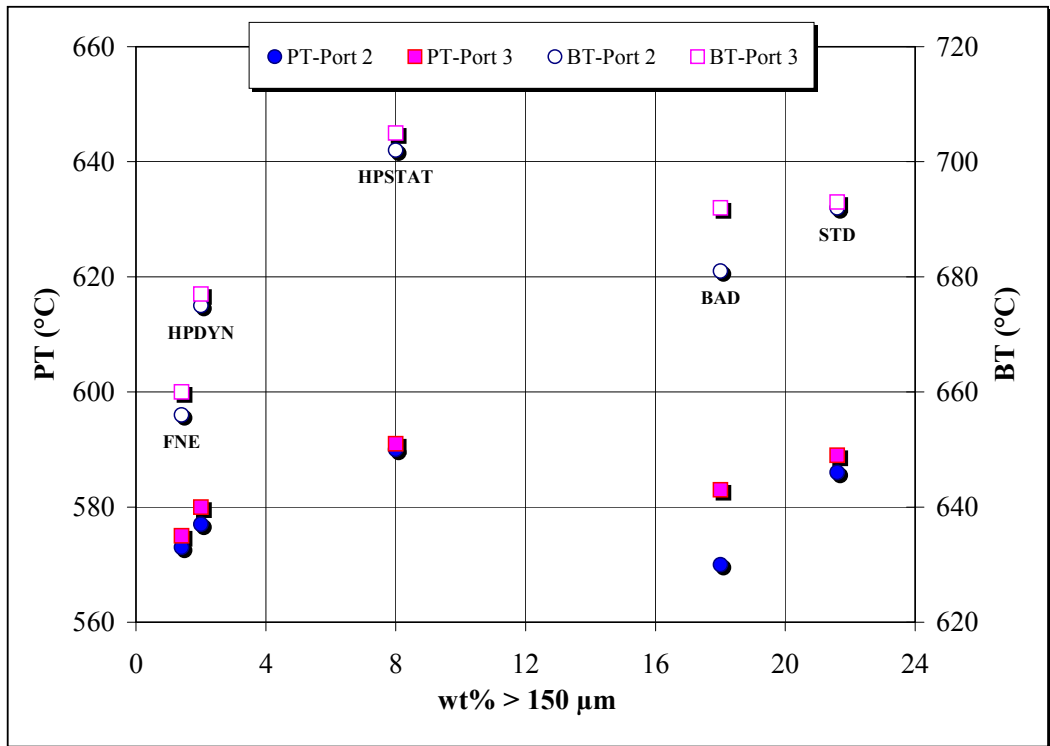
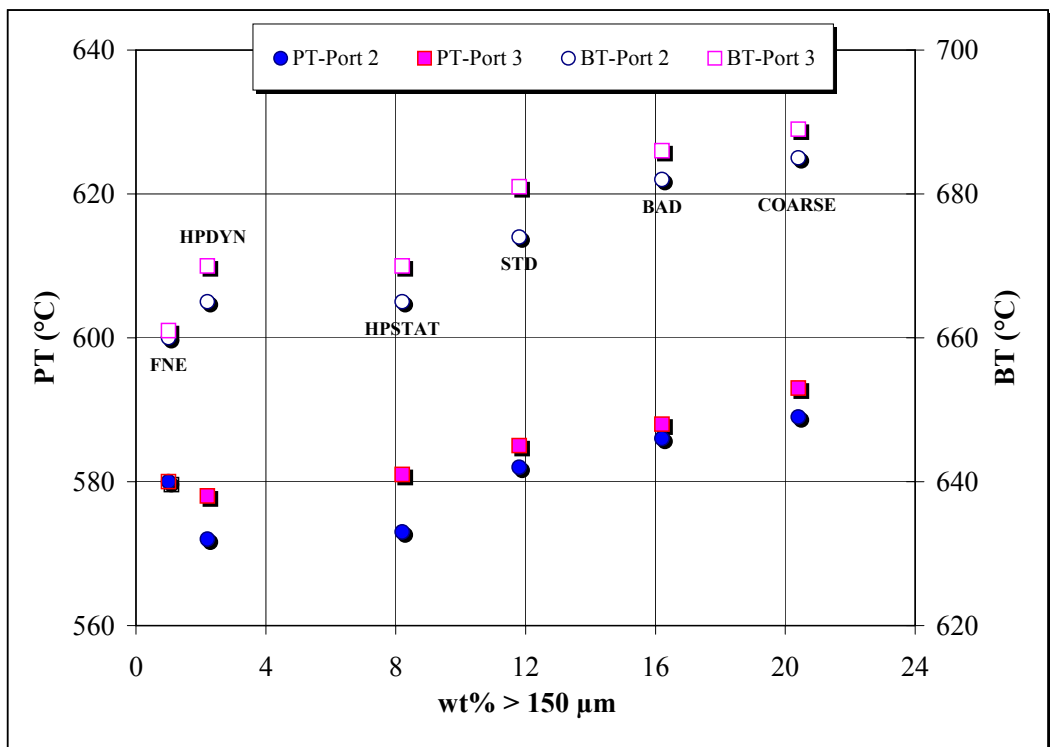


Figure 6.19 PT and BT data as a function of the percentage of particles above 150µm for Carbocol chars from Ports 2 and 3



6.7 Summary

The main conclusions from the experimental work can be summarised as follows:

- (1) The automatic image analysis of the chars obtained from the near-burner region of the CTF indicates a general trend of increasing concentration of thin-walled char (highest ACA5 values) with increasing particle fineness for both coals. The grinds with the lowest percentage of unreactives material gave, consistently, highest ACA5 values.
- (2) A general trend of increasing reactivity with increasing fineness of the coals was observed from the intrinsic reactivity analysis carried out to the chars from Port 1.
- (3) For the unblended coal (FINE, HPDYN and HPSTAT) of the low volatile coal Thoresby, unburnt combustible was found to decrease with increasing particles fineness.
- (4) The coarser grinds of Thoresby coal produced significantly lower unburnt combustible values than expected, comparable with the finest coal grinds. It is unclear if this is attributable to grind size or to the blending procedure.
- (5) For the higher volatile coal Carbocol, unburnt combustible was found to be insensitive to grind quality. It is expected that this phenomenon would not be repeated on full-scale plants. The intrinsic reactivity of the chars was found to increase with increasing particle fineness
- (6) The high performance dynamic classifier is currently the best technology for improving pf quality using standard milling equipment that will reduce combustible-in-ash levels.

CHAPTER 7 CONCLUSIONS AND FURTHER WORK

7.1 Drop Tube Furnace Experiments

In this part of the project, a series of experiments were conducted to characterise chars obtained from a Drop Tube Furnace. The main objective was to investigate the effects of temperature and particle size on char characteristics during high temperature devolatilisation and combustion. An eventual aim of the project was to identify coal properties which have an impact on burnout and how relevant they are in the prediction of coal combustion behaviour. In particular, it was envisaged that this study would help to provide a better understanding of the Reactivity Assessment Program (RAP) and the automatic image analysis of chars.

The coals used in this study, mainly from South America, were found to be vitrinite-rich coals and were all within the bituminous coal range. Vitrinite reflectance analysis of the different coal fractions indicated a narrow range for most of the coals.

The conclusions which arose from the analysis of the pyrolysed and re-fired chars and the correlation of their properties with coals parameters can be summarised as follows:

- (1) The morphological features and concentration of certain types of chars, after pyrolysis, were found to be dependent on the characteristics of the parent coal. The lower rank coals tended to produce predominantly network chars, whereas the higher rank coals produced mainly cenospheric chars.
- (2) Despite the fact that all the coals used in this study were vitrinite-rich, variations in char morphology were evident. This demonstrated that it was impossible to assign any one char type to a single maceral group. It was

apparent that vitrinite generates a wide range of char types depending upon the rank of the parent coal and on the maceral associations within the coal.

- (3) From the data on image analysis of the chars, it was observed that the DTF operating temperature and particle size of the coals have an effect on the amount of thin and thick-walled chars generated. It was clearly evident that the higher the temperature and the lower the particle size, the greater the amount of thin-walled chars and the lower the concentration of thick-walled chars. The increase in ACA5 values with increasing DTF temperature and decreasing particle size was in agreement with the manual char data.
- (4) The intrinsic reactivity, as measured by TGA, of the initial chars was found to decrease with increasing operating temperature and increasing particle size of the coal (i.e. decreasing external surface area of particles). Thus, chars of different size, although from the same coal, are intrinsically different.
- (5) Guasare coal was found to burnout slowly, particularly the coarsest fractions. Its poor burnout performance is clearly due to the formation of thick-walled cenospheric chars during pyrolysis. This means that the percentage of combustible remaining in ash for this coal will increase significantly if it is not properly milled before combustion.
- (6) Some correlation between the properties of the pyrolysed chars and high temperature volatiles with maceral analysis were obtained. However, with the inclusion of rank in the regressions, the correlations improved and this demonstrated the importance of the variation of reflectance of vitrinite. Further correlations of the char properties and high temperature volatiles with % unreactives demonstrated the importance of the Reactivity Assessment Program to assess burnout behaviour of coal. Nevertheless, when considering the complete grey scale histogram, which accounts for the variations in reflectance for all macerals, the correlations were far better. This final approach was considered to be more reliable than the %

unreactives itself since the 190 grey level threshold ignores or includes part of the coal which may or may not be contributing to its reactivity.

7.2 Experiments in the 1MW Combustion Rig

The work in the 1 MW combustion rig was undertaken with the aim of determining the effect of pf particle size distribution on combustion performance of coal. High volatile and a low volatile coals were used for this purpose. Grind specifications were selected to be representative of products that could reasonably be expected from currently available classification technologies. In order to assess the impact of poor mill maintenance a coarse grind was tested.

Maceral composition and most of the properties of the coals did not vary significantly. Vitrinite tended to concentrate in the finest grinds and liptinite and inertinite in the coarsest grinds. The low volatile coal was found to be of higher rank, higher ash content and of similar carbon and hydrogen content to the high volatile coal.

The automatic image analysis of the chars obtained from the near-burner region of the rig (Port 1) indicated a general trend of increasing concentration of thin-walled char (highest ACA5 values) with increasing particle fineness for both coals. The sizes with the lowest percentage of unreactives material gave, consistently, highest ACA5 values.

A general trend of increasing reactivity, decreasing burnout temperature, with increasing fineness of the coals was observed from analysis carried out on the chars from Port 1. A progressive decrease of reactivity with increasing burnout of the chars, from Port 1 to Port 3, was observed.

For the unblended grinds of the low volatile coal, unburnt combustible was found to decrease with increasing particle fineness. The coarser grinds produced significantly lower unburnt combustible values than expected, comparable with the finest coal grinds. It is unclear if this is attributable to grind size or to the

blending procedure. For the higher volatile coal, unburnt combustible was found to be insensitive to grind quality. It is expected that this phenomenon would not be repeated on full-scale plants.

On the basis of the CTF tests, it can be seen that the high performance dynamic classifier is a better option for producing improved pf size distributions.

7.3 Recommendations for Further Work

Image analysis techniques offer advantages in that they are faster and provide more quantitative information and a better degree of objectivity than manual point counting. However, image analysis systems have some difficulties in emulating certain aspects of the human visual system. Despite these inherent difficulties, there has been much success and new improvements in image analysis applied to coal and char characterisation in recent years.

Further refinement of the image analysis techniques for the analysis of coal reactivity and char morphology is required. This should include the ability to distinguish and analyse single coal particles. Useful data would comprise particle size-related measurements, grey scale histogram and maceral associations. This will allow the prediction of char morphology from individual coal particles. The image analysis techniques can be further refined to present char morphology in a format suitable for inclusion in char burnout models.

REFERENCES

- Aiken L.S., West S.G. (1991).** Multiple regression. Newbury Park: Sage.
- Allen M., Cloke M., Lester E., Miles N.J. (1995).** Repeatability of maceral analysis using image analysis systems. *Fuel* 74, 654-658.
- Alvarez D; Borrego A.G., Menéndez R. (1998).** An unexpected trend in the combustion behaviour of hvBb coals as shown by the study of their chars. *Energy & Fuels* 12, 849-855.
- Alvarez D.; Lester E. (2001).** Combustion working Group. Commission III. ICCP.
- Aquino Z.N. (1999).** Effects of coal beneficiation on coal combustion. PhD Thesis. Nottingham University.
- ASTM Standard D388 (1991).** Classification of coal by rank. American Society for Testing and Materials. Philadelphia, P.A., USA.
- Bailey J.G., Tate A., Diessel C.F.K., Wall T.F. (1990).** A char morphology system with applications to coal combustion. *Fuel* 69, 225-239.
- Bailey J.G., Diessel C.F.K., Wall T.F. (1991).** Origin of unburnt combustibles. Report NERDDP-EG-92-1030. Canberra, ACT, Australia: National Energy Research, Development and Demonstration Council, December 1991.
- Bend S.L., Edwards I.A.S., Marsh H. (1989).** Petrographic characterization of coals to relate to combustion efficiency. *Proceedings of the International Conference on Coal Science*, 1989, 437-440. Tokyo: NEDO.
- Bend S.L., Edwards I.A.S., Marsh H. (1992).** The influence of rank upon char morphology and combustion. *Fuel* 71, 493-501.
- Bengtsson M. (1987a).** Combustion behaviour for a coal containing a high proportion of pseudovitrinite. *Fuel Processing Technology* 15, 201-212.

- Bengtsson M. (1987b).** Combustion behaviour for a range of coals of various origins and petrographic compositions. International Conference on Coal Science, 1987, 893-896. Amsterdam, The Netherlands: Elsevier Science Publishers.
- Best P.E., Solomon P.R., Serio M.A., Suuberg E.M. (1987).** The relationship between char reactivity and physical and structural features. American Chemical Society, Division of Fuel Chemistry 32, (4), 138-146.
- Borrego A.G., Alonso M.J.G., Alvarez D., Kalkreuth W., Menéndez R. (1997).** Pf combustion behaviour of Canadian coals in relation to their petrographic characteristics. Proceedings of the International Conference on Coal Science, 1997, 1011-1014. Essen, Germany: A. Ziegler et al. eds.
- BP Amoco plc (2000).** BP Amoco Statistical review of world energy. London: BP Amoco plc.
- British Standard 1016-104.3 (1998).** Methods for the analysis and testing of coal and coke. Proximate analysis: determination of volatile matter content. London: British Standards Institute.
- British Standard 6127 Part 3 (1981).** Petrographic analysis of bituminous coal and anthracite: Part 3 - Method of determining maceral group composition of bituminous coal and anthracite. Milton Keynes, UK: British Standards Institute.
- Bustin R.M., Cameron A.R., Grieve D.A., Kalkreuth W.D. (1983).** Coal petrology, its principles, methods and applications. Short Course Notes Vol. 3. Victoria, Canada: Geological Association of Canada.
- Cai H.Y., Megaritis A., Messenbock R.C., Palacin J., Dugwell D.R., Kandiyoti R. (1997).** Effect of maceral content on volatile release and char combustion reactivity. Proceedings of the International Conference on Coal Science, 1997, 1011-1014. Essen, Germany: Ziegler A. et al. eds.
- Carpenter A. (1988).** Coal Classification. London: IEA Coal Research.
- Carpenter A., Skorupska N.M. (1993).** Coal combustion: analysis and testing. London: IEA Coal Research.

- Chen P., Bodily D.M. (1985).** Separation and characterisation of macerals from Yanzhou coal. Proceedings of the International Conference on Coal Science, 1985, 653-656, Sydney: Australia: Pergamon.
- Clarke G.H. (1988).** Industrial and marine fuels reference book. Butterworths, London.
- Cloke M., Lester E. (1994).** Characterization of coals for combustion using petrographic analysis: a review. Fuel 73, 315-320.
- Cloke M., Lester E., Allen M., Miles N.J. (1995).** Automated maceral analysis using fluorescence microscopy and image analysis. Fuel 74, 659-669.
- Cloke M., Lester E., Gibb W. (1997a).** Characterization of coal with respect to carbon burnout in pf-fired boilers. Fuel 76, 1257-1267.
- Cloke M., Lester E., Gibb W. (1997b).** Morphological and reactivity changes of char during pulverised fuel combustion in a 1MW furnace and a drop-tube furnace. Proceedings of the International Conference on Coal Science 1997, 1007-1010. Essen, Germany (Ed. A. Ziegler et al.).
- Cloke M., Barraza J., Miles N.J. (1997c).** Pilot-scale studies using a hydrocyclone and froth flotation for the production of beneficiation coal fractions for improved coal liquefaction. Fuel 76, 1217-1223.
- Cloke M., Gilfilan A., Lester E. (1997d).** The characterization of coals and density separated coal fractions using FTIR and manual and automated petrographic analysis. Fuel 76, 1289-1296.
- Coalportal (2000a).** Coal mines of Colombia [Online]. Barlow Jonker Pty Ltd. Available at: <URL: http://www.coalportal.com/Mall/coalportal/online_members/documents/exporters-f/Colombia-f.html> [Accessed 10 June 2001].
- Coalportal (2000b).** Coal mines of Venezuela [Online]. Barlow Jonker Pty Ltd. Available at: <URL: http://www.coalportal.com/Mall/coalportal/online_members/documents/exporters-f/Venezuela-f.html> [Accessed 10 June 2001].
- Coinvertir (2000a).** Colombia, energy sector: coal [Online]. Bogota, Colombia: Coinvertir, Invest in Colombia Corporation. Available at: <URL: <http://www.coinvertir.com/sector/coal/coal.htm>> [Accessed 20 June 2001].

- Corporate Information (2001).** Venezuela, coal mining equipment overview [Online]. Milford, CT, USA: The Winthrop Corporation. Available at: <URL: <http://www.corporateinformation.com/data/statusa/venezuela/coalminingequip.html>> [Accessed 14 July 2001].
- Crelling J.C. (1987).** Separation, identification and characterisation of single coal maceral types. Proceedings of the International Conference on Coal Science, 1987, 119-122. Amsterdam, The Netherlands: Elsevier Science Publishers.
- Crelling J.C., Hippo E.J., Woerner B., West D. (1992).** Combustion characteristics of selected whole coals and macerals. Fuel 71, 151-158.
- Crelling J.C., Skorupska N., Marsh H. (1988).** Reactivity of coal macerals and lithotypes. Fuel 67, 781-785.
- Crelling J.C. (1998).** Petrographic atlas - coal macerals [Online]. Carbondale, Illinois: The Southern Illinois University. Available at: <URL: <http://mccoy.lib.siu.edu/projects/crelling2/atlas>> [Accessed 18 July 2000].
- Cumming J.W. (1984).** Reactivity assessment of coals via weighted mean activation energy Fuel 63, 1436-1440.
- Davidson R.M. (1980).** Molecular structure of coal. London: IEA Coal Research.
- Dormans H.N., Huntjens F.J., Van Krevelen D.W. (1957).** Chemical structure and properties of coal XX-composition of the individual macerals (vitrinites, fusinites, micrinites and exinites). Fuel 36, 321-339.
- Dyrkacz G.R., Bloomquist C.A., Ruscic L. (1984).** Chemical variations in coal macerals separated by density gradient centrifugation. Fuel 63, 1166-1173.
- Draper N.R., Smith H. (1998).** Applied regression analysis. 3rd edition. New York, USA: John Wiley & Sons.
- Ecocarbon (1998).** Plan de desarrollo del subsector carbon 1999-2010. Santafé de Bogota: Ecocarbon -Empresa Colombiana de Carbon.
- Essenhigh R. (1981).** Fundamentals of coal combustion, chemistry of coal utilisation, Vol. 2, 1153-1312. New York, USA: Wiley Press.

- Fossil Energy International (2001).** An energy overview of Colombia [Online]. Washington D.C., USA: U.S. Department of Energy. Available at: <URL: <http://www.fe.doe.gov/international/colbover.html>> [Accessed 14 July 2001].
- Gibbins J.R., Man C.K., Pendlebury K.J. (1991).** Determination of rapid heating volatile matter contents as a routine test. 1st International Conference on Combustion Technologies for a Clean Environment, 3-6th September, 1991, 729-741. Vilamora, Portugal.
- Gilfillan A.J. (1999).** Structure and reactivity of coal fractions related to characterisation using total reflectance histograms. PhD Thesis, Nottingham University.
- Gomez H. (1995).** Status of coal exploration in the Atlantic Coast of Colombia. Earth Sciences, Vol. 16. Berlin: Springer-Verlag.
- Goodarzi F., Murchinson D.G. (1978).** Influence of heating rate variation on the anisotropy of carbonised vitrinites. Fuel 57, 273-284.
- Grainger L., Gibson J. (1981).** Coal utilisation: technology, economics and policy. Graham and Trotman Limited, London.
- Haley E., Thomas K.M., Marsh H., Edwards I.A.S. (1991).** Coal char reactivity and burn-off. Proceedings of the International Conference on Coal Science, 1991, 275-278. Newcastle Upon Tyne, UK: Butterworth Heinemann.
- Hamilton L.H. (1969).** Further investigations of structural changes occurring in pulverized coal. Fuel 48, 343-365.
- Hamilton L.H. (1981).** Char morphology and behaviour of Australian vitrinites of various rank pyrolysed at various heating rates. Fuel 60, 909-913
- Harris D.J., Smith I.W. (1991).** The intrinsic reactivity of carbons to oxidising gases: structural changes. Proceedings of the International Conference on Coal Science, 1991, 259-262. Newcastle Upon Tyne, UK: Butterworth Heinemann.
- Harris L.A., Yust C.S. (1976).** Transmission electron microscope observations of porosity in coal. Fuel 55, 233-236.
- Howard J.B. (1981).** Fundamentals of coal pyrolysis and hydrolysis. In Chemistry of Coal Utilisation, Vol. 2. New York, USA: Wiley Press.

- Hunter J.S. (1970).** Statistical design of engineering experiments. New York, USA: AIChE Today Series.
- IEA Coal Industry Advisory Board (1985).** Coal quality and ash characteristics. Paris, France: OECD/IEA.
- Jamieson E.D. (1985).** The cost and availability of Colombian coal. London: IEA Coal Research.
- Jamaluddin A.S. (1992).** Estimation of kinetics parameters for char oxidation. Fuel 71, 311-317.
- Jones R.B., McCourt C.B., Morley C., King K. (1985a).** Maceral and Rank influence on the morphology of coal char. Fuel 64, 1460-1467.
- Jones R.B., Morley C., McCourt C.B. (1985b).** Maceral effects on the morphology and combustion of coal char. Proceedings of the International Conference on Coal Science, 1985, 669-672. Sydney: Australia: Pergamon.
- Kimber G.M., Gray M.D. (1967).** Rapid devolatilisation of small coal particles. Combustion and Flame 11, 360-362.
- Kopp O., Harris L. (1984).** Initial volatilisation temperatures and average volatilisation rates of coal- their relation to coal rank and other characteristics. International Journal of Coal Geology 3, 333-348.
- Kural, O. (1994).** Coal: resources, properties, utilization, pollution. Istanbul, Turkey: Orhan Kural.
- Laurendeau N.M. (1978).** Heterogeneous kinetics of coal char gasification and combustion. Progress in Energy and Combustion Science 4, (4), 221-270.
- Lee C.W., Scaroni A.W., Jenkins R.G. (1991).** Effect of pressure on the devolatilisation and swelling behaviour of a softening coal during rapid heating. Fuel 70, 957-965.
- Lee G.K., Whaley H. (1983).** Modification of combustion and fly-ash characteristics by coal blending. Journal of the Institute of Energy 56, 190-197.
- Lester E. (1994).** The Characterisation of coal for combustion. PhD Thesis, Nottingham University.

- Lester E., Cloke M., Miles N.J. (1993a).** The effect of operating conditions on char produced in a drop-tube furnace. *Fuel Processing Technology* 36, 101-108.
- Lester E., Allen M., Cloke M., Miles N.J. (1993b).** Image analysis techniques for petrographic analysis. *Fuel Processing Technology* 36, 17-24.
- Lester E., Allen M., Cloke M., Miles N.J. (1994a).** An automated image analysis system for major maceral group analysis in coals. *Fuel* 73, 1729-1734.
- Lester E., Allen M., Cloke M., Miles N.J. (1994b).** Maceral analysis by automatic image analysis techniques. 12th International Coal Preparation Congress, 531-537. Poland.
- Lester E., Cloke M., Gibb W. (1995).** Comparison of chars produced in a drop-tube furnace and combustion test facility from coal characterised using image analysis techniques. *Proceedings of the International Conference on Coal Science 1995*, 627-630, Oviedo, Spain: J.A. Pajares and J.M. Tascon eds.
- Lester E., Allen M., Cloke M. (1996a).** The characterisation of char particles using automated image analysis. *Energy and Fuels* 10, (3), 696-703.
- Lester E., Allen M., Cloke M., Miles N.J. (1996b).** Analysis of the problems associated with the use of image analysis for microlithotype analysis on solid coal mounts. *Coalbed Methane and Coal Geology*, Geological Society Special Publication 109, 237-248.
- Lightman P., Street P.J. (1968).** Microscopic Examination of heat treated pulverized coal particles. *Fuel* 47, 7-28.
- Mannini A. (1989).** World coal ports. London: IEA Coal Research.
- Matthias W.H. (1992).** Recent progress in coal structure research. *Fuel* 71, 1211-1223.
- Mc Cown M.S., Harrison D.P. (1982).** Pyrolysis and hydrolyrolysis of Louisiana lignite. *Fuel* 61, 1149-1154.

- Milligan J.B., Thomas K.M., Crelling J.C. (1997).** Temperature-programmed combustion studies of coal and maceral group concentrates. *Fuel* 76, 1249-1255.
- Montgomery D.C. (1997).** Design and analysis of experiments. 4th Ed. New York, USA: John Wiley & Sons.
- Morgan M., Roberts P.A. (1987).** Combustion studies by thermogravimetric analysis. *Fuel* 66, 210-215.
- Morgan P.A., Robertson S.D., Unsworth J.F. (1987).** Coal Combustion characteristics studies at the International Flame Research Foundation. *Fuel Processing Technology* 15, 173-187.
- Morrison G.F. (1986).** Understanding pulverised coal combustion. London: IEA Coal Research.
- Nandi B.N., Brown T.D., Lee G.K. (1977).** Inert coal macerals in combustion. *Fuel* 56, 125-130.
- Nip M., De Leeuw J.W., Schenck P.A. (1987).** Structural characterisation of coals, coal macerals and their precursors by pyrolysis-gas chromatography and pyrolysis-gas chromatography-mass spectrometry. Proceedings of the International Conference on Coal Science, 1987, 89-92. Amsterdam, The Netherlands: Elsevier Science Publishers.
- Oka N., Murayama T., Matsuoka H., Yamada S., Yamada T., Shinozaki S., Shibaoka M., Thomas C. (1987).** The influence of rank and maceral composition on ignition and char burnout of pulverized coal. *Fuel Processing Technology* 15, 213-224.
- Osborne D.G. (1988).** Coal preparation technology. Vol. 1. London: Graham and Trotman.
- Phong-Anant P., Salehi M., Thomas C., Baker J., Conroy A. (1989).** Burnout and reactivity of coal macerals. Proceedings of the International Conference on Coal Science, 1989, 253-256. Tokyo: NEDO.
- Pullen J.R. (1984).** Catalytic coal gasification. London: IEA Coal Research.

- Serageldin M.A., Pan W.P. (1986).** Effect of CaCl₂ on char reactivity kinetics. American Chemical Society, Division of Fuel Chemistry 31, (2), 20-25.
- Schapiro N., Gray R., Eusner G. (1961).** Recent developments in coal petrography. Blast Furnace, Coke Ovens and Raw Materials Proceedings. A.I.M.E. 20, 89-112.
- Shibaoka M., Thomas C.G., Young B.C., Oka N., Matsuoka H., Tamara K., Murayama T. (1985).** The influence of rank and maceral composition of pulverized coal. Proceedings of the International Conference on Coal Science 1985, Sydney: Australia: Pergamon., 665-668. Pergamon.
- Shibaoka M., Thomas C.G., Heng S., Mackay G.H. (1987).** Significance of morphological features of macerals in coal utilization research. International Conference on Coal Science, 1987, 105-110. Amsterdam, The Netherlands: Elsevier Science Publishers.
- Shibaoka M., Thomas C.G., Gawronski E., Young B.C. (1989).** A new concept in the microscopic classification of pf char. Proceedings of the International Conference on Coal Science, 1989, 1123-1126. Tokyo: NEDO.
- Singer J.G. (1981).** Combustion, Fossil power systems. 3rd Ed. Windsor, Ct, USA: Combustion Engineering, Inc.
- Skorupska N.M. (1987).** Coal combustibility. PhD Thesis, Newcastle upon Tyne University, 1987.
- Skorupska N.M. (1993).** Coal specifications – impact on power station performance. Report IEACR/52. London: IEA Coal Research.
- Skorupska N.M., Haley E., Marsh H., Edwards I.A.S. (1989).** An assessment of the properties which control the reactivity of coal chars. Proceedings of the International Conference on Coal Science, 1989, 429-432. Tokyo: NEDO.
- Skorupska N.M., Marsh H. (1989).** The importance of petrographic characterisation of coal for combustion processes. Applied Energy Research. Proceedings of the Institute of Energy Conference, 1989. Swansea, UK.

- Skorupska N.M., Sanyal A., Hesselman G., Crelling J.C., Edwards Marsh H. (1987).** The use of an entrained flow reactor to assess the reactivity of coals of high inertinite content. Proceedings of the International Conference on Coal Science, 1987, 827-831. Amsterdam: Elsevier Science Publishers.
- Singer, S. (1983).** Pulverised coal combustion. Report DOE/ET/10679-T17. P.E.T.C. Pittsburgh, PA, USA: DOE.
- Smith S. E., Neavel R. C., Hippo E. J., Miller R. N. (1981).** DTGA combustion of coals in the Exxon coal library. Fuel 60, 458-462.
- Smith K. L., Smoot L. D., Fletcher T.H. (1993).** Coal Characteristics, structure, and reaction rates. In: Fundamentals of coal combustion for clean and efficient use. Smoot L. D. (ed). Amsterdam, Netherlands: Elsevier Science Publishers.
- Smoot L.D., Smith P. J. (1985).** Coal combustion and gasification. New York, USA: Plenum Press.
- Smoot L.D. (1993).** Fundamentals of coal combustion for clean and efficient use. Coal Science and Technology 20. Amsterdam: Elsevier Science Publishers.
- Solomon P.R., Serio M.A., Carangelo R.M., Markham J.R. (1986).** Very rapid coal pyrolysis. Fuel 65, 182-194.
- Stach E., Mackowsky M.T., Teichmüller M., Taylor G.H., Chandra D., Teichmüller R. (1982).** Stach's textbook of coal petrology. 3rd Ed. Berlin: Gebrüder Borntraeger.
- Steller M., Kalkreuth W., Wiesenkamper I. (1991).** Effect of vitrinite and inertinite fluorescence properties and combustion and hydrogenation reactivities of coals. Proceedings of the International Conference on Coal Science, 1991, 90-93. Newcastle Upon Tyne, UK: Butterworth Heinemann.
- Stopes M.C. (1935).** On the petrology of banded bituminous coals. Fuel 14, 4-13.
- Street P.J., Weight R.P., Lightman P. (1969).** Further investigations of structural changes occurring in pulverized coal. Fuel 48, 343-365.

- Suarez-Ruiz I., Crelling J.C., Bensley D.F. (1991).** Petrographic characterisation of Spanish bituminous coals from the Central Teverga Basins. Proceedings of the International Conference on Coal Science, 1991, 119-121. Newcastle Upon Tyne, UK: Butterworth Heinemann.
- Suuberg E.M., Peters W.A., Howard J.B. (1979).** Product composition and formation kinetics in rapid pyrolysis of pulverized coal: implications for combustion. In: Seventeenth International Symposium in Combustion. Leeds, UK, 20 August 1978, 117-130. Pittsburgh, PA, USA: The Combustion Institute.
- Taulbee D., Dor S., Robl T., Keogh B. (1989).** Density gradient centrifugation, separation and characterisation of maceral groups from a mixed macerals bituminous coal. *Energy & Fuels* 3, (6), 662-670.
- Thomas C.G., Holcombe D., Shibaoka M., Young B.C., Brunckhorst L.F., Gawronski E. (1989a).** Determination of the effect of coal rank and maceral composition on PF combustion reactivity. Proceedings of the International Conference on Coal Science, 1989, 257-260. Tokyo: NEDO.
- Thomas C.G., Shibaoka M., Gawronski E., Gosnell M.E., Phong-Anant D., Brunckhorst L.F., Salehi M.R. (1989b).** Swelling and plasticity of inertinite in PF combustion. Proceedings of the International Conference on Coal Science IEA 1989, 213-216. Tokyo, NEDO.
- Thomas C.G., Shibaoka M., Phong-Anant D., Gawronski E., Gosnell M.E. (1991).** Determination of the percentage reactivities under pf combustion conditions. Proceedings of the International Conference on Coal Science, 1991, 48-51. Newcastle Upon Tyne, UK: Butterworth Heinemann.
- Thompson A.W., Stainsby R.E., Simpson B. (1993).** Collaborative program on NO_x research: Drop Tube studies. International Combustion Report No. 25717. July 1993.
- Tsai S.C. (1982).** Fundamentals of coal beneficiation and utilisation. *Coal Science and Technology* 2, Elsevier Science Publishers.
- Tsai C.Y., Scaroni A.W. (1987).** Pyrolysis and combustion of bituminous coal fractions in an entrained flow reactor. *Energy & Fuels* 1, 263-269.

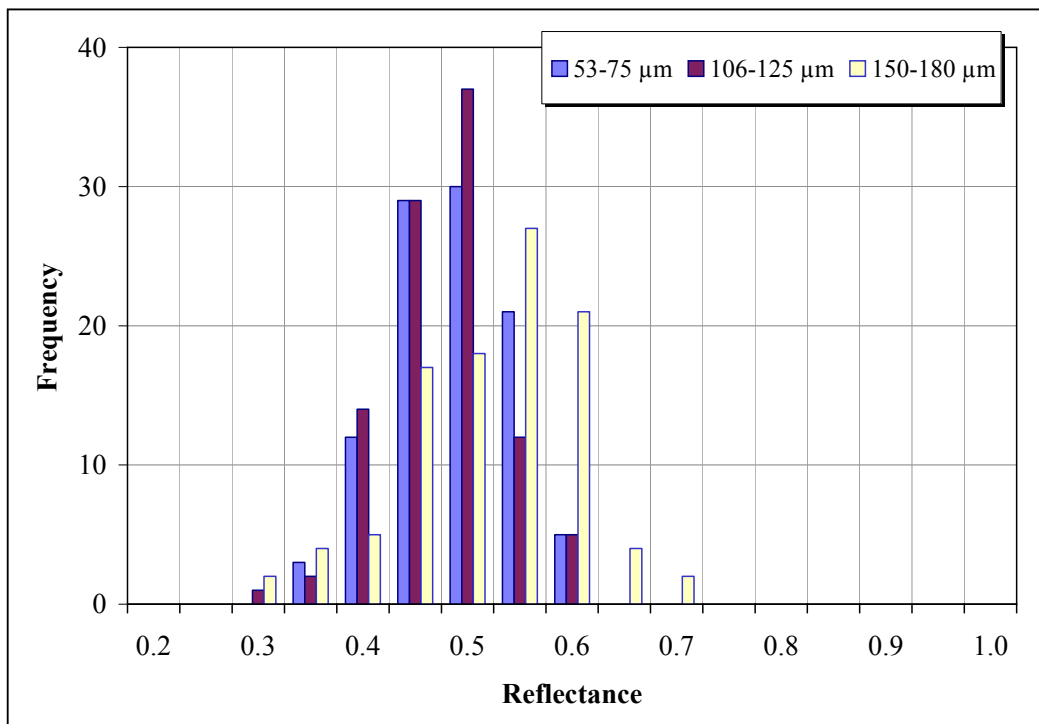
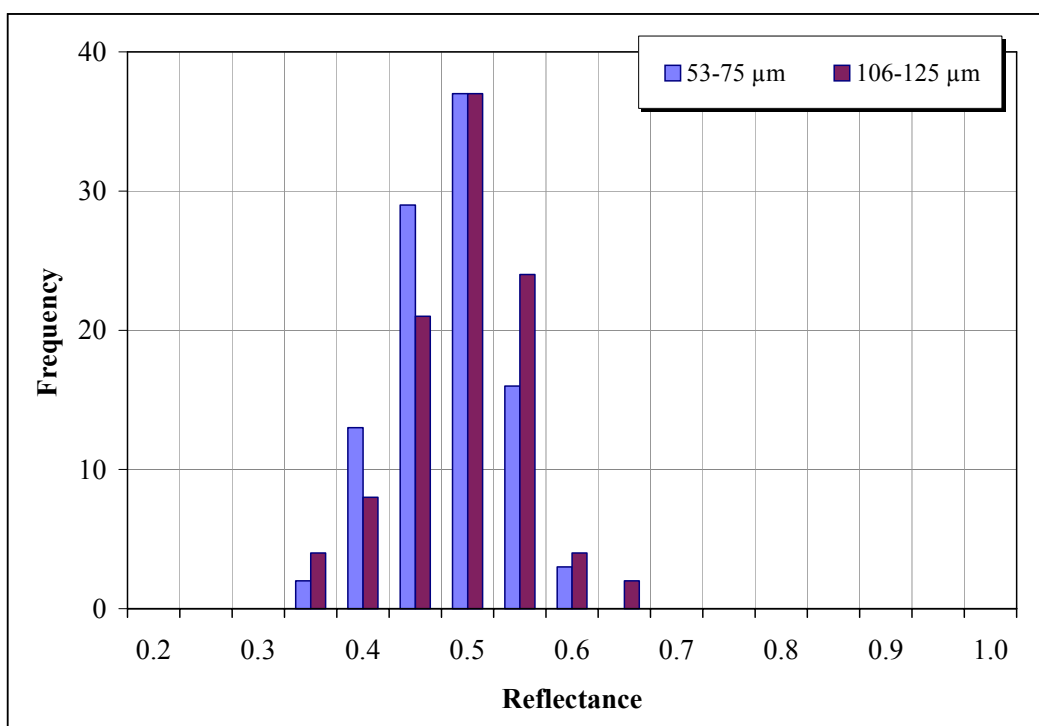
- Unsworth, J.F., Barratt, D.J., Roberts, P.T. (1991).** Coal quality and combustion performance, an international perspective. Coal Science and Technology 19, Elsevier, Amsterdam.
- Van-Krevelen D.W. (1993).** Coal: typology, physics, chemistry, constitution. 3rd Ed., Coal Science Series, Elsevier Science Publishers, Amsterdam.
- Vasquez L.U. (1991).** Venezuelan coal: new projects, new perspectives. In: Coal trading worldwide, Vol. 4. 6th Pacific Rim Coal Conference, 9-12 Jun 1991, 13.1-13.26. Polofsky A H ed. New Jersey, USA: AER Enterprises.
- Vinod H.D., Ullah A. (1981).** Recent advances in regression methods. New York, USA: M. Dekker ed.
- Vleeskens J.M. (1983).** Burnout of coals:- comparative bench-scale experiments on pulverized fuel and fluidised bed combustion. Proceedings of the International Conference on Coal Science, 1983, 599-602. Pittsburgh, PA, USA.
- Vleeskens J.M., Nandi B.N. (1986).** Combustion efficiency and petrographic properties. Fuel 65, 797-802.
- Walker S. (1993).** Major coalfields of the world. London: IEA Coal Research.
- Weaver J.N & Wood G.H. (1994).** Coal map of South America. USA: U.S. Department of the Interior, U.S. Geological Survey.
- World Coal Institute (2000).** Coal, power for progress. 4th Edition. London: WCI.
- Xian D.G., Wang C.C., Zhao Z.G. (1988).** Experimental study on combustion characteristics of pulverized-coal. In: Coal combustion: science and technology of industrial and utility applications. International Symposium on Coal combustion, Beijing, China, 7-10 Sept 1987, 131-137. New York, USA: Hemisphere Publishing Corporation.
- Young B.C., Smith I.W. (1987).** Carbon combustion: the order of reaction in oxygen. Proceedings of the International Conference on Coal Science, 1987, 793-796. Amsterdam, The Netherlands: Elsevier Science Publishers.

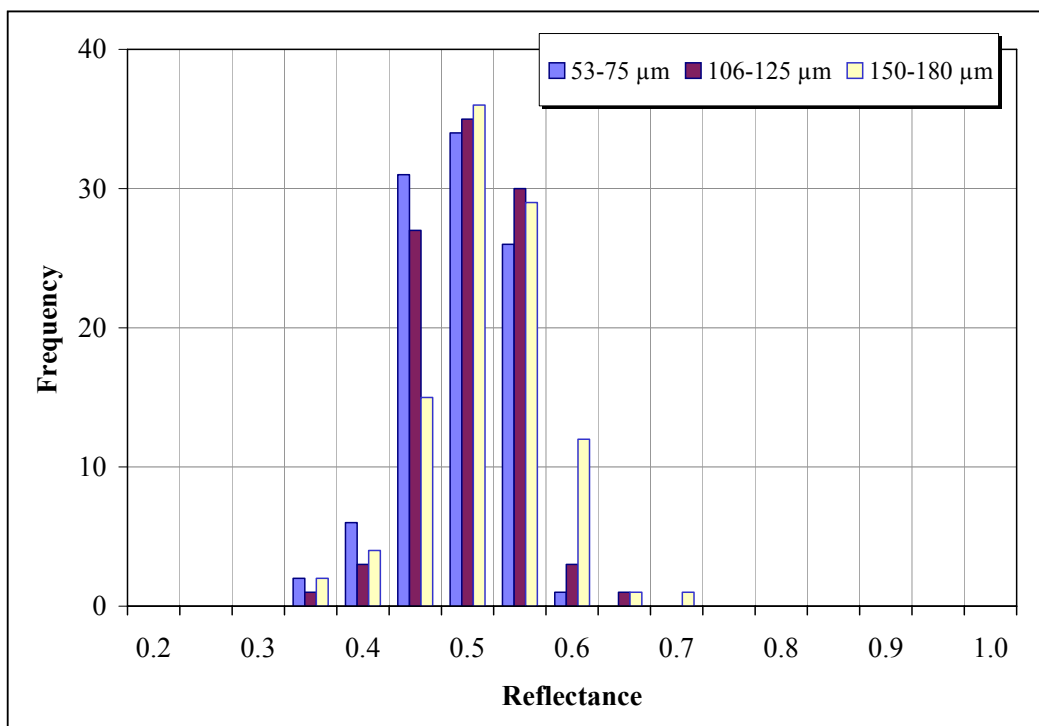
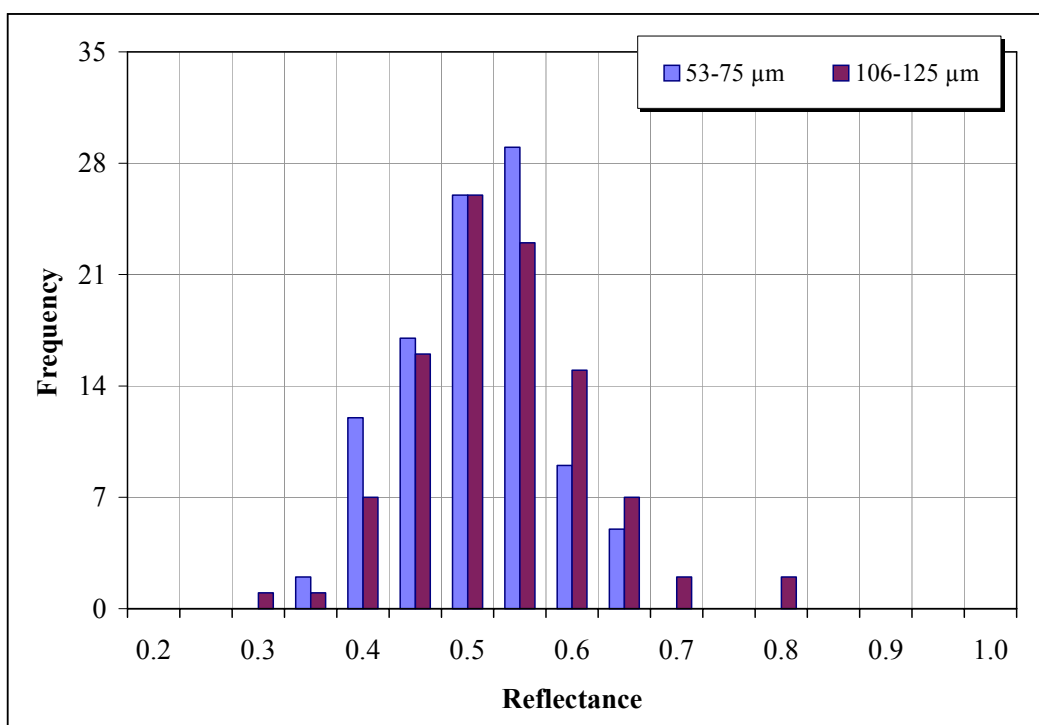
PUBLICATIONS

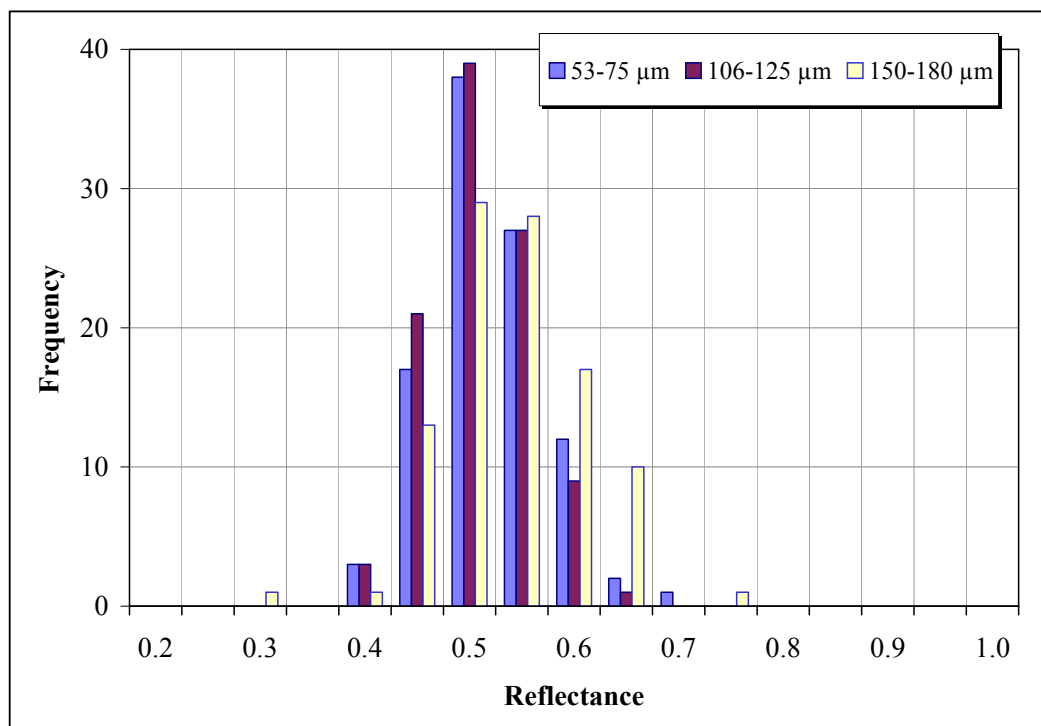
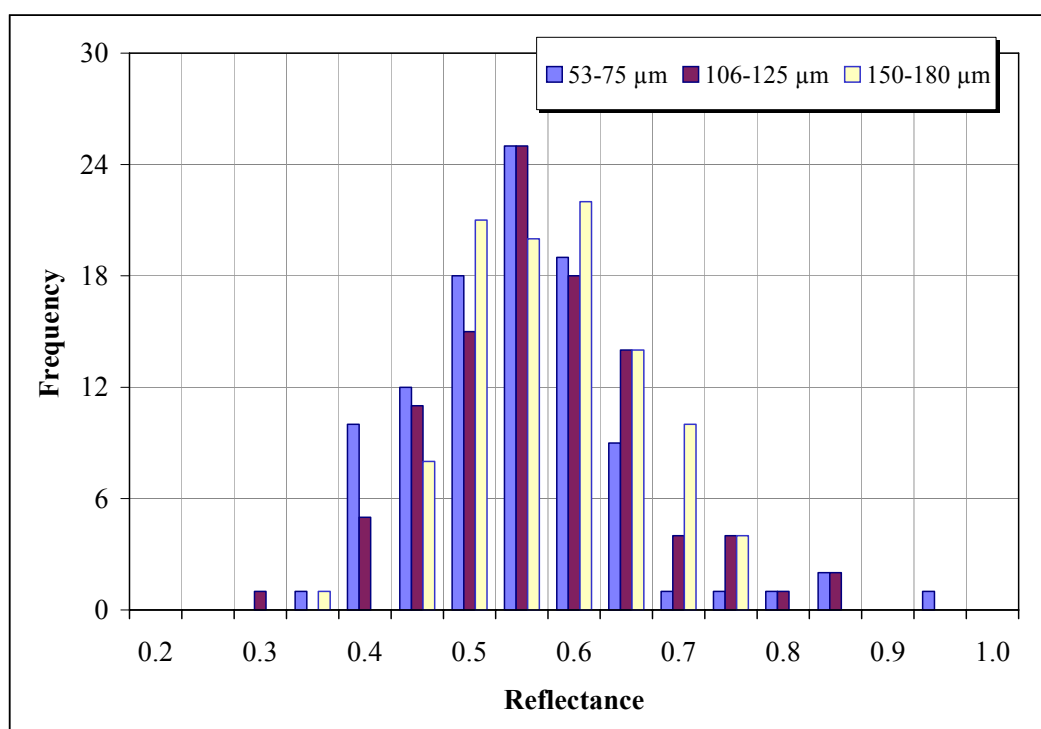
- Barranco R.** Combustion behaviour of South American coals. Compendium of the Research Activity of Colombians in the United Kingdom, Version 1, Colombian Science and Technology Network, 1998. London, UK: Lonsdale Press Ltd.
- Barranco R., Cloke M., Lester E. (2000).** Optimisation of derivative thermal gravimetric analysis of coal by using design of experiments. Proceedings of the IChemE Research Event: Research 2000, Stretching the Boundaries of Chemical Engineering, Bath, 6-7th January 2000, 149.
- Barranco R., Cloke M., Lester E. (2000).** Effects of temperature, particle size, and coal type on char reactivity and morphology during pyrolysis in a drop tube furnace. 3rd UK Meeting on Coal Research and its Applications, Aston University, Birmingham, 12th-14th September 2000.
- Barranco R., Cloke M., Lester E. (2000).** The effect of operating conditions and coal type on char reactivity during combustion in a drop tube furnace [CD-ROM]. Proceedings of the Ninth Australian Coal Science Conference. Brisbane, 26-29 November 2000 [CD-ROM]. Brisbane, Australia: The Australian Institute of Energy.
- Barranco R., Cloke M., Lester E. (2001).** The combustion burnout performance of some South American coals in a drop tube furnace. Proceedings of the 11th International Conference on Coal Science. San Francisco, USA, 30th September-5th October 2001. [Accepted for publication].
- Barranco R., Cloke M., Lester E., Gibb W. (2001).** Study of the combustion burnout performance of some South American coals in a drop tube furnace. Current Research in Combustion: A Forum for Research Students and Young Researchers. Loughborough, UK, 20th September 2001. [Accepted as poster presentation].
- Barranco R., Cloke M., Lester E. (2001).** The morphological characteristics and intrinsic reactivity of char during high temperature devolatilisation. [In preparation for publication].
- Barranco R., Cloke M., Gibb W. (2001).** Char burnout behaviour of South American coals during re-firing in a drop tube furnace. [In preparation for publication].

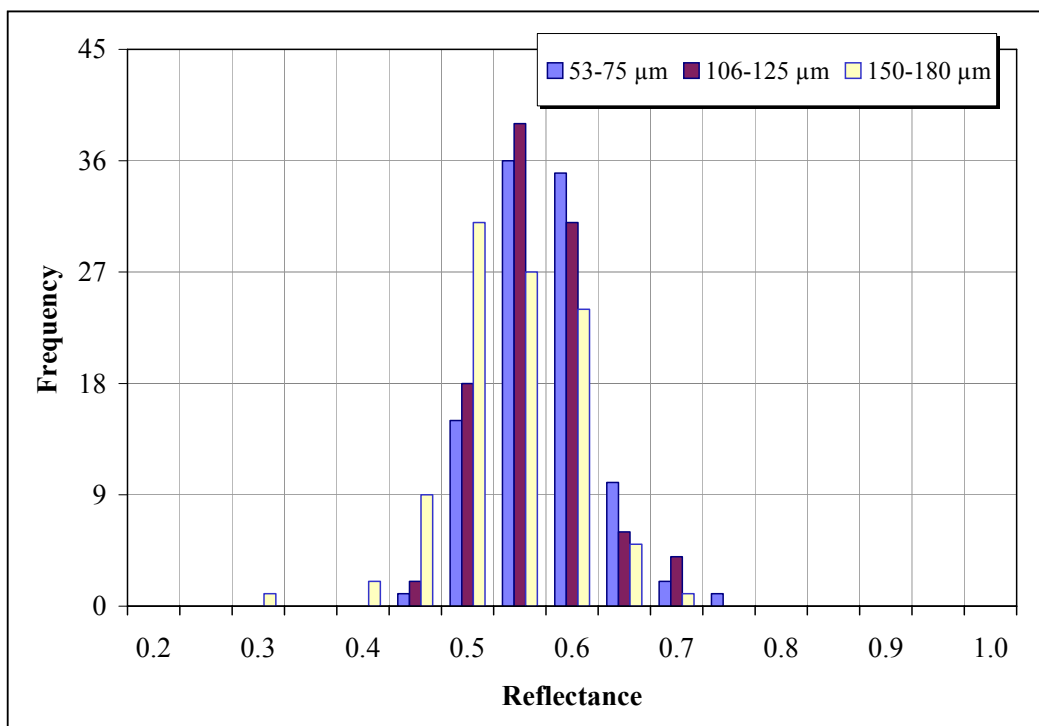
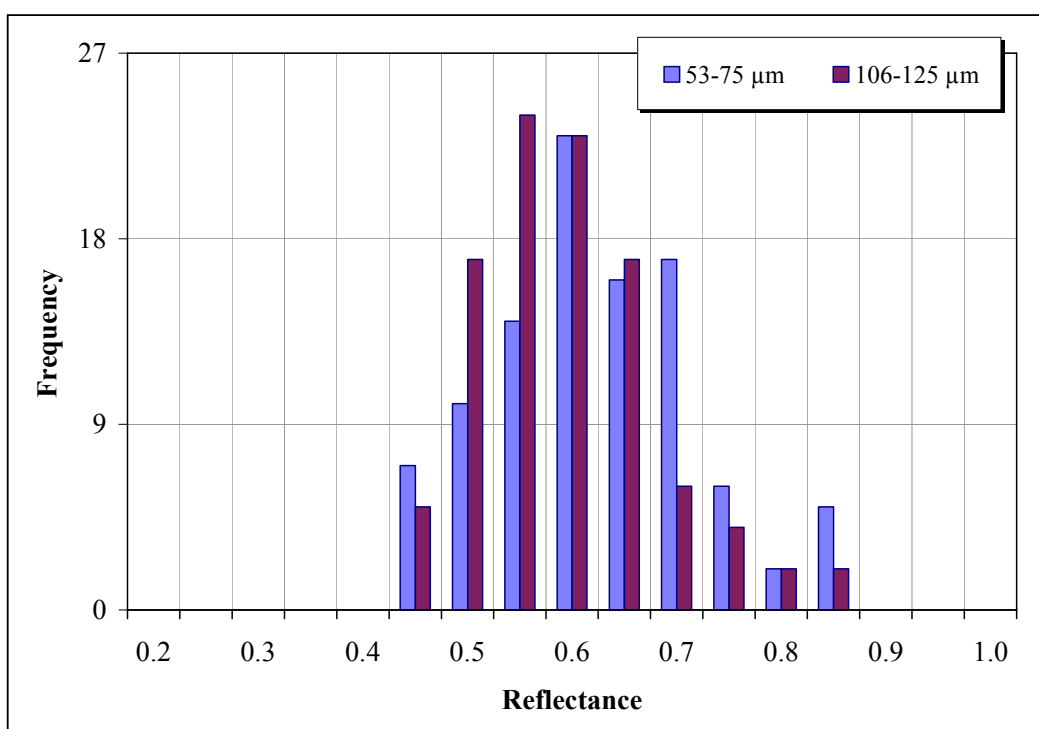
APPENDICES

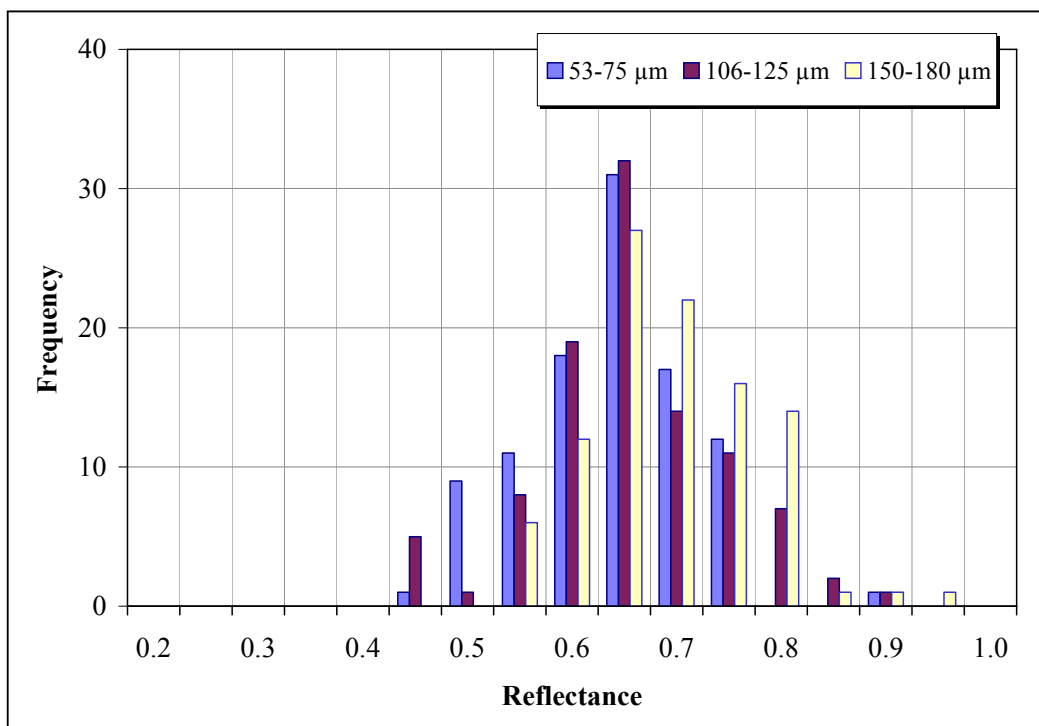
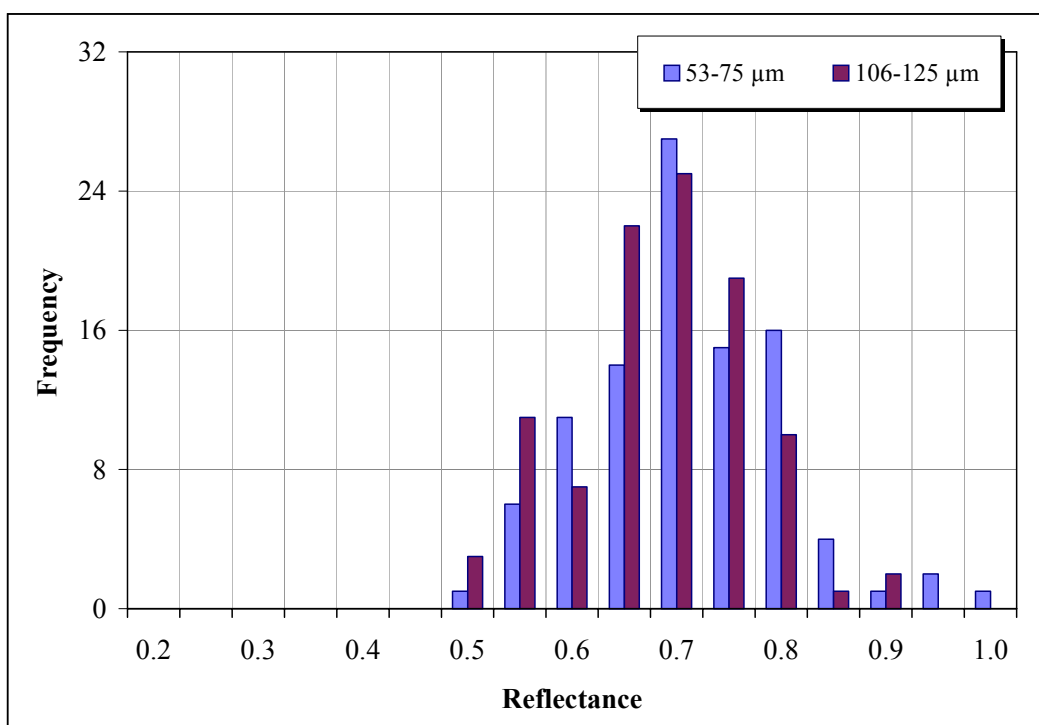
| | |
|---|-----|
| APPENDIX A. Vitrinite Reflectance Histograms of the Coal Fractions | 204 |
| APPENDIX B. Grey Scale Histograms of the Coal Fractions | 210 |
| APPENDIX C. DTA Profiles of the Chars as a Function of DTF Temp. | 216 |
| APPENDIX D. F-Distribution, F-values [Confidence level 95%: $\alpha = 0.05$] | 226 |
| APPENDIX E. DTA Profiles of the Pyrolysed Chars | 227 |
| APPENDIX F. DTA Profiles of the Re-fired Chars | 230 |

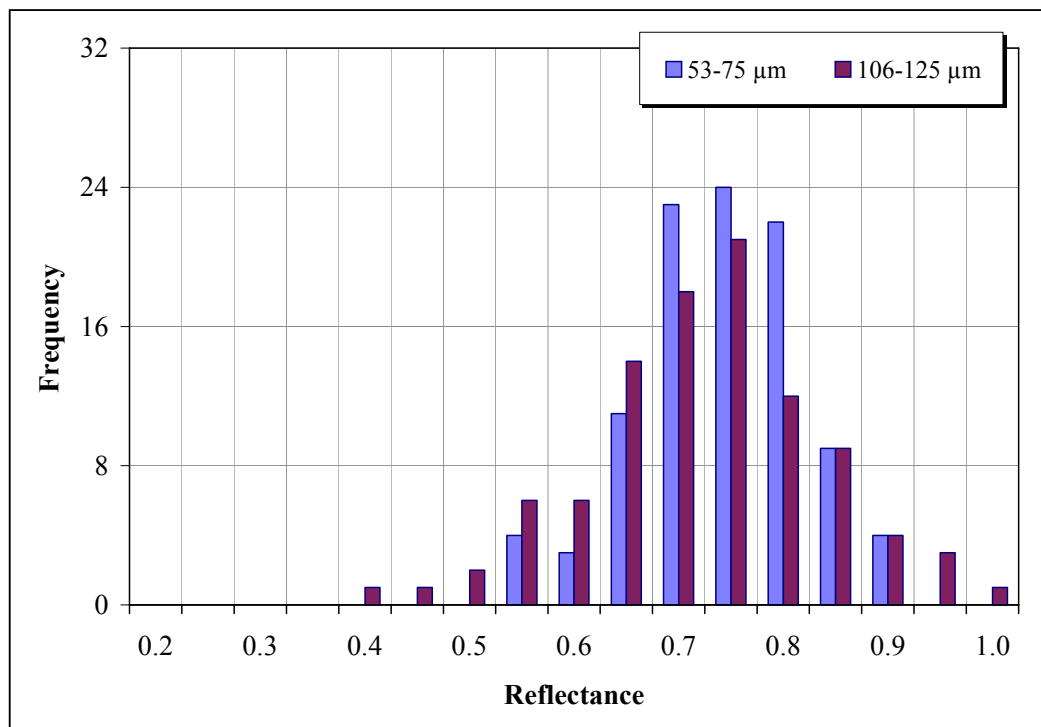
APPENDIX A. Vitrinite Reflectance Histograms of the Coal Fractions**A.1 Bijao****A.2 Fila Maestra**

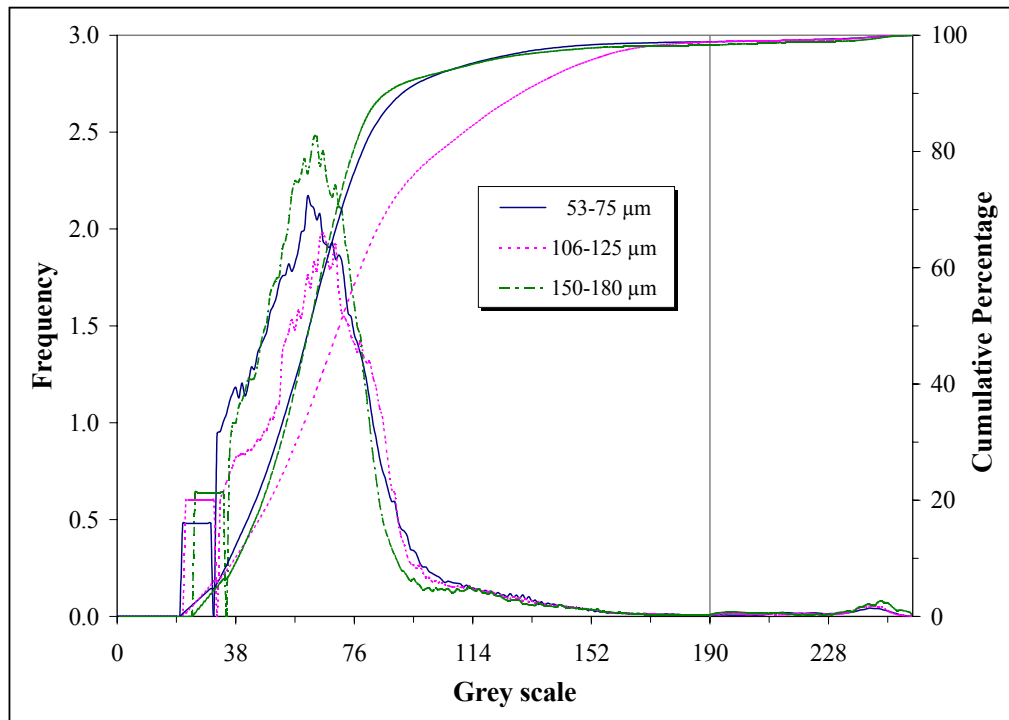
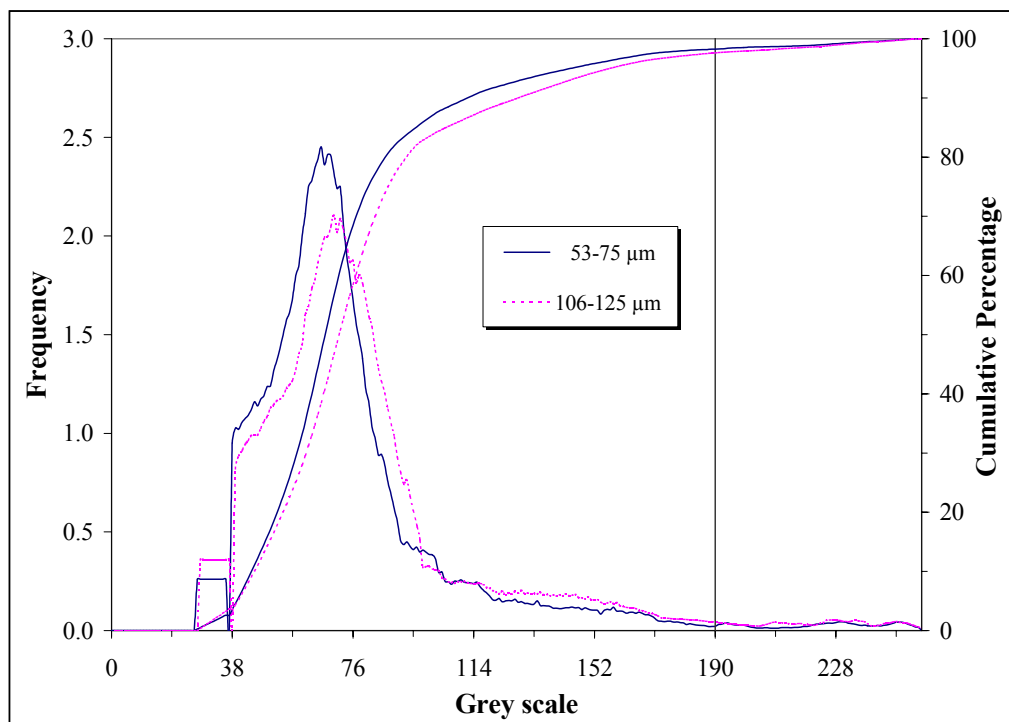
APPENDIX A. Vitrinite Reflectance Histograms of the Coal Fractions**A.3 La Loma****A.4 Oreganal**

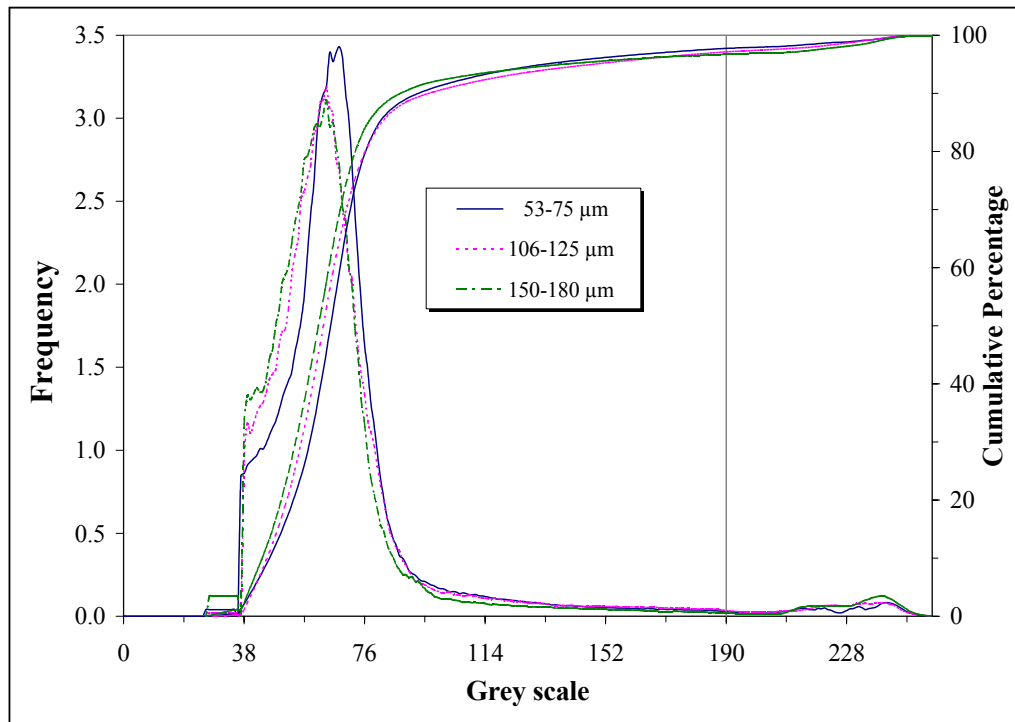
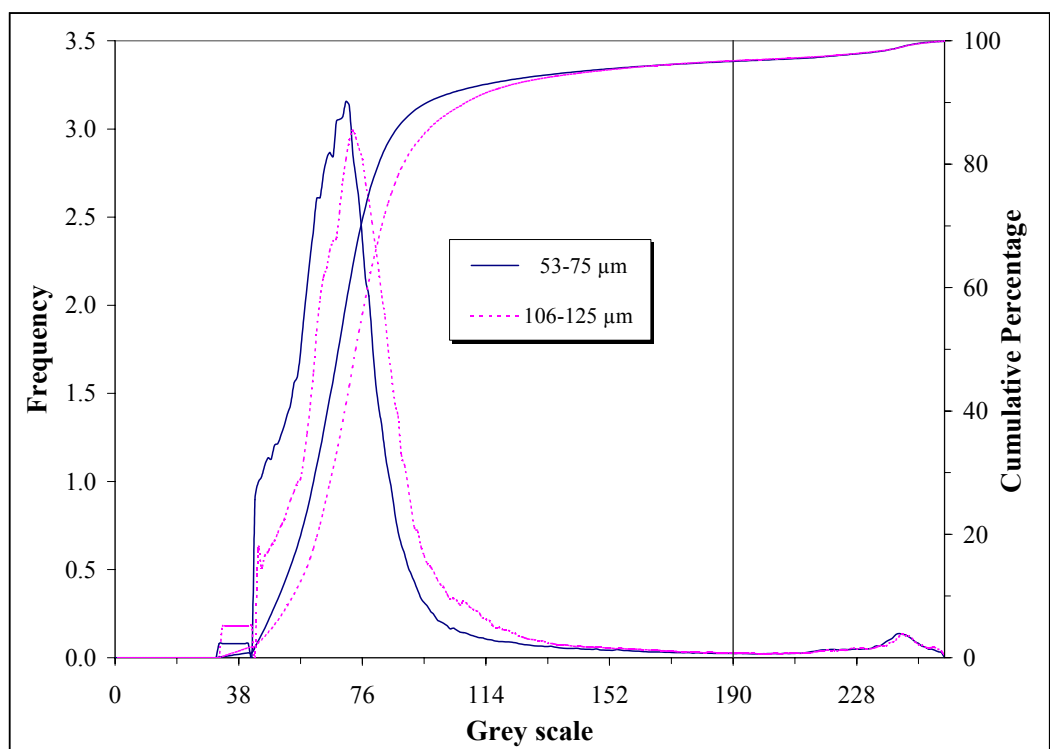
APPENDIX A. Vitrinite Reflectance Histograms of the Coal Fractions**A.5 La Jagua****A.6 El Cerrejon**

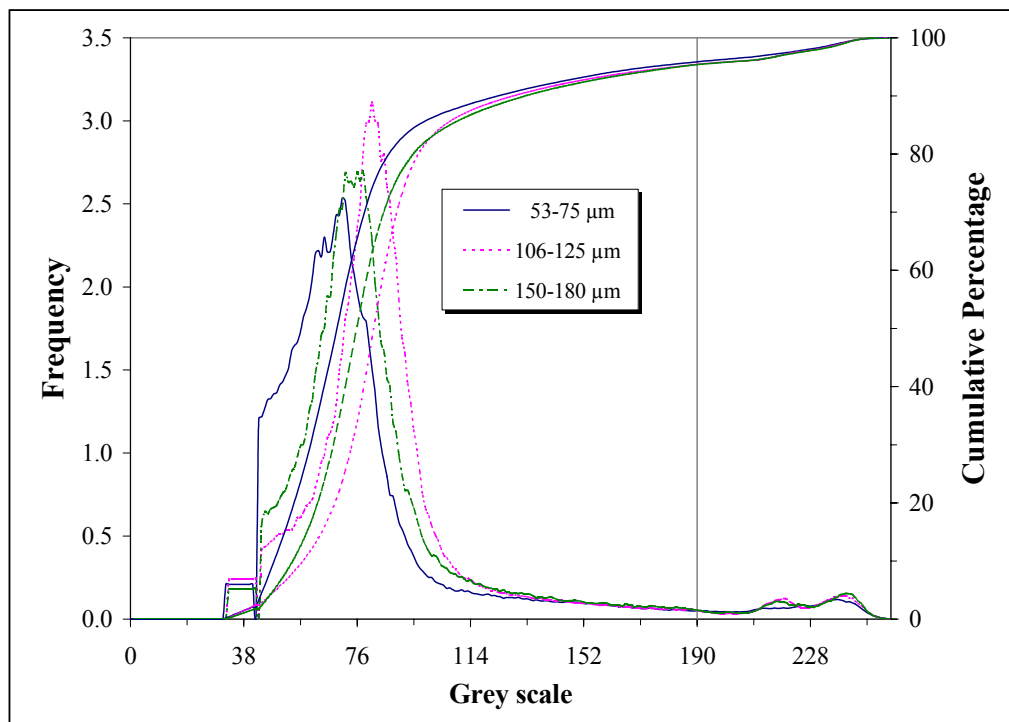
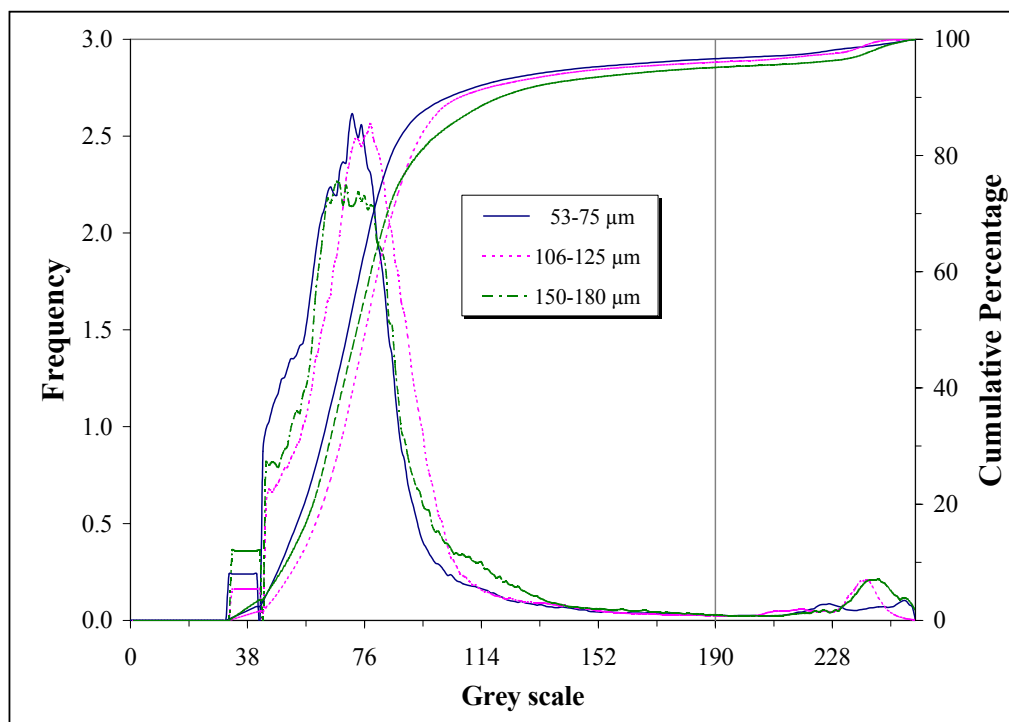
APPENDIX A. Vitrinite Reflectance Histograms of the Coal Fractions**A.7 Caypa****A.8 Paso Diablo**

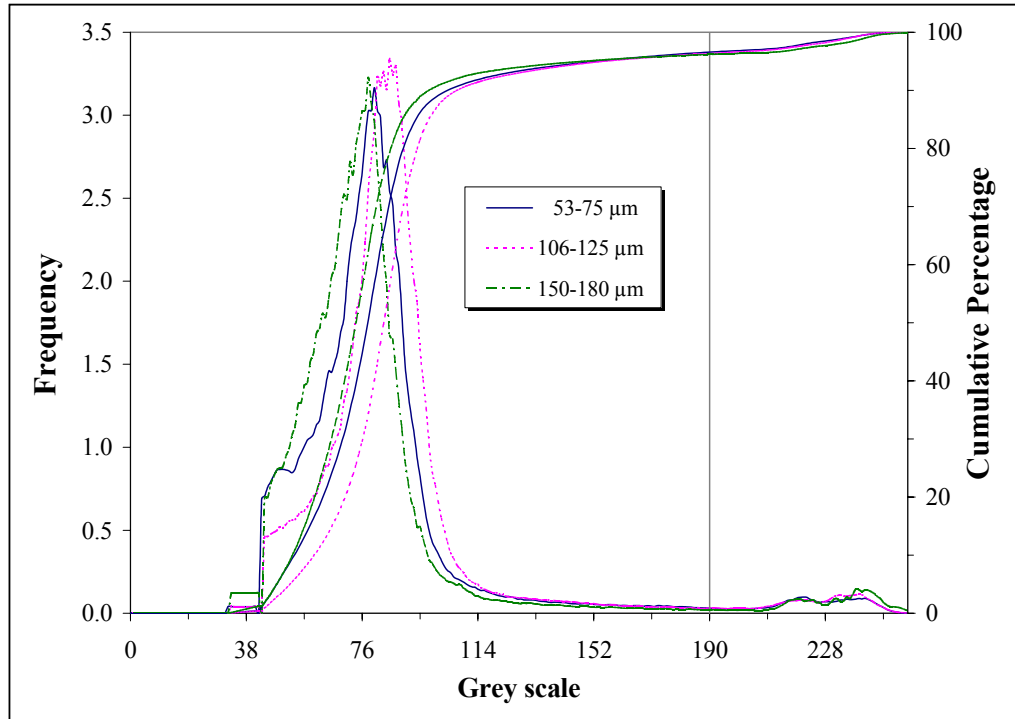
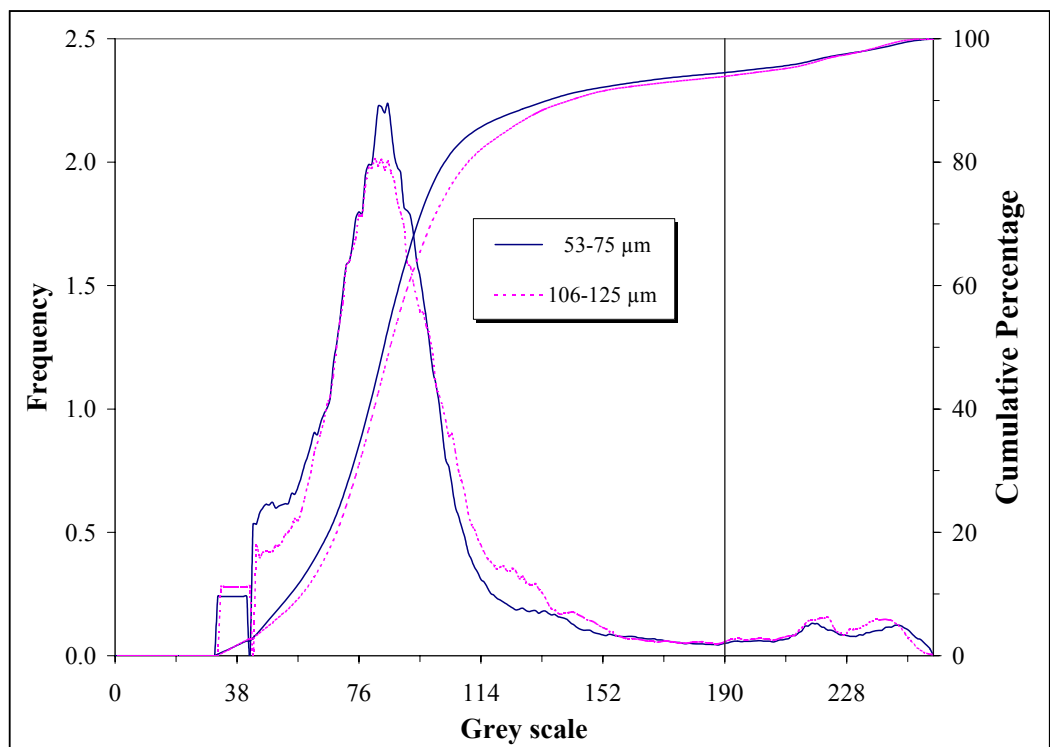
APPENDIX A. Vitrinite Reflectance Histograms of the Coal Fractions**A.9 Guasare****A.10 Maturin**

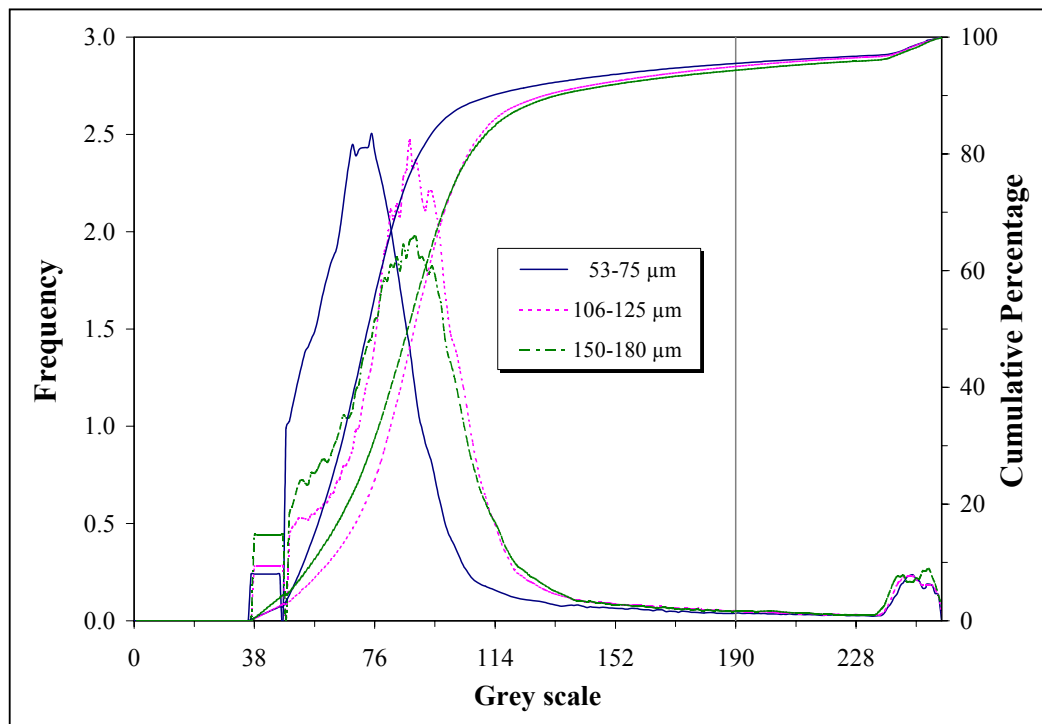
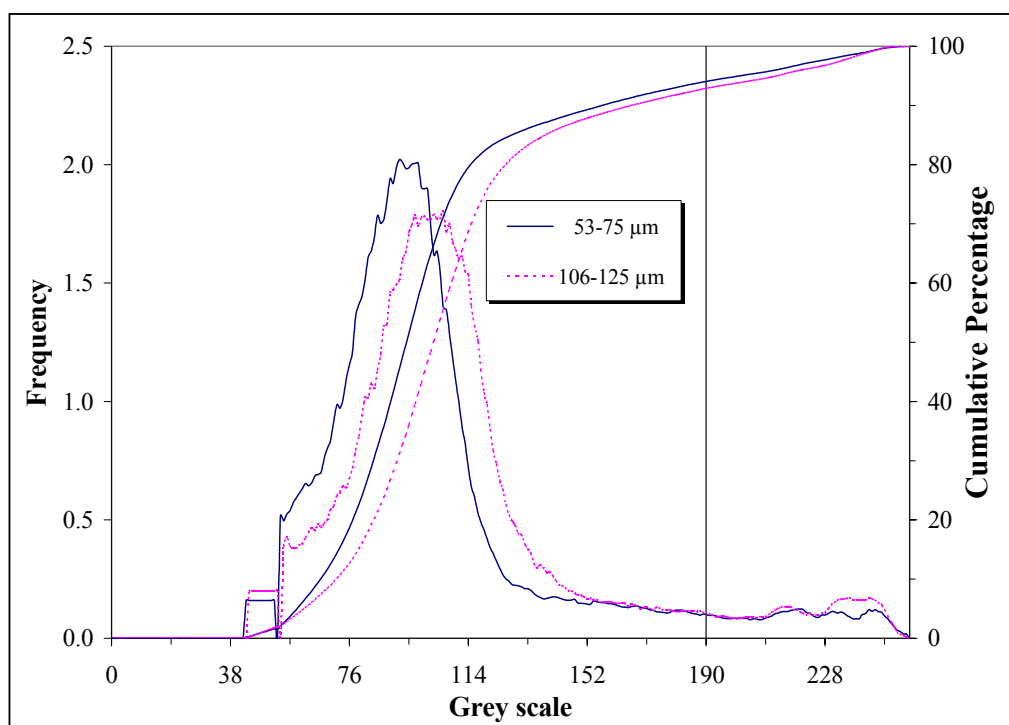
APPENDIX A. Vitrinite Reflectance Histograms of the Coal Fractions**A.11 Ashland**

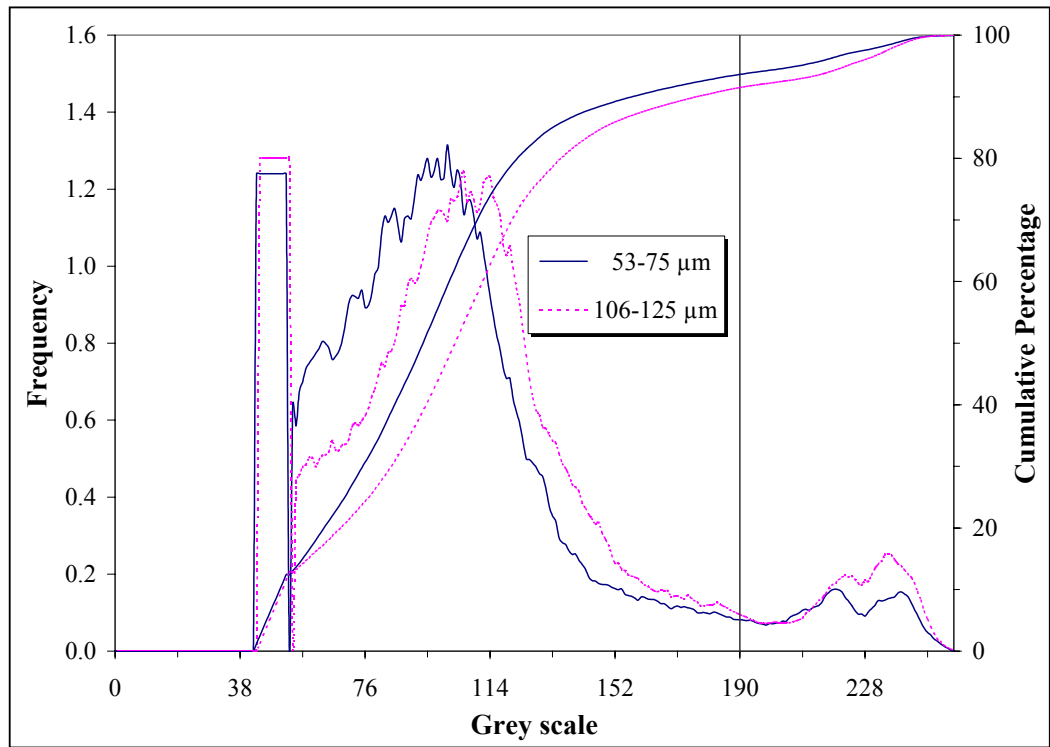
APPENDIX B. Grey Scale Histograms of the Coal Fractions**B.1 Bijao****B.2 Fila Maestra**

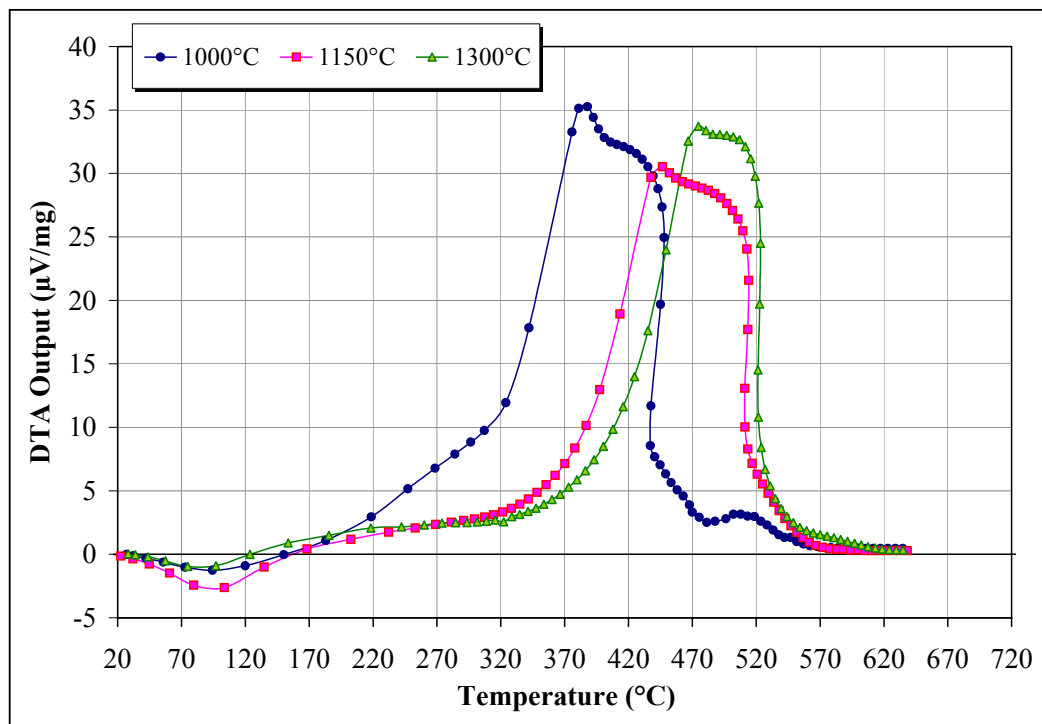
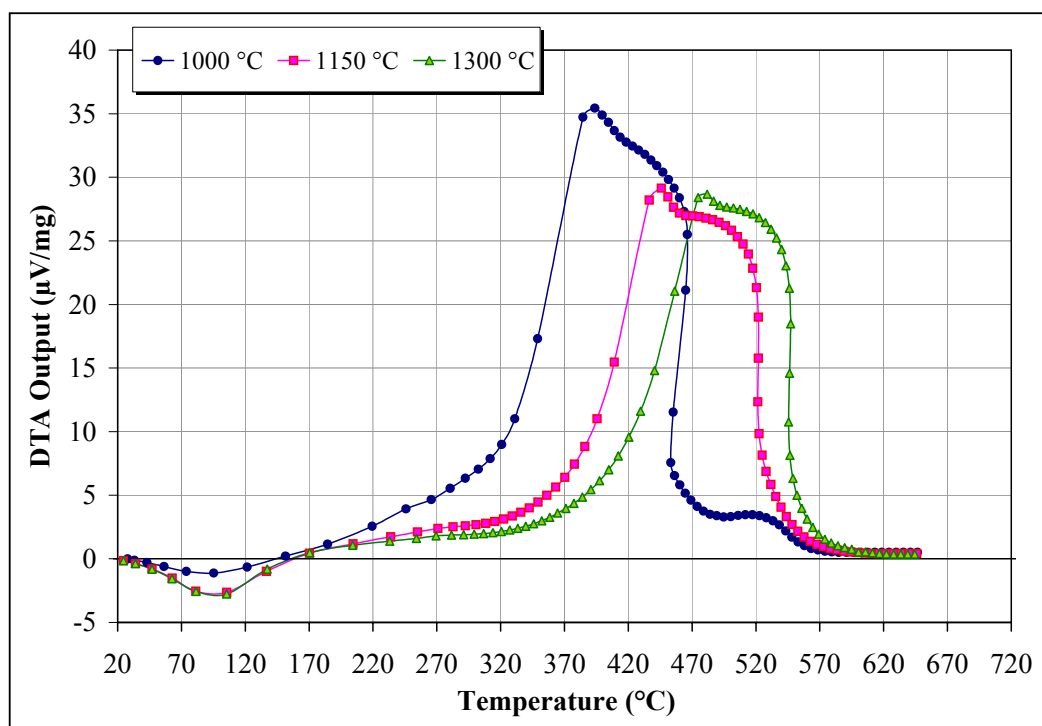
APPENDIX B. Grey Scale Histograms of the Coal Fractions**B.3 La Loma****B.4 Oreganal**

APPENDIX B. Grey Scale Histograms of the Coal Fractions**B.5 La Jagua****B.6 El Cerrejon**

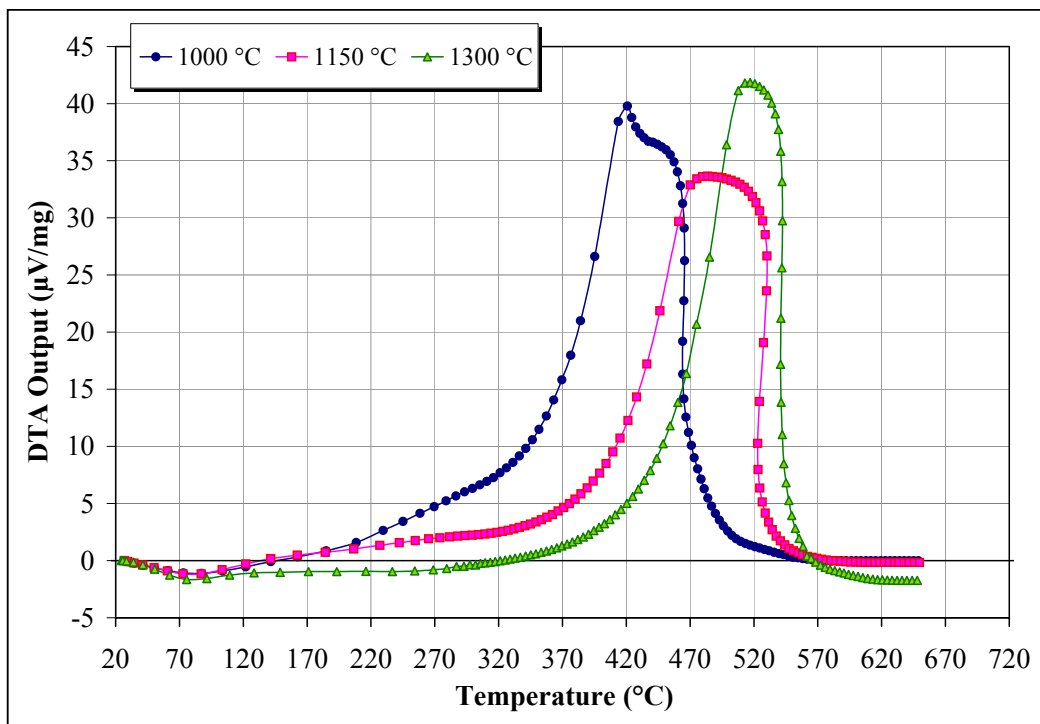
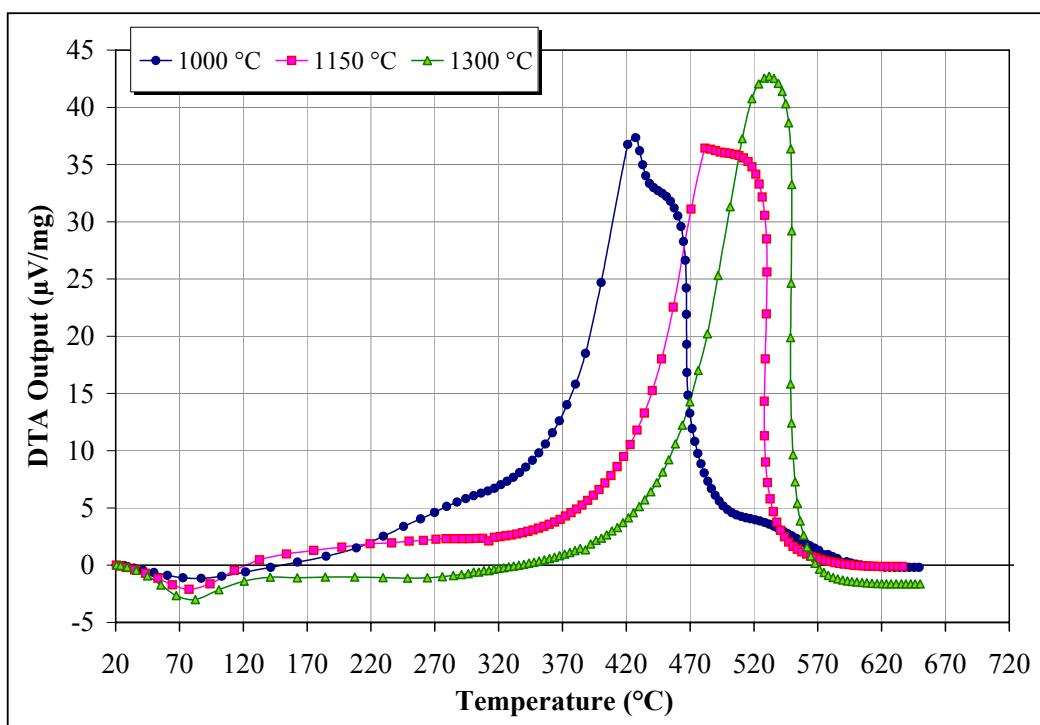
APPENDIX B. Grey Scale Histograms of the Coal Fractions**B.7 Caypa****B.8 Paso Diablo**

APPENDIX B. Grey Scale Histograms of the Coal Fractions**B.9 Guasare****B.10 Maturin**

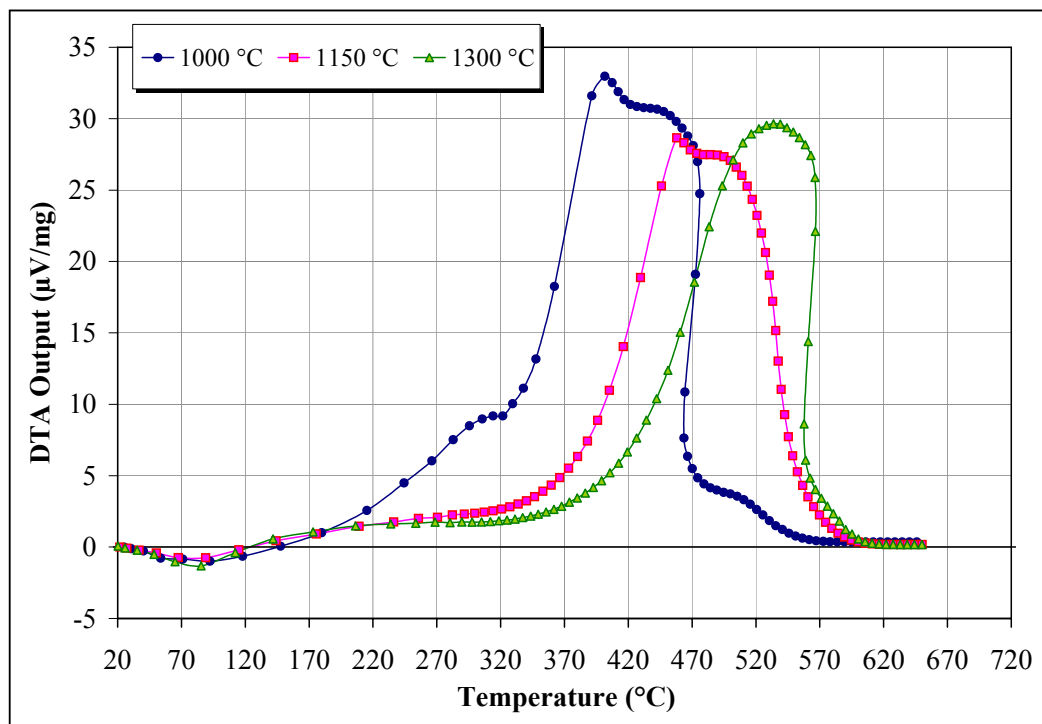
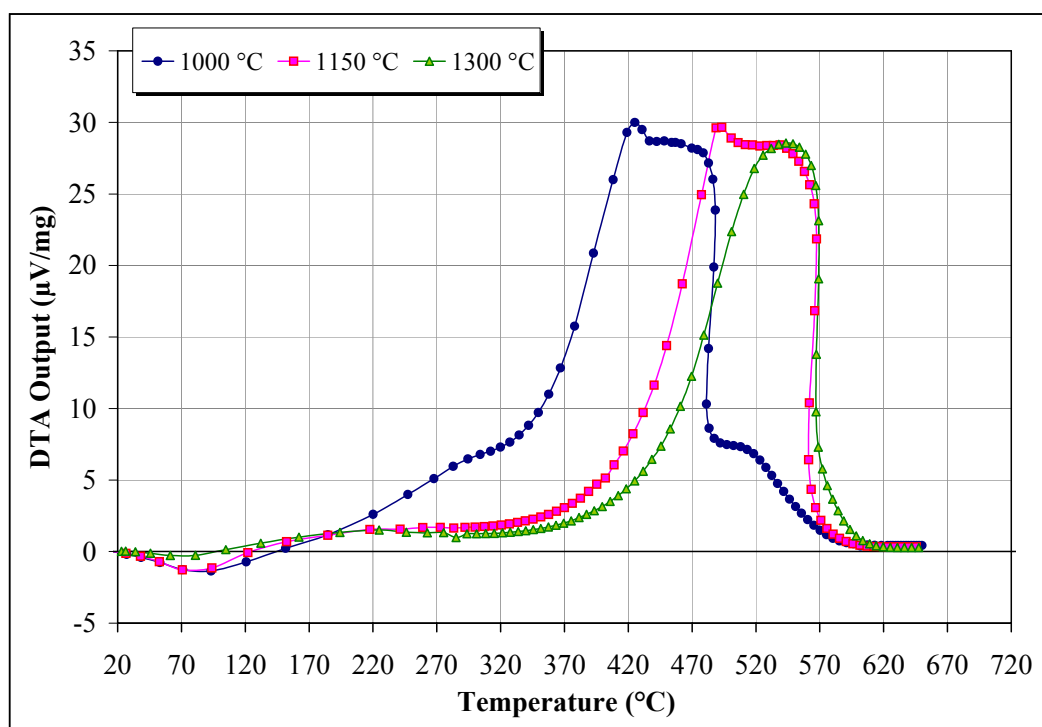
APPENDIX B. Grey Scale Histograms of the Coal Fractions**B.11 Ashland**

APPENDIX C. DTA Profiles of the Chars as a Function of DTF Temperature**C.1 Bijao (53-75 μm fraction)****C.2 Bijao (106-125 μm fraction)**

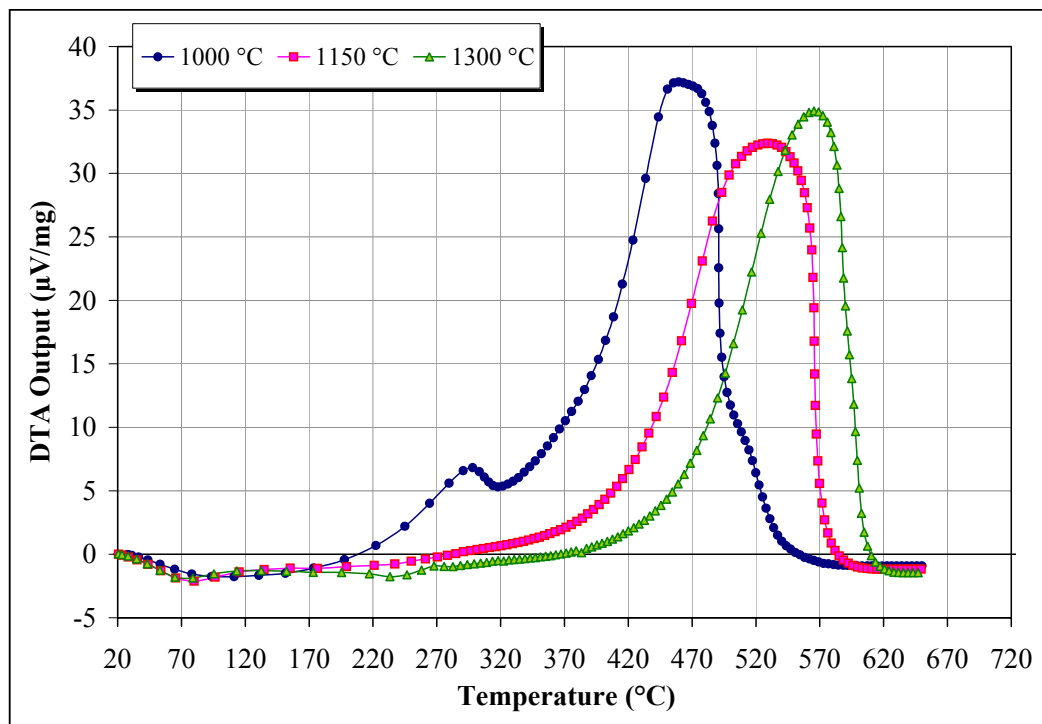
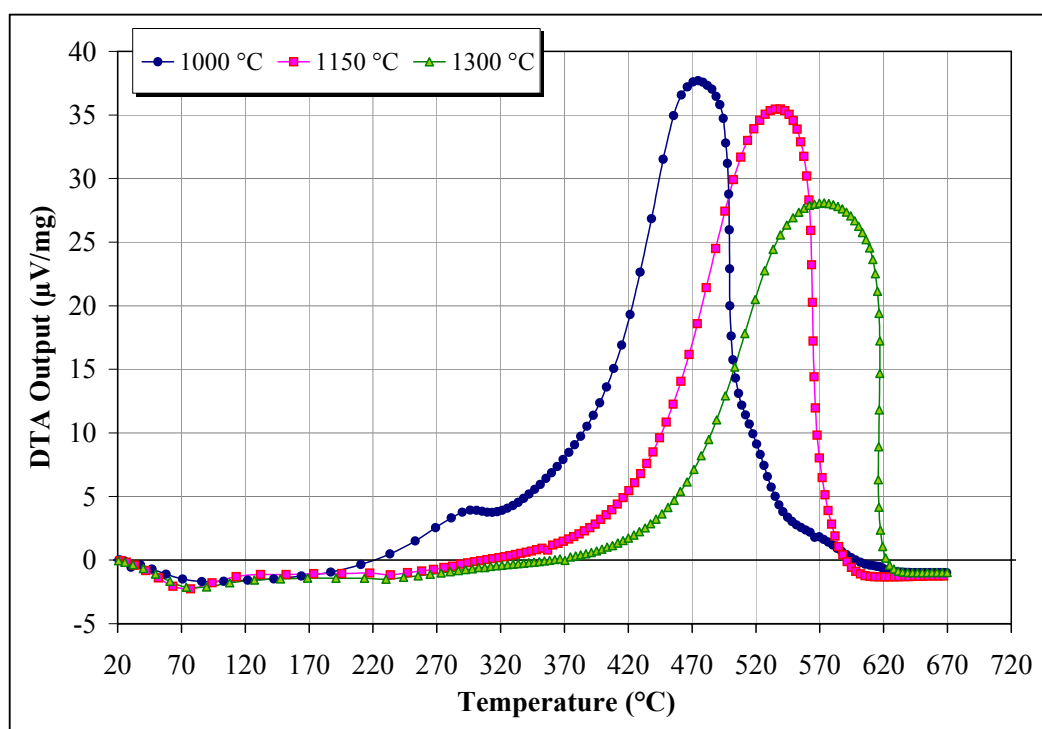
APPENDIX C. DTA Profiles of the Chars as a Function of DTF Temperature

C.3 Fila Maestra (53-75 μm fraction)C.4 Fila Maestra (106-125 μm fraction)

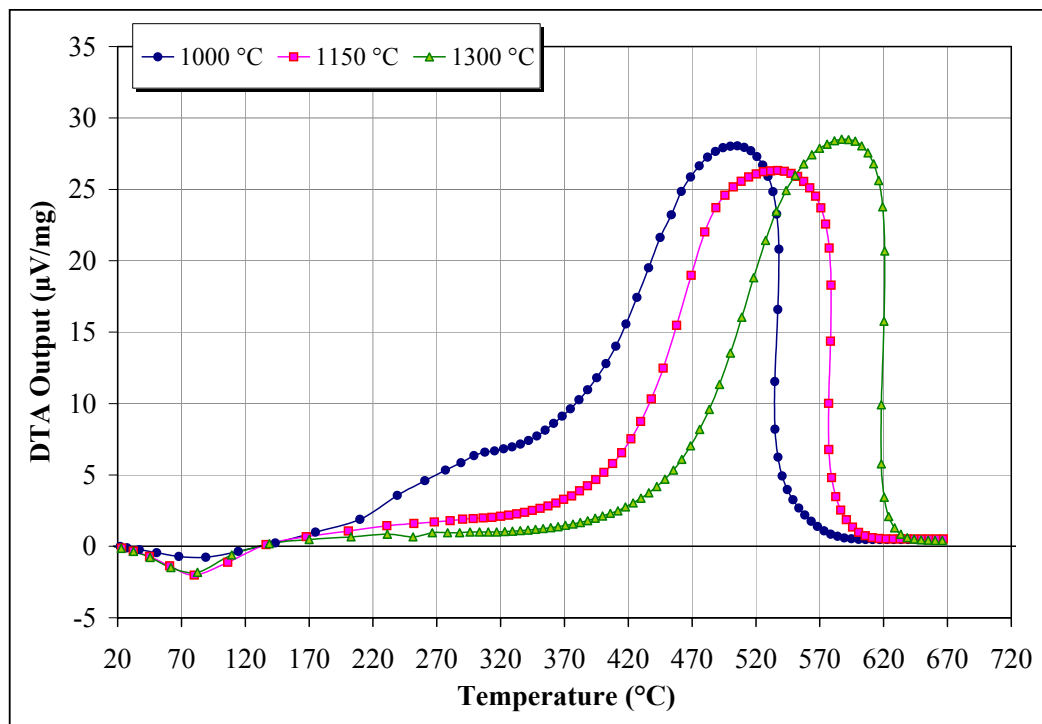
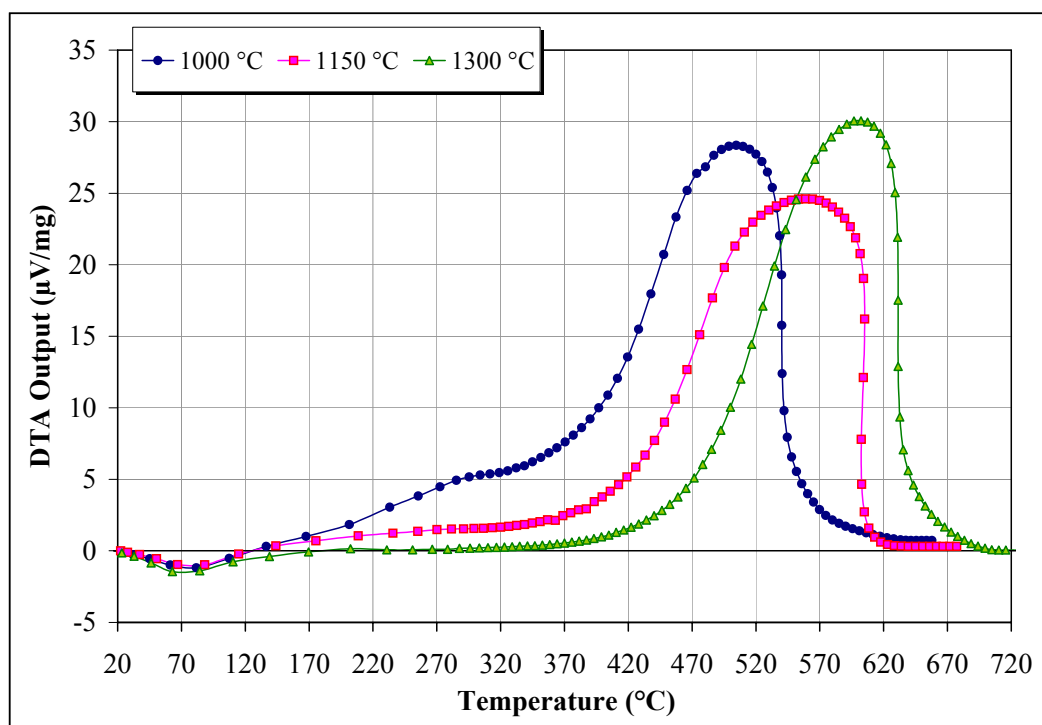
APPENDIX C. DTA Profiles of the Chars as a Function of DTF Temperature

C.5 La Loma (53-75 μm fraction)C.6 La Loma (106-125 μm fraction)

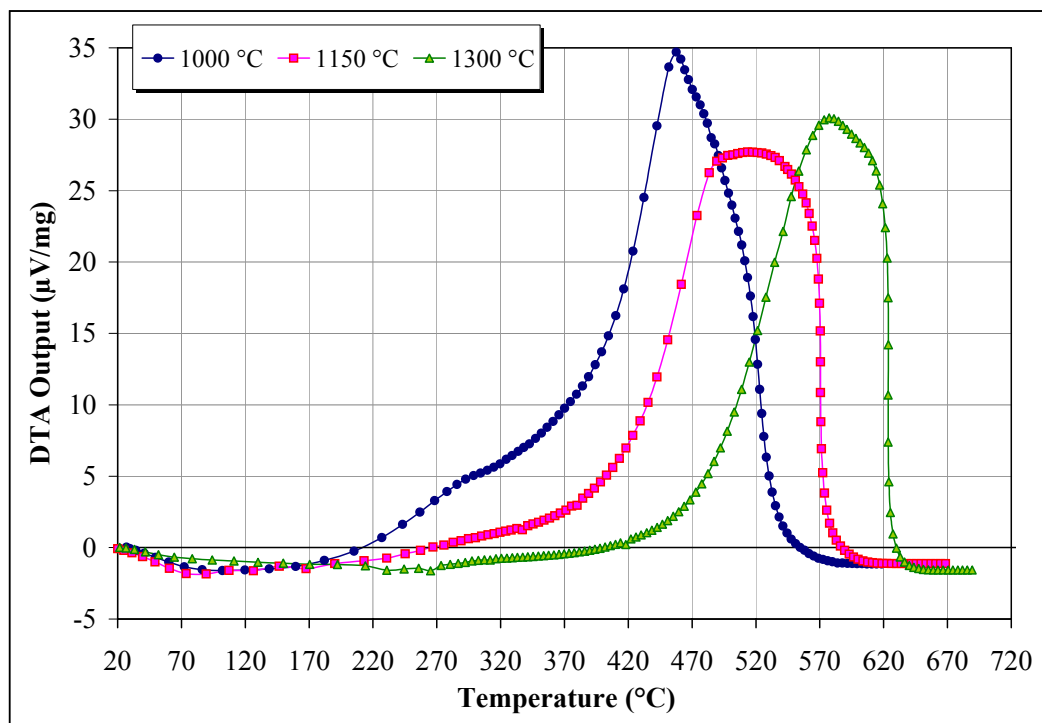
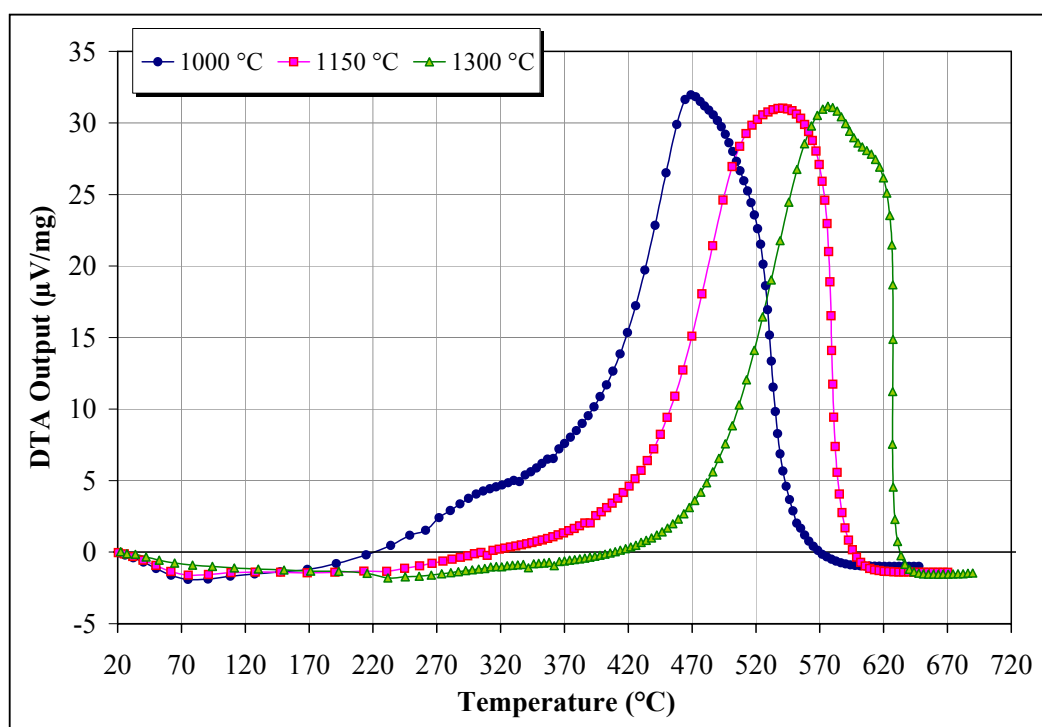
APPENDIX C. DTA Profiles of the Chars as a Function of DTF Temperature

C.7 Oreganal (53-75 μm fraction)C.8 Oreganal (106-125 μm fraction)

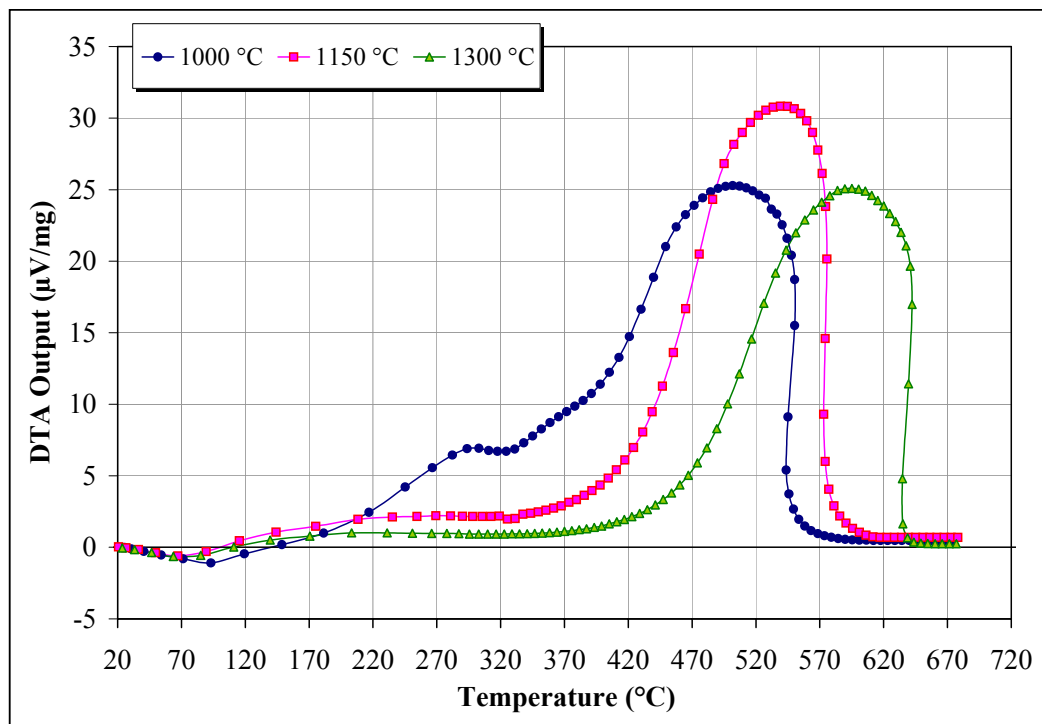
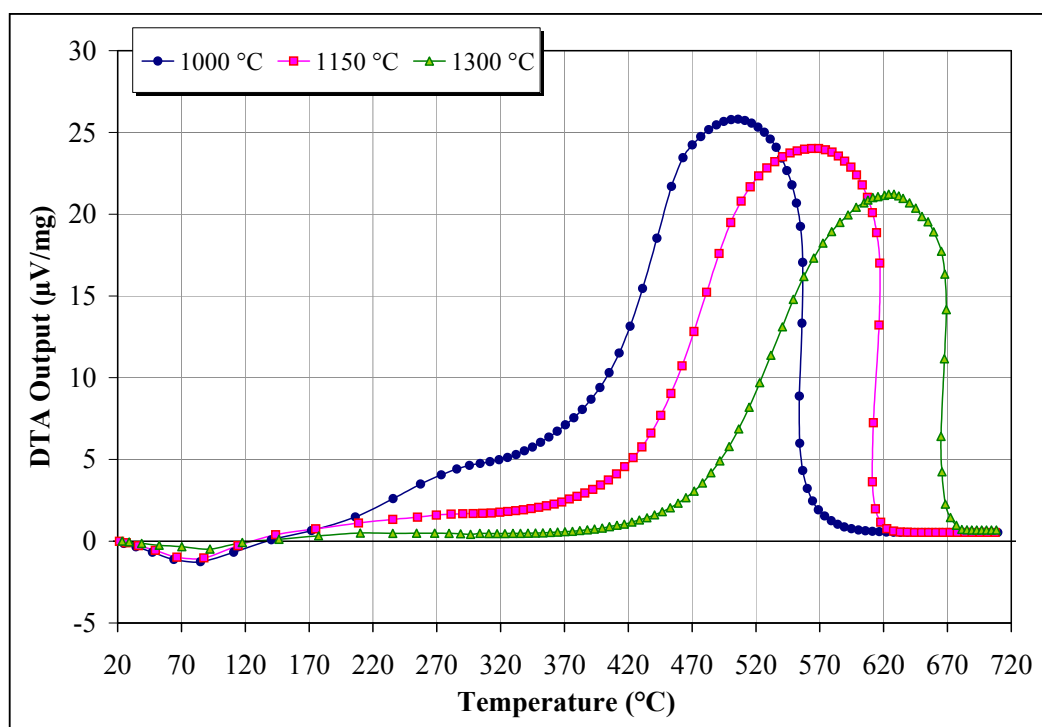
APPENDIX C. DTA Profiles of the Chars as a Function of DTF Temperature

C.9 La Jagua (53-75 μm fraction)C.10 La Jagua (106-125 μm fraction)

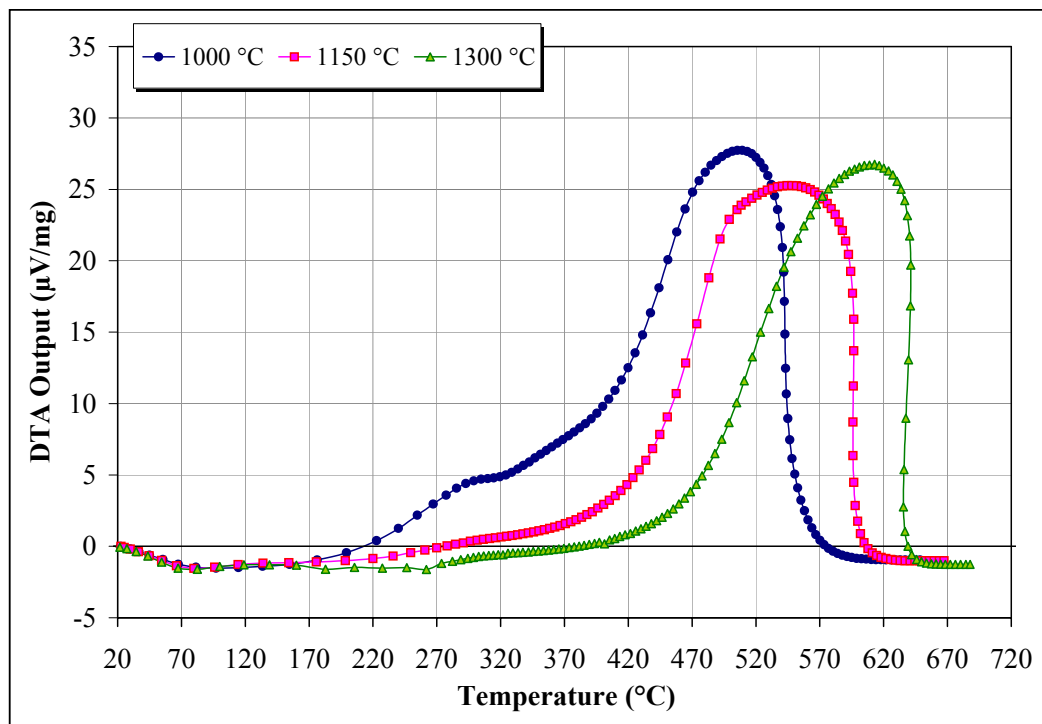
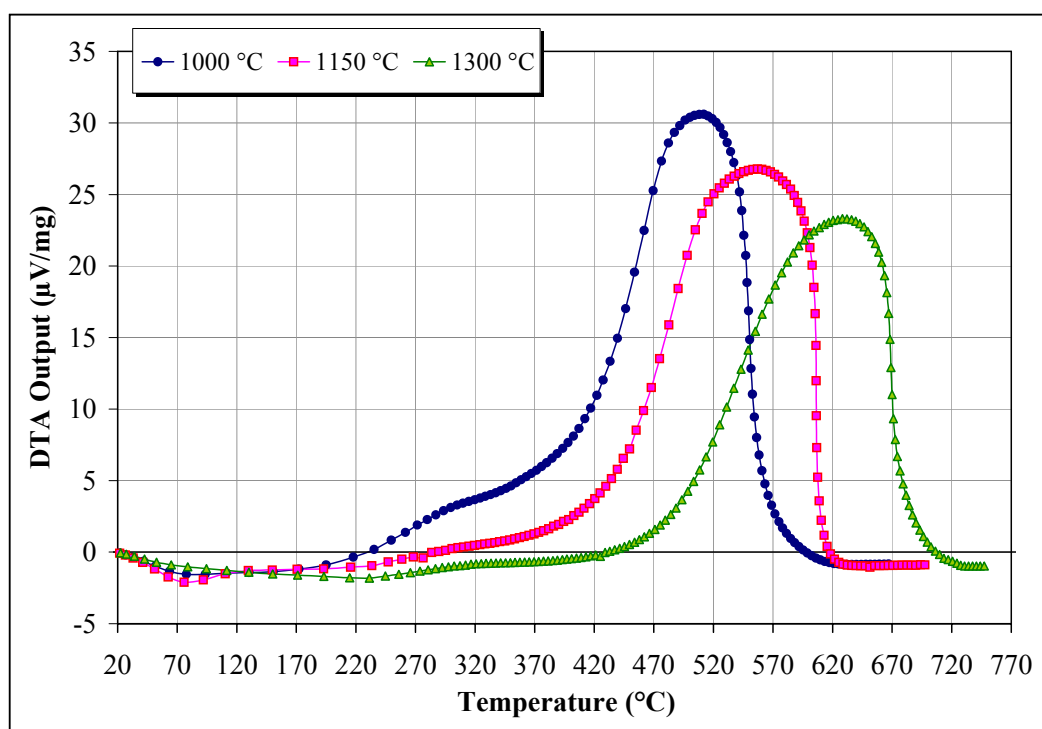
APPENDIX C. DTA Profiles of the Chars as a Function of DTF Temperature

C.11 El Cerrejon (53-75 μm fraction)C.12 El Cerrejon (106-125 μm fraction)

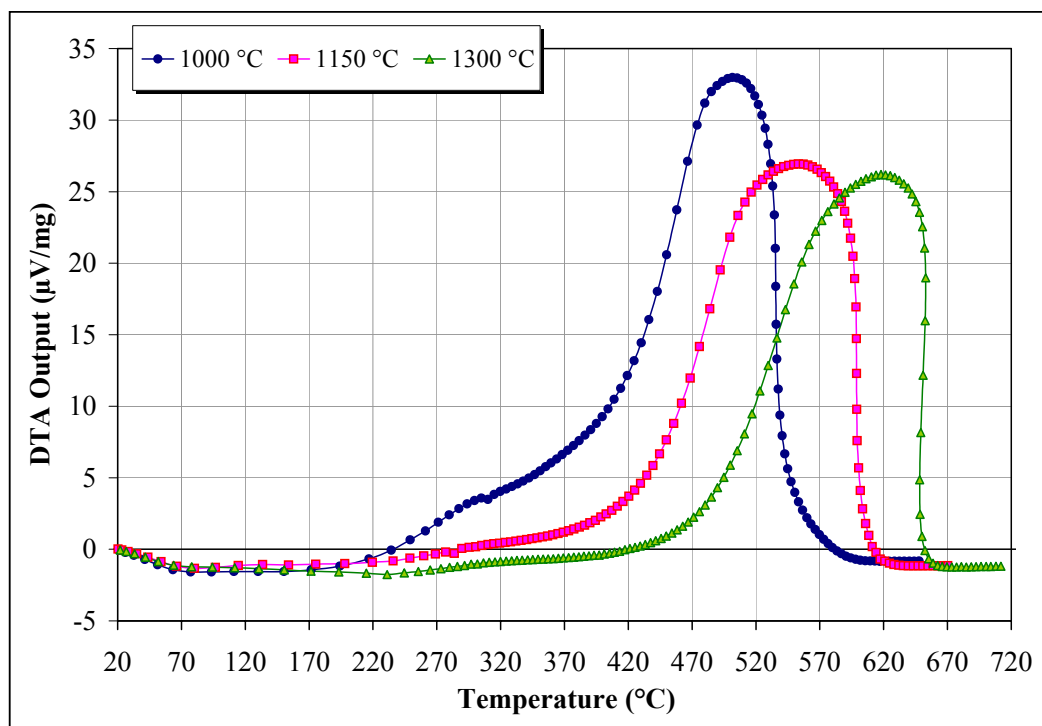
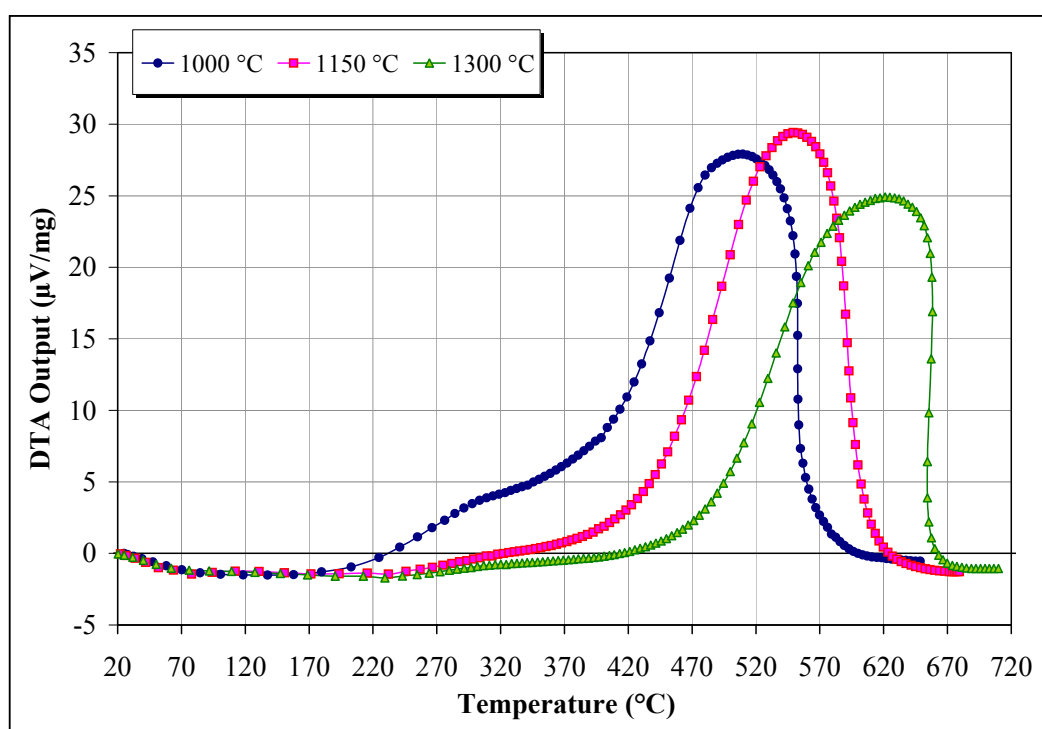
APPENDIX C. DTA Profiles of the Chars as a Function of DTF Temperature

C.13 Caypa (53-75 μm fraction)C.14 Caypa (106-125 μm fraction)

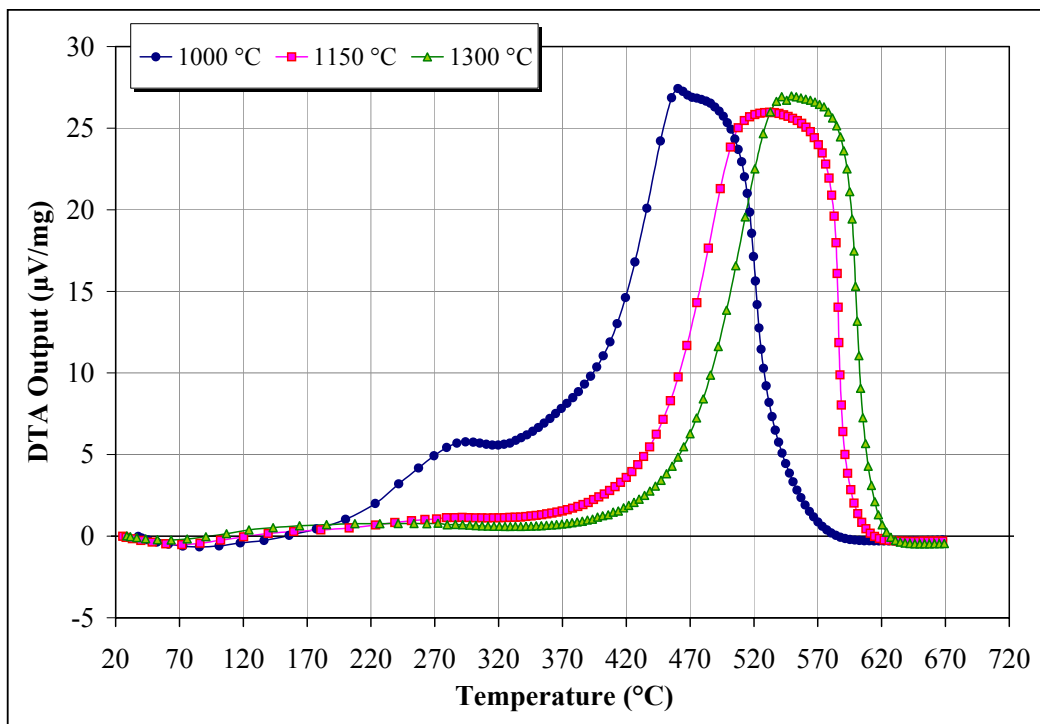
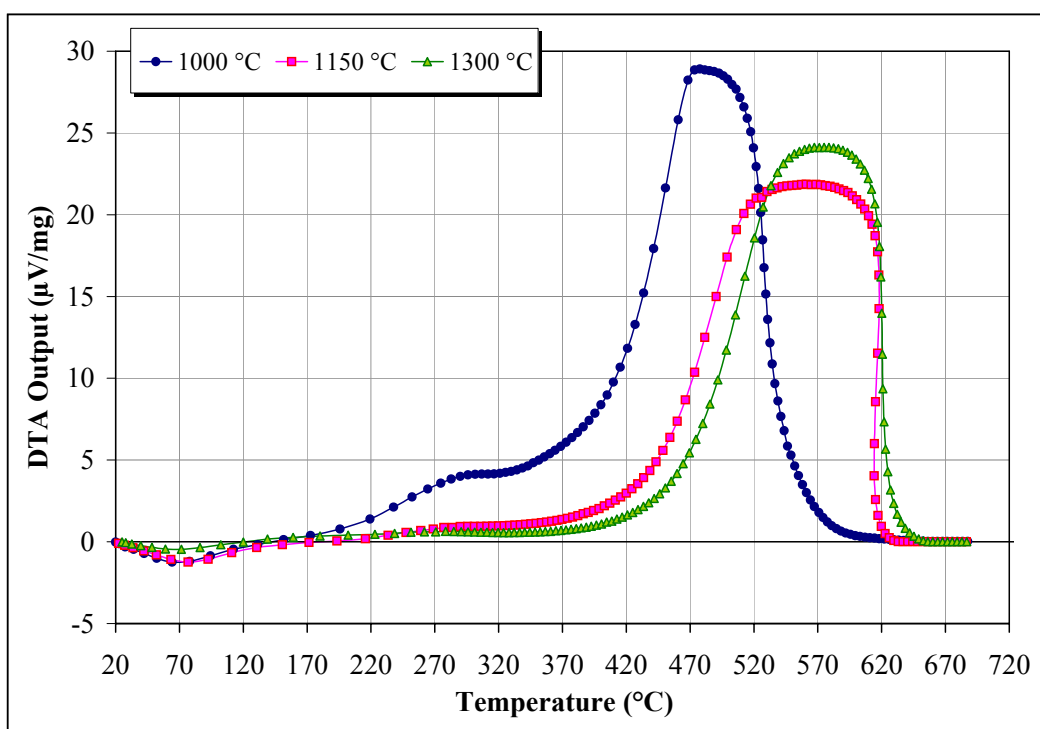
APPENDIX C. DTA Profiles of the Chars as a Function of DTF Temperature

C.15 Paso Diablo (53-75 μm fraction)C.16 Paso Diablo (106-125 μm fraction)

APPENDIX C. DTA Profiles of the Chars as a Function of DTF Temperature

C.17 Maturin (53-75 μm fraction)C.18 Maturin (106-125 μm fraction)

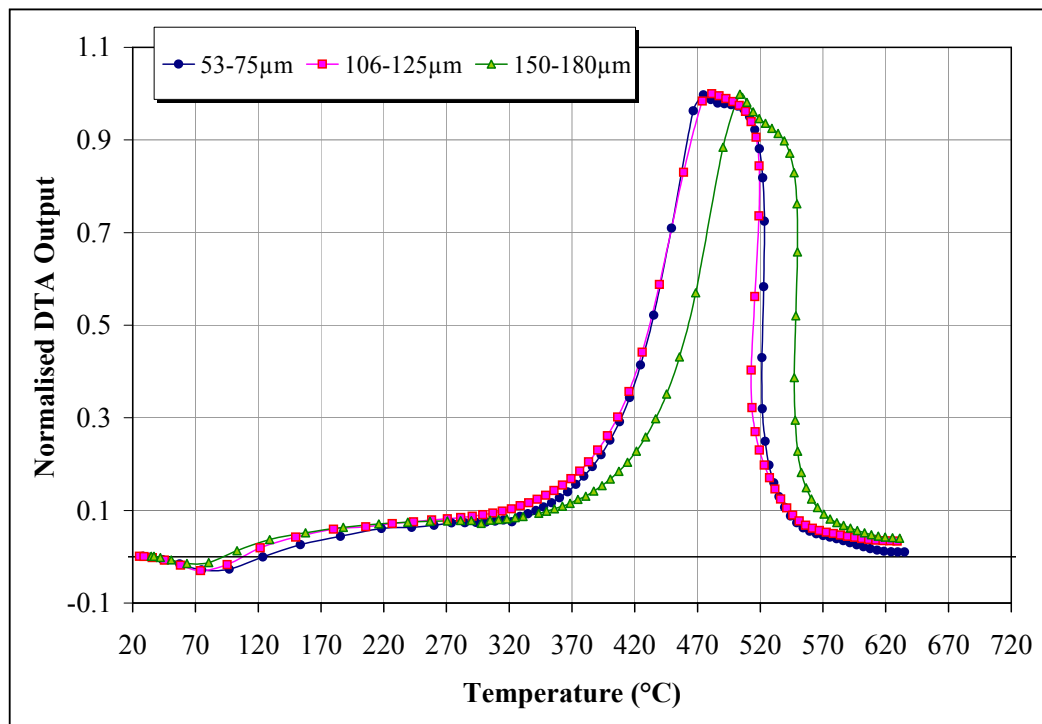
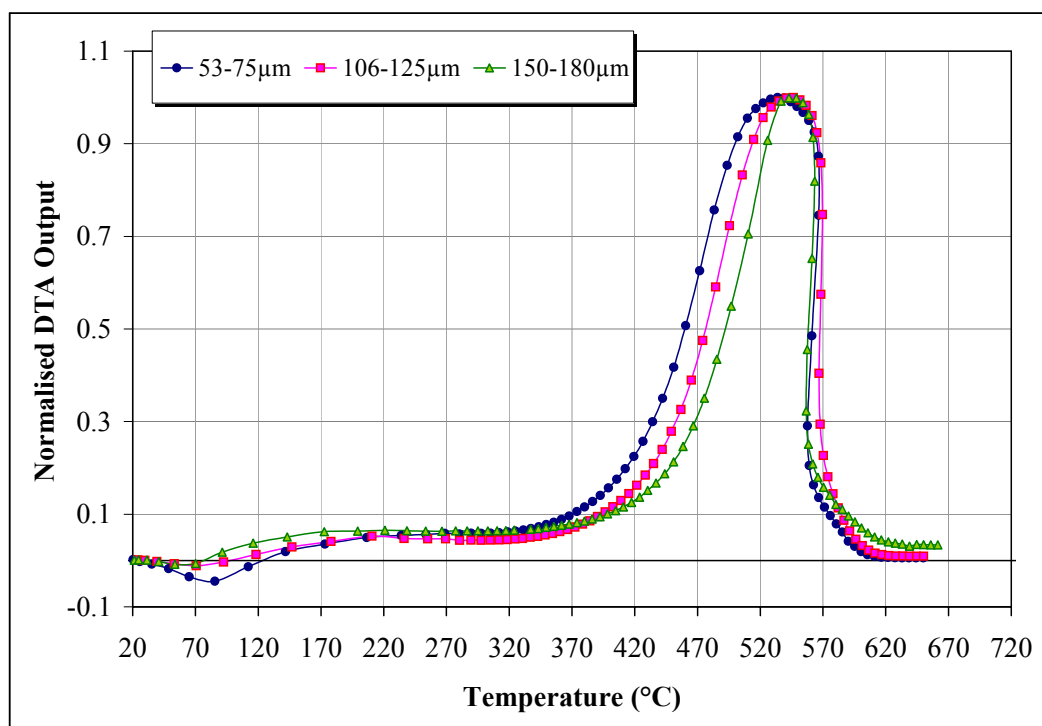
APPENDIX C. DTA Profiles of the Chars as a Function of DTF Temperature

C.19 Ashland (53-75 μm fraction)C.20 Ashland (106-125 μm fraction)

APPENDIX D. F-Distribution, F-values [Confidence level 95%: $\alpha = 0.05$]

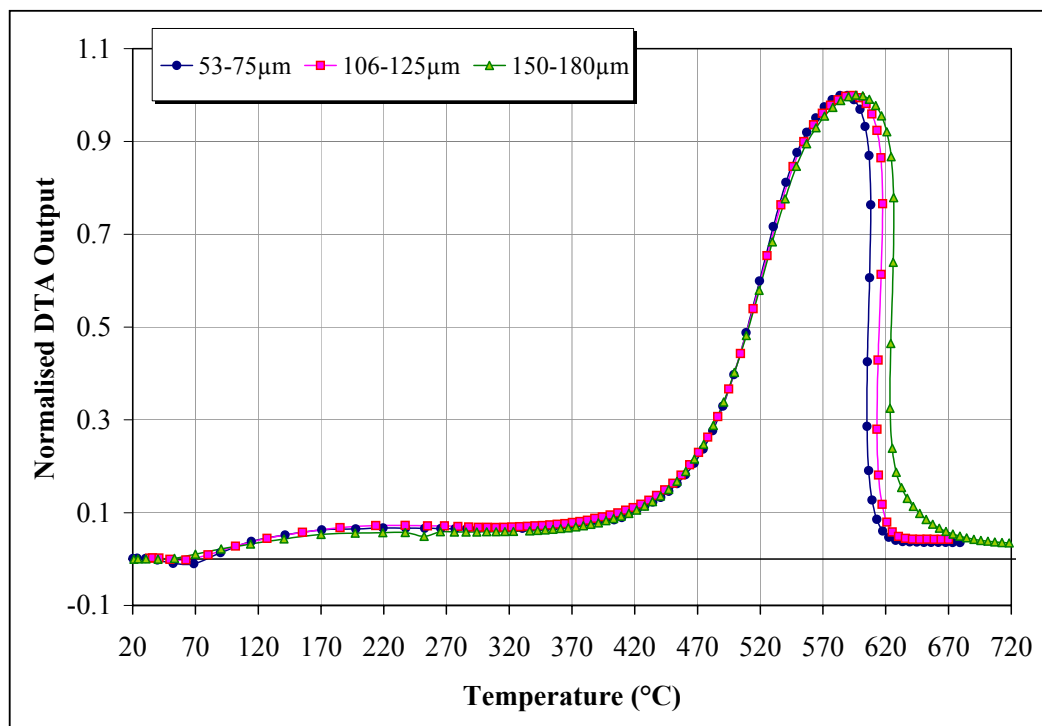
| v_2 \ v_1 | Degrees of Freedom for Numerator ^a | | | | | | |
|---------------|---|-------|-------|-------|-------|-------|-------|
| | 1 | 2 | 3 | 4 | 5 | 6 | 7 |
| 1 | 161.4 | 199.5 | 215.7 | 224.6 | 230.2 | 234.0 | 236.8 |
| 2 | 18.51 | 19.00 | 19.16 | 19.25 | 19.30 | 19.33 | 19.35 |
| 3 | 10.13 | 9.55 | 9.28 | 9.12 | 9.01 | 8.94 | 8.89 |
| 4 | 7.71 | 6.94 | 6.59 | 6.39 | 6.26 | 6.16 | 6.09 |
| 5 | 6.61 | 5.79 | 5.41 | 5.19 | 5.05 | 4.95 | 4.88 |
| 6 | 5.99 | 5.14 | 4.76 | 4.53 | 4.39 | 4.28 | 4.21 |
| 7 | 5.59 | 4.74 | 4.35 | 4.12 | 3.97 | 3.87 | 3.79 |
| 8 | 5.32 | 4.46 | 4.07 | 3.84 | 3.69 | 3.58 | 3.50 |
| 9 | 5.12 | 4.26 | 3.86 | 3.63 | 3.48 | 3.37 | 3.29 |
| 10 | 4.96 | 4.10 | 3.71 | 3.48 | 3.33 | 3.22 | 3.14 |
| 11 | 4.84 | 3.98 | 3.59 | 3.36 | 3.20 | 3.09 | 3.01 |
| 12 | 4.75 | 3.89 | 3.49 | 3.26 | 3.11 | 3.00 | 2.91 |
| 13 | 4.67 | 3.81 | 3.41 | 3.18 | 3.03 | 2.92 | 2.83 |
| 14 | 4.60 | 3.74 | 3.34 | 3.11 | 2.96 | 2.85 | 2.76 |
| 15 | 4.54 | 3.68 | 3.29 | 3.06 | 2.90 | 2.79 | 2.71 |
| 16 | 4.49 | 3.63 | 3.24 | 3.01 | 2.85 | 2.74 | 2.66 |
| 17 | 4.45 | 3.59 | 3.20 | 2.96 | 2.81 | 2.70 | 2.61 |
| 18 | 4.41 | 3.55 | 3.16 | 2.93 | 2.77 | 2.66 | 2.58 |
| 19 | 4.38 | 3.52 | 3.13 | 2.90 | 2.74 | 2.63 | 2.54 |
| 20 | 4.35 | 3.49 | 3.10 | 2.87 | 2.71 | 2.60 | 2.51 |

^a v_1 = Number of Independent Variables; v_2 = Number of Data Points – ($v_1 - 1$)

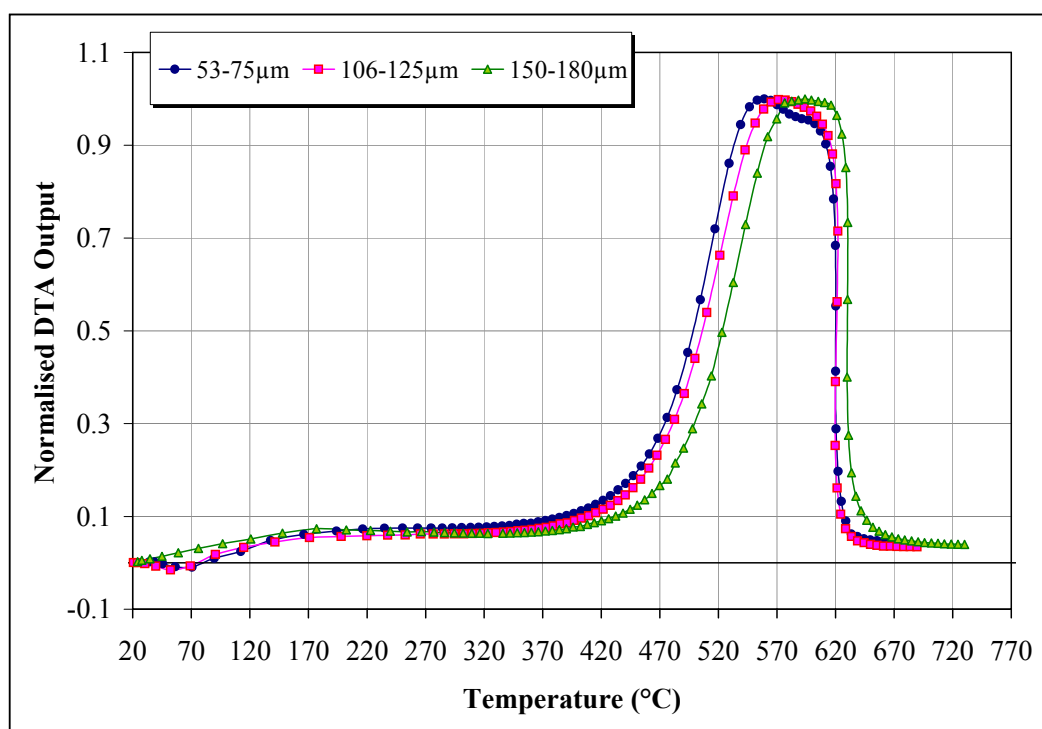
APPENDIX E. DTA Profiles of the Pyrolysed Chars**E.1 Bijao****E.2 La Loma**

APPENDIX E. DTA Profiles of the Pyrolysed Chars

E.3 La Jagua

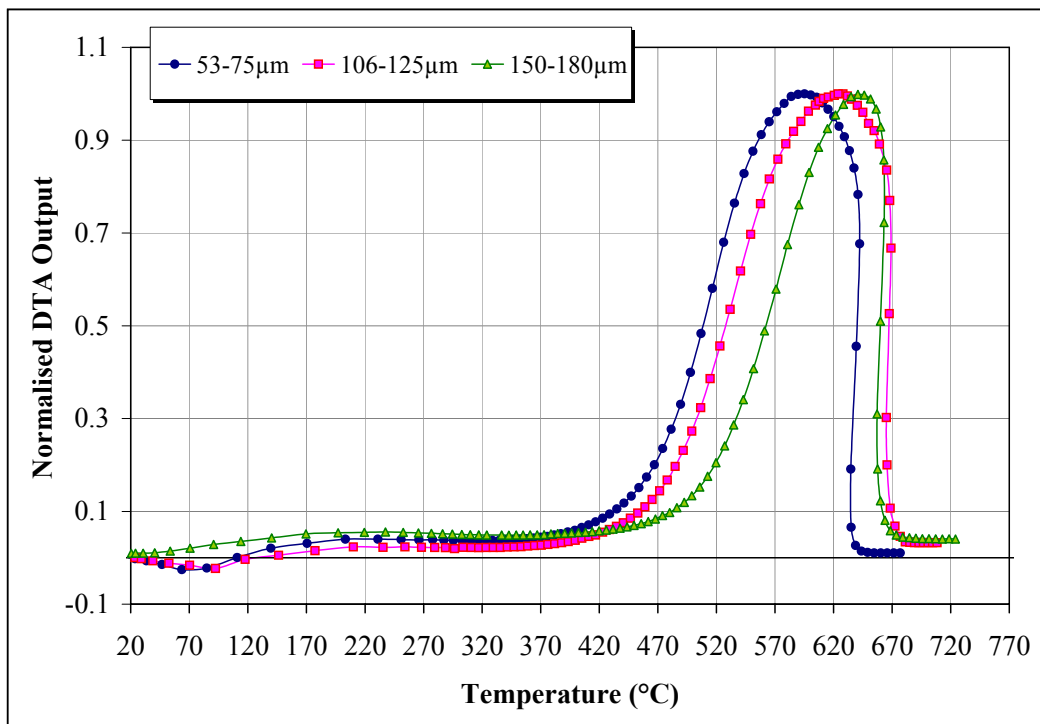


E.4 El Cerrejon

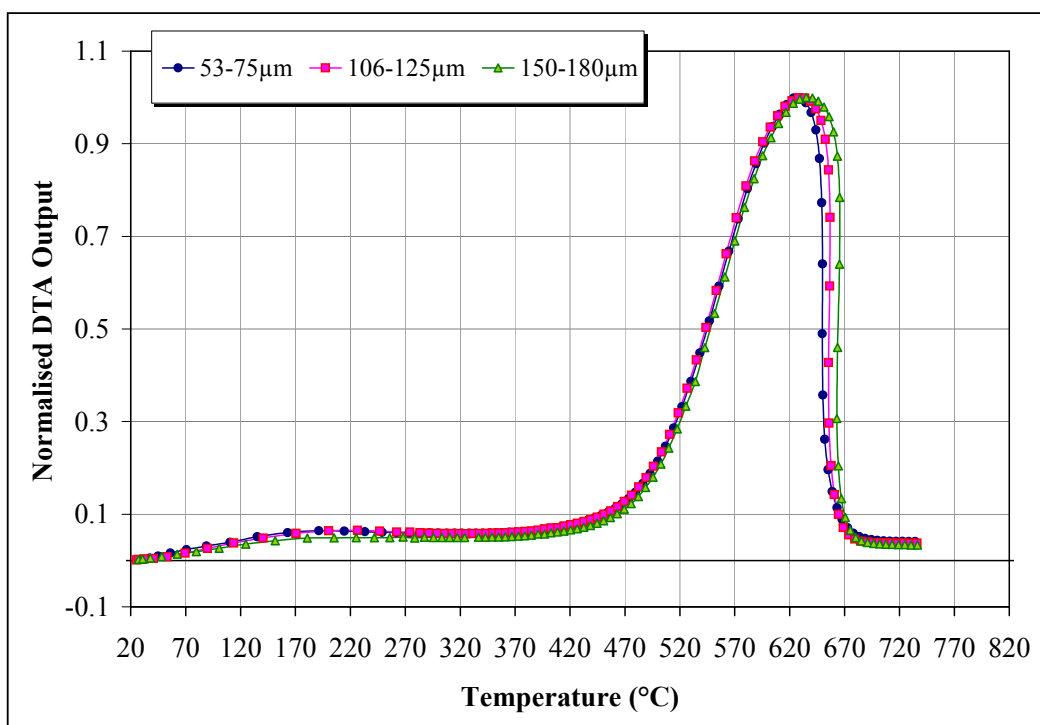


APPENDIX E. DTA Profiles of the Pyrolysed Chars

E.5 Caypa

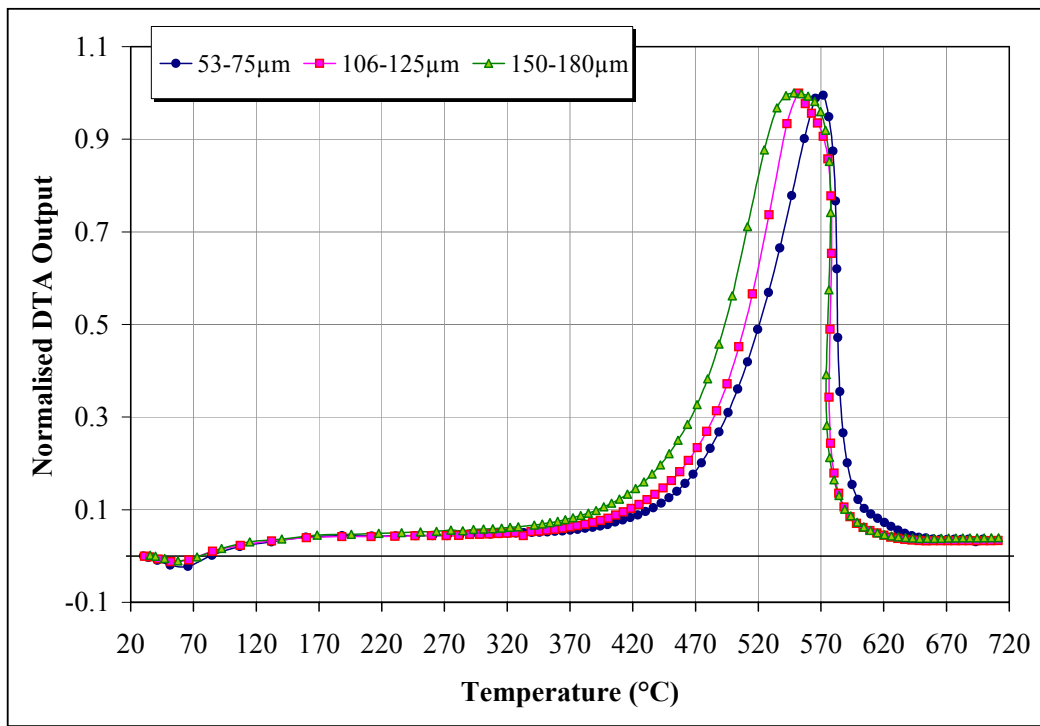


E.6 Guasare

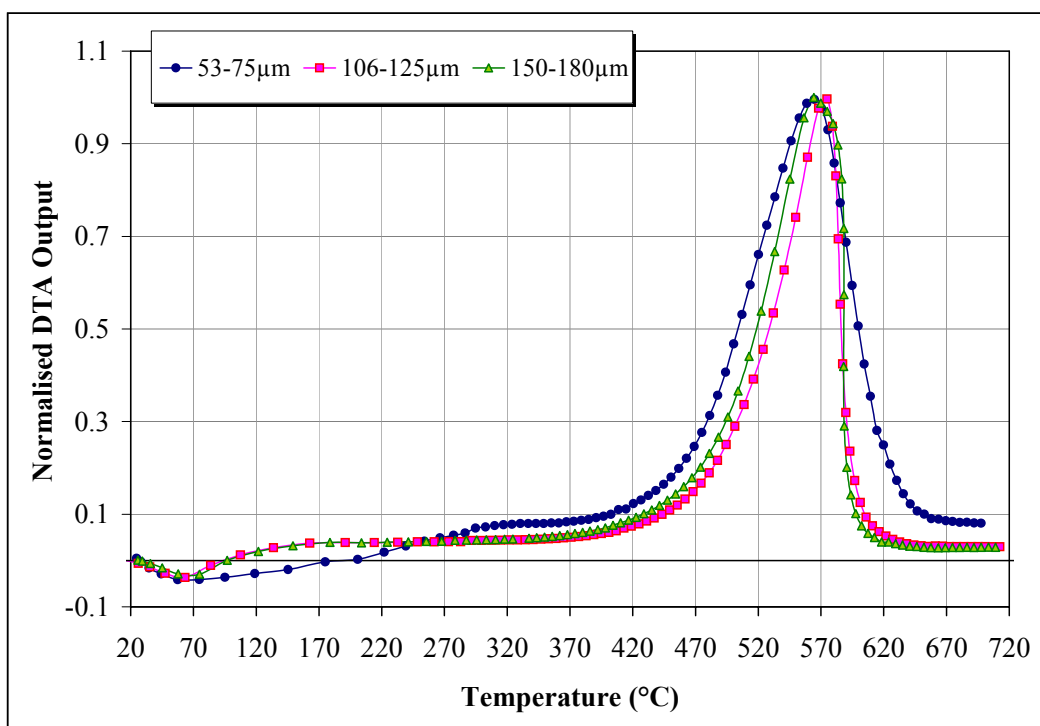


APPENDIX F. DTA Profiles of the Re-fired Chars

F.1 Bijao – 200 ms

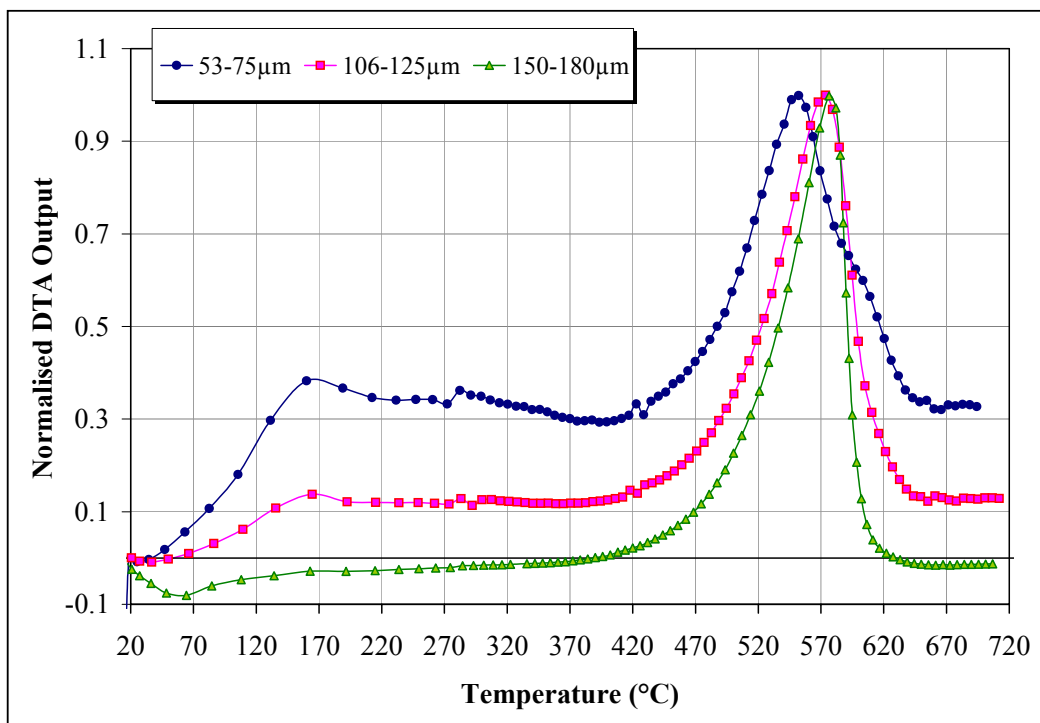


F.2 Bijao – 400 ms

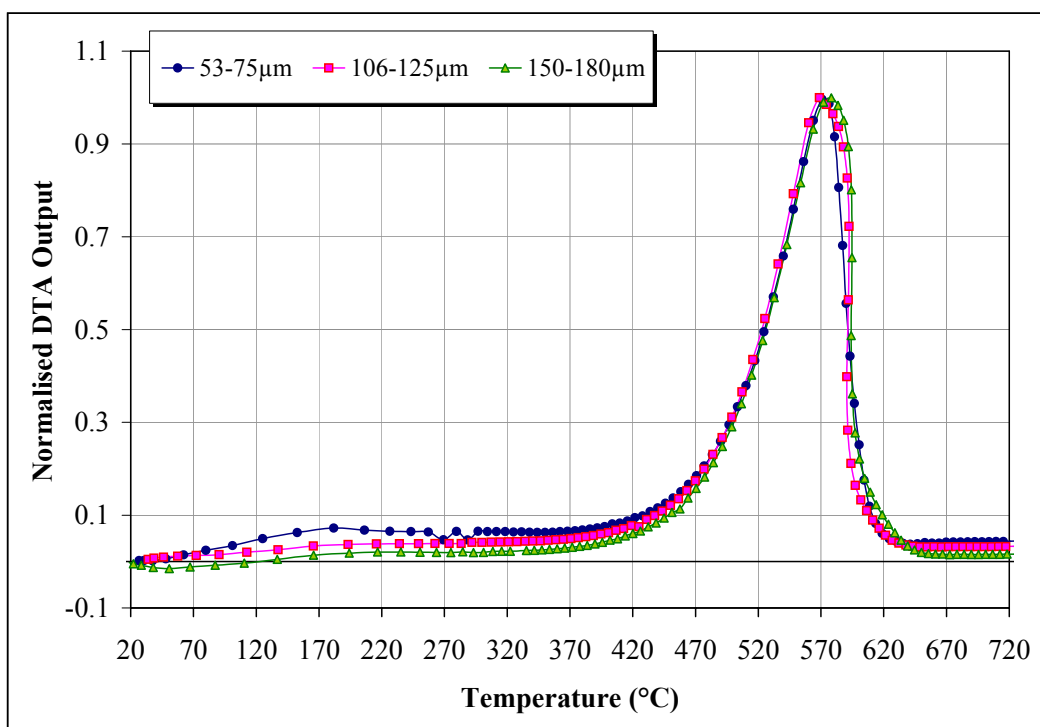


APPENDIX F. DTA Profiles of the Re-fired Chars

F.3 Bijao – 600 ms

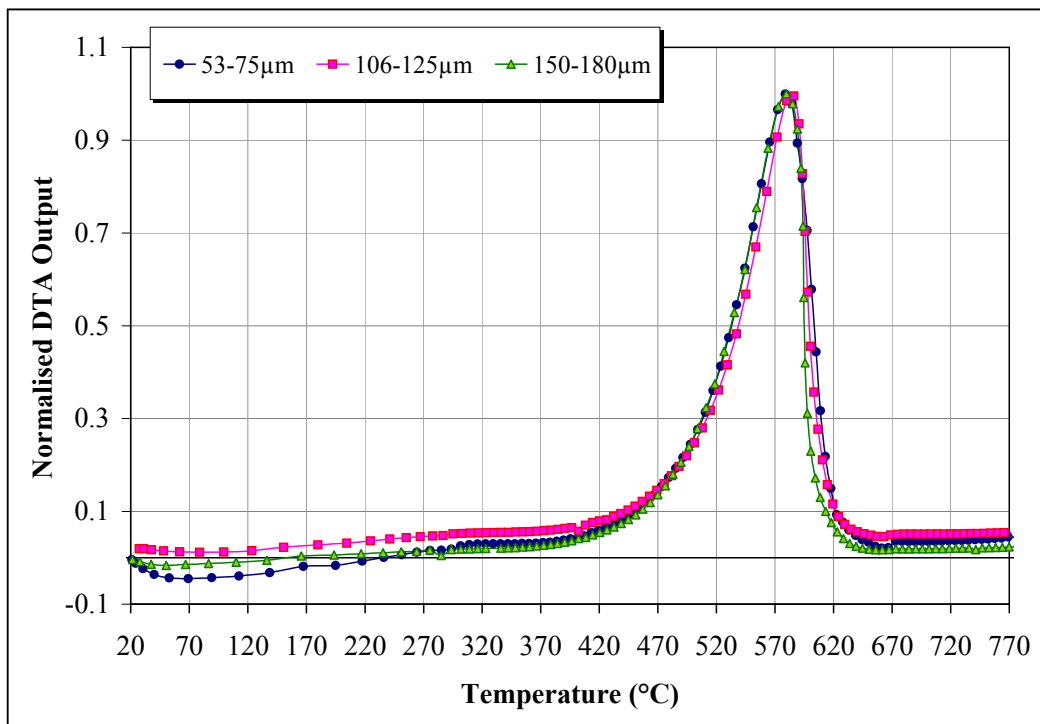


F.4 La Loma – 200 ms

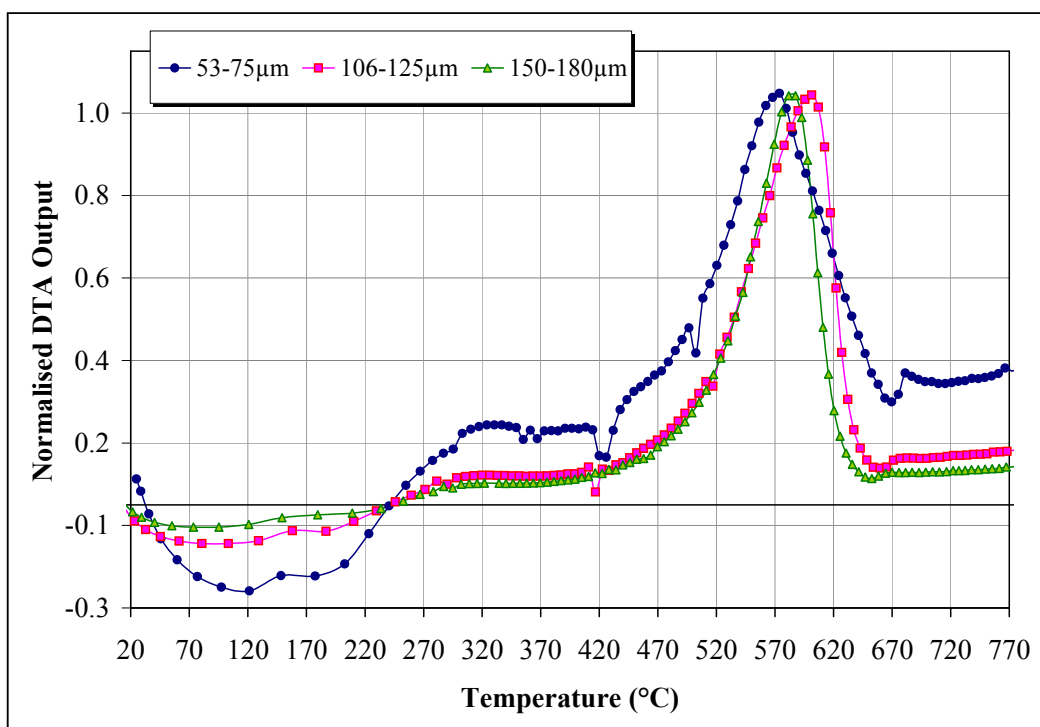


APPENDIX F. DTA Profiles of the Re-fired Chars

F.5 La Loma – 400 ms

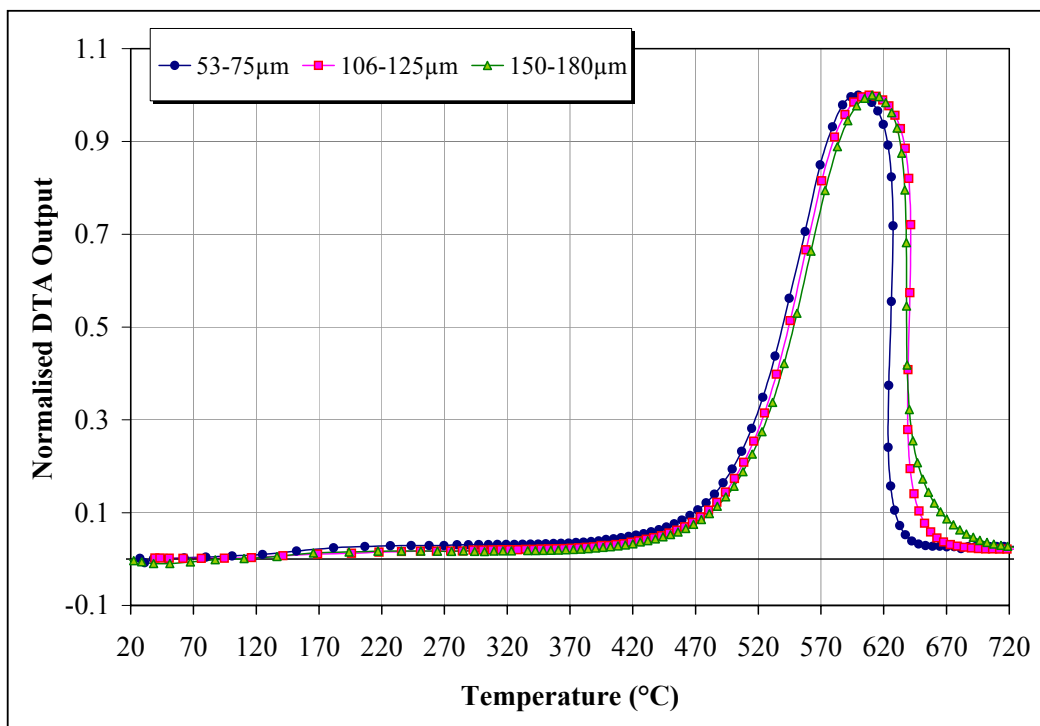


F.6 La Loma – 600 ms

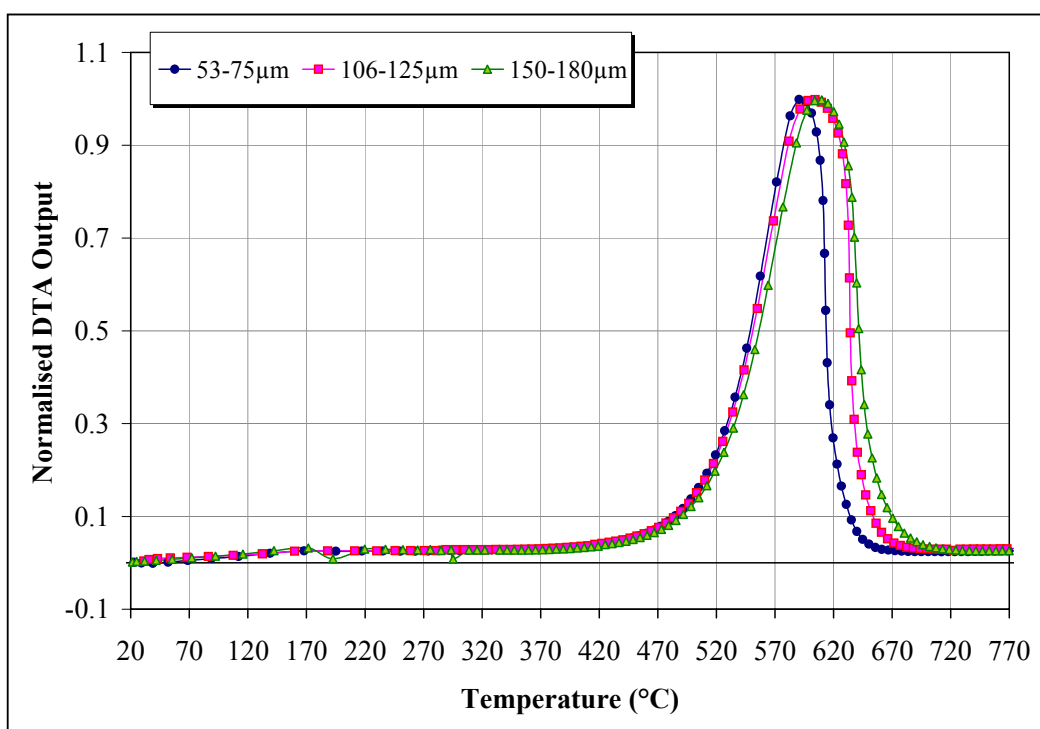


APPENDIX F. DTA Profiles of the Re-fired Chars

F.7 La Jagua – 200 ms

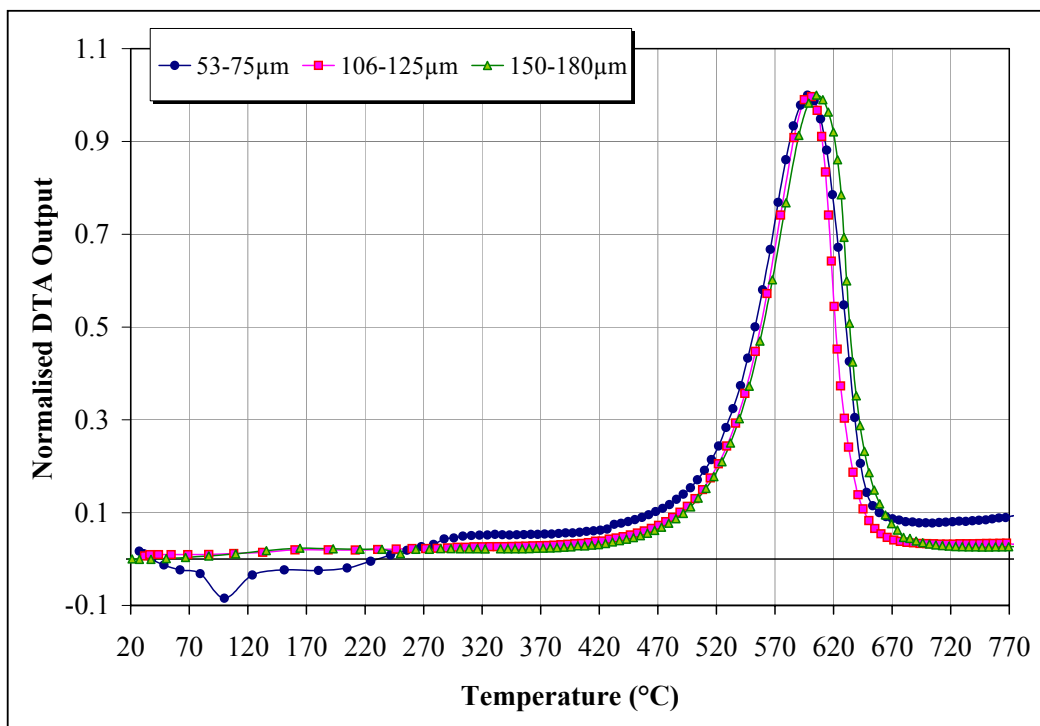


F.8 La Jagua – 400 ms

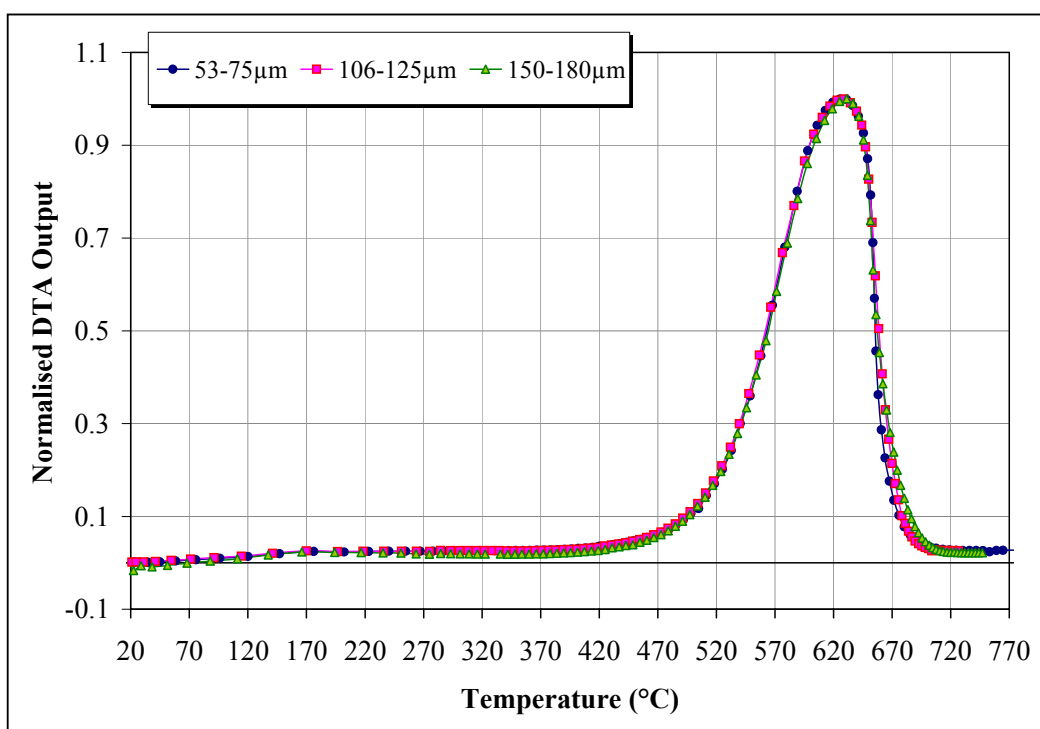


APPENDIX F. DTA Profiles of the Re-fired Chars

F.9 La Jagua – 600 ms

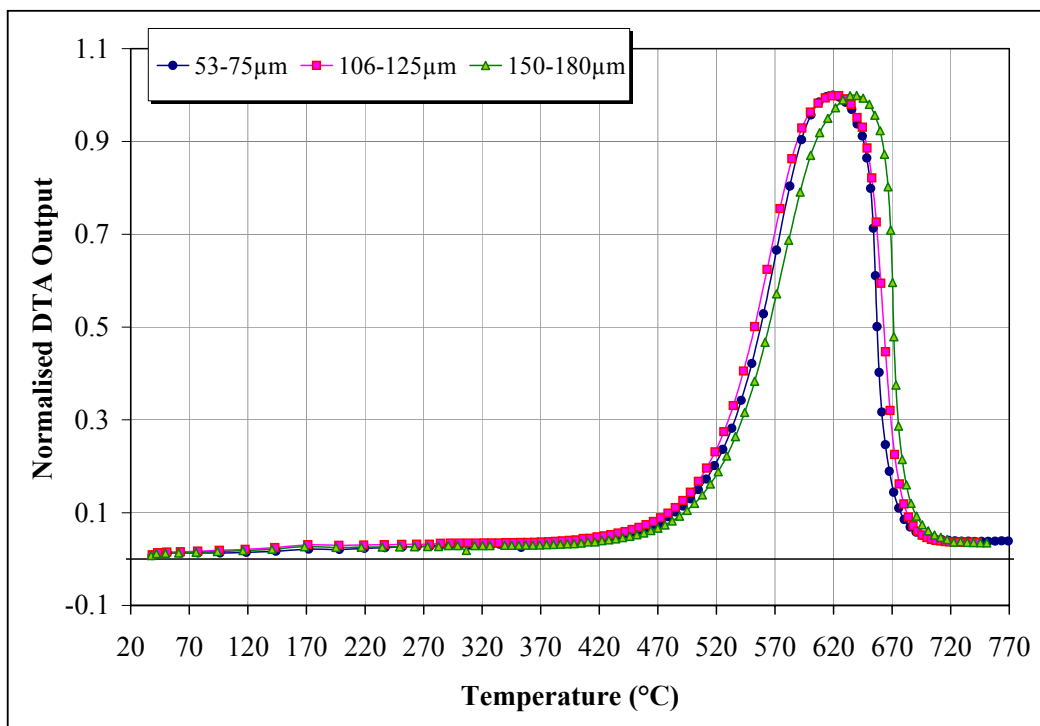


F.10 El Cerrejon – 200 ms

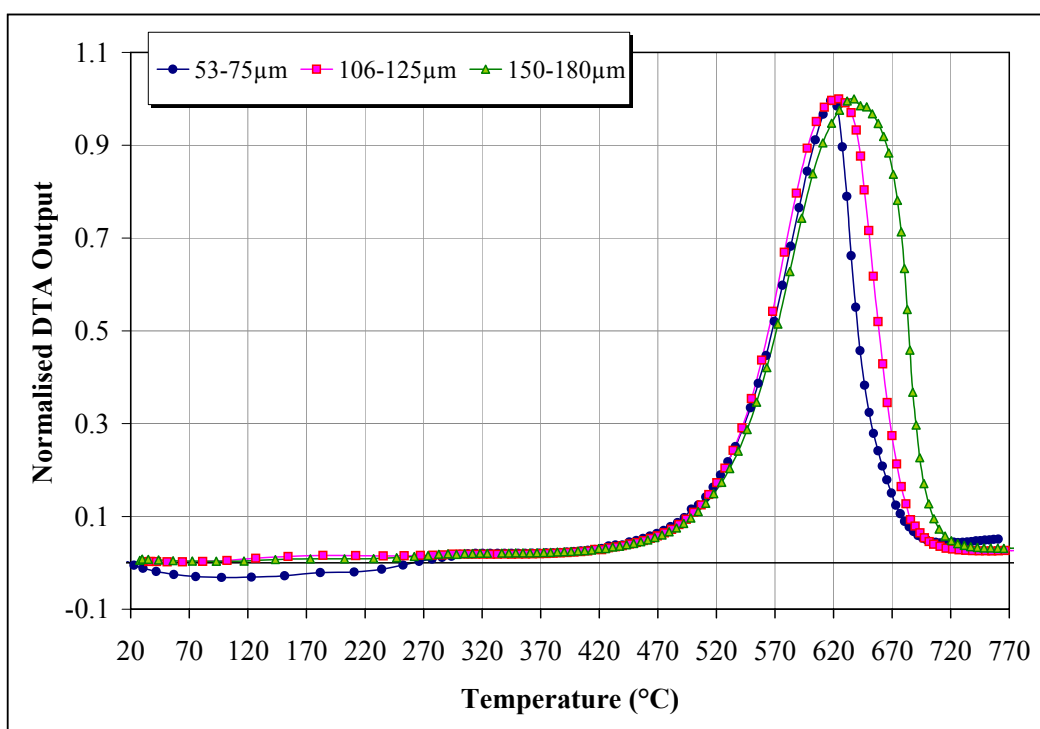


APPENDIX F. DTA Profiles of the Re-fired Chars

F.11 El Cerrejon – 400 ms

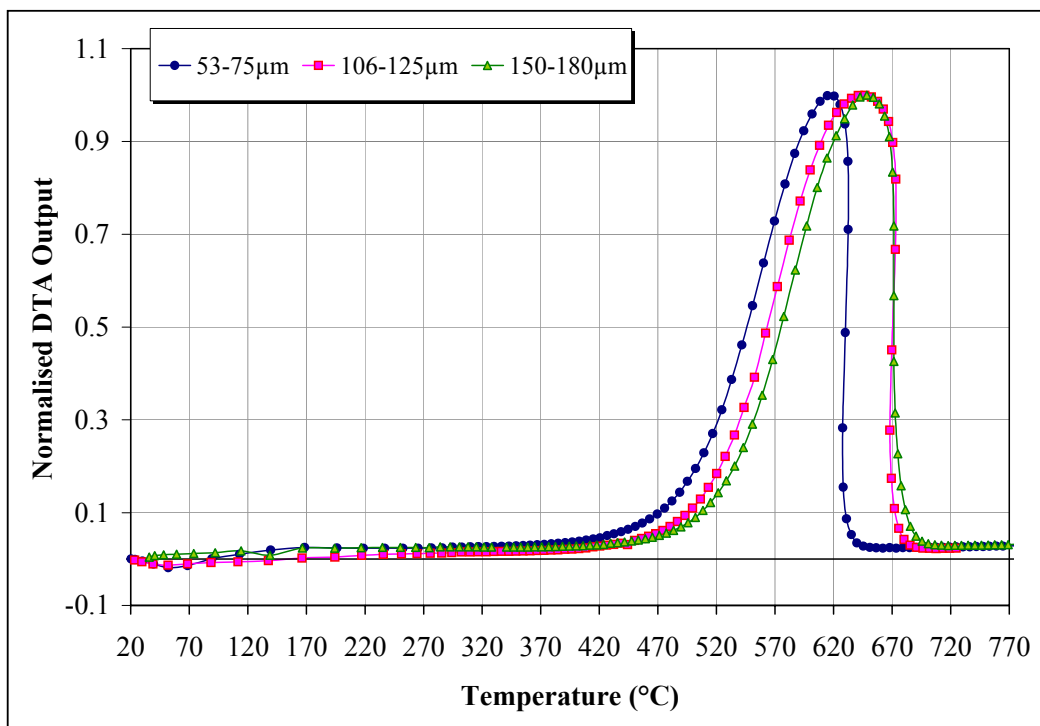


F.12 El Cerrejon – 600 ms

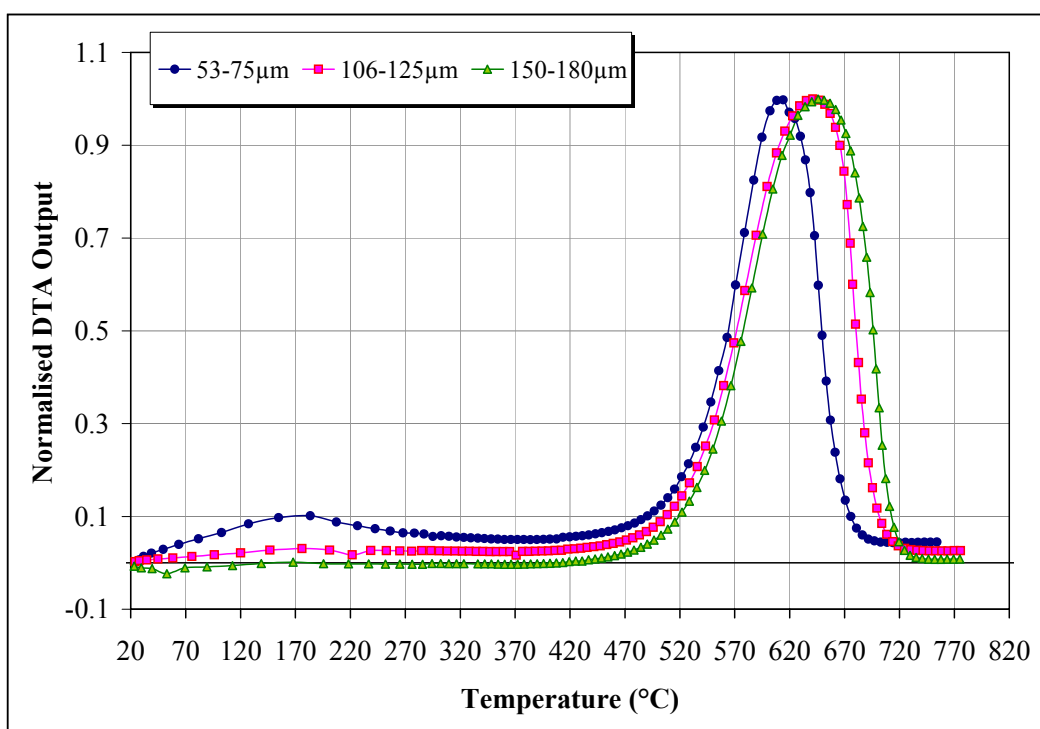


APPENDIX F. DTA Profiles of the Re-fired Chars

F.13 Caypa – 200 ms

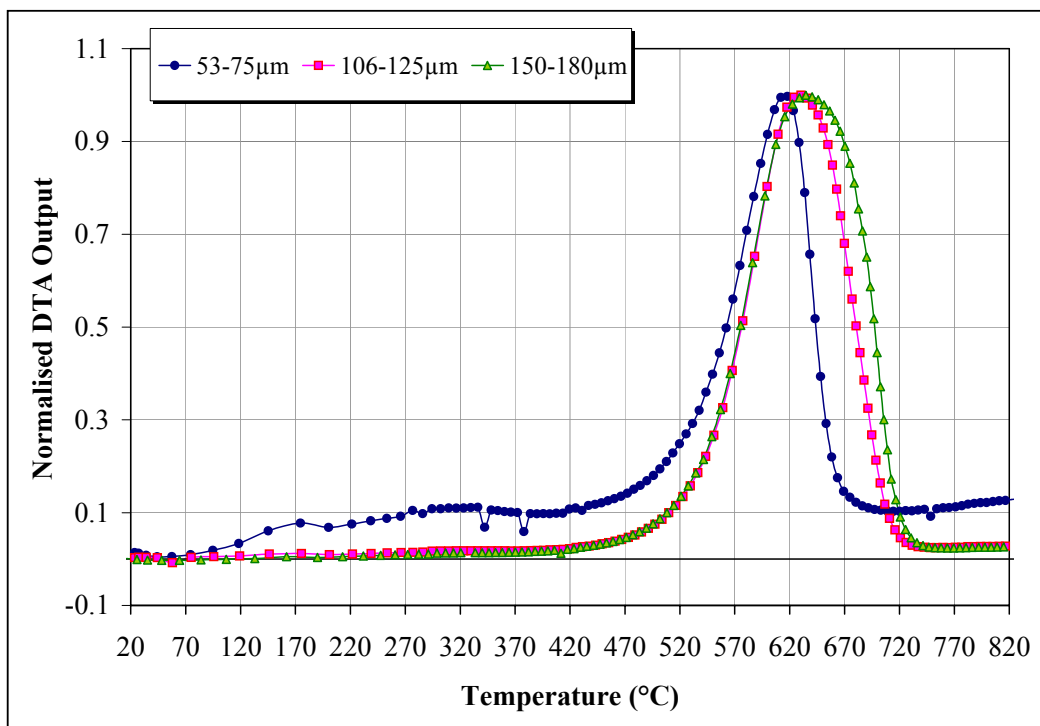


F.14 Caypa – 400 ms

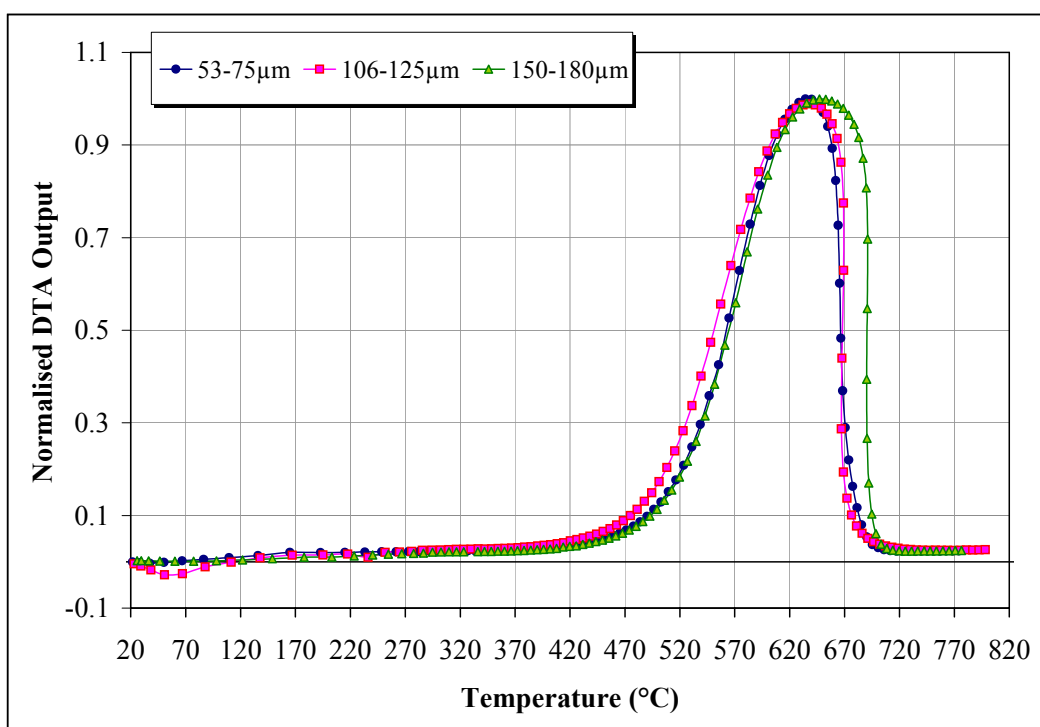


APPENDIX F. DTA Profiles of the Re-fired Chars

F.15 Caypa – 600 ms

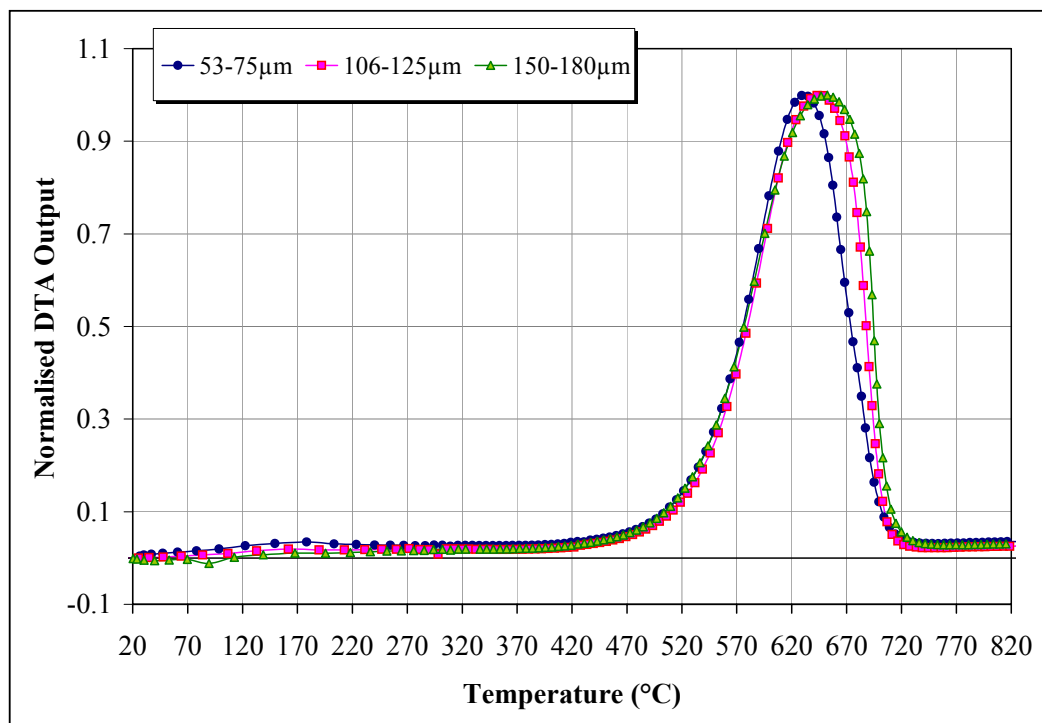


F.16 Guasare – 200 ms



APPENDIX F. DTA Profiles of the Re-fired Chars

F.17 Guasare – 400 ms



F.18 Guasare – 600 ms

